Estimating spatial patterns of soil erosion and deposition in the Andean region using geo-information techniques

A case study in Cochabamba, Bolivia

Promotor:

Prof. B. Schultz, PhD, MSc.
Professor of Land and Water Development
UNESCO-IHE & Wageningen University (WUR)
Delft, The Netherlands

Co-Promotor:

Dr. Ir. C. M. M. Mannaerts
Associate Professor
Department of Water Resources, ITC
Enschede, The Netherlands

Examining committee:

Prof. Dr. Ir. D. Gabriels
University of Gent
Gent, Belgium

Prof. Dr. Ir. L. Stroosnijder
Wageningen University
Wageningen, The Netherlands

Prof. Dr. D. Lobo, MSc.
Universidad Central de Venezuela (UCV)
Caracas, Venezuela

Prof. Dr. L. D. Norton, MSc.
Purdue University
Purdue, USA

Estimating spatial patterns of soil erosion and deposition in the Andean region using geo-information techniques

A case study in Cochabamba, Bolivia

Carlos Saavedra

THESIS

to fulfil the requirements
for the Degree of Doctor of Philosophy
on the authority of the
Rector Magnificus of Wageningen University,
Prof. Dr. M.J. Kropff,
to be publicly defended on
Tuesday, December 6th 2005 at 15:00 hrs
in the auditorium of ITC, Enschede

This publication has been submitted as a Ph.D. dissertation in partial fulfilment of the requirements for the award of the degree of Doctor at Wageningen University, The Netherlands, 6th December 2005.

A mi querida mamá

Table of contents

List of Figures

List of Tables

Acknowledgements

I thought the time to write this section would never arrive, and often I even wondered why I'd ever decided to start on a PhD. Now I've reached the end and it is time to express my gratitude to all the people who have encouraged me to finish this work. For sure, the fulfilment of this research is due to the cooperation of many people. Therefore I can only hope that I mention you all – and those who I forget at this moment, please forgive me and think that despite this lapse I really do appreciate you all.

I would like to begin by saying how greatly indebted I am to my ITC promotor Dr. Ir. Chris Mannaerts, who made it possible for me to embark on my research at ITC. His cooperation and guidance through the years have brought me to the point of successfully completing this thesis. Thank you for always being interested in the progress of my work, and for all your valuable suggestions and finishing touches.

My sincere thanks go to my university promotor Prof. Dr. Bart Schultz, who accepted the challenge to guide me through the development of this thesis. His wise advice and suggestions when we were on fieldwork in the upper and middle valleys of Cochabamba, as well as his valuable corrections to my earlier draft, significantly improved the final dissertation. I would also like to thank Dr. Ir. Herman Depeweg, who spontaneously took on the responsibility of reviewing my thesis and also provided me with much good advice.

I am very grateful to Dr. Karin Pfeffer, whose comments and corrections concerning my first draft made me realize just how far I was straying from the right path. Thank you, Karin; I really appreciate it! I would also like to express my gratitude to Ir. Bart Krol; his comments about my work were a significant contribution in the document.

I would like to sincerely acknowledge the role played by the CLAS/SAIL Project in Bolivia, through the good offices of Dr. Carlos Valenzuela (former director of CLAS) and MSc. Enrique Fernandez (current director), by funding this research. Likewise, I extend my thanks to all the staff at CLAS who in one way or another cooperated in the development of this research.

I am grateful to the Laboratory of Hydraulics (LH-UMSS), headed by MSc. Marco Escobar, for the logistics support while I was working in the Laka-Laka catchment and reservoir alongside scientists involved in other PhD research. I would like to extend my thanks to MSc. Edgar Montenegro, from LH-PROMIC, for his cooperation regarding data and logistics for the study of the Taquiña catchment. My thanks go to MSc. Remco Dost, for his cooperation in installing and setting up the bathymetric survey at the Angostura Lake in Cochabamba. Thanks to Dr Britto for the Portuguese translation.

Thanks to Ms. M. Styczen from DHI for providing me the MIKE BASIN MILW license. I would also like to thank MSc. Elmer Rodriguez, of the CORANI Electric Enterprise, as well as the "Asociación de Riegos La Angostura" and the "Honorable Alcaldia de Vacas", for their economic support.

Thanks to all the staff of the Water Resources Department and to my PhD colleagues. The technical discussions and conversations during the tea/coffee breaks have increased my knowledge of the challenges still ahead in the field of hydrological sciences as we strive to contribute to the food security of our planet.

I would like to thank those researchers in the field of erosion modelling and processes from different countries around the world that unselfishly provided their findings, software and publications, thus greatly contributing to my research.

A thank-you to all my fellow PhD colleagues for their friendship, and for our monthly meetings that gave me renewed spirit when I was sometimes struggling with my study.

The conclusion of my PhD research brings to an end the period of almost four years that I have spent in the Netherlands. I would therefore like to take this opportunity to express my sincere thanks to all the friends I have met along the way. I'm glad to say that I have friends from countries ranging from Albania, Bolivia, Botswana, Costa Rica and Colombia to Italy, the USA and Zimbabwe. During my stay I've been honoured to know such people as Faviana Ines, Julio Cesar, Obed, Bojana, Lyande, David, Mª Fernanda, Claudia, Jamshid, Ivan, Monja, Rafael, Ronald, Sandra Patricia, Johan, Rogier, Carolina, Diana, Robert, Marco, Gustavo, Jorge, Chiara, Antonella, and Arta – to name a few – whose companionship has always made me feel comfortable in Enschede.

Ahora, deseo expresarte toda la gratitud, afecto y amor que te tengo querida mamá. Tu guia desde las etapas mas tempranas de mi vida, tu esfuerzo y duro trabajo así como el amor y las ideas que has inculcado en mi, a lo largo de mi vida, me han permitido salir adelante y terminar mi tesis. Mis palabras son pocas, pero quiero que sepas cuanto aprecio todo lo que tu me has dado. Gracias mami! desde el fondo de mi corazón.

Deseo tambien agradecer a las familias Arnez-Espinoza, Delgado-Arnez y Alvarado-Arnez, por toda la ayuda, afecto, consejos y cariño a lo largo de mi vida, gracias mil!. De la misma manera no puedo olvidar a Andrea, Sonia, Pablo, Lucia y Sergio, personas a quienes vi crecer y son ahora o estan en carrera de ser prosperos profesionales con un gran futuro por delante, muchas gracias por su apoyo, aprecio y amistad. A todos ustedes, los llevo siempre conmigo.

To conclude, I'd like to wish to all those people I have met here success in their lives and professional careers.

GRACIAS

Abstract

Predicting spatial patterns and intensity of soil erosion and sediment redistribution in landscapes can be problematic in areas where few experimental data are available. Yet it is in those data-scarce regions that the ability to extrapolate local field evidence could be most useful in practical applications. Conventionally, soil conservationists and policy makers look at the field scale to judge the on-site impacts of soil erosion on the catchment. Water resource managers, in contrast, usually rely on sediment yield data of gauged catchments to evaluate the off-site effects of erosion intensity and sediment production. In fact, a scale gap can be observed in the approaches used by respectively land and water resources managers.

The increasing availability of satellite data, with spatial resolutions ranging from fine to coarse and temporal resolutions from hourly to monthly, provide a significant information source for mapping, monitoring and predicting current land degradation, as well as for monitoring signals that describe spatio-temporal variations in soil surface characteristics. Moreover, the integrated use of experimental field data with remote sensing imagery allows field evidence to be extended to larger areas.

On the other hand, owing to the increased capabilities of existing GIS platforms, distributed erosion models have evolved and are now commonly used as the georeferenced backbone for the analysis of hydrological and erosion processes. However, the accuracy of their predictions is seriously hampered by the natural complexity and spatial heterogeneity of the processes acting on the landscape itself, coupled with the limited availability of spatio-temporal datasets in ungauged catchments.

Therefore, the aim of this thesis was to use and further develop existing spatially distributed approaches in combination with different geo-information techniques for analysing erosion and sedimentation processes, allowing linkages to be defined between field and basin scales in data-scarce environments. In this study, conceptual models were selected because they represent a compromise between complex data demanding (physically based) models and simple-structure regression (empirically based) models.

The province of Cochabamba in the Central Andes of Bolivia was the focus of this research. The region of the middle and upper valleys of Cochabamba plays an important role in the agricultural sustainability of rural and urban livelihoods. Owing to the semi-arid regime and topographical and geological conditions, however, the impacts of soil erosion are clearly visible and are leading to an increase in the land degradation processes.

Five conceptual model approaches were selected and used, and the results compared regarding their ability to represent erosion and sedimentation phenomena at the regional scale. Hence, erosion and deposition maps for Cochabamba province, with an area of about 54,100 km^2, were derived using the global climate, topography, soil datasets and low-resolution satellite images for land cover. A categorical comparison method was used to validate model predictions based on existing thematic mapping of erosional

intensity. Model accuracies ranged from fair to poor, reflecting fundamental differences in pixel-based modelling and terrain unit mapping. Generalization in the global topographical and soil datasets was seen as the highest source of uncertainty in the model estimates, particularly for the highly variable Andean environment.

A more detailed erosion analysis of a 59.8 km^2 semi-arid catchment was performed using fine- to medium-resolution (5 to 90 m) satellite data for land cover and topography. Rainfall and soil data were obtained by extrapolation from local stations and *in situ* measurements. Accordingly, the five model estimates were compared and validated against an erosion intensity map obtained from multitemporal analysis of a 1961 ortho-photo mosaic and a 2002 SPOT-5 panchromatic orthorectified image, in combination with a digital terrain model and field data. The semi-quantitative validation indicated reasonable model agreement in terms of spatial patterns; however, none of the models was accurate in terms of absolute values and therefore these soil loss estimates should be interpreted with caution.

Detailed sedimentological studies of reservoirs provide high-resolution depositional histories that help to quantify the gross amount of erosion and mean annual sediment yield from the contributing catchments. Hence, the next scale of analysis for understanding the processes of sediment delivery to the channel network and ultimately to the catchment outlet was the reservoir (local scale). For this purpose, three contrasting reservoirs in terms of size and erosive process upstream were studied. A novel and rapid acoustic sonar and GPS-driven survey technique was developed for the purpose. The evaluation of the minimum sample size or point density required to obtain an accurate bathymetric surface was carried out using a split sampling technique and cross validation with several statistics of accuracy.

It was found that the sedimentation rate variability within the reservoirs varied according to the physiography (distance to the river channel, vicinity of the reservoir), topography (gentle, moderate or steep relief), climate (river flows and regime) and reservoir hydraulic conditions (annual flushing, irrigation requirements). The temporal variability was due to the river inflow fluctuation, the exploitation regime and the changes in the reservoir storage capacity.

Finally, the linkages between catchment gross erosion rates and reservoir sedimentation were analysed using spatially distributed sediment delivery ratio (SDR) concepts. This concept is based on the travel time required for detached sediments to arrive at the catchment outlet. Higher delivery ratio (SDR>0.6) were found in 25% of the catchment area, whereas in more than 50% of the area the SDR were lower than 0.2.

Modelling the SDR in the spatial domain and coupling it to the previous catchment gross erosion estimates enabled the net amounts of eroded soil to be estimated. These sediment yield predictions were validated using the reservoir sediment records and were verified for the physiographic and climatic conditions prevailing in this part of the Andes.

Gathering *in situ* environmental information requires strong financial support – seldom unavailable in developing countries such as Bolivia. The findings of this research open

xii

up possibilities for using scarce *in situ* data in conjunction with the ever-increasing remotely sensed data to identify source areas that deliver most of the sediments (not necessarily the most erodings), to identify areas with high erosion rates leading to land degradation where water and soil conservation measures are required, to predict the basin sediment export, and to develop preliminary basin management strategies.

Chapter 1

General introduction

Chapter 1

General introduction

1.1 Problem statement

Soil erosion by water is an important form of land degradation. It is estimated that one sixth of the world's soils are affected by water erosion. Globally, humans impact on around 1,094 million hectares, of which 43% suffer from deforestation and the removal of natural vegetation, 29% from overgrazing, 24% from improper management of the agricultural land and 4% from over-exploitation of natural vegetation (Walling and Fang, 2003). Human-induced land degradation is one of the more destructive phenomena relating to natural resources in the world, and is recognized as a key issue for conservation in the 21st century (Reich et al., 2000). In mountain environments of developing countries, soil erosion regularly constrains rural development and exacerbates poverty by undermining the productive capacity of highland agriculture and livestock raising (Zimmerer, 1993; Lal, 2001).

It is well known that water erosion and sedimentation processes are influenced by a multitude of biophysical and human factors, and occur at different intensities across the landscape. However, the spatial and temporal scales of the processes are still poorly understood, which makes the monitoring and assessment of erosion and deposition processes a complex and cumbersome task, with considerable uncertainty (Figure 1.1). As a consequence, there is a need to improve the understanding of erosion and deposition processes at field, catchment and larger regional scales from the quantitative perspective, in order to be able to analyse their on-site impact on soil productivity as well as their off-site impact on streams (*e.g.,* sedimentation and water quality) (Wickenkamp et al., 2000; Romero and Stroosnijder, 2002).

Localization of erosion-prone areas and quantitative estimation of soil loss rates with sufficient accuracy are of extreme importance for designing and implementing appropriate erosion control or soil and water conservation practices (Shi et al., 2004). Equally, erosion and sedimentation research and a proper understanding of the physical processes are important in order to enhance understanding of landform development across temporal and spatial scales (Slattery et al., 2002; Wainwright et al., 2003).

Erosion and sedimentation embody the processes of rainfall and flow detachment, entrainment or transport and deposition of soil particles. The processes controlling sediment detachment, transport and deposition are complex and interactive (Toy et al., 2002). This complexity results in the lumping of the many sub-processes under the one term "*erosion process*" in many erosion models.

The difficulty in observing and measuring erosion processes during runoff or erosion events, owing to the small spatial and time scales at which the processes occur, necessitates the use of erosion models for the prediction of erosion and sedimentation in

catchments (Jetten et al., 2003). The use of erosion models and "*after the fact*" erosion observations are necessary tools in land resource management (Van Rompaey et al., 2003a). Hence, what is required is a method for predicting soil erosion, sediment transport and deposition in ungauged catchments and under a wide range of climatic, physiographic and land cover conditions.
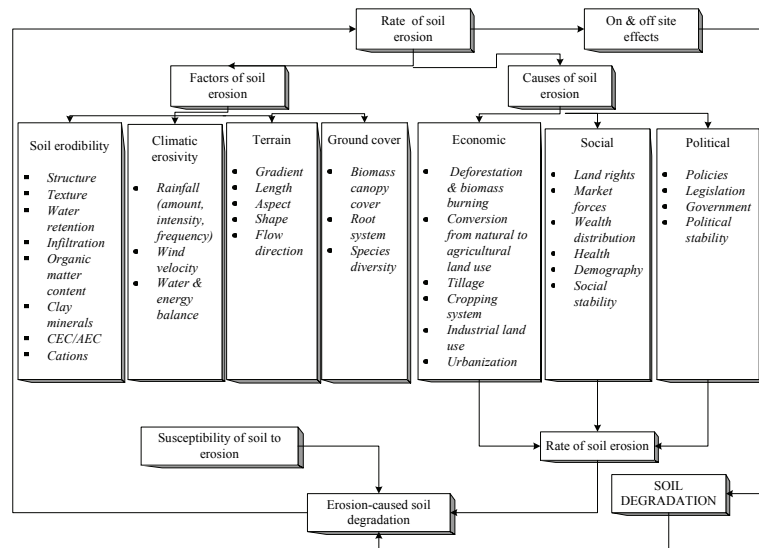
Figure 1.1 Effects of erosion processes in land degradation

Over the last 20 years, there has been remarkable progress in the development of mathematical tools for erosion and sediment transport modelling, with a tendency towards physically or process-based model development (de Roo et al., 1989; Young et al., 1989; Desmet and Govers, 1995; Mitasova et al., 1996; Renschler et al., 1999; Jetten et al., 2003). Most of the current process-based erosion models can be roughly divided into three main groups: plot, field or hillslope scale; catchment scale; and complex landscape models (Merrit et al., 2003).

Although there are numerous models that combine more than one of the above concepts, a number of important issues for effective erosion assessment at catchment and regional scales remain unsolved. For example, many current methods require a large number of experimental input data unavailable in ungauged catchments; important effects of terrain shape are not taken into account; numerical methods used for the model implementation exhibit instabilities when used at high resolutions; and, moreover, detailed spatially variable outputs are limited (Perrin et al., 2001).

The combination of these factors often makes applications of physical models either laborious or simply not practical, particularly for large watershed areas (Pallaris, 2000). Some of the unsolved modelling problems that restrict the use of current models in gaining more insight into the spatio-temporal aspects of erosion and sedimentation

processes and that limit their application in effective erosion prevention for large, complex areas can be identified as follows:

(i) The heterogeneity and complexity of terrain, land cover and soils features across the landscape, and the subsequent need for high spatial resolution treatment in a fully 2D or 3D distributed manner;

(ii) The limited ability to quantitatively describe erosion processes at the fundamental physical level without the use of a minimal number of empirical parameters or inputs;

(iii) The limitations of most numerical methods commonly used in erosion models to simulate and solve water flows (*e.g.,* diffusive wash on soil surfaces) and sediment transport in shallow flows without major assumptions being made;

(iv) The need to integrate model algorithms across different spatial and temporal scales;

(v) The need to validate both spatial and quantitative aspects of model predictions;

(vi) The need for accurate digital elevation or terrain models that require minimal reprocessing or modifications to make them usable for hydrological modelling;

(vii) The continued need for experimental research for deriving soil and land cover input parameters for process-based erosion models, even though the relationships between these parameters are still only poorly understood;

(viii) The need to provide cartographical and graphical visualizations of numerical and model outputs, including dynamic output, in formats that facilitate geospatial analysis and support the natural resource planning and decision-making processes.

It is clear that solving all these problems would require considerable time and effort from many research teams. Accordingly, this research focuses on a selected subset of the above-mentioned problems, *i.e.,* (i), (ii), (iv) and (v).

1.2 Significance of soil erosion and sedimentation in the Andean region of South America

The growing population of Latin America puts a lot of pressure on the agricultural production and practices, and therefore on the soil. Deforestation and inappropriate agricultural practices are causing this region's topsoil to erode at an alarming rate. Although Latin America has the world's largest resources of cultivable land, this reserve is dwindling rapidly (Pla, 1993). Of Latin America's estimated agricultural potential of 576 million hectares, more than half are classified as degraded.

Over 100 million hectares have been degraded by the effects of deforestation, while a further 17 million hectares suffer from overgrazing (Pla, 2003). According to Pla (1996), in South America the policies of agricultural expansion over the last decades have frequently led to land degradation, with a decrease in productivity, an increase in production costs, and an increase in problems related to water supply, flooding, landslides, and the silting of reservoirs, followed by serious economic and social consequences.

In the Andean region (Venezuela, Colombia, Ecuador, Peru, Chile and Bolivia) of South America, a high proportion of the land is characterized by water erosion on steep slopes, which restricts agricultural use (Romero and Stroosnijder, 2002) and livestock

5

raising. A good proportion of the land available for agriculture is found in fragile ecosystems such as humid tropical forests, steep mountain areas, and semi-arid areas (Pla, 2003).

At present, the problems of erosion occur not only in these steep areas but also in areas with more gentle slopes (2% to 8%). Large-scale commercial ranching or plantation agriculture is often directly or indirectly responsible for soil degradation. For example, the clearing of forests to make room for the expansion of farms and ranches means the retentive capacity of soil is lost and the topsoil is much less protected from erosion.
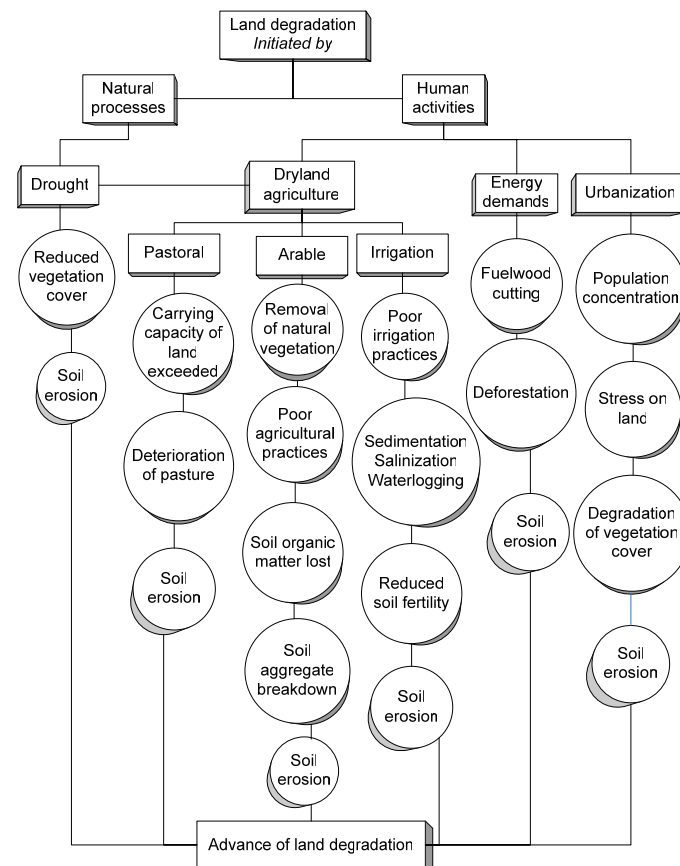
Figure 1.2 Causes of soil degradation

Moreover, much of this new development is on marginal land, often in mountainous regions where rapid erosion is more probable. In addition, a combination of erosion, soil exhaustion and the growing food demand from an expanding population have led to an intensification of agriculture by both small and large farmers (Biscaia, 1987). Traditional methods of letting the land recuperate naturally have been abandoned, and chemical inputs are becoming more prevalent as a means of maintaining production levels.

Bolivia, situated in the heart of South America, is often referred to as the "Tibet of South America". This is because Bolivia's landscape is a mosaic of high mountain peaks, valleys, lowlands, and a very extensive tropical rainforest. A natural consequence of the steep Andean terrain is the severe problem of soil erosion and sedimentation (Bolivar and Mendez, 2000). According to the preliminary land degradation map for the arid, semi-arid and subhumid dry regions of Bolivia (MDSMA, 1996), the provinces of La Paz, Santa Cruz and Cochabamba are affected by a medium to high degree of land degradation in 32%, 33% and 46% of their total area, respectively.

Most of the areas belonging to the provinces of Oruro, Potosi, Chuquisaca and Tarija are currently affected by a high to extreme degree of land degradation and desertification, soil erosion being the most important triggering factor of the land degradation.

In Bolivia, there is generally a good qualitative understanding of the main causes of soil erosion at the local level. However, research is required to get more of the quantitative information needed for predicting potential soil erosion and for selecting or designing management alternatives at the catchment and regional scales (PROMIC, 1995). The lack of appropriate data on erosion rates prevents an objective evaluation of the applicability of conservation practices and models developed elsewhere. As a consequence, some models to predict erosion are used indiscriminately, without scientific evidence of their applicability to a particular situation (Goitia, 1990; Zimmerer, 1994). Owing to lack of research in quantitative erosion, international technical assistance and aid programmes have a reduced influence on soil conservation in Bolivia.

The present strategies and applied research on soil and water management and conservation conducted by national and international organizations reflect the lack of coordination between activities and the inappropriate use of resources not tailored to the needs of the end users. Linking the institutions is essential at the governmental scale. Moreover, the lack of systematic resource inventories at local, regional and national levels in Bolivia is a barrier to matching site characteristics with efficient use and management for erosion control. While soil erosion rates based on field measurements are not available at the catchment or regional scale, they may be surveyed to a small extent at the plot or field scale (Zimmerer, 1993; Prado, 1995; Saavedra and Mannaerts, 2003a). Even so, such data are often not comparable because of non-standardized methodologies and non-uniform experimental conditions.

Furthermore, the meteorological and soil data required for assessing erosion rates and evaluating potentially useful sustainable land management and effective conservation practices are insufficient, both in quantity and quality. Finally, misinterpretation and erroneous conclusions are major worries when using such data for designing conservation measures, for land use planning, and for implementing resource management policies (Dehn, 1995; Millward and Mersey, 1999; Mitasova, 2000). Under these conditions, using highly detailed prediction models that require more hydrological, meteorological and soil data than are available is useless, and may lead to dangerous mistakes in land use and management decisions. Thus, the prediction of water erosion should generally be carried out by applying empirical or conceptual

models rather than physically based methods and models. Research in Bolivia should be directed towards using simple worthwhile methods of predicting impacts and designing management and conservation practices for water and soil conservation and sustainable productivity, as a required step prior to evaluating, validating, and finally selecting farmer-acceptable, economically and environmentally sound technologies (PROMIC, 1995).

Although simulation modelling is a cheap and rapid method of investigation, it cannot replace field data collection and field experiments; however, it may increase the efficiency of these two activities. It is also necessary to keep in mind that good predictions can only be obtained by using models if they are based on good data from field observations and measurements, and not on generated or assumed data (Zehl and Montenegro, 1996; Zarate and Montenegro, 1999; Metternicht and Gonzalez, 2005). In any case, the model user must have appropriate field experience so that unreasonable results can be detected, explained and avoided.

1.3   Aims, objectives and research questions

The general aim of this research is to estimate and compare spatial and temporal patterns and rates of soil erosion and deposition obtained using remotely sensed data and different relatively low data demanding spatial model approaches at regional and catchment scales. In this context, six specific objectives were addressed and each has been achieved by trying to answer several research questions:

(i)   To analyse and review existing modelling approaches and their capacity to represent erosion, deposition and sediment transport dynamics at various spatial and temporal scales.
- What are the potentialities/drawbacks of existing erosion models?
- Are the concepts included in the conceptual erosion models sufficient to represent erosion processes in mountain landscapes?

(ii)   To compare the performance of five relatively low data demanding erosion model approaches to assess erosion at the regional scale, using global coarse-resolution environmental and remotely sensed data.
- Is coarse time series imagery a suitable tool to assess the role of vegetation as protection against erosion at regional scale?
- Can long-term and large-scale erosion monitoring be used to better ascertain the impacts of land management policies and practices on erosion and sediment delivery, and the resulting degradation of soil and water resources?

(iii)   To evaluate the performance of the five erosion models at catchment scale, using soil survey, meteorological, and medium to high spatial resolution remotely sensed data.
- Can erosion be accurately predicted using a combination of fine and coarse spatial resolution imagery?
- Can a limited field data collection suffice to accurately model the pattern of soil erosion and sediment delivery at catchment scale?
- Can spatial erosion estimates be linked across different spatial scales?

(iv)   To validate spatial patterns of erosion predictions, using a soil erosion risk map derived from high spatial resolution imagery and field-surveyed data.

- Can alternative sources of information, such as observed patterns of erosion, be used for model validation?
- Can low data demanding models be used to provide catchment or basin answers and proof that conservation strategies work at these scales?

(v) To assess the applicability of low-cost sonar equipment in combination with GPS (global positioning system) to monitor and determine sedimentation of lakes and reservoirs as an indirect method of estimating sediment yields from contributing catchments.

- Can the integration of a handheld GPS, sonar sounding device and remotely sensed data provide accurate bathymetric surface data in comparison with conventional acoustic surveying?
- How much sediment is deposited in the Angostura reservoir?
- Can the current rate of sediment in the Laka-Laka reservoir reduce its life expectancy significantly?
- What are the causes that trigger the delivery of sediments to reservoirs in mountain landscapes?

(vi) To assess the applicability of spatial sediment delivery ratio (SDR) concepts in mountainous catchments as a linkage between upstream gross catchment erosion and reservoir sedimentation.

- Can the spatial SDR approach be used for sediment yield predictions instead of complex sediment transport equations?
- Can the spatial SDR approach effectively identify the pathways and mechanisms of sediment movement?
- Can data on reservoir sedimentation be used to validate the erosion and sediment yield predictions?

1.4 Outline of the thesis

All aspects of erosion processes, data requirements and models have been researched, starting from a review of existing methodologies, model applications at regional and catchment scales and the estimation of reservoir sedimentation rates by using a novel sonar survey technique. Research by Hill and Schütt (2000), Ranieri et al. (2002), van Oost et al. (2004), and King et al. (2005) demonstrates that geo-information and remote sensing techniques in conjunction with erosion and sedimentation models are powerful tools for generating and supporting such understanding. Therefore, strong emphasis has been put on the use of geo-information techniques for geospatial data handling and processing, and remote sensing as data sources.

In Chapter 1, a general introduction to the research is given, and the significance of erosion and sedimentation processes is presented by contrasting opinions on the severity of the problem worldwide, and in Latin America and the Bolivian Andes in particular. The need for more quantitative estimates of the processes and localization of the process intensities across the landscape is stressed, along with the importance of using remotely sensed data and geospatial tools.

As the basis for a better understanding of erosion and sedimentation processes and models, Chapter 2 gives a brief review of some more important erosion and sediment yield models. Although the scientific literature was screened thoroughly for all existing

model approaches, a complete overview of all models that are currently used to simulate erosion and sediment movement through the landscape, from local to continental scales, was not attempted. Instead, the focus was on selecting a number of model approaches that potentially could be applied to the Andean region, while above all considering the scarcity of experimental data in the researched areas. The process required for selecting an appropriate model is presented, as well as the scaling effects of the input model parameters and their influence on the erosion prediction. The theoretical and algorithm description of the selected models is also presented.

Chapter 3 describes the biophysical characteristics of the region and research area. In addition, it provides insight into the digital image processing techniques used for enhancing, classifying and delineating different data themes derived from satellite data and used in the research (*e.g.,* erosion types or features, land cover, geomorphic units). Emphasis is on the Laka-Laka reservoir and main research catchment. The techniques and advantages of using different remotely sensed data for obtaining the parameters needed to model erosion over the region or catchment (*i.e.,* cover vegetation factor, runoff, land cover fraction) are also reviewed. The soil properties and their variability along topographical gradients within the geomorphic units in the Laka-Laka research catchment are also described in this chapter.

Chapter 4 deals with the application of the five selected models to estimate erosion rates at a regional scale. Here, use was made of coarse spatial resolution global geodata and climate datasets retrievable from the internet. These included databases on global topographical, climate and soil properties and land cover data from satellites. A geospatial modelling resolution of 1 km^2 was used in the assessment. The province of Cochabamba (Bolivia), with elevation ranging between 300 and 5,200 masl (metres above sea level) and an approximate area of about 54,100 km^2, was used as a sample area. A semi-quantitative validation of the predictions was implemented by comparing model predictions with existing erosion intensity maps of a series of sample catchments spread over the middle and upper valleys region of Cochabamba province, in order to derive the degree of agreement between model prediction and observed erosion intensity.

In Chapter 5, the application of the five erosion models at the catchment scale is described. The 59.8 km^2 Laka-Laka reservoir catchment was used for the purpose. Here, use was made of a combination of satellite data of medium and high spatial resolution (*e.g.,* the moderate-resolution imaging spectroradiometer (MODIS) and SPOT-5). The geospatial modelling resolution was increased one order of magnitude to 30 to 100 m. Soil parameters for the erosion models were derived from local survey, sampling, field measurement and laboratory analysis. Climate data were obtained from surrounding meteorological stations. The predicted patterns of erosion and soil loss redistribution were validated by comparing the model predictions with a catchment erosion intensity map derived from a comparison of an orthorectified panchromatic high-resolution (5 m) panchromatic SPOT-5 image (August 2002) with the 1:50,000 ortho-photo mosaic (August 1961).
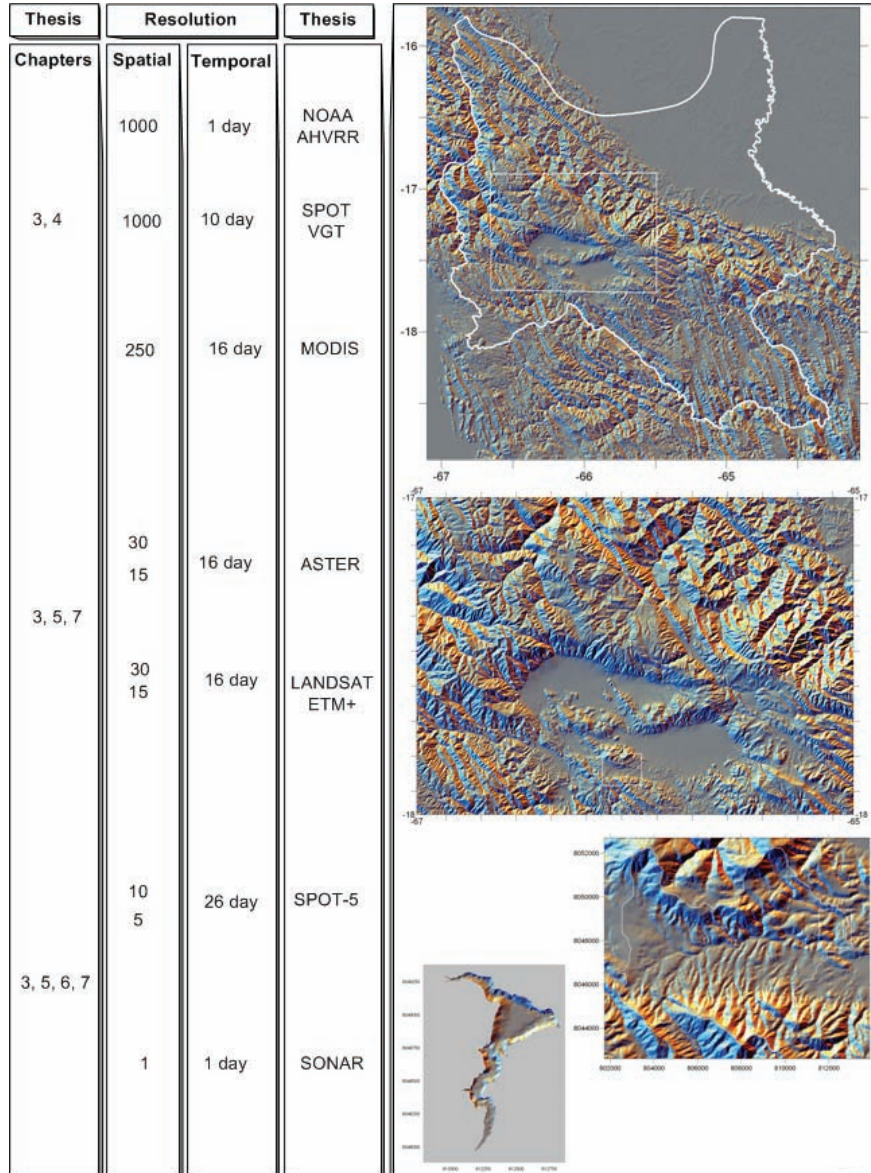
Figure 1.3 Overview of the spatial and temporal resolutions of model simulation and remotely sensed data used in the different chapters

In Chapter 6, the applicability is assessed of rapid, low-cost sonar equipment connected to a GPS instrument for monitoring and determining sedimentation in lakes and reservoirs. Within this research framework, the prime objective was the need for sedimentation data to validate the catchment erosion and sediment yields obtained by the models. Here it is discussed whether the proposed rapid geomatic survey method provides reliable bathymetric surface data that allow deposition patterns in reservoirs to be analysed and sediment yields from the contributing catchments to be estimated. The

influence of the acoustic sounding sampling size on the accuracy of bathymetric surface data is also analysed by using geostatistical methods.

Chapter 7 deals with the analysis of the linkage between gross catchment erosion rates and sediment yield, using reservoir sedimentation data as a quantitative proxy for catchment sediment export. The focus of the research was on intrinsic relationships between both temporal and spatial scales of distributed sediment delivery in a catchment. Four novel spatially distributed SDR concepts were selected and evaluated. The spatial SDR models were coupled with gross catchment erosion estimates (Chapter 5) in order to obtain catchment sediment yield. Validation of the estimated sediment yields from the catchment was carried out by comparing the coupled model predictions with the sediment yields derived from a time series of reservoir sedimentation data (Chapter 6).

In Chapter 8, a synthesis of the research is presented. The methodology developed in this research and the results obtained when estimating soil erosion and deposition patterns at different scales in the Andean region of Bolivia are summarized and evaluated. The realization of the aim and objectives of the research is also discussed. Finally, some limitations of the methods are presented, together with suggestions for application and improvement.

Chapter 2

Erosion processes, model review and selection

Chapter 2

Erosion processes, model review and selection

2.1 Introduction

Many researches, such as those of Romero (2005), Restrepo et al. (In Press), Coppus (2002) and aus Yarina-Kocha (2002), have proved that there is no single erosion or sediment transport model that can be universally applied to the Andean mountain ecosystems. Instead, several modelling alternatives exist, all with potential and limitations that need to be known.

In this chapter, a brief description of the rainfall-induced soil erosion processes is given first. The description is limited to field scale in space and time. Next, a number of selected empirical, conceptual and physically based models are reviewed in terms of their scope, scale, rationale, structural framework, computational procedures and data requirements. Furthermore, examples are analysed to illustrate the application of GIS and remotely sensed data in erosion modelling. Moreover, the concepts of scale and scaling in erosion modelling are also investigated, and methods to upscale or downscale data, models and predictions are presented. Finally, a concise description of the models' selection process used in this research is given, as well as their theoretical background and a short algorithm description. New spatial concepts of sediment delivery from catchments and the four spatial sediment delivery ratio (SDR) models used in this research are described separately in Chapter 7.

2.2 Erosion, deposition and sediment transport processes

Soil erosion by rainfall and runoff is termed "water erosion". It involves the detachment, transport and deposition of soil particles by the erosive forces of rainfall and runoff. Soil erosion occurs in various forms (*e.g.,* splash, sheet, rill, gullies) depending on the stage of progress in the erosion cycle and the position in the landscape. Sometimes the term referring to erosion also indicates where it occurs (*e.g.,* trail erosion, riverbank/riverbed erosion, road slope erosion, cropland erosion). The factors that influence overland flow generation and the detachment and transport of materials over the land surface are shown in Figure 2.1. These factors can be grouped under five major headings: climate and precipitation, relief, soil and bedrock properties, vegetation cover, and human activity.

2.2.1 Soil erosion processes

Erosion by water is induced by naturally occurring phenomena such as rainfall or snowmelt, or artificially by irrigation (Foster, 1982). Detachment of individual soil particles may occur when raindrops strike the surface and overcome the interstitial forces holding the soil particle together. This is commonly referred to as "rainsplash" or "raindrop splash" (Thornes, 1990). As the inducing events continue, water infiltrates

into the soil at a rate controlled by the intensity of the water hitting the surface and the infiltration capacity of the vertical soil profile. The infiltration capacity is a function of several soil hydraulic characteristics that relate the spacing and bonding of soil particles to each other, and the effects of other micro-surface and subsurface characteristics. Water that does not infiltrate begins to pond on the surface. When sufficient depth is achieved on the surface, water will flow in the direction of the steepest unimpeded slope. This initiates the hydrological process referred to as "overland flow" or "runoff". As shown in Figure 2.2, soil particles may be dissolved or suspended in the overland flow, causing the process of sediment entrainment or transport (Julien, 1995).
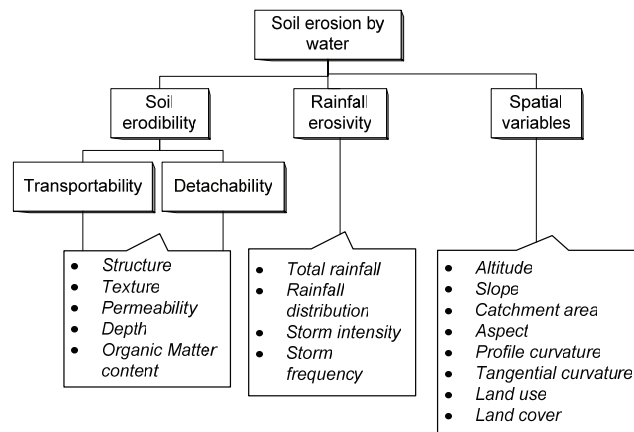
Figure 2.1 The main factors controlling the process of soil erosion by water (source: (Symeonakis, 2001)

Usually, catchments are conveniently divided into the upland or hillslope areas and the channels or drainage system. In the upland areas, overland flow is conceptually divided into rill flow and inter-rill flow mechanisms, which occur on land surfaces. As overland flow converges from various portions of the upland area and becomes more concentrated, it becomes sufficiently erosive to form shallow channels, referred to as "rills". Additional soil particles may become detached as water flows through these rills. In the inter-rill areas, runoff may occur as a very thin broad sheet, sometimes referred to as "sheet flow". Both detachment and transport may occur in the rill and inter-rill areas. As erosive power increases, the small rills may converge to form a large surface channel, called "gullies" (Poesen et al., 2003).

a)   *b)*
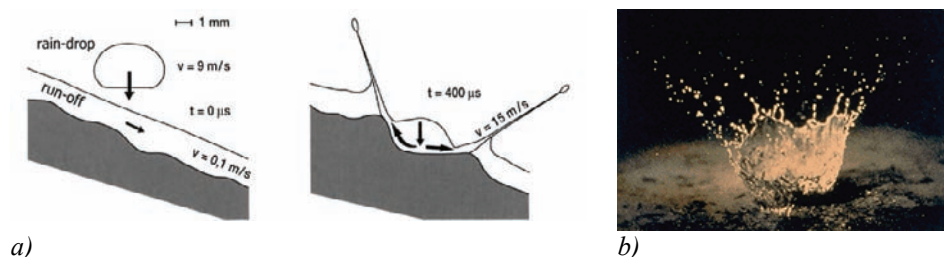
Figure 2.2 Raindrop falling on exposed soil and breaking soil particle to be lost in runoff water: *a)* raindrop velocity, *b)* raindrop impact

As illustrated in Figure 2.3, the rill and inter-rill areas and gullies are the source areas for water erosion. Eventually, if sufficient water continues to flow downslope, it will reach well-defined channels, through which both water and sediment will be carried downstream towards the catchment outlet (Nichols and Renard, 1999). If at any point along the water flow path the velocity is decreased (*e.g.,* change in slope), some soil particles may be deposited because the reduced flows cannot carry that much sediment.

The transport capacity is the maximum amount of sediment that a given flow can carry without net deposition. The detachment capacity and transport capacity are interrelated, and it is their interaction that controls the patterns and magnitudes of both erosion and deposition (Slaymaker, 2003).
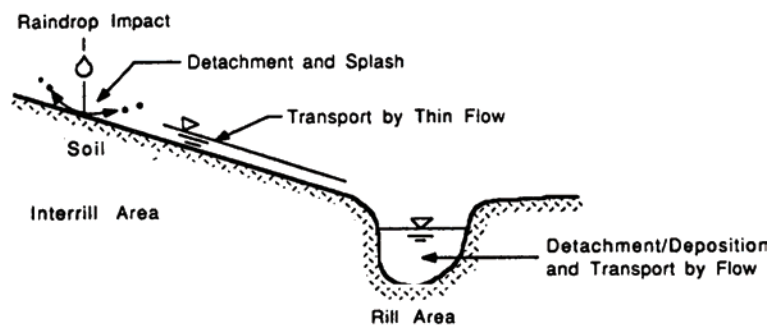
Figure 2.3 Erosion and transport on inter-rill and rill areas (source: Harmon and Doe, 2001)

The dominant character of the process is closely linked to whether the transport or the detachment capacity is the limiting factor. For example, if the detachment capacity of the soil is significantly lower than the transport capacity (*e.g.,* for clayey soils where the inter-particle binding forces are large and resist detachment), then the amount and magnitude of soil erosion is limited by the detachment capacity, which is generally referred to as "detachment-limited erosion" (Van Rompaey et al., 2003b). On the other hand, if the detachment capacity is significantly greater than the transport capacity (*e.g.,* for sandy or loamy soils that are easily detached), then the amount and magnitude of soil erosion is limited by the sediment transport capacity of runoff and referred to as "transport-limited erosion" (Harmon and Doe, 2001).

The amount of sediment actually leaving a site or catchment is a function of the erosional and depositional processes, both on surfaces and in channels, which occur upstream of the discharge point. The amount (mass) of sediment being carried per time unit is called the sediment load. The velocity of entrained sediment passing a given point is the sediment transport rate (Lu and Higgitt, 2001). A mass rate of transport, termed "sediment discharge", can be determined by multiplying the cross sectional area of the channel through which it is passing with the sediment concentration. Sediment yield, as shown in Figure 2.4, is the amount of eroded soil that is delivered to a point in the catchment that is usually remote from the origin of the detached soil particles.

In a catchment, the sediment yield includes erosion from hillslopes, channels and mass wasting (*e.g.,* slumping, sliding, falling), minus the sediment that is deposited after it is eroded and before it reaches the point of interest. As described by Alonso et al. (1995),

17

the sediment yield can be estimated for a given point in a catchment by applying an SDR, which is the fraction or percentage of gross erosion arriving at a given point:

$$SDR = \frac{Y_s}{T_e}$$
(*Eq 2.1*)

where Y_s is the sediment yield at a given point and T_e is the total gross erosion from the catchment upstream of the given point (Figure 2.5). It is hence the total computed gross soil erosion minus all forms of sediment deposition taking place upstream of the designed downstream receptor point (Springer et al., 2001).
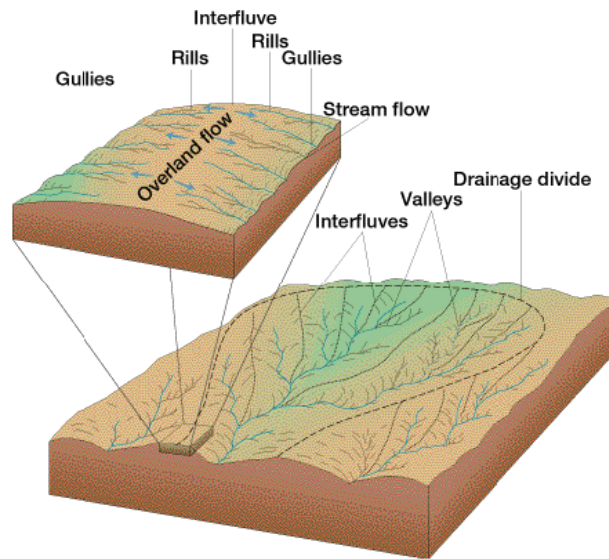
Figure 2.4 Schematic view of rills, inter-rill areas and gullies on a subcatchment (source: Harmon and Doe, 2001)
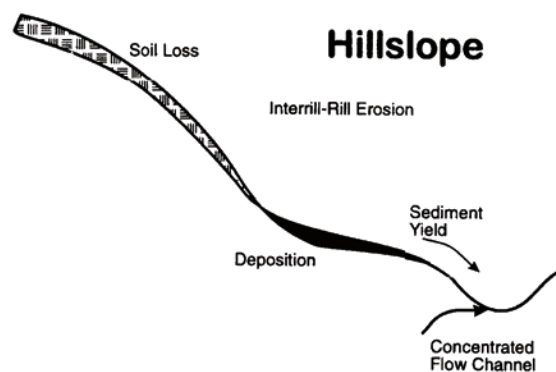
Figure 2.5 Schematic representation of the erosion and deposition from a hillslope to a channel (source: (Flanagan and Nearing, 1995)

18

2.2.2 Gully, channel erosion and sediment routing

In contrast to sheet and rill erosion, the process of gully erosion refers to erosion in channels of concentrated flows which are too deep to be obliterated by cultivation and that usually make a very significant contribution to the total soil loss. Gully flows differ from sheet and rill flows in that raindrop impacts are not an important factor in terms of flow resistance or sediment particle detachment (Poesen et al., 2002). Gully development is considered to be controlled by thresholds, as with rills, although these thresholds have been related to slope and upstream catchment area rather than to flow erodibilities. Channel erosion involves the direct removal of sediment from either the riverbanks (lateral erosion) or the riverbeds. Sediment also enters the stream owing to the slumping of stream banks undercut by channel flow (Bull and Kirkby, 1997). During high flows, a large proportion of the sediment that is transported through the stream network can originate from the stream channel. Most of the erosion types do not necessarily occur in isolation from one another; they are influenced by the landscape as well as rainfall characteristics. Walling and Probst (1997) state that the development of rill and gully erosion requires the concentration of flow and discharges that exceed critical thresholds, and as such will occur as the length of the slope increases. Hence, the dominant erosion process would be expected to follow a downslope sequence of splash-sheet-rill-gully-channel erosion.

Most erosion models tend to predict erosion for just one of these erosion types (*e.g.,* sheet and rill erosion) or at most for a number of them (Summer et al., 1998). The total sediment yield from a catchment is hence given by the sum of all contributing types of erosion existing in the catchment. The detached sediments will be carried along the channel system to the outlet according to a specific mobilization or routing. Sediment availability at a reach depends on local bed and bank erosion, sediment inflow from upstream, and sediment input from overland flow (Rustomji and Prosser, 2001).

Deposition occurs when the transport capacity of overland flow becomes smaller than the settling velocity of particles owing to gravity. These particles are loosely deposited and can be easily remobilized. For example, on the upslope part of erosion plots, where the flow velocity is low because of a small flow-contributing area as well as a short slope length, sediment is easily trapped in depressions or in channel beds. It is remobilized mainly by raindrop impacts. Downslope, an increase in flow velocity enhances the soil particle remobilization and rain-impacted flow transport, depending on slope steepness. The remobilization process is probably more efficient on steeper slopes and, as slope length increases, soil detachment rate decreases and erosion becomes detachment-limited. These processes operate at all spatial scales greater than 10 m^2 or at slope lengths of 5 m or more. Erosion on smaller plots becomes transport-limited and they do not represent the water erosion process adequately. Sediment routing thus involves, as with overland flow, a comparison of sediment availability with the transport capacity of the flow (Pullar and Springer, 2000; van Oost et al., 2004). Usually, the channel erosion process is simulated in the same way as rill erosion, except that splash detachment is not considered and lateral inflows of sediment from the hillsides become important. In the same manner as for rills, the sediment concentration (C_s) can be explicitly computed for each time step in the finite difference scheme, once the array of hydraulic variables, discharge and velocities have been found from a hydrological model.

2.3 A short review of erosion and sediment transport models

Erosion modelling is based on an understanding of the physical laws and landscape processes such as runoff and soil formation occurring in the natural environment. Modelling translates these components into mathematical relationships, describing the fundamental water erosion processes of detachment, transport and deposition (Jetten et al., 2003).

In general, models fall into three main categories, depending on the physical processes simulated, the model algorithms describing these processes, and the data dependency of the model (see Table 2.1). These three categories are the empirical, conceptual and physically based models.

2.3.1 Empirical models

Empirical models are generally the simplest of the three model types. They are based primarily on the analysis of field experiments and seek to characterize the response from these erosion plots using statistical inference. The computational and data requirements for such models are usually less than for conceptual and physically based models (Li et al., 1996). These models usually have a high spatial and temporal aggregation and are based on the analysis of the erosion processes using statistical techniques. They are particularly useful as a first step in identifying the sources of sediments.

However, empirical models are often criticized for employing unrealistic assumptions about the physics of the catchment system, for ignoring the heterogeneity of catchment inputs and characteristics, such as rainfall and soil types, and for ignoring inherent nonlinearities in a catchment system (Foster, 1996). While these criticisms are valid, insufficient meteorological networks and the spatial heterogeneity of soil restrict the use of more complex models. Such models are generally based on the assumption of stationarity, which assumes that underlying conditions remain unchanged for the duration of the study period.

This assumption limits the potential of empirical models for predicting the effects of catchment change. Furthermore, empirical models tend not to be event-responsive, neglecting to model the processes of rainfall-runoff in the catchment (Kandel et al., 2004). Nonetheless, empirical models are frequently used in preference to more complex models as they can be implemented in a situation with limited data and parameter inputs, and are particularly useful as a first step in identifying causes and sources of eroded sediment. Lu et al. (2004) note that, particularly at the larger scale, patterns of sediment delivery and sediment residence time are still poorly understood; hence, prediction of erosion and SDR at these scales is commonly based on empirical or conceptual methods that are applied uniformly in a region.

2.3.2 Conceptual models

Placed somewhere in between empirical and physically based models, conceptual models aim at reflecting the physical processes governing the system but describe them with empirical relationships. These models are typically based on the representation of a catchment as a series of internal and usually linear storages (Sivapalan et al., 2002).

Table 2.1 Erosion and sediment transport models (adapted from Merrit et al. 2003)

Model	Type	Spatial scale	Temporal scale	Input requirements	Outputs
AGNPS	Conceptual	Small catchment	Event/ continuous	High	Runoff, peak rate, erosion, sediment yield
ANSWERS	Physical	Small catchment	Event/ continuous	High	Runoff, peak rate, erosion, sediment, sediment yield
CREAMS	Physical	Plot/field	Event/ continuous	High	Erosion, deposition
EMSS	Conceptual	Catchment	Continuous	Low	Runoff, sediment loads
HSPF	Conceptual	Catchment	Continuous	High	Runoff, flow rate, sediment load
IHACRES-WQ	Empirical/ conceptual	Catchment	Continuous	Low	Runoff, sediment
IQQM	Conceptual	Catchment	Continuous	Moderate	Sediment, sediment load
LASCAM	Conceptual	Catchment/ basin	Continuous	High	Runoff, sediments
SWAT	Conceptual	Catchment/ basin	Continuous	High	Runoff, peak rate, erosion, sediment yield
AGWA	Conceptual/ physical	Catchment/ basin	Continuous	High	Runoff, peak rate, erosion, sediment yield
GUEST	Physical	Plot/field	Continuous	High	Runoff, sediment concentration
KINEROS2	Physical	Hillslope/ small catchment	Event	High	Runoff, peak rate, erosion, sediment
LISEM	Physical	Small catchment	Event	High	Runoff, sediment
EUROSEM	Physical	Small catchment	Event	High	Runoff, erosion, sediment
PERFECT	Physical	Plot/field	Continuous	High	Runoff, erosion
SEDNET	Conceptual/ empirical	Catchment/ basin	Annual/ Continuous	High	Suspended sediment, relative contribution from overland flow, gully and bank erosion processes
T0POG	Physical	Hillslope		High	Erosion hazard
USLE	Empirical	Hillslope	Annual	High	Erosion
RUSLE	Empirical	Hillslope	Annual	High	Erosion
RUSLE-3D	Empirical/ conceptual	Catchment	Annual	Moderate	Erosion
USPED	Empirical/ conceptual	Catchment	Event/ Annual	Moderate	Erosion/deposition
EROSION-3D	Physical	Catchment	Event	High	Runoff, erosion, sediment
MMMF	Empirical/ conceptual	Hillslope/ catchment	Annual	Moderate	Runoff, erosion
THORNES	Conceptual/ empirical	Hillslope/ catchment	Annual	Moderate	Runoff, erosion
EPIC	Physical	Hillslope/ catchment	Continuous	High	Erosion
WATEM	Conceptual	Catchment	Annual	Moderate	Erosion
WEPP	Physical	Hillslope/ catchment	Continuous	High	Runoff, sediment yield, soil loss
MIKE-11	Physical	Catchment	Continuous	High	Sediment yield, runoff
SHETRAN	Physical	Catchment	Event	High	Runoff, peak rate, sediment yield, sediment
SEAGIS	Empirical/ conceptual	Catchment	Annual	High	Erosion, sediment yield
PESERA	Physical	Hillslope/ regional	Continuous	High	Runoff, erosion, sediments
SPL	Empirical/ conceptual	Catchment/ river	Annual	Moderate	Fluvial erosion, river incision

They usually incorporate the underlying transfer mechanisms of sediment and runoff generation in their structure, representing flow paths in the catchment as a series of storages, each requiring some characterization of its dynamic behaviour (Viney and Sivapalan, 1999). Conceptual models tend to include a general description of catchment

21

processes, without including the specific details occurring in the complex process interactions. This allows these models to provide an indication of the qualitative and quantitative effects of land use changes, without requiring large amounts of spatially and temporally distributed input data. Traditionally, conceptual models lump representative processes over the scale at which outputs are simulated (Arnold, 1996).

Recently developed conceptual models have provided outputs in a spatially distributed manner. Alternatively, lumped conceptual models may be applied in a semi-distributed manner by disaggregating a catchment into linked subcatchments, to which the model is applied (Nearing et al., 1994; Arnold, 1996; Marker and Sidorchuk, 2003; Arnold and Fohrer, 2005). Parameter values for conceptual models are typically obtained through calibration against observed data, such as stream discharge and sediment concentration measurements (Doe et al., 1996; de Jong et al., 1999; Zhou and Liu, 2002).

Because parameter values are determined through calibration against observed data, conceptual models tend to suffer from problems associated with the identification of the parameter values; notwithstanding, conceptual models play an intermediate role between empirical and physically based models. Though they tend to be aggregated, they still reflect the hypothesis about the processes governing system behaviour. This is the main feature that distinguishes conceptual models from empirical models. Empirical models make no inferences as to the processes at work; instead they rely on observed or statistical relationships between the causal variables and model output.

2.3.3   Physically based models

These models are based on an understanding of the physics of the erosion and sediment transport processes and describe the sediment system using equations governing the transfer of mass, momentum and energy (Doe et al., 1999; Kandel et al., 2004). In principle, they can be applied outside the range of conditions used for calibration and, as their parameters have a physical meaning, they can be evaluated from direct measurements and without the need for long hydrometeorological records (Smith et al., 1995). They are limited only by the relevance of the physical laws on which they are based. Physically based technology computes erosion using a mathematical representation of fundamental hydrological and erosion processes. Fundamental erosion processes are detachment by raindrop impact, detachment of soil particles by overland flow, transport by raindrop impact, and transport and deposition by overland flow.

The physical models did not emerge until the 1970s, after mainframe computers became readily available. Examples of early physically based models are Aerial Non Point Source Watershed Environment Response Simulation (ANSWERS) (Beasley et al., 1989), Chemicals, Runoff and Erosion from Agricultural Management Systems (CREAMS) (Knisel, 1995), the Water Erosion Prediction Project (WEPP) (Nearing et al., 1989), and more recently the European Distributed Basin Flow and Transport Modelling System (SHETRAN) (Bathurst et al., 1995) and the Soil and Water Assessment Tool (SWAT) (Arnold and Fohrer, 2005). The equations are formulated for use with continuous spatial and temporal data, yet the data used in practice are often point source data to represent, for example, an entire unit area in the catchment. The viability of lumping up small-scale physics to the scale of the spatial grid used in many physically based models is questionable. Nearing et al. (1994) state that model

parameters derived in this manner represent nothing more than fitted coefficients distorted beyond any physical significance. The use of small-scale parameters in small-scale models may lose physical significance at larger scales. Specifically, there is a lack of theoretical justification for assuming that equations apply equally well at the grid scale at which they are representing the lumped aggregate of heterogeneous sub-grid processes.

Likewise, there is little information to show where many of the equations used in the models are valid beyond the small plot scale. In principle, these models are able to simulate the full erosion and sediment yield regime, providing multiple outputs on a spatially distributed basis (Pullar and Springer, 2000). They also have heavy computing requirements and require the evaluation of a large number of parameters on a spatially distributed basis (Perrin et al., 2001; Santos et al., 2003). The advantage of physical models is more their relative transferability, which favours predicting soil erosion and sediment yield under different climate and physiographic land use scenarios and their ability to consider environmental issues such as climate change (Banis et al., 2004).

2.3.4 Current erosion models

As mentioned in the previous section, soil erosion models use mathematical expressions to represent the relationships between various factors and processes occurring in the landscape. These factors generally include topography, meteorological variables, soil properties, and land use and land cover features. A large number of erosion models are based on the famous Universal Soil Loss Equation (USLE) (Wischmeier and Smith, 1978) (*e.g.,* Agricultural Non Point Source Pollution (AGNPS) (Young et al., 1989), ANSWERS (Beasley et al., 1989; Dabral and Cohen, 2001), the Erosion Productivity Impact Calculator (EPIC) (Sharpley and Williams, 1990) and SWAT (Arnold, 1996)). Other models aim at a representation of the catchment in a cascade of planes and channel elements (*e.g.,* the Kinematic and Runoff Erosion model (KINEROS2) (Smith et al., 1995) and the European Soil Erosion Model (EUROSEM) (Morgan et al., 1998)) or they are not intended for use at catchment scale (*e.g.,* CREAMS (Knisel, 1995)). An extensive description and discussion of these models can be found in Merrit et al. (2003).

The USLE (Wischmeier and Smith, 1978) has been the most widely used empirical erosion model. It was developed for sheet and rill erosion based on a large set (*i.e.,* 10,000 plots) of experimental data from agricultural plots and is only valid when applied to a field area up to approximately 1 ha. Although the USLE was developed in the USA, it has been used throughout the world (Pilesjo, 1992; Mellerowicz et al., 1994; Kinnell and Risse, 1998; Bartsch et al., 2002) because it seemed to meet the needs of researchers better than any other available tool (Summer et al., 1998). The mean annual erosion rate is expressed as a function of six erosion factors:

$$A = R \times K \times L \times S \times C \times P \qquad \qquad (Eq\ 2.2)$$

where A [ton ha^{-1} yr^{-1}] is the computed spatial averaged soil loss and temporal average soil loss per unit of area, and R [MJ mm ha^{-1} hr^{-1}] is the rainfall-runoff or erosivity factor. K [(ton ha^{-1})(MJ mm ha^{-1} hr^{-1})$^{-1}$] is the soil erodibility factor representing the soil loss per erosion index unit for a specified soil as measured on a standard plot, which is defined as a length of 22.1 m of a uniform slope of 9% in a continuous clean tilled

fallow. The slope length factor ($L \times S$) represents the ratio of soil loss from the field slope length gradient to the soil loss from a 9% slope under otherwise identical conditions.

C is the vegetation cover and crop management factor or the ratio of soil loss from an area with specified cover and management to soil loss from an identical area under continuous tilled fallow. P is the erosion control practice or support practice factor. It represents the ratio of soil loss with a support practice such as contouring, strip cropping or terracing to soil loss with straight row farming up and down the slope. The USLE concept has been modified and adapted during the past 35 years by a large number of researchers. The Modified Universal Soil Loss Equation (MUSLE) (Williams, 1975), the Revised Universal Soil Loss Equation (RUSLE) (Renard et al., 1997), ANSWERS (Beasley et al., 1989) and the RUSLE-3D (Mitasova et al., 1996; Mitas and Mitasova, 1998; Mitasova, 2000) are all based on the USLE and represent modifications or improvement of the former.

Use of the USLE and its derivatives is limited to estimating gross erosion, and the model lacks the capability to compute deposition along hillslopes, depressions, valleys or in channels. Moreover, the fact that erosion can occur only along a flow line without the influence of the water flow itself restricts the direct application of the USLE to complex terrain. A history of the development of the USLE and its modifications can be found in Lane et al. (1995) and Renard et al. (1997).

CREAMS is a field-scale (less than 5 ha in size) model that predicts runoff, erosion and chemical transport from agricultural areas. The model was developed as a tool to evaluate the effects of various agricultural practices on pollutants in surface runoff and in soil water below the root zone, in response to off-site water quality concerns. It operates in both single storm events or in a long-term average (continuous) mode. The continuous mode is the intended mode of operation and it can predict long-term averages from two to 50 years. Although the CREAMS model uses various aspects of the USLE equation, such as inter-rill erosion by raindrop impact, it differs radically from the USLE empirical formulation in that it uses a physically based approach to calculate the various components of erosion and sediment routing across a field. The model, unlike the USLE, accounts for gully erosion and deposition across the channel and landscape profiles. In this regard, CREAMS represented (Knisel, 1995) a first major technological advance in expressing soil loss as a process-based phenomenon including erosion, transport and deposition (Schmidt, 2000).

The WEPP model (Nearing et al., 1989) was intended to replace the USLE family models and expand the capabilities for erosion prediction in a variety of landscapes and settings. It is a physically based model with distributed parameters that can be used in either a single event or continuous time scale and calculates erosion from rills and inter-rills, assuming that detachment and deposition rates in rills are a function of the transport capacity.

The ANSWERS model developed by Beasley et al. (1989) presented one of the first operational, fully spatially distributed, catchment erosion and sediment yield models. It consists of a water erosion and sediment transport model. The main component of the

erosion/transport model is the sediment continuity equation of Foster and Meyer (1977), and the conceptual basis for the water routing model was taken from Nearing et al. (1994). The ANSWERS project sought to assess the effects of land use, management schemes and agricultural practices using hydrological processes.

The KINEROS2 model is a dynamic semi-distributed physical model (Smith et al., 1995), which treats a catchment as an ensemble of rectilinear surfaces and channels. It is a single-event-based model that uses the Smith/Parlange infiltration model and the kinematic wave approximation to route overland flow and sediments (Julien and Saghafian, 1995).

The EUROSEM model (Morgan et al., 1998) is a physically single-event based model for predicting soil erosion by water from fields and small catchments. It first simulates erosion on a single slope plane or segment. Subsequently, the segments are linked to simulate processes on an entire hillslope. Soil loss is computed as sediment discharges that are defined by the product of the runoff rate and sediment concentration in the flow (de Roo et al., 1996). Detachability by raindrop impact represents the soil erodibility and is derived from measuring the soil cohesion. Overland flow and sediments are routed from inter-rill to rill areas according to the slope. The representation of a catchment by a cascade of plane and channel elements in the WEPP, KINEROS2 and EUROSEM models needs lumping of some parameters for small areas, which represents a drawback when representing large catchments.

SHETRAN (Bathurst et al., 1995; Wicks and Bathurst, 1996) is a physically based, spatially distributed, erosion and sediment yield component of the existing European distributed hydrological modelling system SHE and is for use at catchment scale. For hillslopes (represented spatially by the SHE grid square network), SHETRAN simulates soil erosion by raindrop impact, leaf drip and sheet overland flow (without rilling), and the transport of eroded material by overland flow. For channels, the component simulates the erosion of the bed material and the downstream transport of this material, together with that supplied by overland flow. In the channel sediment routing procedure, it is assumed that the flow can carry any available load of fine sediments (less than 0.062 mm in diameter), but for coarser sediments the load is limited by the calculated transport capacity of the flow (Banis et al., 2004).

CASC2D-SED, developed at the Colorado State University (CSU), is a distributed physically based, hydrological and soil erosion model that simulates the hydrological response of a catchment subject to a given storm event (Julien and Saghafian, 1991; Julien and Saghafian, 1995; Johnson et al., 2000). Rainfall is allowed to vary in space and time. CASC2D-SED can simulate the uphill sediment production and deposition by size fraction at any point in the catchment. The sediment is transported from one cell to the next using the 2D-diffusive wave overland flow routing scheme. A full description of the CASC2D-SED model can be found in Rojas (2002).

Viney and Sivapalan (1999) incorporated a conceptualization of the USLE to predict sediment generation in the Large Scale Catchment Model (LASCAM). Sediment transport involves the processes of channel deposition, re-entrainment and bed degradation, which are assumed to be governed by the sediment transport capacity in

the stream. The sediment transport model conceptualizes processes of existing physically based sediment models, making process description as simple as possible while retaining the capacity to model the effects of land use and climate change (Viney and Sivapalan, 2001). The sediment model includes six global parameters that require calibration against observed sediment load records at one or more locations in the catchment.

EROSION-3D (von Werner, 2000) is a physically storm-event based model for small catchment areas. The physical approach of the erosion model is based on calculating the detachment of soil particles from the soil surface dependent on the momentum fluxes exerted by overland flow or falling raindrops. They are compared with a "critical" momentum flux (Schmidt and von Werner, 2000) that characterizes the specific erosional process of the soil in question. The detachment of solid matter can be computed with the resulting dimensionless coefficient, which is entered into an empirical equation. On the basis of individual rainfall events, the model computes detachment, deposition and net erosion for each grid cell of a catchment area. Additionally, the amount of runoff, sediment concentration, and the grain size distribution (percentage of clay and silt) are calculated.

The Limburg Soil Erosion Model (LISEM) (de Roo et al., 1996; de Roo and Jetten, 1999) is a distributed physically based hydrological and soil erosion model developed for planning and conservation purposes. LISEM incorporates a number of different processes, including rainfall interception, surface storage in micro-depression, infiltration, vertical water movement through the soil, overland flow, channel flow, detachment by overland flow and transport capacity of flow (van der Perk and Slávik, 2003). LISEM does not simulate concentrated erosion in rills and gullies; rather it simulates flow detachment only in the ponded area. This can be seen as intermediate between sheet and rill erosion. Processes describing sediment detachment by rainfall, throughfall and overland flow are included, in addition to the transport capacity of the flow.

SEDNET (Wilkinson et al., 2004) is a spatially distributed sediment budgeting model. It is a steady-state model that was developed for estimating sediment generation and deposition from hillslopes, gullies and riverbanks in a river network. Each river link is connected to an internal catchment that contributes sediment generated from hillslopes or gullies to the link. Models of streambank erosion, flood deposition and sediment transport capacity are used to simulate sediment transport through the river network (Prosser and Rustomji, 2000). Unlike bedload sediment, suspended sediment is an input for all the three aforementioned models. It is assumed that the hillslope erosion does not contribute to the bedload. The mean annual gully-derived sediment that is delivered to a river link from a linked internal catchment is related to the upstream area, the mean cross sectional area of gullies, the gully density, the bulk density of the eroded sediment, and the age of the gullies. Hillslope erosion is estimated using the USLE model.

A hillslope sediment delivery ratio (HSDR) concept is applied to obtain the contribution of suspended sediment from a catchment of a river link from hillslope sources (Prosser et al., 2001). For each link, the rate of lateral erosion from the stream bank and the

characteristics of the river link are used to estimate streambank erosion. Each river link is described by the bank height, lateral migration constants, the *in situ* sediment bulk density, the estimated 1.58 years recurrence interval flow, and the proportion of intact riparian vegetation ordering the link. The transport and deposition of the suspended and bedload sediment fractions are modelled separately in the river network. Bedload is routed by a sediment transport capacity submodel. The capacity of the channel to transport bedload sediment is related to the energy gradient, the sediment transport capacity, the mean channel width, and the settling velocity of bedload particles.

Deposition of suspended sediment in the river network is modelled using floodplain and reservoir deposition submodels. The sediment remaining in suspension is routed through the next river link. A reservoir/lake trap efficiency submodel, based on the work of Brune (1953), is used to estimate sediment deposition in reservoirs. All of the transported bedload is deposited in a reservoir, although a proportion of the suspended loads can pass through the reservoir outlet. The percentage of suspended load trapped by the reservoirs depends on the volume of the reservoir and the mean annual input to the reservoir (deRose et al., 2003).

Only a limited number of erosion and sediment prediction models that are presented in the current literature have been described in this section. It is evident that the selection of an appropriate model involves a number of trade-offs. From the previous description, two extreme model types can be identified: complex conceptual and physically based models with highly detailed representations of the processes being modelled, and models that considerably simplify the process representation. The latter group often exhibit a degree of empiricism and tend to operate on a spatially lumped and/or temporally coarse resolution. The complex models are generally capable of operating either on a continuous basis or in an event-based mode. As yet, there are few examples of models that are capable of simulating on an event basis yet minimize the process representation to only those key processes that control catchment response (Foster, 1996). For land and water management agencies in developing countries, the more complex models are prohibitive in terms of both the time required to develop (*e.g.,* the supporting database) and implement them and the economic resources required for their establishment in areas currently facing alarming land degradation.

2.4   Scale and scaling issues in erosion modelling

Scaling is not exactly the same as scale. Scale refers to a characteristic length or time and can be used either as a qualitative term (*e.g.,* a small-scale process) or as a quantitative measure in space or time dimensions. The spatial dimension represented as coordinates in (*x, y, z*) directions varies temporally along a time domain *t*. There are five accepted meanings of scale used in environmental analysis, namely the cartographic, geographical, process, measurement and modelling scales (Beven, 1995).

Models operate at certain scales, but not necessarily those matching the process or observation scales. Scaling is a change in either spatial or temporal scale and has a certain direction and magnitude (Bogena and Diekkrüger, 2002). It focuses on what happens to the characteristics of an object or process when its scale is changed proportionally. Hydrological and erosional processes (including spatial variability and

relevant physical, chemical and biological phenomena) occur on a wide range of temporal and spatial scales, as indicated in Figures 2.6 and 2.7.
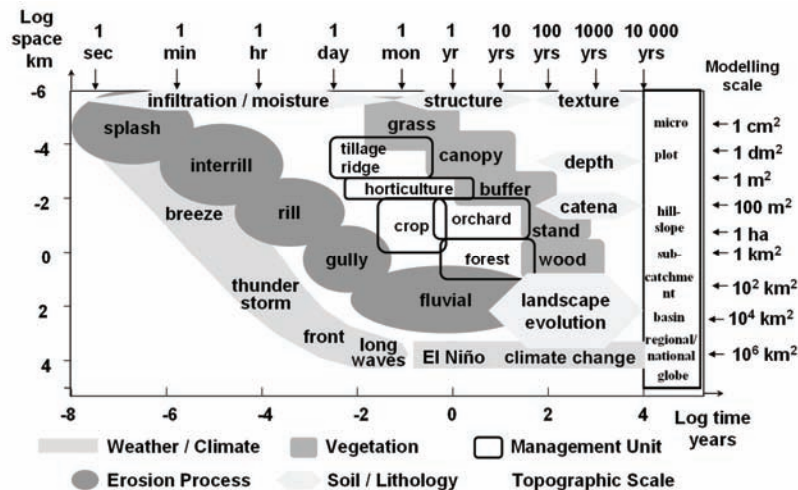
Figure 2.6 Dominant erosion processes at different spatial and temporal scales (source: (Renschler and Harbor, 2002)

Figure 2.7 Scales of interest, spatial and temporal variable properties important for the dominant process at the indicated scale (source: (Renschler, 2003)

To apply the concept of scaling to the erosion process, it should be analysed how topographical attributes change if the spatial resolution of a digital elevation model (DEM) is doubled or how the drainage area changes if the length of a stream doubles (Zhang et al., 2002). One of the major challenges in soil erosion modelling, which has become even more important with the increasing use of models linked to GIS, is the mismatch between the small spatial and temporal scales of data collection and model

conceptualization, and the large spatial and temporal scales of most intended model applications (Renschler and Flanagan, 2003).

Mannaerts (1993), Kirkby et al. (1998) and Zhang et al. (2004b) report that soil erosion model predictions are very sensitive to changes at both the spatial and temporal scales. The major errors in erosion modelling come from incompatibilities between model scale, scale of input parameter data, and the intended scale of the model outputs.

A common issue is that the parameters measured at one scale or several different scales are input into a model built at another scale (Xia and Clarke, 1997; Vigiak et al., 2005). Even if a model operates linearly across the range of model input values, the aggregation of the model parameter values with increasing scale still has bias on the model prediction because of their heterogeneity. Although it is very hard to scale a complex ensemble of parameters and modes to corresponding process scales, it is feasible to identify a few scalable parameters within the complex erosion processes to reduce the scale uncertainty of modelling (Pecknold et al., 1997).

Upscaling and downscaling describe the direction of scale change and require methods such as interpolation and extrapolation or aggregation and disaggregation. The observed data that represent a true pattern of a natural property or process are transformed through a sequence of necessary changes in scales inherent in the data pre- and post-processing in order to apply a spatial erosion model assessment. Any method diminishing the scaling effects could mean a great improvement in modelling results since it seems impossible to completely eliminate the impact of scale on erosion modelling. There are several methods available for translating erosion models across spatial scales. The relevant methods are briefly described below.

2.4.1 Model calibration

The calibration approach is used to adapt a model that is applicable at small scales for application at larger scales, using "calibration" values. This calibration technique consists in setting up an empirically calibrated relationship between fine- and coarse-scale data and requires that both fine- and coarse-scale data are available to perform the calibration (Zobeck et al., 2003). The calibrated model may be treated as valid only within the ranges of input and output data used for the calibration and, moreover, the incorporation of new model variables requires recalibration of the relationship (Xiong and O'Connor, 2000). In practice, it is difficult to carry out measurements for calibration at various scales, especially at very large scales. However, because of the nonlinear processes involved, together with the heterogeneity of the natural system, there is no reason to suppose that the use of calibration values should describe the real processes exactly; however, it does provide a representation rather close to reality (Cabelguenne et al., 1990).

2.4.2 Multiscale models

Since erosion processes change with scales, a set of different models and data is required for various particular scales, such as specifically used at field plot, catchment, regional and/or global scales (Brazier et al., 2001; Veldkamp et al., 2001). Separate scaling methods could be developed for each individual process, and the rules for transition among these could be used to synthesize these separate scaling methods into

an aggregate scaling method that incorporates the behaviour of the ensemble of scales. The plot-scale erosion models may represent physical processes in detail, while a large-scale model can provide a lumped value such as potential cumulative soil erosion at catchment, regional or global scale (Wickenkamp et al., 2000). In doing so, the scale effects are included in each individual model and the erosion process could be accurately simulated. According to Brown and Schneider (1999), the multiscale approach to scaling model application involves efforts to base analyses at larger scales (basin, regional, or global) on cross validation with medium- or fine-scale simulations (reservoir/lake, field, hillslope or catchment). Model parameters obtained from the very detailed data available allow the use of single physically based models across a range of scales.

2.4.3 Lumped models

Classically, erosion models were calibrated and validated for point measurements but did not account for spatial and time variability. Lumped models integrate the increased heterogeneity that accompanies the change in model extent by aggregating across the heterogeneity of the environmental parameters (Picouet et al., 2001). They attempt to incorporate some of the modellers' understanding of the physical processes but do not attempt to represent the physical structure of the catchment area. Therefore predicted variables tend to be spatially averaged (*i.e.*, the average soil loss over the whole catchment). To address this need in upscaling study, the most common way to treat a lumped system is to spatially average the related properties and calculate the mean values for the modelling parameters (Amore et al., 2004). This is based on an assumption that a model is linear in its structure, and no attempt is made to describe the spatial heterogeneity. Alternatively, a more effective way of processing a lumped model is to choose aggregated representative parameters accounting for the heterogeneity. A notable example is using self-similar fractals such as topographical properties for hydrological models in order to represent parameters across scales (Pecknold et al., 1997; Zhang et al., 1999b), since one single set of model arguments across the whole area is applied to perform the model, while the spatial distribution of model results is not taken into account.

2.4.4 Routing models

The model structure remains the same across scales, while the variables (*i.e.*, the fluxes) for the modelled areas are spatially and temporally inferred. Such interaction always occurs in erosional processes, where the model output at a large scale is far from the simple sum of each grid (de Roo, 1998; López and Soto, 2004). When water moves from the top to the bottom of a catchment, and from a small catchment to a large catchment, the values of related hydrological variables in a grid are affected not only by the environmental characteristics within this grid but also by the properties in the surrounding cells (Fan et al., 2004). The runoff in a pixel is determined by the precipitation and infiltration within the grid and water carrying from and discharging to neighbouring grids. The amount of sediment deposited or detached in a grid strongly depends on the movement of both water and sediment in adjacent neighbouring cells (Huang et al., 1999). Hence, the routing approach is usually employed after calculating the drainage direction on the basis of the steepest descent of topography. This technique has been effectively employed in sediment transport models at catchment as well as basin scales (Jain and Kothyari, 2000; Lin et al., 2002; Paringit and Nadaoka, 2003).

2.4.5 Fractal method

Zhang et al. (2002) directly linked the scaling of slope gradient with the fractal dimension of topography. When focusing on the difference in elevation between two points and the distance between them, the variogram equation used to calculate the fractal dimension of topography can be converted to the following equation:

$$\left[\frac{Z_p - Z_q}{d}\right] = \kappa \times d^{1-D} \qquad \qquad \textit{(Eq 2.3)}$$

where Z_p and Z_q are the elevations at points p and q, d is the distance between p and q, κ is a coefficient and D is the fractal dimension. Because the equation $\left[\dfrac{Z_p - Z_q}{d}\right]$

represents the surface slope, it can be assumed that the slope S is associated with its corresponding scale d (cell size) by the equation:

$$S = \kappa \times (d)^{1-D} \qquad \qquad \textit{(Eq 2.4)}$$

This implies that if topography is uni-fractal in a specified range of measurement scale, slope will then be a function of the measurement scale. If a research area is taken as a whole to determine the parameters κ and D, there would be only one value of scaled slope. It is necessary to keep the spatial heterogeneity of slope values.

Analysing the spatial variation of κ and D in different sub-areas, it has been discovered that both κ and D are mainly controlled by the standard deviation of the elevations. Hence, correlation functions are established between κ and D and local standard deviation. When the standard deviation in each pixel is determined by moving a 3×3 pixel window, the spatial distribution of both κ and D is then calculated. Therefore, the slope values for each pixel with finer measurement scales can be successfully estimated on the basis of a coarser-resolution DEM.

2.5 Temporal scale in erosion modelling

From the discussion above, it is clear that the variability, nonlinearity and the interacting nature of erosion and deposition processes over various scales significantly influence the mechanics of surface runoff generation and soil erosion. In particular, the important temporal dynamics of precipitation and surface characteristics (*i.e.,* vegetation cover), which also vary spatially, have strong controls on surface runoff generation and the resulting soil erosion, owing in particular to the nonlinear nature of infiltration, soil detachment and transport processes. These controls are instantaneous phenomena and modelling them ideally requires fine time resolution data, but because data availability is often limited to annual time steps it is often done at annual, and only rarely at daily, time steps.

Therefore, a key consideration in choosing an appropriate erosion deposition model is the time scale at which the erosion processes will be predicted (Veldkamp et al., 2001). Soil erosion by overland flow leads to specific forms of landform development over both short and long time scales (Kandel et al., 2004). In some cases, the landscape can be dramatically modified in a matter of hours as a result of an extreme storm event (Renschler et al., 1999). Thus, rates of soil erosion typically show major variability both within events and between them. This variability is not only a reflection of spatial and temporal variability in the factors that control erosion, such as rainfall intensity and

infiltration, but both the process and stochastic elements of the erosion also vary. The temporal variability of weather, especially rainfall, is extremely important in soil erosion assessment (Kinnell, 2003). Soil erosion totals can be dominated by a few extreme events, thus monitoring as well as simulation studies need to be long enough to capture these erosive events. However, low-magnitude, high-frequency events can also be significant for long-term erosion rates.

The time resolution of a model is commonly known as the "time-step". Typical modelling scales (extents) are plot/local (1 m^2), hillslope (100 m^2), catchment (100 km^2) and regional (>10000 km^2) in space; and event (~1 day), seasonal (~1 year) and long-term (~100 years) in time. Erosion and sediment transport models tend to have been developed from two opposite points of view. Event-based models were developed to look at the response of the modelled area to single storm events. For each event, the model time step is in the order of minutes to hours. The model algorithms were often developed for application to small plots or grid cells in a catchment.

Alternatively, a larger temporal resolution is used in models that explore general trends over time with respect to changes in rainfall, vegetation or land management (Renschler and Flanagan, 2003). The variation in the contributions of eroded sediment within storm events is not considered. A third approach is to use a continuous time step, usually daily, that is responsive to, for example, the development and recession of saturated zones or other processes that can be captured at this time step, yet does not capture land surface response to high-intensity and short-duration events (Wainwright et al., 2003). As computing power has increased, many of the models originally developed to be applied to a single event (*e.g.,* AGNPS, ANSWERS) have undergone modifications and can now be applied as continuous simulations. Those models that have moved from an event-based to a continuous simulation mode often retain the ability to shift between, for example, a daily model time step to finer temporal resolutions during events.

2.6   Remote sensing and GIS in erosion modelling

Soil erosion is influenced by the spatial heterogeneity in topography, vegetation, soil properties and land use, among other factors. All too often, however, predictive soil erosion models do not examine the problem in a spatial context. Soil erosion prediction is relevant at a wide range of spatial scales, from the plot scale to the catchment scale, from the regional scale up to the continental and global scales. At different scales, different processes tend to become dominant, so that the effective focus of the models also changes. At scales from the single erosion plot to the hillslope catena, for example, the timing and volume of overland flow hydrographs are essential, along with their distribution across rill and inter-rill areas. At the larger scales, topography, soil and vegetation patterns become more important. This is where remote sensing and GIS become valuable tools. Remotely sensed imagery and GIS have a long history in erosion modelling.

Numerous studies have shown the potential of remote sensing in soil erosion mapping (Pilesjo, 1992; Metternicht and Fermont, 1998; Reusing et al., 2000; Haboudane et al., 2002; Metternicht and Gonzalez, 2005). At the most basic level, estimates of erosion risk can be derived by classifying pixels according to the percentage of bare soil (see de Jong (1994), Paringit and Nadaoka (2003)). Mathieu et al. (1997), Haboudane et al.

(2002) and Singh et al. (2004) improved this scheme by estimating vegetation parameters from Medium Resolution Imaging Spectrometer (MERIS), Landsat-TM and SPOT-4 imagery and combining them with slopes generated from a DEM to produce an erosion rate map. On the other hand, empirical soil erosion models in combination with soil, climate, vegetation and topography information have been implemented using remote sensing (Dwivedi et al., 1997; Hill and Schütt, 2000; Baban and Yusuf, 2001; Fu et al., 2005). Classification of Landsat-TM imagery has been used to estimate the crop management factor of the USLE (Millward and Mersey, 1999; Zhang, 1999). Methods using satellite imagery to produce maps of vegetation-related variables for soil erosion studies have been compared by de Jong (1994), Leprieur et al. (2000), Symeonakis and Drake (2004), and Tateishi et al. (2004), who found that the normalized difference vegetation index (NDVI) was the most useful.

Since Pilesjo (1992) and Bocco and Valenzuela (1993), researchers involved in these fields have routinely used aerial images. However, changing technologies have created an amazing number of choices, such as hyperspectral and high-resolution imagery (Amarsaikhan and Douglas, 2004), terrain correction (Bishopa et al., 2003), GIS integration (Flugel et al., 2003), and decision support systems (De la Rosa et al., 2004).

Moreover, Wilson and Gallant (2000) argue that the ability to represent elevation in terms of topographical surfaces is central to geomorphological analyses and erosion studies, thus demonstrating the importance of representing topography using an accurate DEM. It is through the distribution of soil that the land surface changes over the long term, so the ability to link sediment transfer with DEM changes (Harmon and Doe, 2001; Peters et al., 2003). The redistribution of sediment will drive the long-term landscape change, which in turn will affect the hydrological processes acting within and over individual hillslopes (van Oost et al., 2000).

Up to this point, it has been demonstrated that erosion assessment and prediction is one of the more widely known GIS applications. Several examples of the integration of GIS and remote sensing can be found in the literature (Dwivedi et al., 1997; Hill and Schütt, 2000; Martínez-Casasnovas et al., 2002; Vaidyanathan et al., 2002; Vrieling et al., 2002). De Roo et al. (1989) combined ANSWERS with GIS technology. De Roo (1998) integrated LISEM and LISFLOOD with a GIS. Grunwald and Norton (1999), Bhuyan et al. (2001) and Paringit and Nadaoka (2003) linked AGNPS with GIS. Other GIS and remote sensing applications are described by Reusing et al., (2000), Leon et al. (2001), Fistikoglu and Harmancioglu (2002), Bartsch et al. (2002), He (2003) and King et al. (2005), among many others.

GIS is thus an important tool for coping with the vast number of spatial data and the relation between data from various sources in the erosion modelling process. The advantages of linking soil erosion models with a GIS include the following:
- The possibility of rapidly processing input data to simulate different scenarios. A GIS provides an important spatial and analytical function, performing the time-consuming georeferencing and spatial overlays to develop the model input data at various spatial scales (Schoorl, 2002; Zhang et al., 2002; Shi et al., 2004).

- The ability to look at spatial variation; thus areas can be simulated at a user-defined resolution (Xia and Clarke, 1997; Qinke et al., 2002; Renschler and Flanagan, 2003).
- The facility of displaying the model outputs (*i.e.*, visualization). Visualization can be used to display and animate a sequence of model output across time and space. Therefore, visualization enables objects to be viewed from all external perspectives, and evokes insight into the data (Mitasova, 1996; Rojas, 2002).

There are different strategies for linking erosion models with GIS, ranging from loosely coupled to tightly coupled arrangements. Pullar and Springer (2000) categorize three levels of integration:

- Loose coupling: the GIS system and the erosion model are separated, and the files must be transferred back and forth externally between GIS and the model.
- Tight coupling: the GIS (typically) provide the shared interface to move the spatial data between the GIS and the separated modelling program.
- Embedded: the model is fully integrated as a component in the host GIS application.

Most of the current integrations of soil erosion models with GIS are examples of the first two approaches. In the third approach, the linkages are problematic owing to the lack of a temporal dimension in most GIS systems. Nonetheless, the PCRaster Environmental Modelling Language and the Geographic Resource Analysis Support System (GRASS) programs with embedded modelling language do build dynamic models, and thus the dimensions of time and space can both be included (Mitasova, 2000; Karssenberg, 2002; Pfeffer, 2003).

2.7   Model selection

In broad terms, it might be said that models are acceptable if they meet their objectives or design requirements. Simply speaking, the reasonableness of the model and the availability of data are the main guiding principles when selecting a model. Physically based models are more appropriate at the small catchment scale; however, they are difficult to use regionally as they are usually high data demanding. The range of complexity between the three types of model (*e.g.,* empirical, conceptual and physically based) is similar with respect to the resource base needed to support model development, calibration, validation and operation. Far more limiting constraints face the modeller, regardless of location, in terms of the presence or absence of available data. The availability of data determines ultimately which type of model can be selected.

Because the aim of this research is to estimate erosion rates by using low data demanding models at catchment and regional scales and with a seasonal time step, the selected model should fit such temporal and spatial scales. However, as described in the preceding sections, most applicable models are derived from field plot or hillslope measurement for rainfall events. If a purely empirical model were selected, the model might need to be calibrated in various environments based on field measurement; hence it is not applicable to all conditions of the research area currently being analysed. If a complex, physically based model is run with too few data and a large part of the area is

simulated with data "assumed" to be constant over a certain part of the area, results are unreliable.

Beven (1995), Brazier et al. (2001) and van Rompaey et al. (2003b) argue that the simpler and less data-intensive conceptual models may be able to perform equally well in terms of overall catchment response, with much less time and effort required to apply them compared with detailed distributed process-based models. Thus, in order to scale a model and its parameters to fit the required scale, conceptually based models are the best choice. A set of 13 criteria were used to evaluate the available erosion models.

Table 2.2 Main characteristics of the selected models

Model	RUSLE-3D	USPED	THORNES	MMMF	SPL
Temporal scale	- Event - Annual	- Event - Annual	- Event - Decadal - Monthly - Annual	- Annual	- Annual
Climatic data requirements	- R-factor - Event EI_{30} - Pluviograph	- R-factor - Event EI_{30} - Pluviograph	- Daily rainfall amounts - Storm duration - Peak intensity - Time to peak	- Rainfall amount - Storm duration - Peak intensity - Time to peak	- Annual rainfall amount
Hydrological data requirements	- Rainfall - Upslope contributing area	- Runoff amount - Peak flow	- Runoff amount - Peak runoff rate	- Hydraulic conductivity - Runoff amount - DEM	- Runoff amount
Runoff generation	-	- Upslope contributing area	- Exponential runoff rate	- Exponential runoff rate	- Upslope contributing area
Main drivers for soil erosion	- Rainfall erosivity - Slope	- Unit stream power	- Flow detachment and transport - Slope	- Rainfall detachment - Transport by runoff - Slope	- Stream power
Size distribution	- Single class	- Single class	- Single class	- Single class	- Single class
Catchment representation	- Raster based	- Raster based	- Raster based	- Raster based	- Raster based

Five of the criteria (class, applications, known limitations, assumptions, agency support/point of contact) were descriptive, and eight (data requirements, model results, cost/complexity, hardware requirements, GIS integration, commercial off-the-shelf integration, graphical interface and ease of use) were evaluative in nature. Five erosion models, namely the RUSLE-3D (Mitas and Mitasova, 1998), the USPED (Mitasova, 2000), the Thornes (Thornes, 1990), the Stream Power Law (Stock and Montgomery, 1999; Barnes and Pelletier, 2001) and the Modified Morgan, Morgan and Finney (Morgan et al., 1984; de Jong et al., 1999; Morgan, 2001) models satisfied these requirements since they permit a combination of soil erosion factors, have a clear definition of physical meaning, are easily parameterizable, can be easily operated and have been previously tested under varied conditions (Table 2.2). The scaling framework presented in Figure 2.8 provides a foundation for addressing scaling issues in the design and use of erosion models for practical decision making. Moreover, because erosion assessment requires careful consideration of all the steps in integration data, modelling, and decision making, each scale in the scaling sequence (Figure 2.9) must be assessed in terms of how data are being transformed. The five models, including their governing equations, are reviewed in the following sections.

PROCESS SCALE	TRUE PROCESS SCALE AND VARIANCE
⬇ Basic scaling ⬇	⬇ Measuring ⬇
MEASUREMENT SCALE	Observation unit (measurement device)
⬇ 1ST Scaling ⬇	⬇ PRE-PROCESSING ⬇
DATABASE SCALE	Common database unit (data availability)
⬇ 2ND Scaling ⬇	⬇ DISCRETIZATION ⬇
MODELLING SCALE	Model unit (model requirements)
⬇ 3RD Scaling ⬇	⬇ MODELLING ⬇
PREDICTION SCALE	Model unit (model design)
⬇ 4TH Scaling ⬇	⬇ POST-PROCESSING ⬇
ASSESSMENT SCALE	Scale of interest (user requirements)
⬇ 5TH Scaling ⬇	⬇ EVALUATION ⬇
MEASUREMENT SCALE	Observation unit (measurement device)
⬆ Basic scaling ⬆	⬆ Measuring ⬆
PROCESS SCALE	TRUE PROCESS SCALE AND VARIANCE

Figure 2.8 Scaling theory for the implementation of an erosion assessment tool (source: (Renschler, 2003)
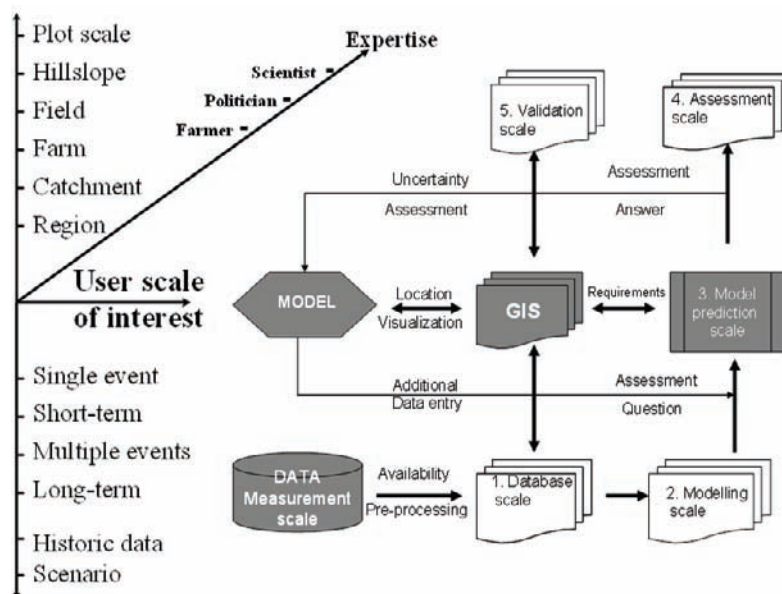
Figure 2.9 Structure of the proposed spatially distributed erosion assessment (source: (Renschler, 2003)

2.7.1   RUSLE-3D

In 1985, the U.S. Department of Agriculture (USDA) decided to revise the USLE in order to improve its performance. As a result, a new equation, the Revised Universal Soil Loss Equation (RUSLE), was developed (Renard et al., 1997). Although this model

still has the basic structure of the USLE in Eq. 2.2, the algorithms for calculating the individual factors have changed significantly.

The RUSLE equation reads:
$$E_{(r)} = R \times K \times LS_{(r)} \times C \times P \qquad (Eq\ 2.5)$$
where $E(r)$ [ton ha^{-1}] is the annual average soil loss, R [MJ mm ha^{-1}hr^{-1}] is the rainfall intensity factor, K [ton ha^{-1} per unit R] is the soil erodibility factor, $LS_{(r)}$ [dimensionless] is the topographical (length-slope) factor, C [dimensionless] is the land cover factor, and P [dimensionless] is the soil conservation or prevention practices factor. The R factor is the sum of the erosion index values for all rainstorms in one year. In an N year period, the R factor is calculated as follows:

$$R = \frac{\sum_{i=1}^{j}(EI_{30})_i}{N} \qquad (Eq\ 2.6)$$

where (EI_{30}) is the erosion index EI_{30} [MJ mm ha^{-1}hr^{-1}] for storm i, and j is the number of storms in the N year period. E [MJ ha^{-1} mm^{-1}] is the total storm kinetic energy and I_{30} [mm hr^{-1}] is the maximum 30 minutes rainfall intensity. A direct computation of the rainfall erosivity factor, R requires continuous rainfall intensity data at a time interval equal to or less than 30 minutes (Yu et al., 2000a). However, long-term data for rainfall amounts and intensities are almost unavailable in the current research area. Renard and Freimund (1994) evaluated erosivity at 155 locations within the continental United States, and developed statistical relationships between the R factor and both total annual precipitation at the location and a modified Fournier coefficient, F (Fournier, 1960), calculated from monthly rainfall amounts as:

$$F = \frac{\sum_{i=1}^{12} P_i^2}{P_a} \qquad (Eq\ 2.7)$$

where P_i [mm] is the average monthly precipitation and P_a [mm] is the average annual precipitation. Derived relationships between the R factor and F developed by Renard and Freimund (1994) were:
$$R = 0.07397 \times F^{1.847} \qquad [r^2 = 0.81] \qquad (Eq\ 2.8)$$
$$R = 95.77 - 6.081F + 0.477 \times F^2 \qquad [r^2 = 0.75] \qquad (Eq\ 2.9)$$

Renard and Freimund (1994) recommended using Eq. 2.8 when F was <55 mm and Eq. 2.9 when F was >55 mm.

The soil erodibility factor K is a quantitative value which is experimentally determined taking into consideration the soil texture, soil structure, the organic matter content and the permeability (Wischmeier et al., 1971).

Determination of the soil erodibility involved assigning values that correspond to the soil types contained within the research area (Torri et al., 1997; Zhang et al., 2004a). Extensive databases of soil samples are in most cases not available at regional scale; however, the information required for the determination of the K factor can be obtained from the soil taxonomy map. At the catchment scale, composite maps identifying soil mapping units derived from a soil reconnaissance survey can be used for the

determination of K values. For each of the soil textural classes, the mean percentage of silt, clay and sand can be derived from the texture triangle, and these values can be used to calculate the geometric mean particle diameter D_g [mm] (Shirazi and Boersma, 1984):

$$D_g = \exp\left[\sum_i 0.01 \times f_i \times \ln(m_i)\right]$$ (*Eq 2.10*)

where f_i [%] is the particle size fraction and m_i [mm] is the arithmetic mean of the particle size i. The K factor can also be assessed using the equation proposed by Römkens et al. (1986):

$$K = 0.0035 + 0.0388 \times \exp\left[-0.5 \times \left(\frac{\log D_g + 1.519}{0.7584}\right)^2\right]$$ (*Eq 2.11*)

When data on soil structure, organic matter and permeability were available, the equation given by Wischmeier et al. (1971) was used:

$$K = \frac{0.01317}{100}\left[2.1 \times 10^{-4} \times M^{1.14} \times (12\text{-OM}) + 3.25 \times (S-2) + 2.5 \times (P-3)\right]$$ (*Eq 2.12*)

where M can be estimated using the expression [%very fine sand + %silt]×[100 - %clay]. OM is the percentage of organic matter, S is the code according to the soil structure and P is the code according to the permeability class.

To incorporate the impact of flow convergence Mitasova et al. (1996) proposed the replacement of the slope-length factor ($L \times S$) by the upslope contributing area per unit of contour width in the RUSLE-3D. The modified $LS_{(r)}$ factor at a point on a hillslope is:

$$LS_{(r)} = (m+1)\left[\frac{A_{(r)}}{22.13}\right]^m \times \left[\frac{\sin \beta_{(r)}}{0.09}\right]^n$$ (*Eq 2.13*)

where $A_{(r)}$ [m^2] is the upslope contributing area per unit of width, $\beta_{(r)}$ [degree] is the steepest slope angle, and m and n are parameters depending on the type of flow.

The cover management factor C reflects the effect of cropping and management practices on the soil erosion rate (Renard et al., 1997). It was derived at the regional scale from the supervised land cover classification map of South America (Eva, 2003). Each land cover class was assigned an individual C factor corresponding to values reported by this soil cover in the literature (Angima et al., 2003). At the catchment scale, the NDVI image from SPOT-5 was used to calculate the C factor, considering that NDVI is highly correlated with vegetative cover and biomass. The C values were calibrated using the RUSLE 1.6 software and field data from individual sample plots. A linear regression was computed between the NDVI values and the corresponding C values from the field (de Jong et al., 1999; Singh et al., 2004).

The effect of contouring and tillage practices on soil erosion is described by the support practice factor P. Wischmeier and Smith (1978) define the support practice factor as the ratio of soil loss with a specific support practice to the corresponding soil loss with up-and-down cultivation. The lower the P value, the more effective the conservation practice is deemed to be at reducing soil erosion. Soil conservation practices cannot be

detected at the regional scale and there are presently no soil conservation practices being utilized by the farmers in the catchment (Flugel et al., 2003). Contemporary agricultural practices consist of up-and-down tillage without the presence of contours, strip cropping or terracing. Given this scenario, the RUSLE-3D model was run with a *P* factor of 1.0 at both regional and catchment scales, reflecting the desire to predict erosion potential under the current conditions of no structural soil conservation support practices.

2.7.2   Unit Stream Power Erosion model (USPED)

Some limitations of the USLE model and its derivatives such as the MUSLE and RUSLE have been outlined in the preceding sections – in particular, that these empirical equations can be used only to estimate gross detachment and lack any capability to compute deposition along hillslopes or depressions. Similarly, these equations represent a soil detachment capacity-limited case, in that the erosion estimates are based on rainfall intensity and raindrop impact on the surface, as expressed by the *R* factor. The influence of terrain on erosion is represented by the topographical factor ($L \times S$), which assumes a uniform slope angle and length along the path of water flow in the RUSLE (Nearing et al., 1994). Improvements to the $LS_{(r)}$ equations in the RUSLE-3D accommodate irregular slopes by incorporating the amount of hillslope convexity and concavity.

According to Mitasova (1999), an additional benefit of the Unit Stream Power Erosion Deposition model (USPED) is that it can predict the spatial distribution of erosion, as well as deposition rates for a steady-state overland flow with uniform rainfall excess conditions. Hence, this model is also applicable to a complex terrain where erosion is limited by the ability of runoff to transport sediment. USPED uses a dimensionless index of sediment transport capacity $T_{(r)}$ and a topographical index E_d, representing the change in transport capacity in the flow direction, to estimate the spatial distribution of both erosion and deposition. The parameter $T_{(r)}$ is derived from the unit stream power theory. The upslope contributing area is used as a proxy for water flux at a given location or grid cell. The index E_d is positive for areas with topographical potential for deposition and negative for areas with erosion potential. The sediment flow rate $q_{s(r)}$ at the sediment transport capacity $T_{(r)}$ (Julien and Simmons, 1985) is described by:

$$\left|q_{s(r)}\right| = T_{(r)} = K_{t(r)} \times \left|q_{(r)}\right|^{m} \times \left(\sin \beta_{(r)}\right)^{n} \qquad \textit{(Eq 2.14)}$$

where $q_{(r)}$ is the water flow, $K_{t(r)}$ is the soil transportability coefficient, and *m* and *n* are constants depending on the type of flow and soil properties. Within the 2D flow formulation, water and sediment flow are represented as bivariate vector fields $q_{(r)}=q_{(x,y)}$, $q_{s(r)}=q_{s(x,y)}$ and net erosion and deposition rate $D_{(r)}$ is estimated as the divergence of the sediment flow (Mitas and Mitasova, 1998):

$$D_{(r)} = \nabla \times q_{s(r)} = \nabla \times \left[T_{(r)} \times s_{(r)}\right] = K_{t(r)} \times i_e \times \left\{\left[\nabla \times A_{(r)} \times s_{(r)}\right]\sin \beta_{(r)} - A_{(r)} \times \left[k_{p(r)} + k_{t(r)}\right]\right\} \qquad \textit{(Eq 2.15)}$$

where $s_{(r)}$ is the unit vector in the steepest slope direction, i_e [m] is the uniform rainfall intensity, $k_{p(r)}$ is the profile curvature or curvature in the direction of the steepest slope, and $k_{t(r)}$ is the tangential curvature or curvature in the direction perpendicular to the gradient. As yet, insufficient experimental work has been performed to develop the parameters needed for USPED; therefore, Mitasova (1997) used the RUSLE parameters to incorporate the approximate impact of soil and cover and obtained a relative estimate

of net erosion-deposition. It is assumed that the sediment flow at sediment transport capacity can be estimated as:

$$T_{(r)} = R \times K \times C \times P \times A_{(r)}{}^m \times (\sin \beta_r)^n \qquad (Eq\ 2.16)$$

where $R \approx i^m$, $K \times C \times P \approx K_{t(r)}$; $LS_{(r)} = A_{(r)}{}^m \times \sin \beta_{(r)}{}^n$; and $m=1.6$, $n=1.3$ for prevailing rill erosion. For prevailing sheet erosion, $m=n=1$. Then net erosion-deposition E_d is estimated as a change in sediment flow rate expressed by a divergence in sediment flow:

$$E_d = div(T_{(r)} \times s) = \frac{\partial(T_{(r)} \times \cos \alpha)}{\partial x} + \frac{\partial(T_{(r)} \times sen\alpha)}{\partial y} \qquad (Eq\ 2.17)$$

where α [degree] is the aspect of the elevation surface or direction of flow minus gradient direction.

2.7.3 Modified Morgan, Morgan and Finney (MMMF)

Morgan et al. (1984) developed a method to predict annual soil loss from field-sized areas on hillslopes. It presents a straightforward, hybrid conceptual and physical approach to predict annual soil losses. The model consists of a water phase and a sediment phase. In the water phase, annual rainfall and the number of rainy days are used to determine the kinetic energy of rainfall for soil detachment and the volume of surface runoff (Morgan, 1995; Morgan, 2001). In the sediment phase, soil erosion is considered to result from the detachment of soil particles by raindrop impact and the transportation of those particles by overland flow.

The modified version (MMMF) enables the use of a cumulative sediment transport capacity algorithm, remote sensing imagery and a DEM (de Jong et al., 1999). The model characterizes the terrain using the DEM, and uses combined coarse and high multitemporal remotely sensed data to account for vegetation properties and soil moisture changes. The model estimates annual soil loss by evaluating both rainfall soil detachment and sediment transport over the soil surface. The lowest of the two values is taken as the soil loss at a particular location, indicating the erosion-limiting factor (Shrestha et al., 2004).

Mean annual rainfall R_a [mm] and the rainfall intensity I [mm hr^{-1}] are used to compute the kinetic energy for splash detachment E [J m^{-2}] using the following equation:

$$E = R_a \times (11.9 + 8.7 \times \log_{10} I) \qquad (Eq\ 2.18)$$

The critical value for soil moisture storage R_c [mm] is derived from several soil and land cover parameters, which include soil moisture at field capacity MS [weight %], bulk density B_d [gr cm-3], hydrological rooting depth R_d [m], and the ratio of actual to potential evapotranspiration E_t/E_o.

$$R_c = 1000 \times MS \times B_d \times R_d \times \left[\frac{E_t}{E_o}\right]^{0.5} \qquad (Eq\ 2.19)$$

The amount of overland flow Q [mm] is a function of the soil moisture storage, annual rainfall and the mean rainfall per rainy day in the year R_o.

$$Q = R_a \times \exp\left[\frac{-R_c}{R_o}\right] \qquad (Eq\ 2.20)$$

Excess rainfall becomes overland flow, which is drained downhill using a multiple routing algorithm to generate the potential cumulative overland flow Q_{cum} [mm]. This map is combined with the saturated hydraulic conductivity K_s [mm hr^{-1}], slope steepness S [degree] and, after masking out the hydrological channel network CH [0, 1], the distributed transport capacity map DT_c is obtained.

$$DT_c = [Q_{cum} - K_s] \times \sin(S) \times CH$$

(Eq 2.21)

The transport capacity T_c [kg m^{-2}] map is computed from the distributed transport capacity map, the slope S [degree], and the C factor of the RUSLE that accounts for effects of vegetation cover and soil tillage.

$$T_c = 0.001 \times C \times DT_c^2 \times Sin(S)$$

(Eq 2.22)

Soil detachment by rainfall F [kg m^{-2}] is based on empirical relationships between rainfall energy E [J m^{-2}], the soil detachability index K_m [g J^{-1}], expressed as soil splash detachment per unit of rainfall kinetic energy, and the percentage of rainfall interception by vegetative cover P_i [%].

$$F = 0.001 \times K_m \left[E \times \exp(0.05 \times P_i) \right]$$

(Eq 2.23)

Finally, the mean annual soil loss rate at cell i [kg m^{-2}] is estimated as the minimum of sediment available and transport capacity.

2.7.4 Thornes model

Soil erosion models must organize energy (overland flow and slope), resistance (erodibility of soil) and protection (vegetation cover) together in a physical and simple way. After analysing the competition between vegetation growth and soil erosion, Thornes (1985; 1990) put forward a conceptual erosion model by combining sediment transport and vegetation protection. It contains a hydrological component based on a storage type analogy, a sediment transport component and a vegetation growth component (Thornes et al., 1996). When modelling the competitive behaviour of vegetation and erosion, Kirkby et al. (1998) indicated that erosion is reduced exponentially in relation to the bare soil value by increased vegetation cover.

The value b equal to -0.07 was used to budget inputs and outputs to the soil storage from weathering, erosion, organic matter production, and decomposition. Thornes et al. (1996) determined that the maximum power value for overland flow is m=2 and for slope n=1.67, which represent the maximum capacity of sediment transportation. The minimum exponent value for vegetation cover is b=-0.07, which is the response to maximum capacity of vegetation protection to soil erosion. Satisfactory results were obtained when this model was used to simulate the water erosion in both humid and semi-arid areas (Wainwright, 1994; Symeonakis, 2001). Hence, the Thornes erosion equation reads:

$$E = K_t \times OF^2 \times s^{1.67} \times e^{-0.07 \times v_c}$$

(Eq 2.24)

where E [mm month^{-1} or mm day^{-1}] is erosion expressed as a denudation rate, depending on the time step of the model, K_t is a factor representing soil susceptibility to erosion and calculated from soil grain size, OF [mm per time step] is the overland flow derived from hydrological submodels of varying complexity, s [m m^{-1} or degree] is the slope gradient and v_c [%] is the fraction of vegetation cover.

A modification of the runoff curve number (CN) method (SCS, 1972) developed by Zhang et al. (2002) was used to derive the monthly runoff. The method assumes that the daily rainfall approximates an exponential frequency distribution within each day; then the rain day frequency density (J_i) is:

$$J_i = \left[\frac{n}{r_o}\right] \times e^{-\frac{r_i}{r_o}}$$

(Eq 2.25)

where n is the number of rain days per month, r_o [mm day^{-1}] is the mean rainfall intensity per rainy day each month, and r_i [mm] is the daily rainfall. The rainfall distribution per month in Eq. 2.25 was used to adjust the CN model. When the rainfall is less than the initial abstraction I_a [mm], there is no overland flow. Therefore, Zhang (1999) describes the monthly overland flow OF_i [mm] as:

$$OF_i = \int_{I_a}^{\infty} OF_p \times J_i \times \Delta r$$

(Eq 2.26)

where OF_p is the overland flow in a rainfall event and is estimated as follows:

$$OF_p = \frac{(r_i - I_a)^2}{(r_i - 0.8S)}$$

(Eq 2.27)

where $I_a = 0.2 \times S$, S is the potential retention [mm] and is estimated as: $\frac{25400}{CN} - 254$, and

CN [0 - 100] is the runoff curve number that is dependent on factors such as land cover, soil type and soil texture. The OF_i [mm] can be calculated using an approximate method, that is:

$$OF_i = \sum \Delta r \times OF_p \times J_i$$

(Eq 2.28)

where $\Delta r = \frac{r_{i_{max}} - I_a}{n}$, $r_i = I_a + i\Delta r$ and supposing r_{imax}=500 mm per rain day as a basic simplification.

2.7.5   Stream Power Law (SPL)

Mountain ranges evolve over millions of years towards a steady-state topography in which the rate of rock uplift due to the convergence of tectonic plates is more or less equal to the rate of erosion via rivers (Whipple and Tucker, 1999). The stream power law model for fluvial erosion states that erosion is proportional to the product of river slope and discharge. In terms of geological time, changes in discharge lead to changes in river slope in order to attain equilibrium between uplift and erosion. The calibrated SPL model incorporates climate and channel geometry to quantify denudation across the orogeny (Tucker and Whipple, 2002). The simplicity of this law for quantifying bedrock incision has resulted in its use in landform evolution models and as an erosion indicator. Channel width generally correlates inversely with slope and incision. However, where channel width does not correlate properly with slope, this suggests that other local controls such as lithology or sediment supply play a role (Phillips and Marion, 2001).

Quantifying denudation in this way provides a new perspective for evaluating controls on incision and the hypothesis of erosional control on the kinematic evolution of the Central Andes. Detachment-limited bedrock incision is often modelled as a power

function of unit stream power or shear stress. According to Stock and Montgomery (1999), the stream power incision equation can be written as:

$$E = K_l \times A^m \times S^n$$
(Eq 2.29)

where E [m yr^{-1} per area unit] denotes erosion or denudation rate, K_l [m^x yr^{-1}] is the erosion coefficient encompassing the effects of lithology, soil and climate, A [km^2] is the upstream drainage area and S [m m^{-1}] is the slope gradient. According to Whipple and Tucker (1999), three different choices of m and n values can represent river incision rates as a function of three distinct controls, namely, total stream power (m=1, n=1), stream power per unit of channel width (m=0.5, n=1) and shear stress (m=0.5, n=2/3).The exponents m and n were more closely related to the geological setting in the research areas and they were established at values of m=0.5 and n=1. Values of K_l can vary over several orders of magnitude (Finlayson et al., 2002a). Research in several bedrock environments carried out by Howard et al. (1994), Whipple et al. (2000) and Barnes and Pelletier (2001) report values of K_l ranging from 4.4×10^{-7} to 1.3×10^{-3} m$^{0.2}$ yr^{-1}.

In most mountainous catchments, the use of the upstream contributing area as a proxy for discharge may potentially overestimate the increase of discharge along the portions of the river as it flows down the drenched flank of the main mountain chain. To compensate for this discrepancy between contributing area and discharge, Finlayson and Montgomery (2003) have modified the river incision relation to include discharge explicitly for providing a spatially distributed index of erosion potential (ε) at the scale of orogeny. The modified equation then reads as:

$$\varepsilon = K_l \times Q^m \times S^n = K_l \times \varsigma \sum \left(A_{(r)} \times P_a \right)^m \times S^n$$
(Eq 2.30)

where $A_{(r)}$ and P_a represent the upstream area and net annual precipitation, respectively, and ς is a parameter that brings observed annual net precipitation values of a subcatchment in agreement with gauged annual discharge estimates.

2.8   Summary

From the descriptions and explanations given in the previous sections it is shown that:

- There are four main driving forces of erosion processes: (i) climatic forcing mainly through precipitation, including potential change such as variations in frequency and magnitude of events; (ii) topographical forcing presenting the potential energy gradients for the erosion and sediment transport processes; (iii) land cover changes active at different spatial and temporal scales and intensity, and of both natural (*e.g.,* long-term climate induced) or man-made nature; (iv) human activities affecting land cover, soil and local topography, such as deforestation, land abandonment, soil displacement by agricultural tillage, road construction and land levelling, and special cases such as forest or vegetation fires.
- The main tool for analysing the effects of such forcing by climate, physiographic or human factors on soil erosion is modelling. For erosion and sediment transport modelling, a wide set of tools is available for predicting soil loss or deposition. Empirical models have limitations in predicting the spatial distribution of overland flow and soil loss over the land surface since they cannot be universally applied, they are not able to simulate the movement of water and sediment over the land, and they cannot be used outside the range of conditions for which they were developed. The erosion scientific community supports the use of a physically based

approach because individual erosion processes are described and effects of variables on soil erosion are described by how these variables affect the fundamental processes represented in the model. However, due to the complexity in their mathematical representation, the parameterization of these models is extremely time-consuming and requires a huge amount of data (*e.g.,* the WEPP model requires more than 200 parameters). Most of the data are unavailable in areas where water and soil conservation planning are required – more so than in areas where the model has been developed.

- With the advent and spread of GIS, erosion modelling has increasingly aimed at providing spatially distributed prediction. GIS tools have enhanced exponentially the possibilities of handling spatial information such as topography, soil and land use, thus simplifying the implementation of spatially distributed models.

- Traditionally, most erosion research has been conducted at one particular scale and has ignored problems of scale transfer relating to results. In particular, research on individual processes has taken place at finer scales (*e.g.,* laboratory, experimental plots) for practical reasons (*i.e.*, design of soil conservation strategies for agriculture).

- Because of complex and nonlinear interactions between erosion processes, the extrapolation of results and their transfer from small scales to larger scales is not straightforward. Shifts in spatial and temporal scales therefore give rise to the emergence of characteristic processes represented at each scale. Some components in coarse-scale understanding have frequently been omitted from models, or are poorly represented (*e.g.,* runoff generation, linkages between slope and channel processes, soil surface characteristics control on infiltration, hydraulics and spatial organization of runoff and sediment transport, and biological control on soil properties). At all modelling scales, there seems to have been a shift to the conceptual approach owing to lower data demand and consideration of the physical processes in analysis.

- Appropriate representation of processes, even if simplified, can allow a better transfer of data and knowledge across a range of scales. Although there is no general methodology for scale changes, the recognition of similar objects, variables and patterns at different scales eases extrapolation for upscaling and downscaling.

- From scaling theory, it should be remembered that any spatial erosion modelling assessment approach in the geospatial domain requires a sequence of essentially six scaling steps to transform erosional processes into decisions, namely, measurement scale, database scale, modelling scale, prediction scale, assessment scale and validation scale (Figure 2.8).

- A key issue in the selection of the models used in this research was to make the best use of the scarce and scattered *in situ* information available so that the results of the simulations would adequately support the implementation of erosion control strategies. It is true that an improved model performance, independent of whether an empirical or physically based model is used, will depend upon forcing data resolution. However, demanding very high-resolution data or continuous monitoring is ideal, but it is not a solution in response to this phenomenon. Minimum data, minimum parameters and minimum calculating load to obtain the best simulation results may make distributed erosion models easier, as well as popular, to apply in ungauged catchments.

- Conceptual models offer a compromise between the need to explicitly deal with the main physical processes and the limited data availability, and may therefore be appropriate in characterizing the distribution of erosion within the catchment (*i.e.*, van Rompaey et al. (2003a) and Vigiak et al. (2005) obtained acceptable results with a simple transport-limited erosion model whose main driving factor was topography). Hence, for the present study five distributed conceptual models were selected based on a set of criteria of which the more important were (i) relatively low data demanding, (ii) ease of use, (iii) easier parameter estimation, (iv) GIS integration, (v) time scale, (vi) integration of remote sensing data, and (vii) potential for improvements.
- The five selected models allow the prediction of the location of erosion source and/or depositional areas, as well as the quantity of soil loss and deposition (*i.e.,* the USPED model). They predict erosion rates on a monthly and/or annual basis, taking into account the spatial distribution of the hydrological and erosional model variables.

Chapter 3

Description of the study area

Chapter 3

Description of the study area

3.1   Introduction

In this chapter, the general settings of the region and research areas (Figure 3.1) are presented. First, a brief description of the Bolivian Andean region is given. According to the Bolivian Ministry of Sustainable Development and Environment (MDSMA, 1996), this ecoregion is characterized by natural geological erosion and sedimentation phenomena of high intensity, as well as man-induced accelerated land degradation processes and desertification. Next, a more detailed description of the main characteristics of the sample areas used in the regional- and catchment-scale assessments is given (*i.e.*, the province of Cochabamba and the Laka-Laka catchment). Lastly, a number of lake and reservoir sites used for sediment yield assessments in this study are also described.

The specific objectives of this chapter are (i) to describe the biophysical characteristics of the research areas; (ii) to identify the main geomorphic units from a 1:50,000 digital orthophoto mosaic; (iii) to determine the soil characteristics and model parameters in the catchment from a reconnaissance soil survey, *in situ* experiments and laboratory data; (iv) to determine the temporal variation of the vegetation cover, using time series of remotely sensed data, and (v) to delineate soil erosion types and patterns of the research catchment, using high spatial resolution satellite imagery (SPOT-5).

3.2   Bolivian Andes

The Andean Cordillera extends for 5,000 km along the western coast of South America, reaching its greatest width of 700 km in the Central Andes of Bolivia (Montgomery et al., 2001). The tectonic style of the orogen varies significantly, both along and across the strike (Figure 3.2). Landlocked Bolivia sits astride the Andes in the west-central part of the South American continent. In Bolivia, the Andean mountain belt is very large and deformed by thin skinned tectonics (Guyot et al., 1999; Aalto et al., 2003). The back arc orogenic wedge is formed by the Cordillera Oriental (Eastern Cordillera), which limits the enigmatic high plateau Altiplano (Guyot et al., 1990) and the sub-Andean zone, and is characterized by the elbow shape of the mountain range (Bolivian Orocline) and high relief (several summits over 6,000 masl). It has overthrust and supplied its adjacent foreland sedimentary basin with sediments since upper Oligocene times. The present axis of the Bolivian Orocline separates the High Amazonian drainage basin in the north from the Pilcomayo drainage basin in the south. As such, it defines the country's five geographical zones: the *High Mountains* (Western and Eastern Cordillera) and *Altiplano* in the west, the semitropical *Yungas* and *temperate valleys* of the Eastern Cordillera slopes, and the *tropical lowlands* (*llanos*) in the eastern region, encompassing more than 55% of the country (Ribera et al., 1996). Notwithstanding the complicated geological patterns that favour erosion, few data are presently available to measure or evaluate the actual geological erosion rates of the Andean Cordillera (Guyot et al., 1996).
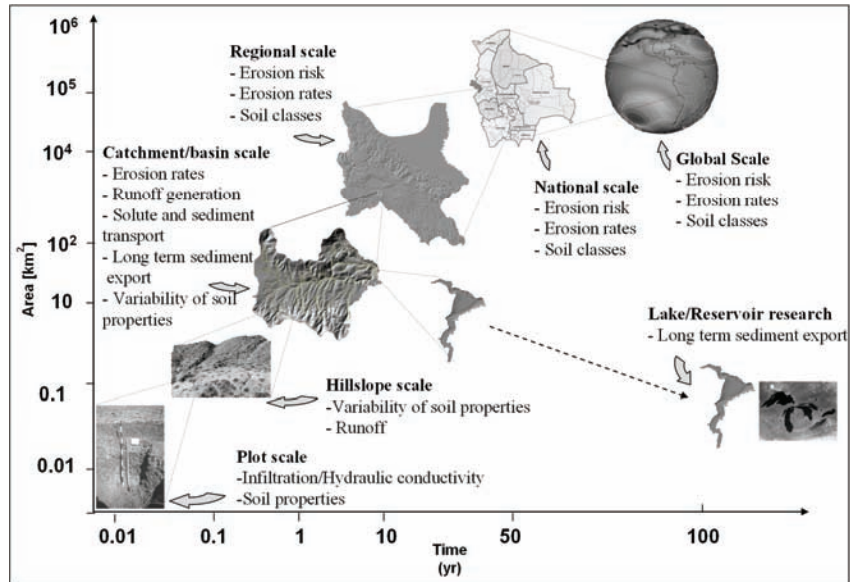
Figure 3.1 Location of the nested research areas (from top to bottom: Bolivia, Cochabamba, Laka-Laka catchment, catchment hillslope, Laka-Laka reservoir and soil sampling)
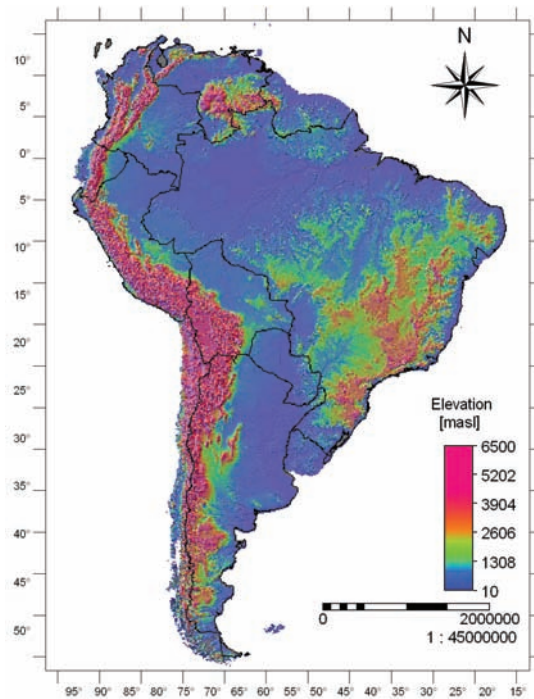
Figure 3.2 Relief map of the Andean Cordillera from the U.S. Geological Survey (USGS) 30 arc-second DEM (GTOP030)

50

3.3   Cochabamba province

Cochabamba is the third largest populated province in Bolivia, with an area of approximately 54,100 km^2. It lies between latitudes 16º 30' and 18º 00' S and between longitudes 64º 30' and 67º 30' W. It is located in the dissected mountains of the intermediate zone between the Altiplano in the west and the Santa Cruz floodplains to the east.

3.3.1   Climate

Although the province of Cochabamba lies entirely within tropical latitudes, the climatic conditions vary widely from tropical in the lowlands to polar in the highest mountain chains. Temperatures depend primarily on elevation and show high variability. In most locations, rainfall is heaviest during the summer, and annual amounts tend to decrease from north to south (Salazar and Montenegro, 1997). Figure 3.3 shows the average monthly rainfall amount measured at four stations located in different climatic regions. It shows the concentration of rainfall in the period from December to March and indicates a large seasonal variability (Johnson, 1976). According to the *Köppen* (1938) classification, three climatic regions are found in Cochabamba, namely dry, temperate humid, and tropical rainfall regions.

Temperatures and rainfall amounts in the Cordillera vary drastically (Montes de Oca, 2002). In the Altiplano, the average daily minimum temperature is less than -5ºC. Sheltered valleys through the Cochabamba Cordillera have mild temperatures (17ºC to 25ºC) and low to moderate rainfall amounts averaging from 400 to 760 mm annually. Temperatures drop with increasing elevation, however, and snowfall is possible at elevations of about 3,500 masl, with the permanent snow line being at around 4,600 masl. Areas above 4,650 masl have a polar climate with glaciation features.

The north and eastern lowland areas have a tropical wet climate with high temperatures, high humidity and high rainfall throughout the whole year (Jette and Rojas, 1998). Average daily maximum temperature is more than 30ºC all year in most locations. The rain-bearing northeastern winds, blowing across the Amazon basin, bring significant rainfall amounts. Rainfall often occurs in brief thunderstorms, sometimes accompanied by strong winds and hail. In the high mountain regions the average annual temperature is about 8°C, with an annual rainfall ranging from 600 to 1,000 mm, and in the valleys around 17°C, with rainfall from 400 to 650 mm. In the tropics (low floodplain), mean temperatures are over 25°C and rainfall ranges from 1,000 to 3,000 mm (MDSMA, 1996).

3.3.2   Physiography

Three main physiographic units can be distinguished in Cochabamba: the Cordillera, sedimentary basins and tropical areas, all formed during the Tertiary orogeny (Beck, 1988). The Eastern Cordillera enters Cochabamba from the northwest section. It presents a high rolling plain, with elevations from 4,200 to 5,200 masl interspersed irregularly with high peaks – too high to be exploited for large-scale grazing.
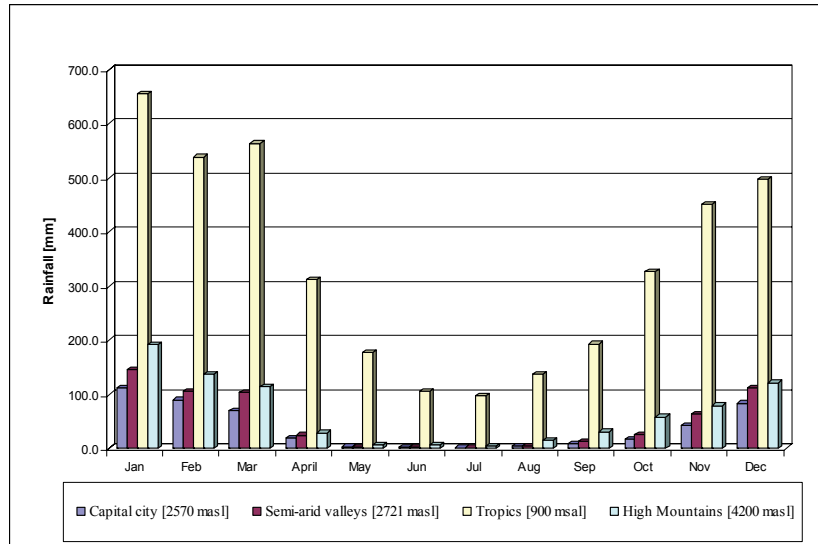
Figure 3.3 Monthly rainfall distribution at four physiographic regions in Cochabamba (1961 to 2003)
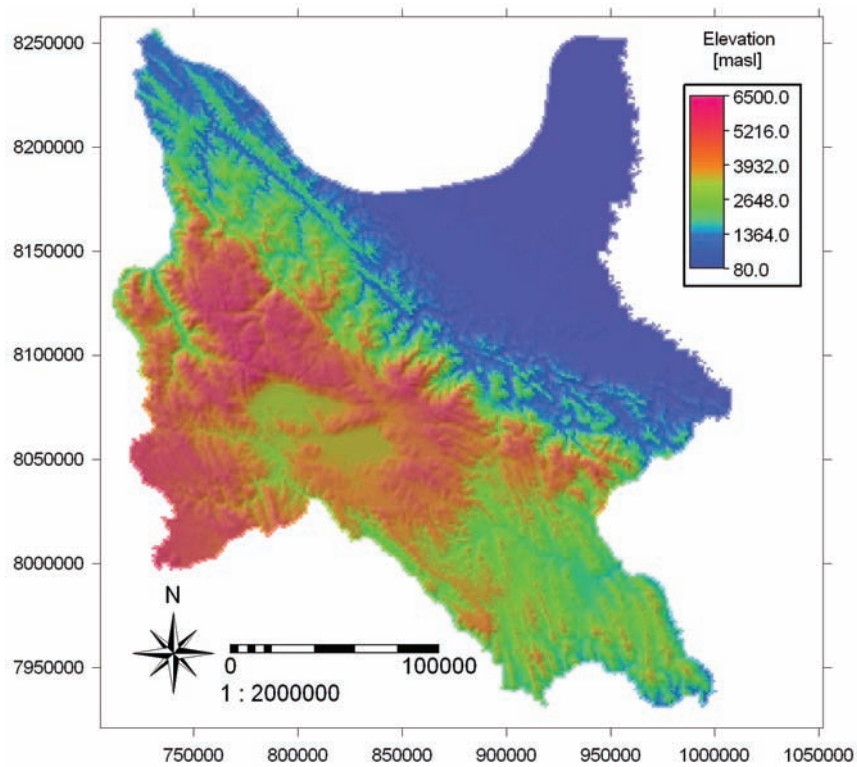
Figure 3.4 Digital elevation model of Cochabamba from the SRTM data

The eastern slopes of the Cordillera gradually descend in a series of complex N-S mountain ranges and hills, with elevations ranging from 3,200 to 4,000 masl, which form the sedimentary basins (Montes de Oca, 2002). These areas are favourable for crops and settlement.

Alluvial soils occur in the low areas, but erosion has followed the removal of vegetation in many places. The area is characterized by intense geomorphic activity, including water erosion (*e.g.,* rills and gully systems), slope movements and fluvial activity, leading to medium to high annual sediment exports (Lara, 1985).

The valley floors range from 2,000 to 3,000 masl and these lower elevations mean milder temperatures than those in the mountains. The north and northeastern lowlands consist of tropical rainforests.

Because much of the topsoil is underlain by a clay hardpan, drainage is generally poor, and heavy rainfall periodically converts vast parts of this region to swamps. Although comprising over 60% of the Cochabamba territory, this region is still sparsely populated (CLAS, 2003). These different physiographic zones define the complex topography of Cochabamba (see Figure 3.4). The 90 m resolution digital terrain model (DTM) was derived from the Shuttle Radar Topographic Mission (SRTM) data and the elevation ranges from 5,200 masl in the highest mountains (Tunari Cordillera) to 190 masl in the eastern floodplains (lowlands).

3.3.3   Geology and soils

The geology is dominated by sedimentary and igneous rocks, ranging from sandstone and quartzite to siltstones and shale, and calcareous marls to recent alluvial deposits. Rocks in the high mountain fronts include quartzites, conglomerates, sandstones, siltstones and shales of Cambrian age. A strip of Precambrian schist and quartzites occurs at the mountain footslopes, while the lower hills to the south consist of Ordovician and Silurian shales and siltstones (GEOBOL, 1992; GEOBOL, 1998).

During the Quaternary, large volumes of sediments were accumulated in the valleys of Cochabamba, namely, upper valley or *Valle Alto*, Sacaba valley, and the middle and lower valleys. They occur as large coalescing alluvial fans composed of weakly consolidated and poorly sorted sediments, with textures ranging from very coarse boulders in a gravelly sandy matrix to loams and clays. The overall texture becomes increasingly finer downstream, grading to lacustrine loams and clays deposited in the lacustrine environment in the central part of the valleys (GEOBOL, 1998). According to Montes de Oca (2002), the Cochabamba valleys of tectonic origin are narrow (5 to 10 km wide) and predominantly a Paleozoic and Mesozoic basement (Ordovician, Silurian and Cretaceous periods). The Ordovician section is composed of a lower sequence of siltstones, claystones and sandstones (*Cuchu-Punata* formation), and an upper sequence of quartzitic sandstones (*San Benito* formation). The Silurian section contains a lower formation of quartzites and clay grits (*Cancaniri* formation), covered by claystones (*Uncia* formation).

Mesozoic sedimentary rocks of the Cretaceous period are also found overlying the Paleozoic rocks. They are mainly limestones and marls at the bottom (*Molino*

formation), underlying a flysch-type sequence of calcareous sandstones, marls and clays (*Santa Lucía* formation). During the Paleocene, molassic deposits (*Morochata* formation) were laid down, which consist of conglomerates covering a small part of the area. The bottom of the valleys is filled with a thick sequence of Quaternary deposits, beginning with Pleistocene lacustrine deposits consisting of clays, and sandy and silty clays in the lower areas, which develop into fluvio-lacustrine and fluvial sediments towards the top. In the foothills on the lateral slopes, coarse deposits have accumulated (*i.e.,* agglomerates, gravels and coarse sands related to the alluvial fans of a number of torrential streams descending from the neighbouring highlands) (Barnes and Pelletier, 2001).

The lowland region is geologically young. The process of Amazonian sedimentation is continuing as the sediment-laden white-water rivers course down from the Cordillera, continuously changing their channels and depositing and re-depositing their sediments along the way. The sediments of this region are mostly of alluvial origin from the late Pleistocene and Quaternary, while beneath is a Tertiary marine molasse. The region belongs to a pericratonic basin underlain by the ancient Brazilian shield, with various faults and diaclasations. The plain has little local relief, but elevational changes of a few metres may determine an area's local water regime and biota.

3.3.4 Land cover and vegetation

The province of Cochabamba presents an enormous variety of land cover and vegetation. For purposes of describing their characteristics and geographical distribution, the land cover vegetation map of South America (Eva et al., 2002) was used (Figure 3.5). The high Andean mountains and Altiplano regions present large areas of "montane grasslands" with characteristic species such as *Festuca dolichopylla*, *Stipa ichu,* and *Calamagrostis minima* (Beck, 1988). The wet puna is covered with grasses and shrubs. Sedges and rushes dominate areas with poor drainage. Above 4,000 masl, the vegetation in wet areas (or *bofedales),* includes floating submerged cushion plants. Large cushions are formed by *Distichia muscoides, Oxychloe andina* and *Plantago tubulosa*. Common trees in the area are *Buddleja coriacea* (Kiswaras) and *Polylepis spp* (Lara, 1985)*.* The wet puna includes small mountain chains with typical microclimates, in which species such as *Satureja boliviensis, Calceolaria spp*, *Mutisia ledifolia, Senecio spp*, *Senna aymara,* and *Ephedra americana* are found. Montane grasslands presenting patches of *Festuca poa* are located from the northeast to the southeast section of the Eastern Cordillera, with altitudes ranging from 3,500 to 4,000 masl and with a semi-humid climatic regime. Montane shrublands with species such *Baccharis* and *Caceol sp* are also characteristics of this region (Vaneberg, 1988).

In the sub-Andean valleys, there is predominance of "semi-arid woodlands". The woodlands are dominated by species such as *Schinopsis haenkeana* (Soto), *Acacia caven* (Churqui), *Prosopis laevigata* (Algarrobo), *Aspidioosperm sp* (Quebracho blanco), *Salix humboldtiana* (Sauce), *Schinus molle* (Molle), *Choricia insignis* (Toborochi) and *Tipuani tipu* (Tipa) (Vaneberg, 1988; Lopez, 2003). The semi-arid shrublands are composed of often spiny species such as *Dodonea viscose* (Chacatea) and *Bachharis dracunculifolia* (Tola), or by trees composed entirely of stiff, spiny branches such as *Prosopis kuntzei* (bizarre leafless tree locally called Lanza-Lanza), cacti such as *Neoraimondia herzogiana* (Giant caraparí), and several species of *Ephedra*

andina (Pinco) and *Minthostachys acutifolia* (Muña) (Nagashiro, 1992; Beck et al., 1993). Subhumid deciduous forests are distributed in the eastern section of Cochabamba at an altitude of less than 900 masl. The forest covers the non-consolidated sediments forming low hills east of the foothills of the mountains. Among the dominant trees are *Terminalia oblonga* (Verdolago), *Astronium urundeuva* (Cuchi), *Cybistax antisiphylitica* (Tajibillo), and *Zeyheria tuberculosa* (Jopo de mono) (Kessler et al., 2001).
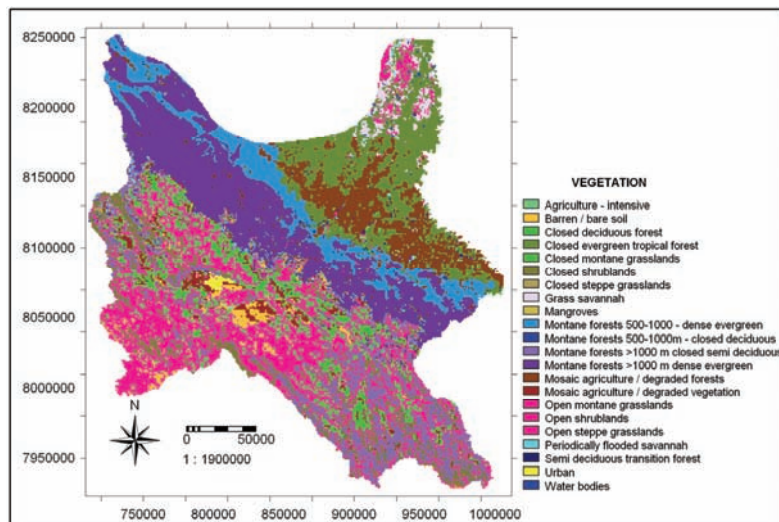
Figure 3.5 Land cover map of Cochabamba derived from the South America vegetation map

Seasonal humid Amazon rainforest located in the northeastern region of Cochabamba starts at areas below 1,100 masl. According to Libermann (1991), the forest is characterized by a large number of species that reach their southern limit of distribution with species such as *Astrocaryum sp*, *Iriartea deltoidea*, *Attalea sp*, *Socratea exorrhiza* (Palms) and trees such as *Swietenia macrophylla* (Mara), *Cedrela odorata* (Cedro) *Terminalia amazonica* (Verdolago), *Calophyluum brasilience* (Palo maria), *Ceiba pentandra* (Mapajos) and *Hura crepitans* (Ochoa). Seasonally inundated forest along the major rivers in the rainforest zone is called *várzea*. These areas have been greatly disturbed by slash-and-burn agriculture, and species such as *Hura crepitans* (Ochoa), *Ochroma pyramidale* (Perea), *Poulsenia armata* (Ficus) and *Ceiba petandra* (mapajos) are found (Navarro, 1997). Finally, the humid sabana reaches contiguously into the humid forests. Ribera et al. (1996) affirm that vast areas of grasses such as *Andropogon bicornis* and *Hymenachne amplexicaulis* are predominant in this region.

3.4 Laka-Laka catchment

3.4.1 Catchment choice

The Laka-Laka catchment is close to the town of Tarata and is about 35 km southeast of Cochabamba (Figure 3.6). According to Zimmerer (1993), this semi-arid region has presented signs of medium to high levels of soil erosion since 1953. The catchment belongs to the mountainous part of the upper valley or Valle Alto ecosystem. The Laka-Laka catchment was selected for scientific as well as practical reasons:

- Since conceptual models have been selected, a proper choice would be a catchment of medium size. The bigger a catchment, the larger the spatial units affected by erosion. Therefore, the effectiveness of the models can be spatially assessed more effectively in terms of how representative the real erosion processes are simulated.
- Since one of the ultimate objectives of erosion modelling is to define some alternative mitigation measures, a catchment little affected by soil conservation measures had to be chosen.
- The existence of a reservoir at the outlet provided an ideal opportunity for direct estimation of the catchment sediment yield.

Of the available options the Laka-Laka catchment matched these requirements best:
- The catchment is representative of the surrounding catchments and environment.
- The catchment is of a medium size with an area of about 59.8 km^2.
- Current conservation measures consist of only a few check dams in some tributaries or areas, with high gully or debris flow activity and very few terraces (CORDECO, 1991).
- A total number of 120 families live in the catchment. There are five villages, so there are good opportunities to involve farmers in potential soil and water conservation programmes.
- The Laka-Laka reservoir, located at the catchment outlet and operational since 1992, is affected by serious sedimentation problems (Torrico, 1999).

The catchment lies between latitudes 17° 35' 13" and 17° 40' 37" S and longitudes 66° 3' 10" and 66° 9' 12" W. Elevation ranges from 2,780 to 3,500 masl and slope angles are generally steep. The DEM of the catchment is shown in Figure 3.7(a).

As mentioned, a dam has been constructed at the catchment outlet. Construction of the dam started in May 1990 and its operation began in July 1992. The dam construction was part of the Laka-Laka Multipurpose Project (Figure 3.8). The aim of this project was to store 6 Mm^3 of water from the Calicanto and Viscachani rivers on an annual basis (LH-UMSS-PROMIC, 1999). The new supply of water was intended to irrigate 500 ha of agricultural land downstream of the catchment with a discharge of 500 to 560 l s^{-1}. A drinking water supply for Tarata town was also considered. The high turbidity of the reservoir water, owing to the high sedimentation process in the reservoir, made the treatment too expensive.

3.4.2 Climate and hydrology

According to the Thornthwaite classification, the climate in the area is dry semi-arid, with a high water deficiency in winter and occasional heavy thunderstorms in summer. At Tarata, 10 km from the catchment, the average annual rainfall is 504 mm for the period 1960 to 2003 (Tarata meteorological station). Most of the rain (77%) and all heavy storms occur in the period from December to March. It is only during these large storms that runoff occurs in the catchment (Salazar and Montenegro, 1997).

Figure 3.9 shows the average monthly rainfall. It shows the concentration of rainfall in the period from December to March and a high standard deviation that indicates a large interannual variability.

a)

b)
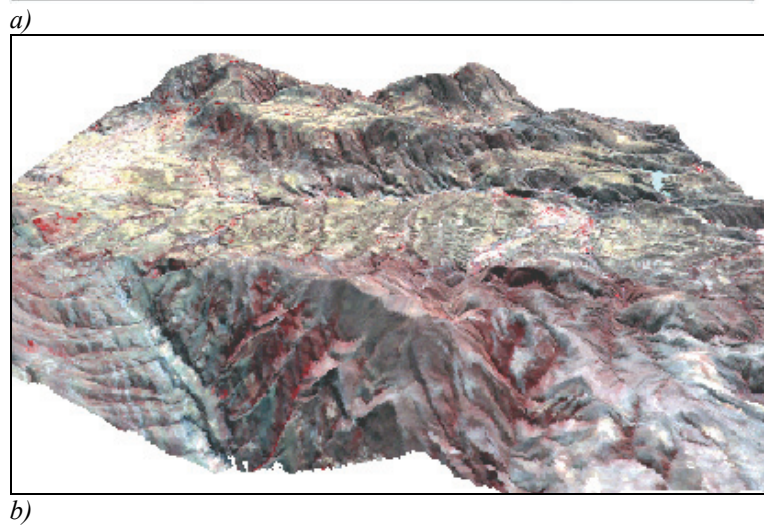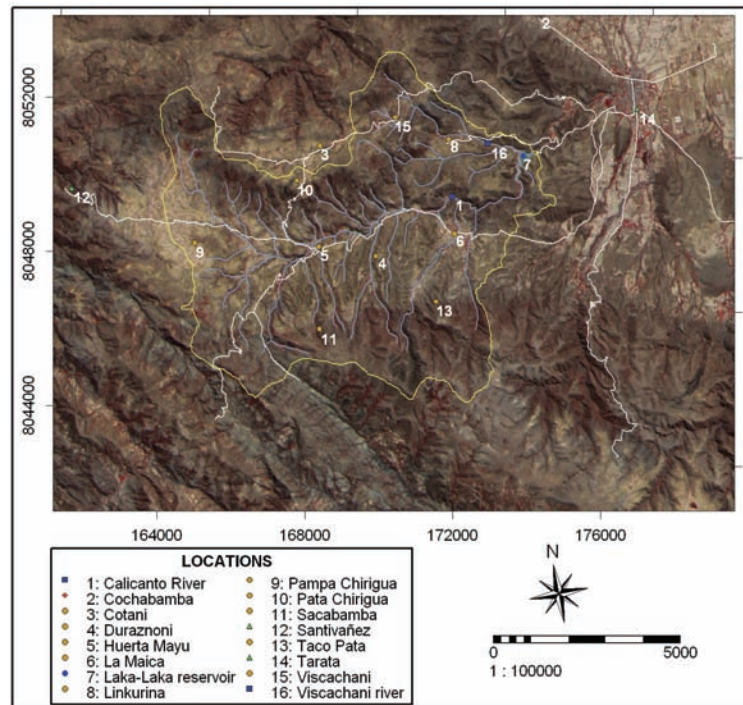
Figure 3.6 General location of the Laka-Laka catchment: *a)* ASTER false-colour composite image with the main towns and rivers, *b)* SPOT-5 false-colour composite 3D image (acquisition date: August 19th, 2002)

a)

b)

c)

d)
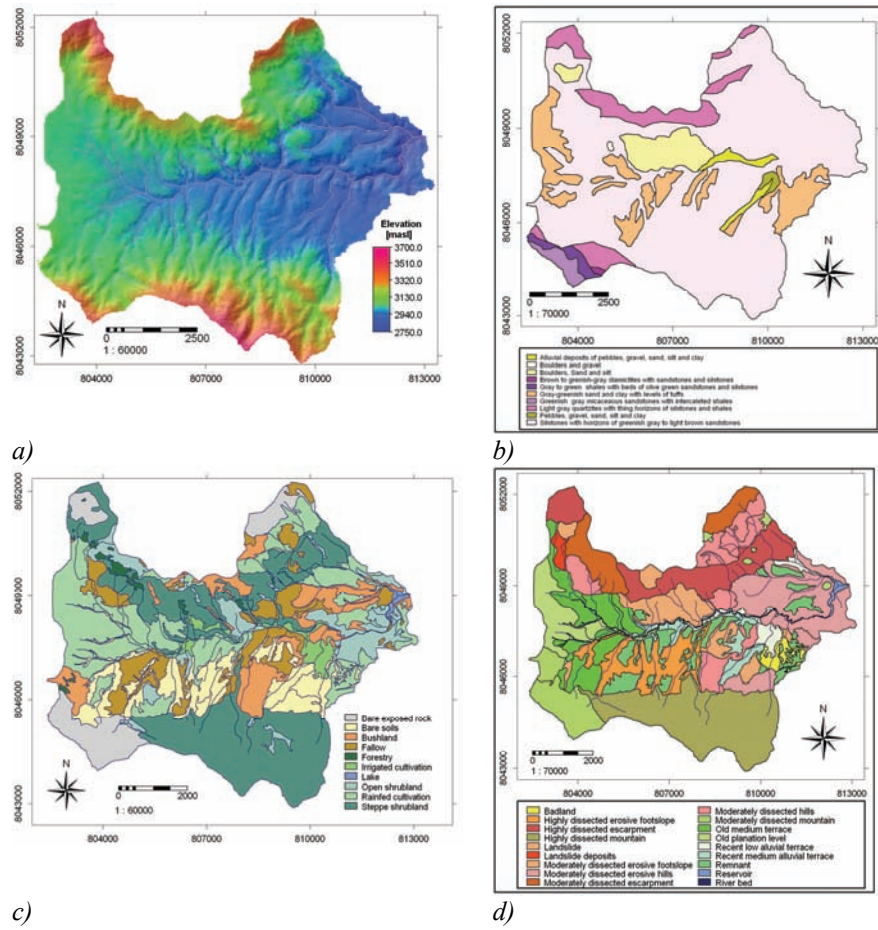
Figure 3.7 Thematic maps of the Laka-Laka catchment: *a)* DEM, *b)* geology, *c)* land cover, d) geomorphic units

Figure 3.8 General views of the Laka-Laka dam and reservoir

Winters are dry and cold in the southeastern region of the catchment, known locally as *Pampa Chirigua*. Data for the past 30 years indicate that the mean minimum temperature in June was -5 ºC. Over the same period, the average temperature in the warmest month (November) was 28ºC, and the annual average temperature was 18ºC.
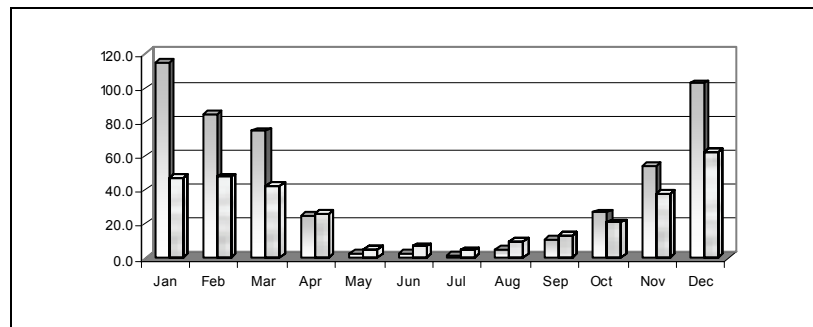
Figure 3.9 Monthly rainfall distribution at Tarata meteorological station over the period 1960 to 2003

The annual potential evapotranspiration according to Penman-Monteith formulae (Allen et al., 1998), using climate data from the past 30 years, is estimated to be 1,583 mm. Rainfall does not satisfy water requirements for rainfed agriculture and a moisture deficit exists for most crops, particularly from April to November.

The catchment is exposed to strong winds, which are relatively intense and more frequent from August to October, especially during the afternoon hours. Average monthly wind speed ranges from 5.2 km hr^{-1} in March to 16.5 km hr^{-1} in September. The dominant wind direction is from northwest to southeast during the wet season (November to March), and changes to southwest during the dry season (April to November). The soil textural analysis revealed that the soils in the catchment are in principle permeable. However, infiltration rates are significantly reduced by surface sealing and crusting attributable the high clay content in the second and third horizons of the soil profiles.

3.4.3   Geology

The catchment lies in the Andean region of the semi-arid valleys and contains two different morphological environments: mountain ranges and sedimentary basins, both formed during the Tertiary orogeny. The mountain chains in the southern and northern parts of the catchment are composed of Ordovician, Silurian and Quaternary rocks (Claure, 1996; GEOBOL, 1998). Quaternary landslides can be observed and were formed by the combined action of topography, gravitational force, and reduced transport. A sequence of siltstone and shale interbedded with greenish grey to light brown sandstone, with low resistance to erosion, cover most of the catchment (*Anzaldo* formation).

Light grey quartzite with thin horizons of siltstone and shale (*San Benito* formation) are present in the southern and eastern parts of the catchment and also in the southern bank of the river Calicanto. Quaternary landslides comprised of boulders, sand and silt are observed in the north-central bank of the main river. Next to it, a sequence of alluvial deposits consisting of pebbles, gravel, sand, silt and clay can be observed in the north

bank of the river. Alluvial deposits and terraces constitute the riverbanks at the intersection of the Calicanto and Viscachani rivers. Alluvial sediments ranging from conglomerates to silt and clay are located predominately in the frontal area of the alluvial fans (GEOBOL, 1998). Well-developed brown to greenish grey diamictites with sandstones and siltstones (*Cancañari formation*) and greenish grey micaceous sandstones with intercalated shales (*Catavi formation*) are present at the southwestern part of the catchment. There are also Quaternary conglomerates in the central and eastern parts of the catchment. The Quaternary material is a mix of boulder, gravel, silt, sand and clay from alluvial, colluvial and lacustrine deposits (Figure 3.7b)

3.4.4   Geomorphic mapping and soil characterization

The general characteristics of the catchment were studied during a field reconnaissance survey in which information on the geology, geomorphology and soils in particular was gathered. The major thematic units were identified by interpreting 1:50,000 black-and-white aerial photographs taken in August 1961 and very high resolution (VHR) panchromatic/multispectral SPOT-5 imagery taken in August 2002.

Taking into account the fine spatial resolution of the panchromatic VHR SPOT-5 and its information content, it can be noted that the planimetric accuracy of the delivered image as regards ground sample distance (GSD) is relatively poor owing to a number of geometric distortions. The inherent geometric accuracy of images and their approximate georeferencing (computed for some product levels from the source of the satellite, the orbital position and the imaging geometry) need to be improved. Orthorectification is the process that converts images into map-like (metric quality) form by accurately removing satellite-, scanner- (camera), and terrain-related distortions (Bishopa et al., 2003). The resulting ortho-image can then be directly applied in GIS or mapping-oriented applications (*e.g.,* terrain analysis, thematic information extraction, area measurement).

Hence, the 5 m resolution panchromatic VHR SPOT-5 (12,000×12,000 cells, level 1A) was orthorectified by means of 90 selected ground control points (GCP) measured with a differential Geographic Positioning System (GPS) and 30 m DEM data using ERDAS 8.7 Ortho-Base with root mean square error (RMSE) of less than 0.89. Twenty of the distributed GCPs were located within the research catchment. An object-to-pixel transformation using the GCPs was computed using the model provided in the SPOT-5 data. Post-processing for radiometric improvement of the ortho-image was applied.

The corrected image was then used to orthorectify both the multispectral SPOT-5 bands of 10 m resolution (6,000×6,000 cells, level 1A) and the 15 1:50,000 aerial photographs covering the Angostura floodplain and the Laka-Laka catchment, thereby obtaining a photo mosaic with 5 m resolution (Figure 3.10a).

Next, a contrast stretch of 1% saturation was performed for each band to enhance those landscape features of particular relevance in this research. The research area was clipped for preparing the thematic maps of the catchment. Six basic image elements, namely, colour/tone, texture, shape, size, pattern and association, together with ground truth observations made in the catchment, and collateral data about the topography, were used for extracting geomorphic features. Based on the resulting classification and

field observation, 18 representative plots measuring 30×30 m were selected (Figure 3.11) and distributed over five geomorphic units (Table 3.1). In each plot, representative soils were described and classified into specific soil units.

In the catchment, several geomorphic units were distinguished: escarpment, mountain, hills, landslides, footslope, remnants, old planation level, low and medium terraces (Figure 3.7 d). The mountains and hills from the Anzaldo formation present a strong degree of dissection and usually have a thick regolith of weathered shale sensitive to mass movements. Slopes often have a pronounced micro-relief owing to the high density of grazing. On the south-facing slopes, soils have a well-developed silt loam A_h *horizon* over a clear yellowish brown *B horizon* with a texture of loam to clay loam and some evidence of clay translocation in the form of illuviation cutans on ped faces. On the north-facing slopes, soils are often truncated, and rills and gully erosion are common alongside paths.

Table 3.1 Physical soil properties at 18 selected sites for soil description. H is the soil horizon, D [cm] is the depth of the soil layer, B_d [gr cm^{-3}] is the bulk density, FC [%] is the water content at field capacity, *WP* [%] is the water content at wilting point, *AW* [%] is the available water, *Sa* is the percentage of sand, *Si* is the percentage of silt and *Cl* is the percentage of clay, OM [%] is the organic matter, K_s [mm day^{-1}] is the hydraulic conductivity and *I* [mm day^{-1}] is the infiltration capacity

Nº	Physiographic unit	H	D	B_d	FC	WP	AW	Sa	Si	Cl	OM	K_s	I
1	Old planation level	A1	22	1.34	12.3	4.9	7.38	36	51	13	0.97	59	*18.5*
		A2	27	1.52	24.2	18.2	6.03	28	31	41	0.45		
		A3	14	1.58	18.2	8.65	9.64	40	39	21	0.3		
		A4	17	1.35	38.3	20.9	17.44	22	16	62	0.01		
2	Old medium terrace	B1	28	1.46	11.8	4.66	7.22	42	41	17	1.11	64	*21.5*
		B2	14	1.28	16.2	8.33	7.96	29	44	27	0.52		
		B3	15	1.38	14.6	7.26	7.37	29	47	24	0.45		
		B4	15	1.84	15.3	6.42	8.96	31	45	24	0.15		
3	Moderately dissected mountain	C1	23	1.7	15.4	5.67	9.75	33	51	16	0.6	94	*38.8*
		C2	21	1.5	17.3	9.05	8.27	32	40	28	0.45		
		C3	36	1.59	21.3	10.6	10.7	29	37	34	0.23		
4	Recent low alluvial terrace	D1	60	1.2	11.5	6.04	5.5	37	47	16	0.97	60	*26.4*
		D2	60	1.4	18.4	8.16	10.2	25	47	28	0.08		
5	Remnant	E1	12	1.41	11.1	5.21	5.95	53	35	12	1.7	56	*50.2*
		E2	24	1.53	14.4	7.47	6.97	45	43	12	0.82		
		E3	39	1.66	22.6	11.5	11.1	28	38	34	0.45		
6	Old planation level	F1	41	1.52	16.7	7.06	9.66	37	47	16	2.37	200	*90.7*
		F2	12	1.3	23.3	13.6	9.76	25	35	40	0.67		
		F3	22	1.7	23.5	13.3	10.2	17	35	48	0.3		
7	Landslide	G1	10	1.46	10.8	4.95	5.86	47	41	12	1.04	195	*46.7*
		G2	30	1.48	14.0	6.83	7.24	36	42	22	0.08		
8	Recent medium alluvial terrace	H1	30	1.25	27.2	13.4	13.8	25	56	19	2.73	124	*42.7*
		H2	23	1.35	13.8	6.07	7.77	37	43	20	0.52		
		H3	18	1.37	15.5	7.41	8.1	33	49	18	0.74		
		H4	29	1.4	17.0	7.84	9.23	25	53	22	0.52		
9	Moderately dissected erosive footslope	I1	15	1.38	7.5	3.65	3.92	54	36	10	0.3	201	*50.2*
		I2	18	1.7	20.1	8.6	11.59	42	30	28	1.26		
		I3	22	1.41	24.2	17.29	6.94	23	21	56	0.38		
10	Moderately dissected hills	J1	35	1.45	13.5	5.47	8.03	39	47	14	1.33	150	*11.4*
		J2	23	1.48	12.6	6.77	5.83	39	45	16	0.74		
		J3	18	1.5	16.06	6.71	9.35	27	53	20	0.74		
		J4	*38*	*1.46*	*15.6*	*6.58*	*9.1*	*36*	*44*	*20*	*0.6*		

Table 3.1 Continuation: Physical soil properties at 18 selected sites for soil description. H is the soil horizon, D [cm] is the depth of the soil layer, B_d [gr cm^{-3}] is the bulk density, FC [%] is the water content at field capacity, WP [%] is the water content at wilting point, AW [%] is the available water, Sa is the percentage of sand, Si is the percentage of silt and Cl is the percentage of clay, OM [%] is the organic matter, K_s [mm day^{-1}] is the hydraulic conductivity and I [mm day^{-1}] is the infiltration capacity

N°	Physiographic unit	H	D	B_d	FC	WP	AW	Sa	Si	Cl	OM	K_s	I
11	Old medium terrace	K1	31	1.39	12.9	5.43	7.5	55	34	13	0.97	101	36.9
		K2	35	1.38	24.5	16	8.5	15	9	76	1.04		
		K3	29	1.63	23.9	16.3	7.6	28	10	62	1.11		
12	Highly dissected erosive footslope	L1	16	1.44	9.97	4.24	5.7	48	37	15	1.55	109	38.7
		L2	14	1.29	15.3	8.43	6.9	38	37	25	0.82		
		L3	20	1.61	25.7	15.8	9.9	8	39	53	0.52		
		L4	30	1.77	21.6	13.3	8.3	34	33	33	0.15		
13	Remnant	M1	16	1.42	6.4	2.96	3.4	56	33	11	0.89	180	90.1
		M2	16	1.05	8.49	4.52	3.9	68	17	15	0.23		
		M3	34	1.7	17.6	5.43	12.5	58	25	17	0.38		
		M4	14	1.44	23.9	13.2	10.7	34	21	45	0.02		
14	Highly dissected erosive footslope	N1	16	1.34	9.97	4.6	5.4	54	35	11	0.76	154	3.0
		N2	12	1.6	17.9	8.25	9.7	44	39	17	0.91		
		N3	15	1.32	18.3	9.61	8.6	40	37	23	1.82		
		N4	15	1.43	13.5	5.8	7.7	60	21	19	1.44		
15	Badlands	Q1	58	1.36	16.1	8.54	7.5	38	45	17	2.66	74	91.8
		Q2	13	1.41	23.9	12.6	11.4	23	18	59	1.44		
		Q3	27	1.38	22.6	12.2	10.4	32	19	49	0.68		
16	Moderately dissected erosive hill	R1	54	1.65	22.6	9.09	13.5	33	34	33	1.9	68	28.9
		R2	20	1.33	27.9	14	13.9	18	13	69	1.52		
		R3	14	1.7	23.1	11.5	11.6	35	28	37	0.61		
17	Remnant	S1	47	1.4	12.2	6.3	5..9	54	35	11	1.37	150	17.6
18	Moderately dissected erosive hill	T1	19	1.31	19.5	10.2	9.3	40	41	19	2.43	141	30.1
		T2	18	1.43	17.7	9.52	8.2	44	39	17	1.22		
		T3	42	1.33	20.2	12.3	7.9	24	63	13	0.53		
		T4	20	1.53	28.1	16.2	11.9	25	55	20	1.1		

The soils have relatively thin and weakly developed A_h *horizons* and a less developed *B horizon* with less clay cutans and slightly coarser texture (silt loam to loam). They lack the distinct textural change between the A_h and *B horizons*. Most of the shallow soils are free of lime. The remnants, terraces and old planation levels that extend into the adjacent mountain valleys, especially in the southern part, are composed of sediments horizontally bedded and finely textured with local gravel intercalation. Gully development is strong, with gullies having complex slopes determined by slight differences in lithology. Non-eroded loamy soils occur with a clear A_h *horizon* overlying a *B* or B_t *horizon*.

The stripped bedrock escarpments are an important unit in the catchment. Over large areas, the regolith or hard rock is close to the surface. Consequently, the soils are shallow and consist of a thin (about 10 cm) gravelly sandy to loamy A_h *horizon* over weathered rock. The erosion that took place on these steep slopes and obviously resulted in the removal of earlier formed soils and regolith is believed to have taken place under the more humid conditions that occurred in the late Pleistocene. Dissected erosive footslopes present a coarse texture and poorly sorted bouldery to stony deposits over hard rock. Downstream of this syncline, the arid landscape consists of steep slopes with hardly any regolith soil. The rivers (Calicanto and Viscachani) present steep and narrow riverbeds, underlain by poorly sorted, very coarse textured, deposits. On the

lower slopes there are hardly any soils, the slightly weathered bedrock being exposed at the surface over large areas.

3.4.5   Land cover and land use

Agricultural land is cultivated in a labour-intensive way. Most of the farmers lack funds and cannot afford any mechanical equipment, so essentially all agricultural work is done by human and animal power (Zimmerer, 1993; Denniston, 1995). The steep slopes also make mechanization almost impossible. Oxen are used for ploughing, while weeding and harvesting are done manually. Croplands are mostly located on the small river terraces along the main river courses. Rainfed agriculture is also practised along the hilltops, footslopes and on the old planation levels (high plateaus) in the southern region of the catchment. The main crops are wheat, corn, and potatoes.

The steeper slopes are mainly developed for grazing by sheep and goats, which results in intensive removal and stripping of scarce vegetation (Garcia, 1992). This is considered one of the triggering factors for the erosion processes, resulting in sheet-wash, rill formation, ephemeral gullies and soil creep on the slopes (Geerken and Ilaiwi, 2004). Deep active gullies exist on the hills, footslopes and old planation levels, which incise the sediments to a depth of more than 4 m. In some places, the incision may be as deep as 10 m. Xerophytic land cover is dominant in the whole catchment, though the percentage of this vegetation cover varies from zone to zone. On the very steep slopes, where the topsoil is very shallow and stony, vegetation hardly grows at all. However, on medium and intermediate slopes shrubs and sparse native grasses are present, with vegetation cover greater than 25%, while shrublands with vegetation cover greater than 45% can be observed on both sides of the high mountain relief (Figure 3.7c).

The grasses and shrubs belong mostly to the Graminae, Cyperaceae, and Plantaginaceae families. Native grasses such as *Stipa ichu* (Paja brava) are scattered over the catchment. Shrubs such as *Acacia macracantha*, *Prosopis alba*, *Dodonaea viscose* and *Bacharis sp* are located mostly in the side hills and footslopes. Native trees such as *Scinus molle* and *Scinus fasciculatus* are randomly distributed (Lopez, 2003). Exotic species such as *Eucalyptus globulus* and *Pinus patulata* have been introduced through reforestation. The orthorectified multispectral images and the orthophoto showed that land cover in the catchment is highly dynamic. Over the past 45 years, areas with bare soil have increased by 1.9 km^2, whereas areas with rainfed and irrigated agriculture have decreased by 6 km^2; changes in land cover were therefore not homogeneous. The area with bush and shrub vegetation increased (3.9 km^2) through regeneration of natural vegetation. In order to derive the land cover map, an unsupervised classification using a histogram peak cluster technique to identify dense areas or frequently occurring pixels was first carried out (Escadafal, 1994; Haboudane et al., 2002). The cluster module was carried out first to generalize the level of clustering, retaining all spectral classes.

Based on the histogram of the clustering results, nine well-defined spectral classes were selected (Jensen, 1996; Mücher et al., 2000). Each class was checked in the field using GPS eTrex Summit from Garmin^{TM}. Fifty ground data sites were visited and checked in the field. A minimum of 200 cells were selected as training areas for each class (Leprieur et al., 2000; Flugel et al., 2003). A spectral signature file for each class was subsequently created. These signature files were used by the maximum likelihood

classifier to categorize the continuum spectral data in the entire image (Mücher et al., 2000). The supervised classification accuracy of each land cover was evaluated using a stratified random sampling design. A confusion matrix was produced, from which the overall accuracy was estimated at 75% and a kappa index of agreement of 0.70 was obtained.

3.4.6 Delineation of soil erosion types and features using remote sensing

The assessment of the actual erosion at the catchment scale was conducted using the method based on both ground and high spatial resolution remotely sensed data (Metternicht and Fermont, 1998). An erosion feature map was generated by classifying separately the orthorectified SPOT-5 and photo-mosaic images in combination with field ground truth data (Figure 3.10). First, an unsupervised classification was performed using the K-means clustering algorithm, employing all four image bands (Sujatha et al., 2000; Amarsaikhan and Douglas, 2004). The preliminary classification represented with different degrees of intensity four main erosion features, namely, *inter-rill erosion*, *rill erosion*, *gullies* and *channel and bank erosion*, which were used for defining training areas (Ma et al., 2003).

The 50 georeferenced field observations (ground data) were collected during the dry season, contemporaneous to the acquisition of the four SPOT-5 multispectral bands. Field observation comprised the description of soil sites and surface dynamics. Point data were gathered from auger holes, minipits, and some full pits. Soil surface features such as topsoil crust colour, percentage cover of surface rock fragments, and vegetation type and percentage cover were determined (Rubio and Bochet, 1998). The false-colour composite (FCC) image and the topographical maps, along with the field observation, were then used to obtain the final erosion feature map using Gaussian maximum likelihood method.

Likewise, a visual classification was used in order to delineate the intensity of soil erosion on the photo mosaic for the period of 1961. Areas with similar intensity of water erosion process were delineated, distinguishing between areas with no visible signs of erosion, areas with inter-rill and rill erosion, and areas affected by gully erosion. It was determined that 9.3 km^2 of areas affected by inter-rill and rill erosion 55 years ago had become incised by deep gullies. This increase in gully density is related to land abandonment, to natural degradation of the soil, and to a lesser degree to change in vegetation cover and/or soil erodibility caused by agricultural practices. A description of the spatial distribution and intensity of the erosion types is given next.

3.4.6.1 *Mass movements*

On the steep slopes, many gullies and mass movements have occurred. These mass movements transport large amounts of sediment to the reservoir. The occurrence of these mass movements is related to stripped bedrock slope, a result of the present dry climatic conditions where soil formation is limited and all weathered rock is directly removed by mass wasting during intensive rainfall events.
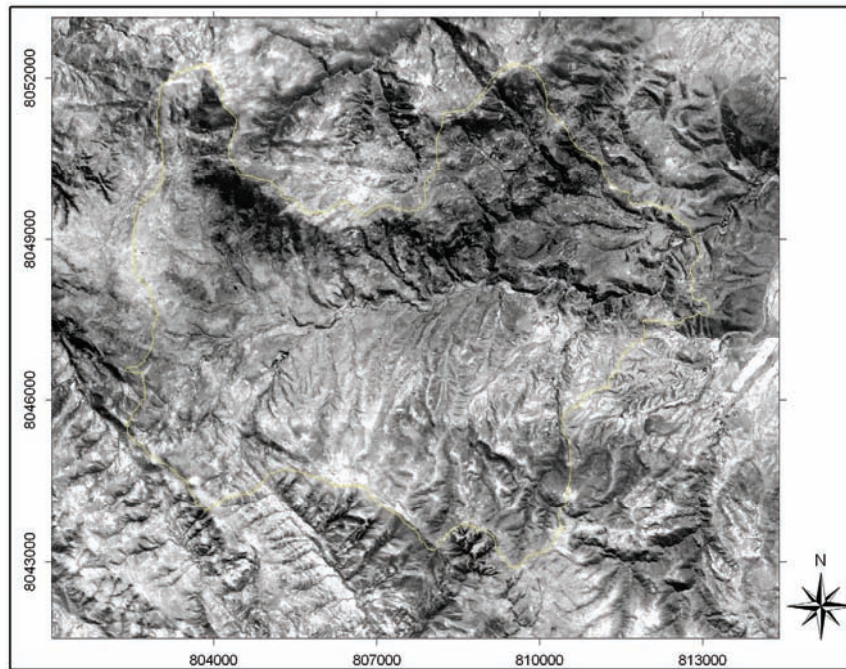
a)
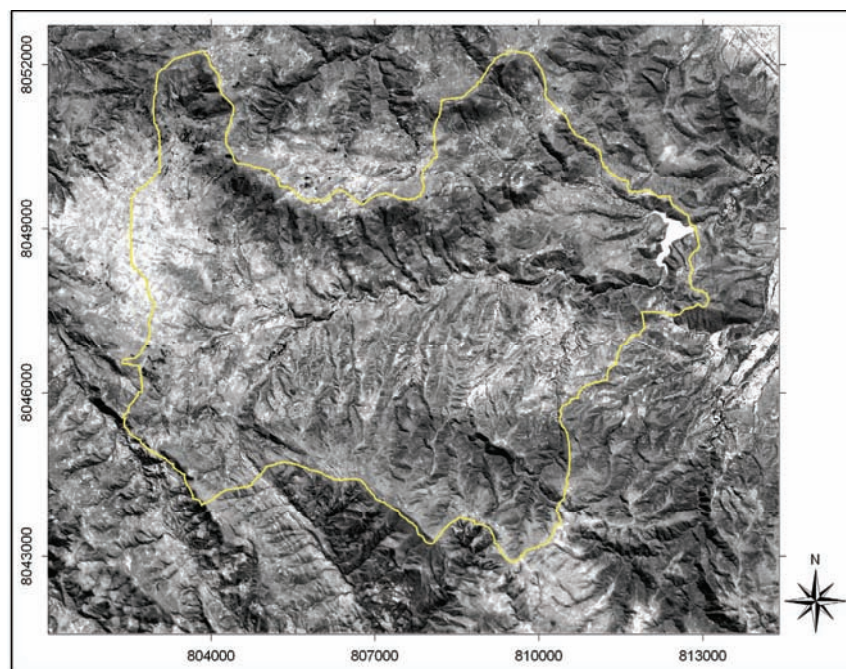
b)

Figure 3.10 *a*) Subset of the orthophoto covering the Laka-Laka catchment (1961), *b*) subset of the orthorectified panchromatic SPOT-5 in the catchment (2002)

3.4.6.2   Gullies

The differences in the characteristics of the gully systems are defined according to the lithological areas where they occur and the degree of gully wall retreat they present.

The presence of deep gullies intersecting steep slopes in the fluvio-lacustrine sediments is a common characteristic occurring along the south side of the Calicanto river. These sediments contain dispersive clays and are therefore easily eroded. Remnants of the slopes and terraces are constantly being eroded by slumping and subsequent headward retreat of the gullies (Martínez-Casasnovas et al., 2004). Moderate active gullies are more directly connected to the channel network. Stable gullies, on the other hand, are often situated on the upper parts of hills and do not have a direct connection to the channel network. Field observations have shown that most gullies do not change shape dramatically during single storms (Poesen et al., 2002). Many of the headcuts and gully sides are only active intermittently and none of them showed signs of rapid retreat.

3.4.6.3   Rills and diffusive wash

Rill and inter-rill erosion occurs in the upper steep slopes with a very high grazing density. Rills are found mostly on the steeper parts of cultivated fallow soils and in areas where surface runoff concentrates, such as in topographical depressions. Cropland downslope of fallow land seems more susceptible to rill erosion than other cropland areas. Fallow land produces significant amounts of surface runoff (Cerdan et al., 2002). The presence of surface stoniness and soil crust cover indicates areas where rill and inter-rill erosion are active processes. In most parts of the catchments (*e.g.,* footslopes and hills) where the threshold for resilience has been trespassed, the catchment has become very sensitive to rill and ephemeral gully erosion, which is translated into hillslopes being severely eroded (Vandekerckhove et al., 2000). Erosion features are less visible on the alluvial terraces and lacustrine plains. Ephemeral and active gullies along with slumps near the mountain fronts can be observed.

3.4.6.4   Erosion dynamic in the catchment

Based on the explanation provided in the preceding sections, it is possible to describe the model of erosion in the Laka-Laka catchment as follows:

- Gully systems have developed in different areas because of varying vegetation cover, soil properties, and responses to intense rainfall and intensity according to the topographical positions. Whereas on the vegetated upper and lower slopes most of the rainfall infiltrates and little runoff is produced, the strongly eroded footslopes produce large amounts of runoff. The middle slopes react immediately.

- Consequently, the middle slopes are regarded as transportation zones for runoff and sediments. When the runoff reaches the lower slopes, it will infiltrate; however, when the runoff drains into the gullies that cut through all topographical positions, the runoff and its sediment will finally reach the channels, and soil will be exported from the catchment.

- During extreme precipitation events, all topographical positions contribute directly to the main channels as Hortonian overland, even the vegetated lower slopes. In the case of such events, soil erosion takes place on a massive scale and can be regarded as the main landscape-forming process.

Figure 3.11 A typical soil profile in the catchment
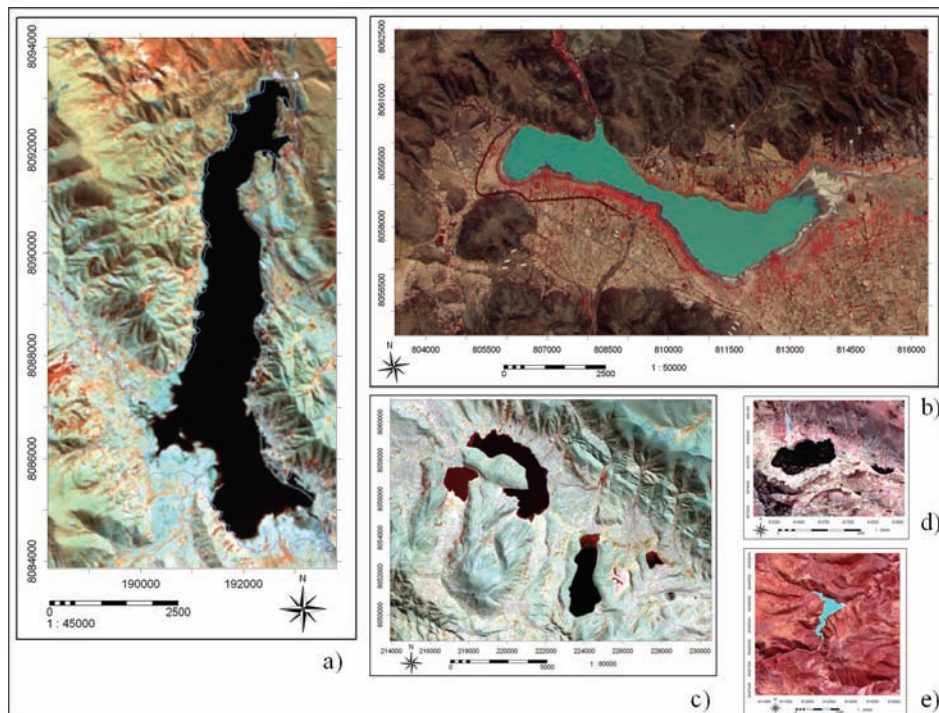
Figure 3.12 False-colour composite images: *a)* Corani reservoir, *b)* Angostura reservoir, *c)* Vacas lakes system, *d)* Larati lake, *e)* Laka-Laka reservoir

Soil losses during an extreme event, including the devastating power of hail impact on erosion, are many times higher than during more regular thunderstorms.

3.5 Reservoir and lakes

A number of lakes and reservoirs are found in the study area. They constitute one of the main sources of water supply for the main valleys and the city of Cochabamba. The lower, middle and upper valleys remain a predominantly agricultural region. Because of its low precipitation, a significant number of crops are irrigated, which contributes to the water requirements of the valley (Agash, 2003). The high volumes of water needed for irrigation and demanded by the large population make water resources management one of the key elements in the sustainable development of the valleys and the urban region. To deal with this situation, the construction of dams has been promoted, providing irrigation water for intensified crop production in some cases (*e.g.,* Angostura, Totora Q'ocha, Laka-Laka reservoirs), and supporting hydroelectric power generation in others (*e.g.,* Misicuni and Corani reservoirs).

3.5.1 Corani reservoir

The Corani reservoir is an artificial lake constructed at an elevation of 3,245 masl for hydroelectric power generation (Figure 3.12). The main river affluents to the reservoir are the *Corani, Kenko, Candelaria, Tablas, Tholamayu* and *Kayarani*. Downstream of the dam two operating plants are located: Corani and Santa Isabel. Further downstream, some important sites have been identified for potential future hydroelectric developments. Originally in 1966, the reservoir surface covered an area of about 1,140 ha, with a total volume of 82 Mm^3 (SGT, 1998).

In 1983, the dam and the spillway were raised to 5 m. At the same time, a tunnel 12 km long and 2 km of channels were constructed in order to engross the following water courses: *Pajchahuayco, Khentimayu, Rumichaca, Alisomayu* and *Cinturillas*. This system is called the *old Málaga* intake. The rain gauge installed at the Corani dam registered a total of 2,968 mm for the period 2003, exceeding the 48 years long-term annual mean precipitation of about 2,582 mm. Because of the strong shadow and rainfall gradient from NE to SW, the mean annual precipitation for the catchment is about 1,550 mm. The catchment area covers 298 km^2. Cropland, pastureland and forest are the most important land uses. Steep rolling uplands, with mountain ranges along the streams, and a humid regime are characteristics of this ecosystem.

3.5.2 Angostura reservoir

The Angostura reservoir is an artificial reservoir constructed at an elevation of 2,707 masl for irrigation purposes. It is located 17 km from the city of Cochabamba, along the old main road to Santa Cruz. The reservoir started to operate in 1947, with an initial capacity of 100 Mm^3. It reaches its maximum capacity at an elevation of 7.5 m. It is able to irrigate 5,800 ha distributed over three main units: south, central and north, all located in the middle valley of Cochabamba.

The tributaries to the Angostura reservoir are the *Sulty, Pocoata, Siches, Chaqui Mayu,* and *Laka-Laka* rivers, all forming the Upper Valley drainage basin of 1,992 km^2. The long-term mean precipitation at the Tarata meteorological station is 504 mm. Land use in this basin is primarily cropland, grasslands, shrublands and sparse forest, with areas

prone to erosion, especially in the mountainous areas. The topography varies from flat areas in the valley, floodplain and fans to very steep in the mountains and hills.

3.5.3 Laka-Laka reservoir

The small reservoir of Laka-Laka is located 3 km from Tarata town and 35 km from the city of Cochabamba. It consists of a *concrete gravity dam,* with a height of 31.5 m. The main tributaries are the Calicanto and Viscachani rivers. It was designed to irrigate 500 ha of agricultural fields with a discharge of 500 l s^{-1}, and to provide drinking water to Tarata and other neighbouring villages (5,000 inhabitants in total) at a design rate of 150 litres per person per day (LH-UMSS, 1994). The original capacity at normal level (2,805 masl) was estimated as 2.6 Mm^3, with a reservoir area of about 28.45 ha.

3.5.4 Lakes

The lake system of the region of *Vacas* is situated 65 km south of the city of Cochabamba. The altitude ranges from 3,120 to 3,340 masl, with varying topography and a cold subhumid climate. The lake system, characterized by an endorheic pattern, is formed by the *Parco Qocha, Jutuntuyo, Acero Qocha, Pilahuito* and *Khollpa Qocha* lakes. Owing to the lack of data on the original topography or previous bathymetric surveys, it was decided not to use these lakes in the present research.

Chapter 4

Regional-scale erosion modelling using global coarse-resolution satellite data and geodata

Chapter 4

Regional-scale erosion modelling using global coarse-resolution satellite data and geodata

4.1   Introduction

In the previous chapters, the importance of being able to estimate erosion rates from plot to continental scale has been shown extensively. Nevertheless, three additional reasons are provided to emphasize the importance of estimating soil erosion at larger regional scales. First, soil erosion has a range of environmental impacts, including loss of organic matter and soil nutrients, reduction of crop productivity and degradation of downstream water quality (Lal, 2001). The integrated impacts of erosion often reveal their importance only at a larger catchment or regional scale.

Secondly, effective control of soil erosion is a critical component of natural resource management if the aim is to approach sustainable agriculture and acceptable ecosystem integrity (Pimentel et al., 1995). Erosion maps at national, regional, basin and catchment scales are useful for guiding investment prioritization for effective remediation programmes if resources in those areas are limited and have to be spatially allocated with care (*i.e.,* predictions for Australia (Lu et al., 2001), Italy (van der Knijff et al., 2000), England (Brazier et al., 2001), France (Bissonnais et al., 2000) or continental estimates in Europe (Kirkby et al., 2004) and Africa (Zhang et al., 2002)).

Thirdly, to support estimates of soil erosion contributions and their impacts, the effects of changes in climatic conditions, vegetation and land use on soil erosion rates need to be better understood and assessed at wider basin, regional and even continental scales.

This chapter consequently focuses on large-scale modelling of water erosion processes, using the province of Cochabamba as the sample area. A general description of the setting and biophysical characteristics of the researched area was presented in the preceding chapter. The objective of this chapter is to assess the performance of five low data demanding models in their ability to predict spatial patterns and rates of soil erosion and deposition at the regional scale. Moreover, the use of global- and continental-scale remotely sensed climate, land cover and digital elevation data for regional erosion assessment is also evaluated.

4.2   Data and methods

All data used for this regional assessment were collected from public data servers. They present global environmental and satellite data products provided by space agencies, international organizations or research institutions. After screening the available datasets, it was decided to build and evaluate two modelling scenarios: a baseline (I) and a present-day scenario (II). The baseline scenario represented the International

Panel of Climate Change (IPCC) 30-year baseline climate period (1961 to 1990), commonly used as the starting point and reference for climate change research (IPCC, 1996). This strategy was found convenient at the provincial and national scales.

Table 4.1 Summary of information on the data sources used in the regional erosion modelling

Data	Resolution Space	Time	Acronym/ name	Source
Topography	1 km	n.a. [a]	HYDRO-1k	Global elevation derivative database http://lpdaac.usgs.gov/gtopo30/hydro/index.asp
Topography	30-90 m	2000 [b]	SRTM	Shuttle Radar Topographic Mission Data (SRTM) ftp://e0mss21u.ecs.nasa.gov/srtm/
Topography	15-30 m	2002 [b]	ASTER	Advanced Spaceborne Thermal Emission and Reflection Radiometer http://edcdaac.usgs.gov/dataproducts.asp
Topography	10-20 m	2002 [b]	SPOT-5	SPOT stereo pair data and DEM http://spotimage.com
Topography	5m	1961-1987 [b]	n.a.	Aerial photo coverage; also used for land cover Instituto Geografico Militar (IGM), Bolivia
Land cover	1.1 km [d]	1 day [c]	AVHRR	NOAA AVHRR satellite active archive system http://www.saa.noaa.gov/nsaa/products/welcome http://edcdaac.usgs.gov/1KM/comp10d.asp http://lpdaac.usgs.gov/glcc/sa_int.asp
Land cover	1 km	10 day [c]	SPOT –VGT (vegetation instrument)	Short Wave Infrared (SWIR), sensitive to soil and vegetation moisture content http://free.vgt.vito.be/ http://www.spot-vegetation.com/
Land cover	250 m	16 day [c]	MODIS	Medium Resolution Imaging spectrometer VNIR data http://edcdaac.usgs.gov/order.asp
Land cover	20-30 m	16 day [c]	Landsat-7 ETM	Landsat Thematic Mapper (+Enhanced) data http://glovis.usgs.gov
Land cover	15 m	5 day [c]	ASTER	Aster VNIR data http://edcdaac.usgs.gov/order.asp
Land cover	10-20 m	6 day [c]	SPOT-4 & 5	SPOT multispectral and panchromatic data http://sirius.spotimage.fr/anglais/welcome.htm
Precipitation	2.5-3.75 degrees	1900-1998	CRU-05	Global monthly precipitation dataset - Climatic Research Unit, UEA, UK http://www.cru.uea.ac.uk/cru/data/tmc.htm http://eos-webster.sr.unh.edu/SR/
Precipitation temperature	0.5-0.1 degrees	1930-1998	LBA CRU-CL 2.0	Large-scale Basin Experiment - Amazonia, LBA HYDRONET database; UNH, US http://www.sr.unh.edu http://beija-flor.ornl.gov/lba/
Precipitation	0.25 degree	1998-present	TRMM	Tropical Rainfall Measuring Mission data http://lake.nascom.nasa.gov/data/dataset/TRMM/ http://tsdis.gsfc.nasa.gov/tsdis/tsdis.html
Soil data	5 arc-minutes	n.a.	GSDTG	Global Soil Data Task Group dataset (IGBP-DIS) http://www.daac.ornl.gov/SOILS/igbp.html

(a) not applicable; (b) acquisition date; (c) theoretical revisit time; (d) horizontal resolution at nadir

The baseline scenario evaluation included the following data: (i) a 30-year time series of gridded average climate and precipitation dataset from the Climatic Research Unit – Average Climatology 2.0 (CRU-CL 2.0); (ii) one-year National Oceanic & Atmospheric Administration – Advanced Very High Resolution Radiometer (NOAA-AHVRR) derived 10-day composite normalized difference vegetation index (NDVI); (iii) the South America land cover map from the Land Process Distributed Active Archive Centre (LP DAAC); (iv) the HYDRO-1k, 1 km global DEM from the National Centre for Earth Resources Observation & Sciences (EROS); and (v) the global soil properties database from the International Geosphere and Biosphere Programme Data and Information System (IGBP-DIS).

The second present-day scenario evaluation included newly released continental-scale satellite data and geodata on South America: (i) a six-year period (1998 to 2003) of three-hourly and daily satellite rainfall data from the Tropical Rainfall Measuring Mission (TRMM); (ii) a six-year time series of NDVI imagery (1998 to 2003) from the SPOT-Vegetation instrument (SPOT-VGT); (iii) an up-to-date land cover map of South America from the Global Vegetation Monitoring Unit of the Joint Research Centre (JRC-GVT); (iv) 90 m resolution DEM from the Shuttle Radar Topography Mission (SRTM); and (v) a taxonomic soil unit map at scale 1:250,000 of Cochabamba province. Table 4.1 shows more details of the data sources.

All these data generally presented coarse resolutions and are commonly used in continental and global studies and large-scale analysis. After extracting the data from the databases, appropriate format conversions were applied wherever necessary and all layers were gridded to a 1 km scale resolution using georeferenced digital resampling techniques. All data were georeferenced in the universal transversal mercator (UTM) coordinate system (UTM zone 19, WGS-84 ellipsoid). The following sections introduce a concise description of the data used for deriving the erosion model input parameters.

4.2.1 Topographical data

Topography is one of the prime inputs to any erosion and hydrological model, since it defines the effect of gravity on the movement and flow of water and sediments. A number of DEMs are readily available today, with resolutions ranging from 30 arc-seconds to as high as 30 m. The elevation and derived topographical variables used in the baseline and present-day scenario evaluations were derived from two different spatial resolution sources, namely, HYDRO-1k and SRTM. HYDRO-1k is a geographical database developed to provide a comprehensive and consistent global coverage of topographically derived data at 1 km grid resolution. It includes streams, drainage basins and ancillary layers and was derived from the global 30 arc-second elevation data (GTOPO30).

For the second present-day scenario evaluation, the freely available 90 m or 3 arc-second spatial resolution SRTM data were used. The SRTM is a radar interferometry dataset derived from the Endeavour shuttle mission in February 2000, a joint project of the National Geospatial Intelligence Agency (NGIA) and the National Aeronautics and Space Administration (NASA). SRTM tiles were pre-processed to extract topographical parameters (*e.g.,* slope, upslope contributing area).

A characteristic feature of the unedited SRTM data is numerous data voids originating from a number of factors such as shadowing, layover or other radar-specific causes. Water surfaces generally produce very low radar backscatter and often result in noisy images. The surface of the DEM may thus be "speckled" with negative elevation values. To overcome this problem, missing elevation points were filled with values derived from the surrounding area by using the spline interpolation technique. While the patching procedure is suitable for repairing small closed areas of missing elevation data, it would not be an appropriate method for filling in missing data for large open-ended areas such as an entire missing valley or mountain range, which are sometimes encountered in the SRTM-DEM (Wrigth, 2002).

4.2.2 Parameter data related to land cover and vegetation

Land cover data assist in improving the representation of physical land processes such as erosion or hydrological processes. Land cover data have been successfully employed in studies of vegetation-atmosphere interactions, evaporation, transpiration and runoff (Loveland et al., 1999). Vegetation cover then plays an important role in erosion modelling. There is common acceptance that the rate of soil erosion is reduced exponentially as a function of vegetation cover. However, vegetation cover changes spatially and temporally, which makes it difficult to measure in the field, especially over large areas; hence, remote sensing is commonly applied in this situation.

4.2.2.1 Land cover

The 1 km resolution land cover characteristics database jointly developed by the U.S. Geological Survey (USGS)-EROS, the University of Nebraska-Lincoln (UNL) and the JRC of the European Commission (Brown et al., 1999) was used for the baseline scenario evaluation. An unsupervised land cover classification was first derived from the monthly composite of the AVHRR-NDVI time series imagery covering 1992 to 1993. For extensive post-classification, stratification was necessary to resolve the spectral temporal confusion between disparate land cover types (Belward et al., 1999).

A new land cover map of South America was launched by JRC in 2002 (Eva et al., 2002). This updated land cover map was used for the present-day scenario evaluation. This map uses satellite data from multiple sensors (*i.e.,* microwave and optical sensors on earth observing satellites (Along Track Scanning Radiometer (ATSR-2), SPOT-VGT, JERS-1 radar data, Operational Linescan System (OLS), GTOPO30)). Land cover is classified in more than 40 classes at a spatial resolution of 1 km.

4.2.2.2 NDVI

Temporal vegetation indices (*e.g.,* NDVI, LAI) for the baseline scenario evaluation were derived from NOAA-AVHRR satellite data (1.1 km resolution at nadir). AVHRR data can be retrieved on a daily basis, permitting high temporal resolution. Pre-processed 10-day composite AVHRR-NDVI images from the period 1992 to 1993 were converted to monthly NDVI values.

For the present-day scenario evaluation, SPOT-VGT 10-day composite NDVI time series, atmospherically and geometrically corrected for the period 1998 to 2003, were used. The vegetation instruments 1 and 2 (VGT1/VGT2) have been on board the SPOT-4 satellite since 1998 and 2002, respectively, and have enabled high temporal resolution NDVI production up to the present. The NDVI time series for Cochabamba province was clipped from a whole file set of zipped files downloaded from the server using the CROP-VGT interface (Griguolo, 2003). These NDVI time series were normalized to NDVI values using the equation below (SPOT, 2000):

$$NDVI = a \times DN + b \qquad \qquad \text{(Eq 4.1)}$$

where NDVI is the Real NDVI with values ranging from -1 to 1, DN is the digital number per pixel, a is a constant with a value of 0.004 and b is another constant with a value of -0.1.

4.2.3   Climate data

Owing to its high variability and spatial heterogeneity relative to other climatological variables, rainfall is one of the more difficult variables to measure and monitor at scales required for studying land surface processes. Much of the research into techniques for estimating areal precipitation and related climatological parameters at larger scales relies on instruments such as geostationary satellites (*e.g.,* Geostationary Operational Environmental Satellite (GOES), Meteosat), passive microwave techniques (*e.g.,* Special Sensor Microwave Imager (SSM/I)), radar techniques (Tropical Rainfall Measuring Mission Precipitation Radar (TRMM PR)) and indirect techniques (*e.g.,* GOES Precipitation Index (GPI)).

Complete spatial representations of surface climate are currently available with global coverage on internet data servers. For evaluation of the baseline scenario, the climatic grid data from the CRU-CL 2.0 dataset (New et al., 2002) was used. This dataset includes seven global meteorological variables, namely, precipitation, wet day frequency, temperature range, relative humidity, sunshine duration, ground frost frequency and wind speed. These data (10' latitude/longitude grid) were interpolated from the datasets of station means for the period 1961 to 1990. Meteorological ground station data (precipitation and temperature) from most of the existing meteorological stations were used to validate the CRU-CL 2.0 data for the Cochabamba region. This resulted in the historical long-term 30-year monthly averages (1961 to 1990). This period is commonly referred to as the "baseline scenario period" for climate change studies (IPCC, 1996).

For the present-day scenario evaluation, the high temporal resolution satellite dataset for surface climate over global land areas referred to as TRMM was used. TRMM is a spaceborne large-scale precipitation data series that holds monthly (TRMM V6-3B43) and three-hourly (TRMM-V6-3B42) precipitation gridded data at 0.25 degree spatial resolution for the period 1998 to present (TRMM, 1998).

a)   *b)*
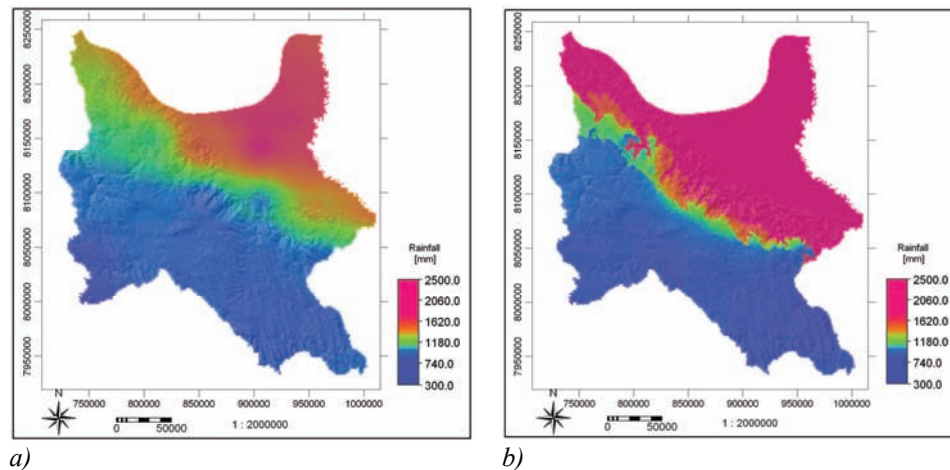
Figure 4.1 Spatial rainfall distribution: *a)* long-term annual rainfall (1961 to 1990) from CRU-CL 2.0, *b)* annual rainfall average using TRMM (1998 to 2003)

In order to assess the quality of the CRU-CL 2.0 and TRMM precipitation grids, the annual estimates were compared with the annual precipitation grid derived from 121 meteorological ground station data points by using the ordinary kriging method. As in the case of many less developed countries, time series of climatological variables are not available on a long-term basis; therefore the only period with any consistency in the data in Bolivia is from 1960 to 1979.

The analysis shows that in the semi-arid Andean region precipitation values are positively correlated with CRU-CL 2.0 and TRMM values with a Pearson coefficient of determination (R^2) of 0.65 and 0.70 respectively (Figure 4.1). However, considerable underestimation was observed for the tropical areas where annual rainfalls can easily reach 3,000 mm and more, as against those derived by the satellite having averages of 2,300 mm for TRMM (3B43-V6), 2,100 mm for TRMM (3B42-V6) and 2,400 mm for CRU-CL 2.0.

4.2.4 Soil data

For use at continental and regional scales, only three large-scale soil databases and maps exist: (i) a 1:5 million scale FAO-UNESCO Soil Map of the World and derived soil properties (FAO, 2003), (ii) a 1:1 million scale FAO Land and Water, Soil and Terrain database for Latin America and the Caribbean (FAO, 1998), and (iii) 1:5 million global soil data products (IGBP-DIS, 2000). The soil data used in the baseline evaluation were derived from the IGBP-DIS CD-ROM. This global soil database contains data on soil properties and soil units on a 5 arc-minutes grid. The soil data system enabled soil information and maps for Cochabamba to be generated at resolutions adopted for the different erosion models. Derived surfaces of organic carbon density, nutrient status, water-holding capacity and heat capacity are provided for modelling and inventory purposes.

For the present-day scenario evaluation, the 1:250,000 soil unit map was used, as prepared by the Regional Secretary of Agriculture in 1990 (Jette and Rojas, 1998) and updated by the Center for Aerospace Survey for Natural Resources Management (CLAS, 2003). Eighteen soil classes were identified, according to main terrain and soil characteristics such as texture, chemical composition, lithology and land cover.

4.3 Distributed erosion modelling

Individual GIS layers were built for each erosion model input parameter (*e.g.,* climate, soil, relief, vegetation cover) and combined using geospatial modelling procedures in ILWIS® (Koolhoven et al., 2004) to predict soil losses in the spatial and temporal domains. The spatial output grid cell resolution was set to 1 km. Temporal data resolution was set to a monthly time step. Monthly soil loss results were then aggregated to annual values. The datasets of the two baseline and present scenarios were used as grid layer inputs for the five models described in Chapter 2: (i) the RUSLE-3D model (Renard et al., 1997; Mitasova, 2000), with a modified *LS*-factor (Moore and Wilson, 1992; Desmet and Govers, 1996b); (ii) the Thornes model (Thornes, 1985; Thornes, 1990); (iii) the Stream Power Law (SPL) model for fluvial erosion (Finlayson et al., 2002b), (iv) the Modified Morgan, Morgan and Finney (MMMF) model (Morgan et al., 1984; de Jong et al., 1999); and (v) the Unit Stream Power Erosion and Deposition (USPED) model (Mitasova, 1999). The following

sections provide an outline of how the erosion parameters were derived, including an assessment of their utility for regional erosion monitoring.
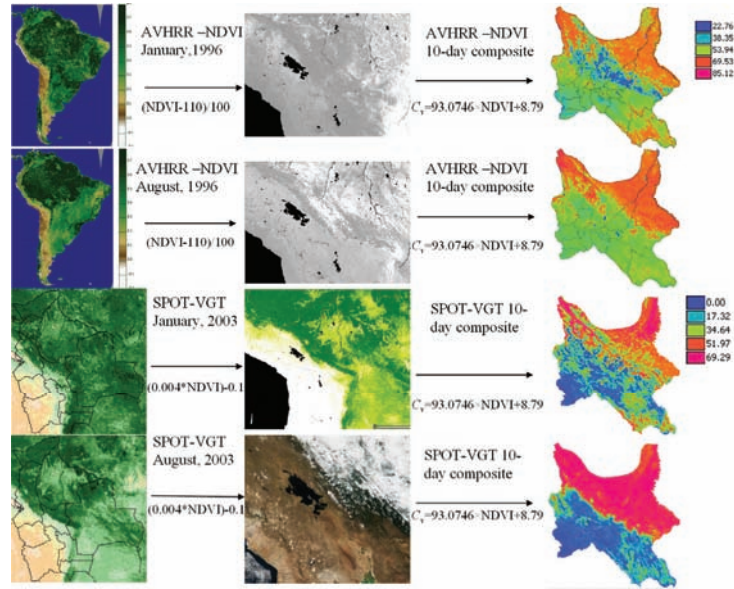
Figure 4.2 Use of NOAA–AVHRR and SPOT-VGT satellite data (10-day composite NDVI) for the land cover percentage determination over Cochabamba
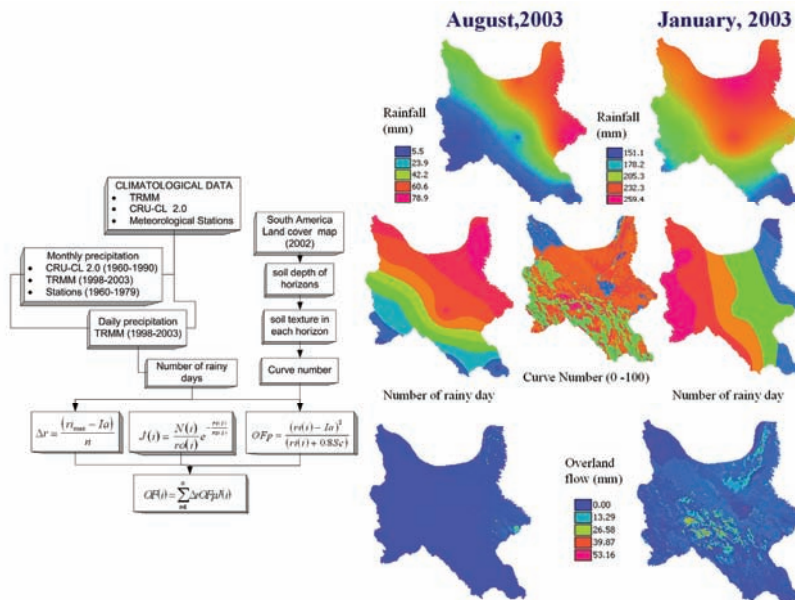
Figure 4.3 Spatial distribution of monthly runoff using land cover, rainfall and soil satellite data

79

4.3.1 Vegetation parameters

The vegetation-related parameters, which account for the protection given by the canopy cover and ground cover, have to be considered when attempting to model erosion at the regional scale. Accurate information about the spatial distribution of the fraction of vegetation cover types is hence of utmost importance. Here, the processed monthly NDVI time series from AVHRR and SPOT imagery is used as an input for the regression relationship developed by Zhang et al. (2002), who related the NDVI values to the fraction of vegetation cover v_c [%] using the equation:

$$v_c = 93.07466 \times NDVI + 8.79815 \qquad \textit{(Eq 4.2)}$$

Figure 4.2 illustrates the use of the NOAA-AVHRR and SPOT-Vegetation data for estimating the fraction of vegetation cover in the study area. For most land uses except croplands, mainly seasonal or perennial vegetation and quasi-permanent soil surface cover control the factor *C*. For representing the effect of land use and land cover, the RUSLE-3D, USPED and MMMF models use the factor *C* to express the effect of vegetation and surface cover.

Seasonal changes in the land cover and derived parameters may be important. In perennial crops such as coffee and banana stands, these parameters may be assumed to be fairly constant, but for annual agricultural crops this assumption is questionable. However, at this large assessment scale, crop management practices such as intercropping and the lack of well-defined crop calendars make the change in land cover characteristics in the season extremely difficult to characterize. Seasonality of the factor *C* was therefore not considered further at the regional scale, and annual values were employed for the simulation. This approach was judged reasonable, taking into account that four out of the five models (the Thornes model was the exception) were run on an annual time step.

The value of the *C* factor is the average soil loss ratio weighted by the erosivity distribution of rainfall during the year. Obtaining most sub-factors needed to evaluate the soil-loss ratio or *C* factor values is unfeasible at the 1 km cell size. Therefore, the effect of vegetation was evaluated considering only vegetation canopy effect, using the vegetation fraction derived from the NDVI. Referenced *C* values were crossed with literature values, relating generalized land use types to annual *C* factor values (*e.g.,* USDA Agricultural Handbook 703 (Renard et al., 1997)) to obtain average values for the *C* factor (see Table 4.2).

It is admitted that this regional *C* factor evaluation approach used in the initial stages of this research (Saavedra and Mannaerts, 2003b) and prior to the main field research campaign is only approximate. More extensive ground validation is needed to derive appropriate relationships between vegetation and surface cover effects on erosion that are applicable to large spatial scales.

4.3.2 Soil parameters

Information required to determine the soil erodibility or *K* factor and related soil erosion parameters (*e.g., B_d, MS, K_s.*) for the baseline scenario were derived from the IGBP-DIS soil data products (IGBP-DIS, 2000). The soil texture and organic matter content of topsoil (0 to 30 cm) were used to calculate the *K* factor at 1 km cell size.

Table 4.2 Land use data input for the erosion models: *HC* is the hydrological soil conditions, *C* is the cover management factor, R_d [m] is the root depth, E_t/E_o is the ratio of actual to potential evapotranspiration, P_i is the percentage of rainfall interception

Land cover	HC	C	R_d	E_t/E_o	P_i
Agriculture-intensive	Poor	0.1	0.15	0.67	26
Barren / bare soil	Poor	1	0.05	1	5
Closed deciduous forest	Poor	0.01	0.2	0.9	35
Closed evergreen tropical forest	Good	0.001	0.21	0.91	37
Closed montane grasslands	Poor	0.09	0.19	0.85	31
Closed semi-deciduous forest	Poor	0.03	0.205	0.89	32
Closed shrublands	Poor	0.04	0.18	0.8	30
Closed steppe grasslands	Fair	0.06	0.17	0.81	28
Desert	Poor	1	0.055	0.05	5
Grass savannah	Poor	0.011	0.14	1	35
Mangroves	Poor	0	0.14	1	40
Montane forests 500-1000 m - dense evergreen	Fair	0.089	0.13	0.95	36
Montane forests 500-1000 m - open evergreen	Poor	0.09	0.135	0.94	35.9
Montane forests 500-1000 m - closed deciduous	Fair	0.091	0.136	0.93	35.8
Montane forests 500-1000 m - closed semi-deciduous	Poor	0.092	0.137	0.92	35.7
Montane forests 500-1000 m - transition forest	Poor	0.093	0.138	0.91	35.5
Montane forests >1000 m closed semi-deciduous	Poor	0.095	0.139	0.89	35.4
Montane forests >1000 m dense evergreen	Good	0.096	0.125	0.9	35.6
Montane forests >1000 m open evergreen	Fair	0.097	0.123	0.895	35.3
Montane forests >1000 m transition forest	Poor	0.098	0.121	0.88	35.2
Montane forests >1000 m closed deciduous	Poor	0.099	0.12	0.897	35.1
Mosaic agriculture / degraded forests	Poor	0.11	0.122	0.7	26
Mosaic agriculture / degraded vegetation	Poor	0.12	0.111	0.75	25.5
Open evergreen tropical forest	Fair	0.001	0.18	0.93	36.1
Open montane grasslands	Poor	0.13	0.13	0.85	30
Open shrublands	Poor	0.14	0.12	0.82	29.5
Open steppe grasslands	Fair	0.15	0.11	0.81	28
Periodically flooded savannah	Poor	0	0.2	0.9	36
Permanent snow / ice	Poor	1	0.2	1	40
Semi-deciduous transition forest	Poor	0.145	0.15	0.9	34
Shrub savannah	Fair	0.125	0.13	0.89	30
Sparse desertic steppe shrub / grasslands	Poor	0.5	0.11	1	5
Urban	Poor	0	0	1	0
Water bodies	Poor	0	0	1	0

Table 4.3 Soil input data for the erosion models: *MS* [weight %] is the soil moisture, B_d [gr cm^{-3}] is the bulk density, K_s [cm hr^{-1}] is the hydraulic conductivity, *HSG* is the hydrological soil group, K_m [g J^{-1}] is the soil detachability index and *K* is the soil erodibility factor according the U.S. customary and international system units (SI)

Soil unit	Texture	MS	B_d	K_s	HSG	K_m	K [USA]	K [SI]
Alfisol	Sandy clay	0.28	1.27	0.3	Group D	0.3	0.15	0.0197
Andisol	Silt loam	0.25	1.36	1.71	Group B	0.9	0.55	0.0725
Entisol	Sandy loam	0.276	1.41	2.01	Group A	0.7	0.3	0.0395
Entisol, Alfisol	Sandy clay loam	0.26	1.35	0.34	Group C	0.1	0.18	0.024
Inceptisol, Alfisol, Vertisol	Silty clay	0.35	1.24	0.25	Group D	0.5	0.28	0.037
Entisol, Inceptisol	Loamy sand	0.16	1.45	3.61	Group A	0.3	0.26	0.0343
Entisol, Inceptisol, Alfisol	Loam	0.23	1.36	0.83	Group B	0.8	0.36	0.0474
Entisol, Inceptisol, Alfisol, Vertisol	Silty clay loam	0.33	1.25	0.36	Group D	0.8	0.2	0.0264
Entisol, Inceptisol, Histosol	Silt	0.3	1.38	3.05	Group B	1	0.6	0.079
Entisol, Inceptisol, Ultisol	Silt loam	0.25	1.36	1.95	Group B	0.9	0.55	0.0725
Entisol, Andisol	Sandy loam	0.275	1.39	2.02	Group A	0.7	0.36	0.0474
Histosol	Loam	0.24	1.35	0.85	Group B	0.8	0.38	0.05
Inceptisol	Silt loam	0.25	1.37	1.75	Group B	0.9	0.55	0.0725
Inceptisol, Alfisol	Clay loam	0.35	1.26	0.35	Group D	0.7	0.3	0.04
Inceptisol, Alfisol, Ultisol	Sandy clay loam	0.26	1.35	0.35	Group D	0.1	0.2	0.0264
Inceptisol, Ultisol	Loam	0.23	1.37	0.83	Group B	0.8	0.39	0.051
Ultisol	Clay loam	0.35	1.25	0.35	Group D	0.7	0.32	0.0422
Vertisol	Clay	0.45	1.15	0.15	Group D	0.05	0.12	0.0159

For the present-day scenario, a recently published regional soil taxonomy map produced by CLAS (2003) enabled the soil erodibility to be estimated based on the RUSLE model equations (Eq. 2.12). The soil detachability index K_m for the MMMF model was obtained from literature (Morgan et al., 1998; Morgan, 2001), using the topsoil textures (Table 4.3). Soil moisture at field capacity MS and topsoil bulk densities B_d were also derived, using literature, from comparable soils in South America (Yang et al., 2003).

4.3.3   Topographical parameters

Slope steepness, slope length, and upstream contributing area are fundamental input requirements for most soil erosion models. These inputs can be derived from a DEM within an appropriate GIS environment. After pre-processing of the DTMs (*i.e.,* HYDRO-1k, SRTM), the D8 steepest decent flow routing algorithm (Jenson and Domingue, 1988) was applied to determine the upstream contributing areas. This algorithm was used in spite of criticism (*i.e.*, it permits flow only in one direction, fails to adequately represent divergent flow over convex slopes, and may lead to bias in the flow path orientation compared with multiple flow algorithms) (Tarboton, 1997; Schauble, 2003).

The selection of D8 was based on the consideration of the DEM spatial resolution (1 km); if the multiple flow algorithm was chosen, some false topographical artefacts may have been created. Next, a three-dimensional analysis of the terrain surface for an optimized calculation of the $LS_{(r)}$ by using Eq 2.13 and Eq 2.16 was implemented. By doing so, other than parallel patterns of sediment flow lines that may actually be converging or diverging from the given computational cell were taken into account. These topographical parameters are computed from the first- and second-order derivatives of terrain surface approximated by regularized spline with tension (Mitasova et al., 1996).

4.3.4   Hydrological parameters

Overland flow is a variable of prime importance in water-induced erosion processes. Although the impact of raindrops detaches soil particles, it is flowing water that transports the detached soil particles to areas of concentrated flow and, depending on the sediment load and the transport capacity of the flow, detaches or re-entrains previously detached particles or deposits particles being transported. Runoff occurs on hillslopes when surface depression storage and either soil moisture storage, in the case of prolonged rain, or the infiltration capacity of the soil, with intense rain, is exceeded (Morgan, 1995).

The rainfall-runoff process is believed to be highly nonlinear, time varying, spatially distributed and not easily described by simple models. Two major approaches (empirical and physically based) are used nowadays. Considering the data available, a distributed remote sensing approach, based on a modification of the SCS Curve Number model (SCS, 1972) proposed by Zhang et al. (2002), was chosen for estimating spatial overland flow at a monthly time step (see Figure 4.3). In order to implement the hydrological submodel, daily rainfall data are used. The model assumes an exponential distribution of daily rainfall depths and a theoretical maximum daily rainfall amount, which when added yield a probabilistic estimate of monthly runoff volumes (Eq 2.28).

When using the SPL model, Finlayson and Montgomery (2003) proposed the use of the upslope contributing area as a proxy for discharge, so that approximate estimates of monthly and annual discharge were generated by combining the runoff volume map with the flow accumulation map, as expressed in Eq 2.30.

4.4   Results and discussion

4.4.1   Spatial distribution and rates of erosion and deposition: model comparison

4.4.1.1 *Baseline scenario evaluation*

The soil loss values estimated by each model were grouped into five erosion intensity classes, using a frequency distribution analysis. The spatial distribution patterns of the different erosion intensity classes of the baseline scenario are shown in Figure 4.4.
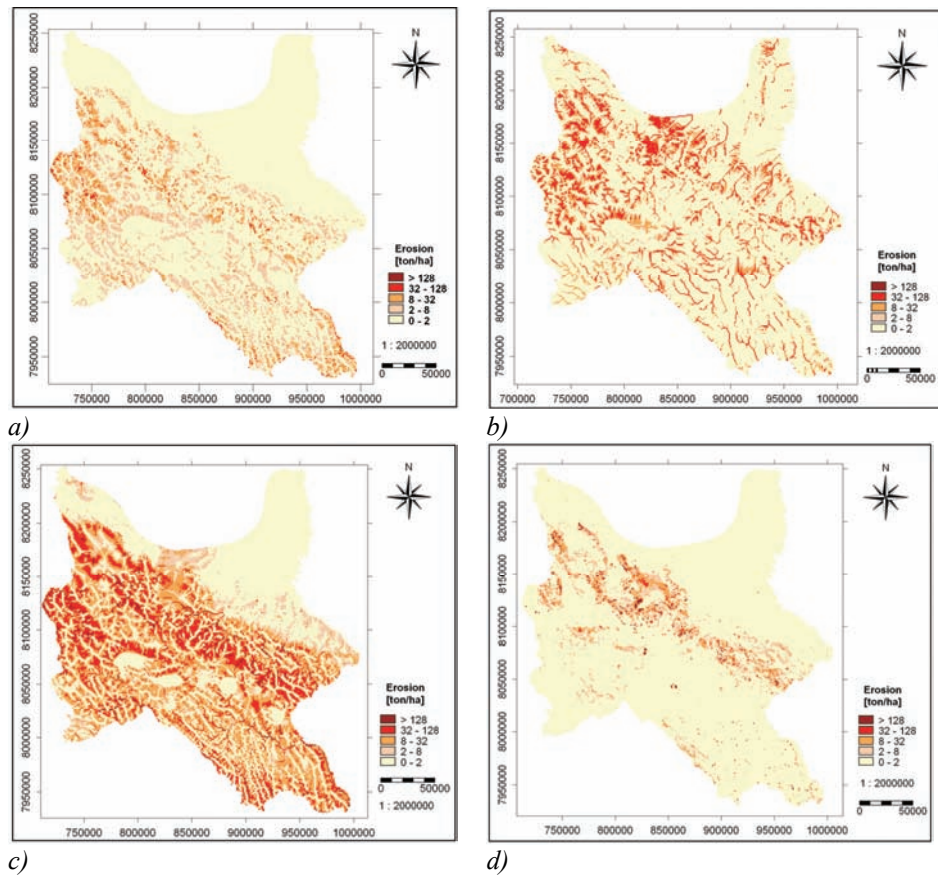
Figure 4.4 Spatial distribution of soil loss and predicted erosion rates in the baseline scenario evaluation: *a)* RUSLE-3D, *b)* MMMF, *c)* SPL, *d)* THORNES
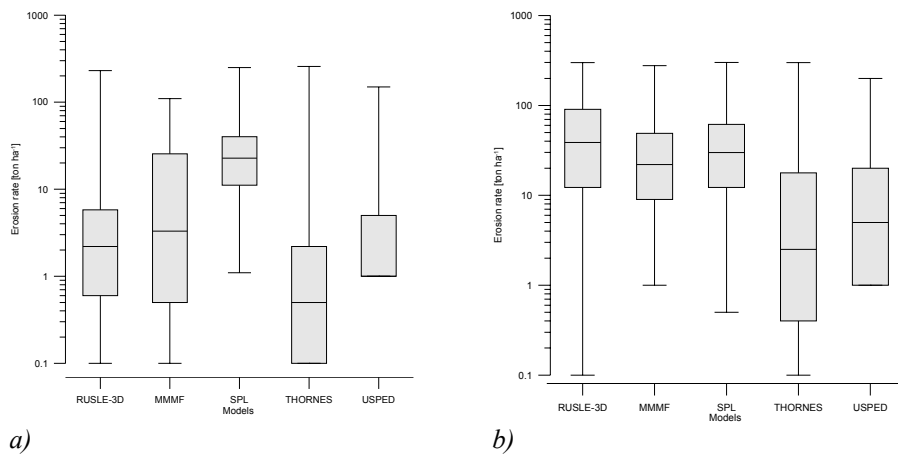
Figure 4.5 Box-plot of the erosion rate estimated by the models: *a)* baseline scenario evaluation, *b)* present-day scenario evaluation

a)

b)

c)

d)
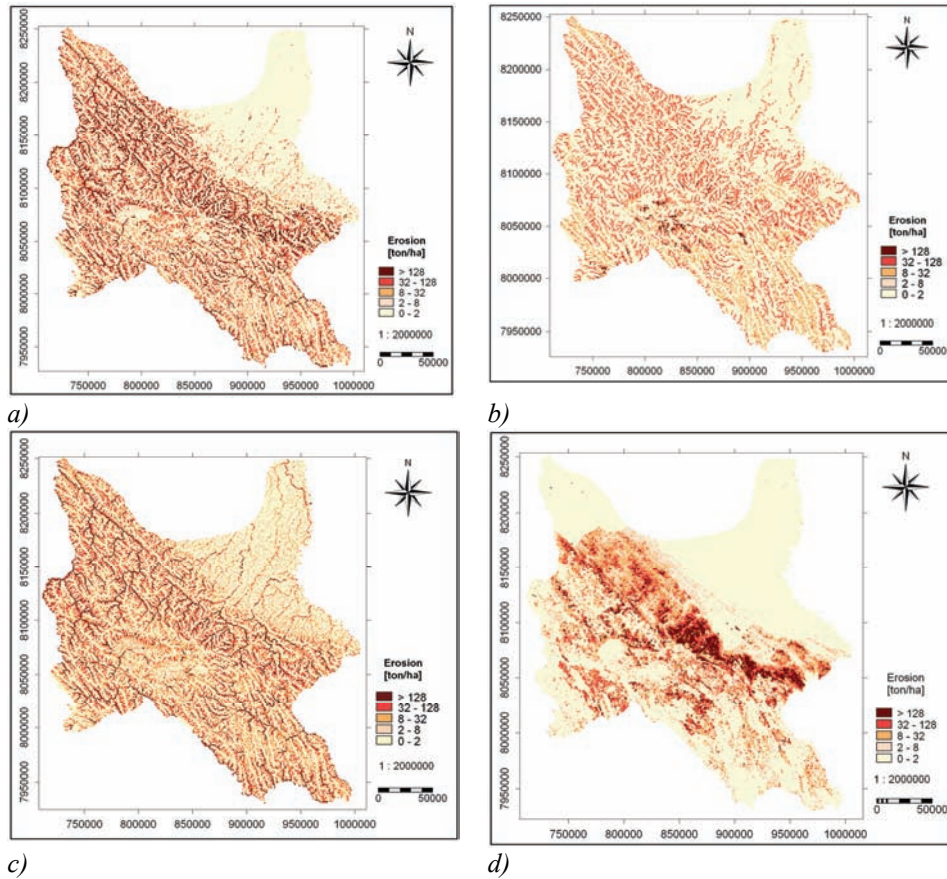
Figure 4.6 Spatial distribution of soil erosion and predicted soil loss rates in the present-day scenario evaluation: *a)* RUSLE-3D, *b)* MMMF, *c)* SPL, *d)* THORNES

Table 4.4 Area of different erosion classes in Cochabamba according to the baseline scenario evaluation

N	Rate of erosion [ton ha^{-1}]	Erosion risk class	RUSLE-3D		MMMF		SPL		THORNES		USPED	
			Area [km^2]	Area [%]	Area [km^2]	Area [%]	Area [km^2]	Area [%]	Area [km^2]	Area [%]	Area [km^2]	Area [%]
1	0-2	Low	40521	74.6	40111	74.3	25927	47.9	47353	87.6	31099	57.4
2	2-8	Medium	9000	16.9	4131	7.6	4388	8.1	4030	7.4	4544	8.4
3	8-32	High	4050	7.5	4229	7.8	13557	25.1	1961	3.6	3796	7
4	32-128	Very high	505	0.9	5629	10.4	9459	17.5	491	0.9	2075	3.7
5	>128	Extreme	24	0.04	0	0	769	1.3	265	0.5	369	0.7
6		Deposition									12217	22.8
Total			54100	100	54100	100	54100	100	54100	100	54100	100

85

The highest rates of erosion are found along the Eastern Andean Cordillera (*e.g.,* the high mountains and the mountain ranges) in the western part of the province, while lower erosion values are found in the tropic and subhumid region. Predicted soil loss rates obtained with the five models range from 0 to 260 ton ha^{-1} yr^{-1}, or a range of [0 - 26,000 ton km^2 yr^{-1}], and are shown in Figure 4.5.

The highest annual denudation for the 54,100 km^2 region representing Cochabamba province, according to the five model predictions, is provided by the SPL [9.4×10^7 ton yr^{-1}], while the lowest is given by the RUSLE-3D [1.4×10^7 ton yr^{-1}] model. Likewise, the highest average annual estimated erosion rate is provided by the SPL [17.3 ton ha^{-1} yr^{-1}] and the lowest by the RUSLE-3D [2.5 ton ha^{-1} yr^{-1}] model. Table 4.4 relates the erosion intensities obtained by the different models to the percentage area that is affected. If a pixel with a soil loss rate below 2 ton ha^{-1} yr^{-1} is defined as low erosion, more than 128 ton ha^{-1}yr^{-1} is defined as extreme, and in between as medium, high and very high. It is estimated that about 68.4% of the province experiences low erosion, 10.4% faces medium erosion, whereas 12%, 7.7% and 1.5% face high, very high and extreme erosion, respectively.

Based on a qualitative field verification of the erosion model outputs in the region using a rapid georeferenced erosion appraisal approach, the reliability of the model predictions was verified in the first instance. From the analysis, it is concluded that the model predictions using the baseline scenario data in absolute and qualitative terms should be categorized as ranging from poor to fair. In terms of relative spatial patterns of erosion, the spatial prediction provided by the MMMF and SPL can be considered acceptable.

4.4.1.2 *Present-day scenario evaluation*

Research by Thieken et al. (1999), Grimm *et al.* (2002), van Rompaey et al. (2003c) and Van Oost (2005) concludes that erosion model predictions perform better when high-resolution input data are used. The data used for the present-day scenario evaluation correspond to more recent continental and global satellite data available. Hence, improvements in the accuracy of mapping spatial patterns could be expected when using the present-day scenario evaluation data. Accordingly, erosion (and deposition for the USPED model) estimates from each model were regrouped into five erosion intensity classes and their spatial distribution patterns are shown in Figure 4.6. Field verification indicated that the spatial erosion patterns obtained with the present-day scenario data were more consistent with reality than the baseline scenario evaluation.

From the aggregated time series of erosion maps derived for the period 1998 to 2003, it is predicted that on average for all the models about 1.0×10^8 tonnes of soil are mobilized annually by rainfall-induced erosion across the province, with an annual average erosion rate of 19 ton ha^{-1} yr^{-1} or 1,900 ton km^{-2} yr^{-1}. This is almost twice as high as the previous estimation using the baseline data scenario (Saavedra and Mannaerts, 2003b). Accordingly, the highest annual denudation is provided by the SPL model [1.4×10^8 tonnes], whereas the lowest is given by the MMMF [0.6×10^8 tonnes]. Likewise, the highest average predicted erosion rate is provided by the SPL [27 ton ha^{-1}], whereas the MMMF [11.2 ton ha^{-1}] gives the lowest estimate.
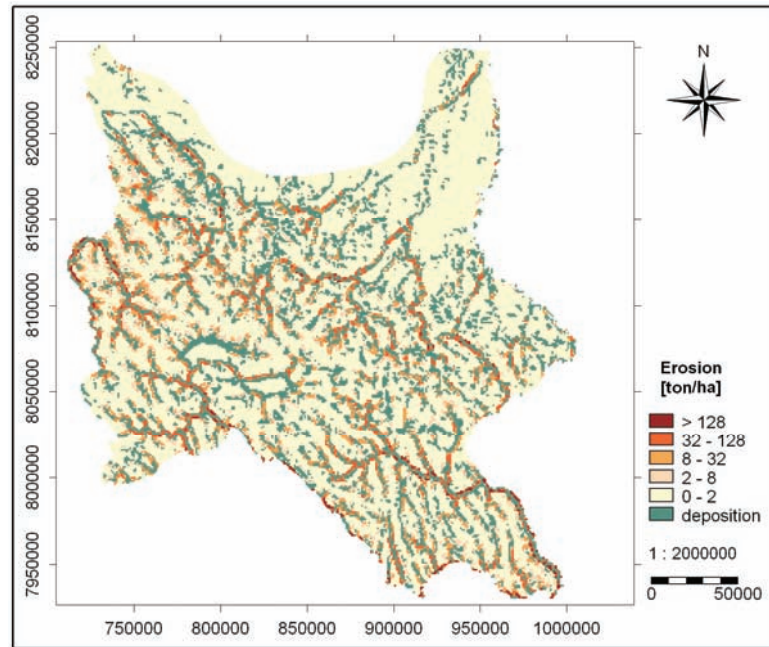
a)
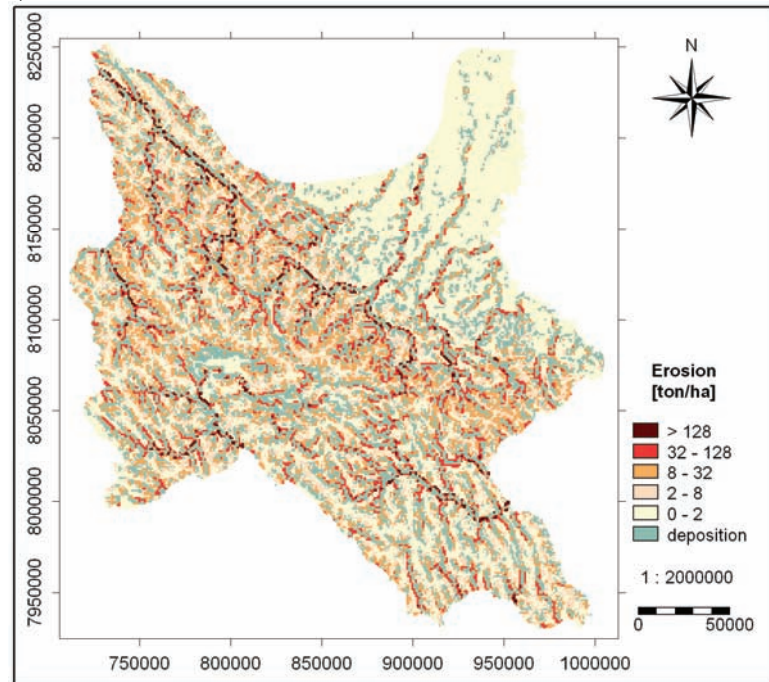
b)

Figure 4.7 Comparing the spatial pattern and rates of soil loss predicted by the USPED model using the baseline and present-day scenario data

Consequently, it is predicted that on average about 56% of the province experiences low erosion, whereas 10% of the area faces a medium soil loss. The proportion of the area with high, very high and extreme intensity of erosion is 15%, 13% and 6%, respectively. Overall, 19% of the area is eroded at a rate greater than 30 ton ha^{-1} yr^{-1}, considered the continental average rate (Guyot et al., 1990; Aalto et al., In press), showing the potential to target priority regions and areas for erosion control measures or programmes in the province.

From the monthly estimates provided by the Thornes model, it is evident that most of the erosion occurs at the end of the dry season, when a low vegetation cover coincides with high rainfall intensity. All the model predictions show that the Andean region presents areas with high erosion rates because it is subject to long dry periods, followed by heavy bursts of erosive rainfalls falling on steep bare slopes with fragile and thin soils. In contrast, the sub-Andean lowlands and floodplain regions present low soil loss rates, owing to the very low energy gradients for erosion in combination with a high perennial vegetation cover.

Under any given rainfall regime, the maps indicate clearly that the reduction of protective ground cover increases the risk of soil losses. Soil loss distributions appear rather well delineated and the pixels containing large values of soil erosion correspond to severely degraded areas on the ground. In fact, the multitemporal dataset of the SPOT-VGT images (1998 to 2003) covering the phenological vegetation cycles enabled the identification of areas where the density of vegetation is very low or absent.

Although the reliability of the predicted spatial erosion patterns in the present-day scenario evaluation across the province is significantly improved, soil loss estimates for the Andean region are still only fair in terms of absolute values.

The differences between the two scenario evaluations clearly indicate that errors, reliability and uncertainty of the modelling results are quite dependent on the space-time resolutions and quality of the input data, besides the model representations. A very important source of uncertainty in the predictions is related to the soil parameters extracted from the soil taxonomy map (*i.e.,* texture, erodibility, etc). The spatial resolution of this map is far too low or, in other words, the generalization in this soil map is far too high to represent terrain and soil variability in susceptibility to erosion. For those models using estimates of runoff volumes and runoff rates (*i.e.,* the Morgan and Thornes models), another limitation may be related to the algorithms used for the estimation of overland flow and runoff, (*i.e.,* the frequency distribution of storm rainfalls (Kirkby et al., 2000) and the fact that important sediment transport processes are not explicitly included. High-frequency rainfall events are crucial for generating overland flow; however, their effect on the long-term (*e.g.,* seasonal or continuous) prediction is reduced by using the exponential frequency distribution within each month.

Furthermore, additional studies address the need for using high-resolution DEMs for a better estimation of soil loss rates. It has been extensively demonstrated that the mean $LS_{(r)}$ and the mean erosion rates vary with a factor of three to six when a 1 km DEM (HYDRO-1k) is used as against a 90 m DEM such as the SRTM topographical dataset.

At coarser grid resolutions, the mean slope decreases significantly. The maximum grid cell slope gradient corresponding to a 90 m DEM in the study area is over 100%, whereas the maximum slope is equal to 55% if a 1 km DEM is used (Figures 4.8 and 4.9). These results clearly show that the $LS_{(r)}$ and the total soil loss are also strongly influenced by the quality and resolution of the DEM database (Figure 4.7).
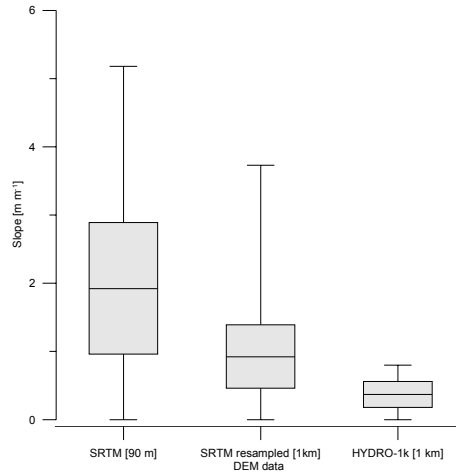
Figure 4.8 Box-plot of slope gradient variability for different DEM data

a)   *b)*
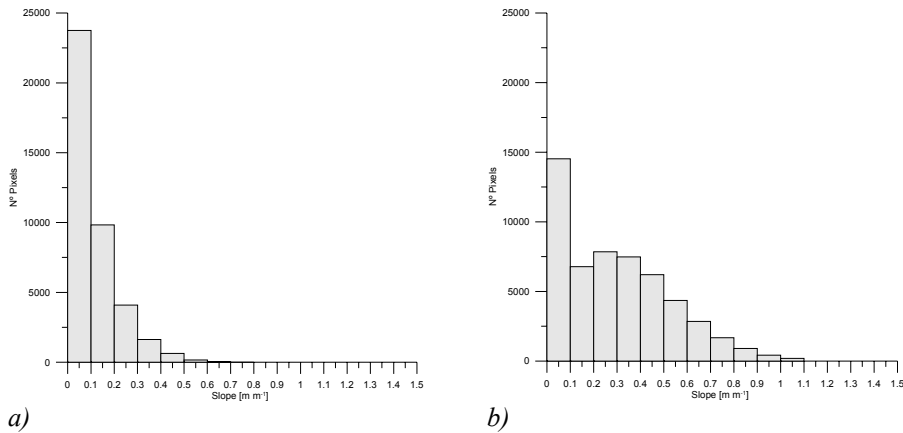
Figure 4.9 DEM histogram: a) HYDRO-1k, b) SRTM resampled to 1 km cell size

Finally, all the five selected models use a lumped hybrid representation of the major erosion process on land surfaces. Some model concepts were derived from experimental inter-rill and rill erosion data. Although inclusion of flow accumulation algorithms for the evaluation of runoff or slope lengths adds a representation of linear erosion processes (*e.g.,* gullies, small channels) to the models, no explicit gully erosion or mass wasting procedures are included in the five model approaches used. Despite these limitations, the use and validation procedure of simple, low data demanding, modelling approaches can be justified in those data-scarce environments and countries, using operational continental and global satellite data and geodata.

4.4.2   Model validation

Differences in the spatial distribution patterns of erosion and deposition and also in the absolute values derived from the model intercomparison are significantly influenced by the weights each individual model assigns to the major erosion controlling factors, such as lithology, soils, vegetative cover, slope gradients and rainfall rate.

Yet, although the most up-to-date continental large-scale satellite data and geodata were used in this assessment, it is clear that there are still uncertainties involved in the erosion estimations, which, in turn, increases the importance of validating the accuracy of the spatial predictions. However, this is rather problematic in countries such as Bolivia, where it is very difficult, if not impossible, to obtain and acquire long-term and direct soil erosion measurement data for either small plots or larger catchment areas. A fully quantitative validation of erosion rates is hence not feasible. Instead a method proposed by Kirkby et al. (2004) was used to determine the overall reliability of the model predictions. This method uses a categorical comparison of gridded model estimates, with soil erosion estimates at smaller scales derived either by the application of a physically based model or from geomorphic erosion intensity surveys and soil erosion risk assessments.

The available information for the regional validation (Figure 4.10) consisted of catchment erosion risk assessment studies done using geomorphological field surveying in combination with aerial photo interpretation. From these ground surveys, erosion risk maps can be derived using expert-based (Bissonnais et al., 2000; Baban and Yusuf, 2001), factorial scoring (Kirkby et al., 2000; Pallaris, 2000) or fuzzy logic methods (Metternicht and Gonzalez, 2005). Model validation data were provided by regional development agencies such as the Integrated Catchment Management Program (PROMIC, 1995), the Development Program for the Arque and Tapacari Valleys (PRODEVAT, 1999), and a research centre (CLAS, 2000) whose the aim was to foster and implement integrated catchment and sustainable natural resources management in the Bolivian mountainous region (Figure 4.11).

A scheme of the validation procedure is shown in Figure 4.12. From a comparison between the Thornes model prediction and the erosion risk intensity map of the Llave catchment in the Tunari mountain range near Cochabamba city (see Figure 4.9), it can be observed that 64% of the catchment area is mapped in the same class or differs in one class from the validation dataset. Areas overestimated by two classes or more represent 9%, whereas underprediction by more than two classes encompasses 24% of the area validated. The degree of agreement [%] of all model predictions with observed erosion intensity is shown in Table 4.6.

The values of reliability obtained in this research are lower than those reported by van Rompaey et al. (2003c). This can be attributed to the much wider range of climates and landscapes, ranging from high mountain basins to tropical lowland areas, encountered in our regional research area. To date, erosion model validation assessments of this kind have mostly been done in more homogeneous climatic and physiographic regions (*i.e.*, Belgium and Italy (Van Rompaey et al., 2001; Verstraeten and Poesen, 2001; Verstraeten et al., 2002; Van Rompaey et al., 2003a).

Table 4.5 Area of different erosion classes in Cochabamba according to the present scenario evaluation

N	Rate of erosion [ton ha^{-1}]	Erosion risk class	RUSLE-3D Area [km^2]	Area [%]	MMMF Area [km^2]	Area [%]	SPL Area [km^2]	Area [%]	THORNES Area [km^2]	Area [%]	USPED Area [km^2]	Area [%]
1	0-2	Low	33266	61.5	36221	67.0	30313	56.1	32245	59.7	16591	30.9
2	2-8	Medium	2118	3.9	3075	5.7	3323	6.1	7155	13.2	9615	17.7
3	8-32	High	5746	10.6	6367	11.8	8480	15.7	7325	13.5	8818	16.2
4	32-128	Very high	8770	16.1	8110	15.	9124	16.9	5165	9.6	4384	8.1
5	>128	Extreme	4200	7.7	327	0.5	2860	5.2	2210	4	754	1.4
6		Deposition									13948	25.7
	Total		54100	100	54100	100	54100	100	54100	100	54100	100

Table 4.6 Degree of agreement in relation to the land degradation risk assessment in the Llave catchment

Class	Area [km^2]	RUSLE-3D AAP[a] [km^2]	DA[b] [%]	MMMF AAP [km^2]	DA [%]	SPL AAP [km^2]	DA [%]	THORNES AAP [km^2]	DA [%]	USPED AAP [km^2]	DA [%]
Low	7.0	4.4	61.8	5.6	78.9	4.3	61.8	1.9	27.2	3.8	54.3
Medium	17.7	0.8	4.5	1.9	17.7	3.1	17.1	7.5	42.3	7.8	43.8
High	15.7	6.0	38.3	2.2	15.7	6.1	38.3	3.8	24.5	1.9	12.0
Very high	3.3	0.9	25.9	0.2	3.3	0.3	9.0	0.6	19.2	0.7	20.6
Total	43.8	12.0		9.9		13.7		13.9		14.2	
Weighted accuracy			24.5		47.6		23.6		27.5		39.7

[a] AAP: accurate area prediction, [b] DA: degree of agreement

Table 4.7 Degree of agreement in relation to erosion features from Tintaya catchment

Erosion Features	Tintaya Area [km^2]	RUSLE-3D AAP [km^2]	DA [%]	MMMF AAP [km^2]	DA [%]	SPL AAP [km^2]	DA [%]	THORNES AAP [km^2]	DA [%]	USPED AAP [km^2]	DA [%]
Slight inter-rill and rill erosion	41.4	24.3	57.9	28.5	68.0	24.3	57.9	26.9	64.1	11.3	26.8
Moderate inter-rill and rill erosion	50.5	0.8	1.7	3.3	6.6	9.1	18.3	9.7	19.4	9.9	19.9
Severe inter-rill and rill erosion	12.0	1.7	13.8	0.9	7.5	1.4	11.8	0.1	0.6	1.5	12.7
Slight active gullies	18.5	4.6	24.8	3.5	19.1	5.8	31.3	0.3	1.5	0.9	5.0
Moderate active gullies	5.3	2.4	45.8	1.6	29.6	2.4	45.1	0.3	5.2	0.3	5.0
Severe active gullies	28.4	1.9	6.7	5.7	20.0	1.5	5.4	0.6	2.0	2.0	5.0
Channel erosion	3.4	0.6	16.9	1.1	31.6	0.6	17.8	0.1	2.6	0.0	7.2
Total	159.5	36.3		44.6		45.2		37.9		26.0	
Weighted accuracy			46.2		50.0		42.0		50.6		20.6

A similar validation result was obtained when the erosion intensity map of the Tintaya catchment was used as a validation dataset. It was observed that 56% of the catchment area was mapped in the same class or with a one class difference between the Thornes model prediction and the erosion feature map. Areas overestimated by the model by two classes or more represent 14% of the total areas, whereas underprediction by two classes is observed in 29% of the validation area (Table 4.7).

These findings are in accordance with Gobin and Govers (2003a), who state that when the Pan-European Soil Erosion Risk model (PESERA) was validated through a categorical comparison between measured and predicted erosion rates, a general underestimation of 52% for predicted erosion rates above 1 ton ha^{-1} yr^{-1} and an overestimation of 69% for predicted rates below 1 ton ha^{-1} yr^{-1} were found. Moreover, Nearing (1998; 2000) states that soil erosion models usually tend to overpredict small soil losses and underpredict large soil losses.
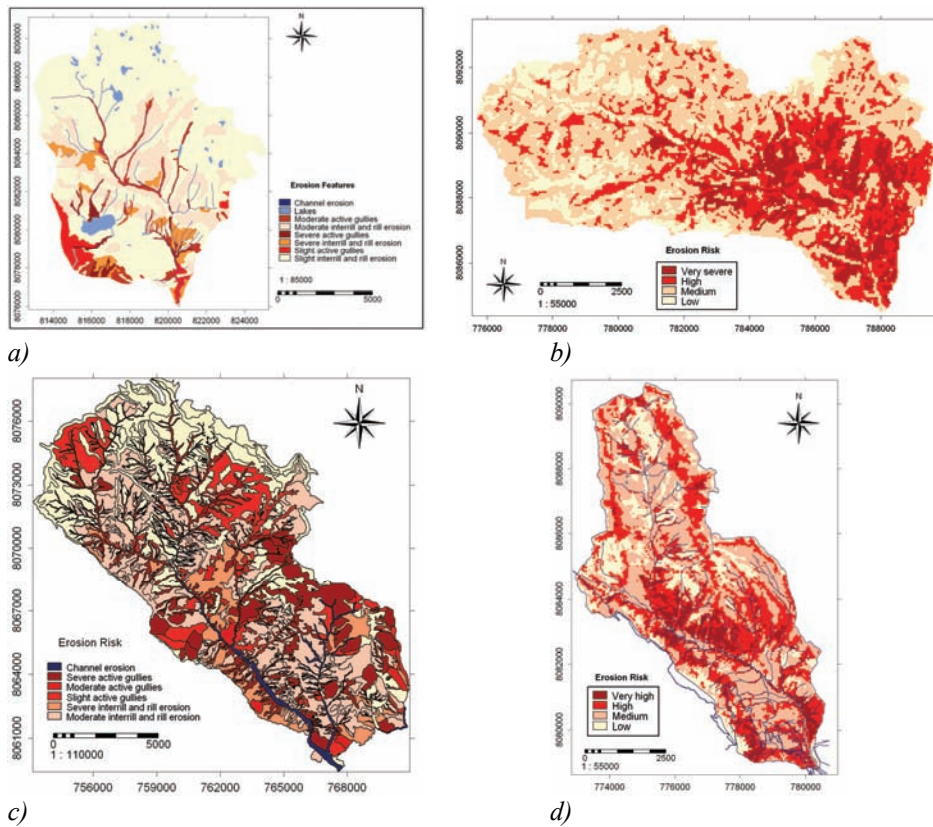
Figure 4.10 Erosion features map used for the regional validation: *a)* Quenko Mayu catchment *c)* Tintaya catchment. Erosion risk maps used for the regional validation *b)* Chocaya catchment, *d)* Llave catchment
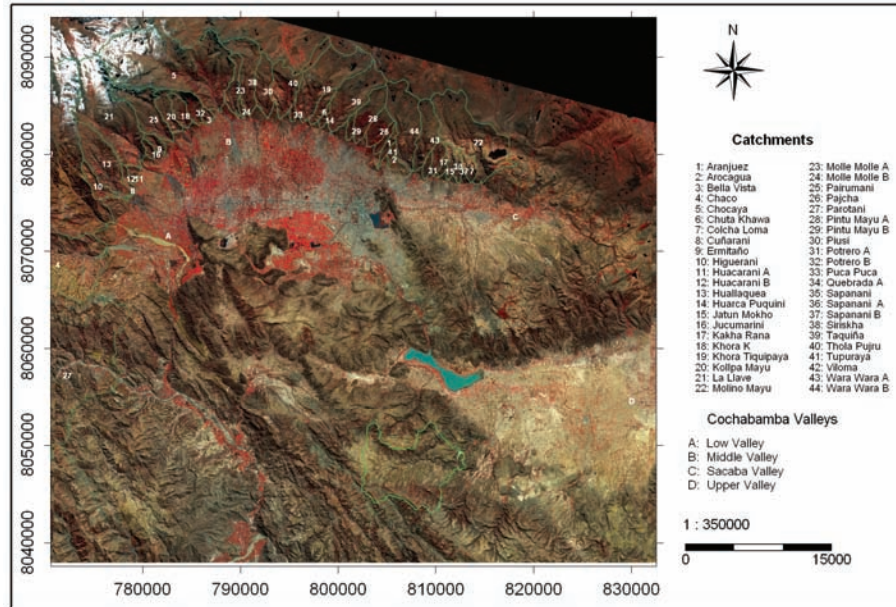
Figure 4.11 Tunari cordillera catchments system on a SPOT-5 false-colour composite
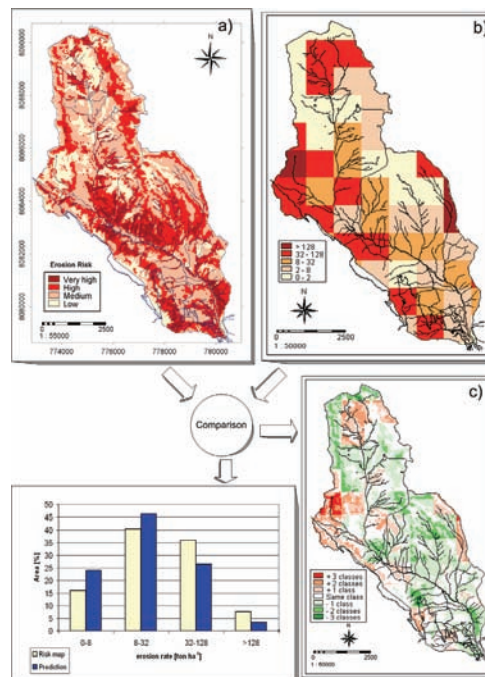
Figure 4.12 Scheme of the validation at the regional scale

From the validation analysis, it can be seen that for steeper areas (*e.g.,* mountain fronts, steep escarpments and cliffs), the SPL, the RUSLE-3D and the Thornes models overpredict amounts of eroded soil. The SPL model overemphasizes the effect of the fluvial bedrock incision (*e.g.,* channel and bank erosion) occurring in environments of this kind, whereas the RUSLE-3D and the Thornes model overemphasize the effect of topography and slope. Conversely, the MMMF and the Thornes model underestimate the soil loss in areas with less than 40% of slope gradient, some of which are experiencing higher erosion rates.

This can be explained by analysing the overland flow generation mechanisms in both models. Although the overland flow routine implemented in the Thornes model uses daily rainfall and an exponential frequency distribution, application of this concept in semi-arid regions with strong seasonal rainfall seems problematic. Moreover, the runoff algorithm does not consider the short-duration rainfall intensity distribution, so that short periods of intense rainfall that generate brief Hortonian overland flow are masked out. The MMMF model generally yields the lowest soil losses. This might be explained by the fact that soil detachment by overland flow is not considered in the model structure and this process plays an important role in mountainous areas.

In addition to the marked influence of erosion factors such as soil erodibility, rainfall erosivity and runoff on the model estimates, the RUSLE-3D and USPED models demonstrate the importance of the influence of topography on the spatial distribution of soil erosion and deposition for complex topography. Both models estimate the soil detachment pattern according to the geometry of the terrain and replace slope length by upslope contributing area as a measure of water flow path length. These models capture the impact of a wider range of flow types, and in turn they include the combined, averaged impact of sheet and rill flow on hillslopes, as well as concentrated flow erosion and potential for gully formation, so that the impact of gullies from field observations are incorporated owing to the associated effect on the $LS_{(r)}$ function.

Although no single model gives accurate results, model performance was categorized in increasing order of performance as follows: SPL<USPED<RUSLE-3D<THORNES<MMMF. Given the ranges of agreement obtained through the cross validation, the quality of the input data and the scale of the analysis, the results obtained with the present-day scenario evaluation when using these relatively simplified model approaches are encouraging.

4.5   Conclusions

In many countries and regions of the world, gathering experimental field plot and catchment data on erosion is usually difficult for a variety of reasons. Long-term and verified experimental datasets are scarce or even absent, and the study area selected is no exception. However, governments or local authorities in these places are usually in need of regional natural resource assessments to enable them to better allocate both financial and human resources for development purposes. A need therefore arises to search for assessment methods based on remote data and applicable to larger regions. This chapter has described the efforts of performing a regional-scale erosion assessment using remote but up-to-date global and large-scale continental datasets. Furthermore, a

number of modelling concepts have been evaluated in combination with the data sources.

The potential use of freely available global and continental satellite data and geodata has been shown. In particular, the use of high temporal resolution satellite data such as SPOT-VGT and the TRMM data for time series rainfall analysis proved to be valuable for monitoring land cover and vegetative cover seasonality, as well as rainfall dynamics, and consequently such data are an aid in assessing and monitoring soil erosion and deposition patterns across the landscape.

The predicted spatial patterns of erosion are consistent with regional erosion assessment from the literature (Walling and Fang, 2003; Yang et al., 2003). It is indicated that the areas of high soil erosion can be accounted for in terms of steep unstable terrain, and the occurrence of highly erodible soils and low vegetation cover. This can be due to important vegetation removal by human activity or other factors.

When comparing the soil erosion rates across the different landscapes of the study region, it was observed that soil erosion is located in the Andean region and in most of the semi-arid areas. The monthly soil erosion estimates by the Thornes model illustrated that this is mainly caused by high rainfalls in the onset of the rainy season, when ground vegetation cover (*e.g.,* grasses and shrubs) is still absent. Likewise, the presence of the Eastern Cordillera chain stretching from northwest to southeast has an influence on the rainfall occurrences. Modelled soil erosion rates are relatively low in the tropical rainforest and the arid areas owing to, respectively, high density of vegetation cover and little to no rainfall and erosivity. Overall, it was estimated that areas affected by very high and extreme erosion encompass about 20% of the total area of the province.

At this coarse scale, all five models proved to be more sensitive to topographical gradients, runoff accumulation and the fraction of vegetation cover parameters. Soil moisture storage and the soil detachability or erodibility index showed a more moderate sensitivity.

Inevitably, substantial uncertainties exist in the coarse grid regional erosion maps presented in this chapter. Estimated soil losses represent annual averaged soil erosion generated within each 1 km^2 cell. The digital soil erosion maps give an approximation of sediment source areas and erosion intensity but do not represent sediment yields from the cells, catchments or region. Sediment yields from hillslopes or catchments are usually significantly lower than the hillslope erosion or soil detachment rates, as most of the sediments travel only a short distance and are locally deposited before getting into the drainage network. In turn, it is found that the uncertainty associated with the results depends more on the spatial and temporal data and on the model resolutions, quality and generalization found in several of the global input data layers than on the intrinsic model algorithms themselves.

A generalized lack of quantitative soil erosion measurements and monitoring data in Bolivia and in the research area in particular hindered a classic quantitative model validation. The model outcomes were therefore verified by using georeferenced field checking and a semi-quantitative categorical method that relies on evaluating the degree

of agreement between the predicted erosion rates and catchment soil erosion type and intensity maps obtained using a combination of field surveying, aerial photo interpretation and/or expert knowledge.

From the validation analysis, it is concluded that the MMMF, the RUSLE-3D and the Thornes models give slightly better erosion estimates and spatial distribution patterns. The RUSLE-3D and USPED models may possibly provide some better predictions in mountain landscapes if higher-resolution elevation data or imagery (*i.e.*, 30 m, 15 m) are available or used. The fact that erosion in semi-arid landscapes is more transport-limited because of the more ephemeral nature of runoff, limiting the transport of sediments over large distances, may favour the applicability of these models. The validation datasets represent a number of representative catchments of the "middle valley" region of the province; however, other validation data (*e.g.,* sub-Andean, mesothermic valley and tropics) are necessary to ensure a complete validation of the models for the whole region.

Even though in quantitative terms the erosion rates obtained in this regional assessment may not be very accurate, and even uncertain in absolute value, the model outputs can still be used to identify erosion-prone areas with a good degree or level of confidence. The hotspots pinpointed by the models can then be further verified and monitored using a combination of ground survey data and/or higher-resolution satellite images (*e.g.,* ASTER, Landsat-7 ETM and SPOT-5) and similar erosion model approaches to gain a more accurate estimate of erosion. Furthermore, these results can also be used to determine or shed more light on whether soil erosion is due to anthropogenic activity (*e.g.,* agricultural practices, land abandonment) or natural causes such as climate change, desertification or geotectonical activity.

In summary, the five modelling approaches presented here are versatile, can accommodate heterogeneous data resolutions, and do not require the use of model parameters unavailable at regional or national scales, particularly in developing countries. All data needed to implement a regional erosion monitoring system is available on the internet in near-real time.

Thus, it would be feasible to establish an erosion monitoring system at regional scale that could keep us abreast of the land degradation status and situation, and gradually build up a time series of data that would allow the analysis of temporal trends in erosion. Another advantage for policy making is that scenario analysis for different land use and climate changes is possible using this approach.

Chapter 5

Catchment-scale erosion modelling using medium-resolution satellite imagery and limited ground data

Chapter 5

Catchment-scale erosion modelling using medium-resolution satellite imagery and limited ground data

5.1 Introduction

In the previous chapter, the erosion rates across the province of Cochabamba were modelled using continental environmental and remotely sensed data in the context of the regional modelling assessment. In this chapter, data from a field reconnaissance survey, a meteorological station, a topographical map, as well as aerial photographs and high spatial resolution satellite data, are used to parameterize model inputs. A more detailed analysis of the erosional processes that take place within the catchment was carried out by using both high-resolution imagery (2002) and aerial photographs (1960).

This chapter focuses on four major points. The first deals with the implementation of the selected erosion models themselves. The second deals with the evaluation of the reliability of the model predictions, using a semi-quantitative method of validation. In the third section, an analysis and discussion of the model parameters that may induce an under- or over-prediction in the soil loss estimates is carried out in order to select a suitable erosion model for semi-arid mountain catchments. Lastly, the possibility of using regional erosion estimates for catchment-scale prediction is investigated. Soil loss prediction in the catchment areas that is derived from continental datasets is compared with the estimates derived using a field dataset at the catchment scale, in terms of absolute values as well as their spatial distribution.

Hence, the aim of this chapter is to compare and evaluate the performance of five erosion models in a semi-arid mountain catchment, in particular (i) to assess the reliability of model predictions of spatial patterns of erosion by comparing them with mapped erosion features extracted from high-resolution satellite imagery, (ii) to assess whether low data demanding models can be used as an effective tool for quantifying rates of soil erosion in semi-arid ungauged catchments, and (iii) to compare predicted erosion rates obtained using continental environmental and remotely sensed data (1 km) with predictions (30 m) obtained using field-surveyed data and high spatial resolution satellite imagery.

5.2 Data and methods

The research was undertaken in the Laka-Laka catchment where considerable soil erosion had occurred prior to 1953 (Zimmerer, 1993). The general setting and biophysical description of the catchment is given in Chapter 3. Data to parameterize the models were gathered during the dry season (June to July) of 2003, when an intensive field survey campaign was carried out. To model erosion and deposition in mountain catchments with steep topography, such as Laka-Laka, requires an adequate DEM, as

well as other data describing the spatial distribution of rainfall, soil, land cover and land use properties. The data available for the catchment include (i) the Moderate Resolution Imaging Spectroradiometer (MODIS) derived 16-day composite NDVI from a continental database with 250 m cell size, generated by the Earth Observation System Gateway (EOS) for the period 2003; (ii) the HRV SPOT-5 scene taken in August 2002; (iii) scale 1:50,000 aerial photographs taken in August 1961; (iv) scale 1:50,000 topographical map with 20 m contour intervals and the SRTM-DEM data; (v) soil data derived from the soil reconnaissance survey, which include profile sampling at 18 point locations in the catchment area; (vi) scale 1:100,000 geological map; and (vii) 30-year long-term rainfall data from the Tarata meteorological station, and hourly rainfall data being derived from the Pampa Chirigua station.

In order to compare the scaling effect on erosion estimates, a higher spatial resolution was used (30 m), but the same temporal resolution as in the regional assessment (seasonal time step). The modelling results were semi-quantitatively validated by comparing model spatial pattern prediction with erosion patterns derived from processing the SPOT-5 scene, aerial photographs and ground truth data. The following sections discuss in detail the most important factors and how they were derived to apply to GIS coverages.

5.2.1   Climate and erosivity

The climate in the catchment is strongly influenced by the presence of the Eastern Cordillera stretching across Cochabamba from the northwest to the southeast. This semi-arid Andean region, including the Laka-Laka catchment, is strongly affected by an orographic effect on the precipitation and temperature, and is referred to as the "upper valley" of Cochabamba. It presents a considerable positive skewness of the annual rainfall distribution (*i.e.,* some heavy rains represent most of the annual precipitation, while light rains are more or less insignificant). A dry autumn and dry winter period (March to September) is followed by a gradual occurrence of rainfall in spring (September to December) and a maximum rainfall in mid-summer (December to March). The extreme rainfall events with the highest hourly and half-hourly intensities occur in January and February. The Tarata meteorological station is located 5 km from the catchment and is the only station with daily rainfall data in the vicinity of the catchment. Figure 5.1 shows the daily rainfall distribution for the period 1990 to 2003. The Pampa Chirigua station is located in the upper western section of the catchment. Hourly rainfall information in this station was only available for the years 1990, 1991, 1992, 1993, 1994 and 2000 (Figure 5.2).

In modelling erosion with the RUSLE-3D and the USPED models, the erosivity factor R [MJ ha^{-1} mm hr^{-1}] quantifies the effect of raindrop impact and reflects the amount and rate of runoff likely to be associated with rain. To obtain the factor R by the RUSLE methodology (Wischmeier and Smith, 1978), high-resolution rainfall measurements at a small time scale (*e.g.,* minutes) are required, as well as accurate computation of the rainfall erosivity EI_{30} of each storm.

The EI_{30} calculation is a very onerous procedure, involving the analysis of the hyetograph for every rainfall event >13 mm (erosive storm) over a sufficiently long period. Rain showers need to be separated in time by at least six hours from the

previous or the following event, and showers of at least 6.35 mm in 15 minutes should be retained. For each erosive storm between January 1990 and December 1994, data from the Pampa Chirigua station were used to compute EI_{30} according to the RUSLE handbook instructions (Renard et al., 1997). The EI_{30} is obtained by multiplying total storm energy E by the maximum 30-minute intensity I_{30}.
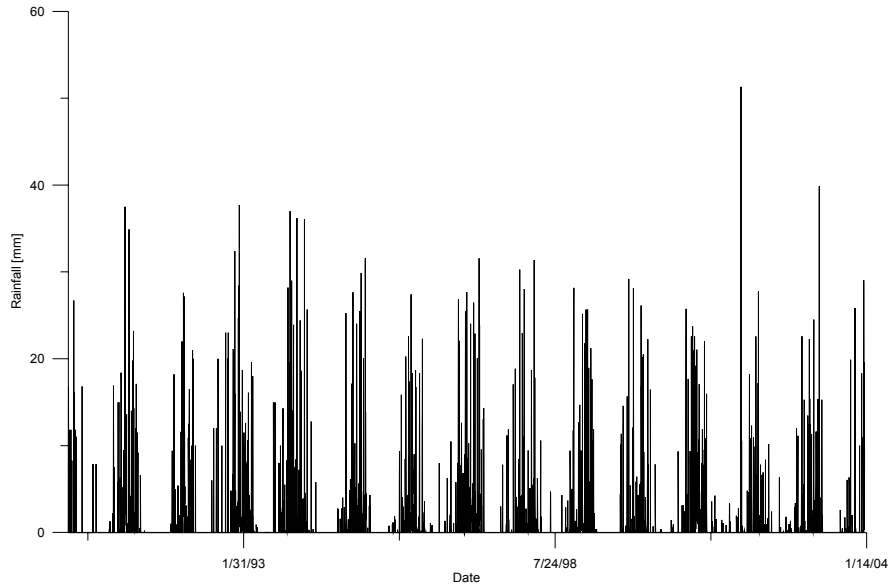
Figure 5.1 Daily rainfall distribution for the 1990 to 2003 time series (Tarata station)

a)   *b)*
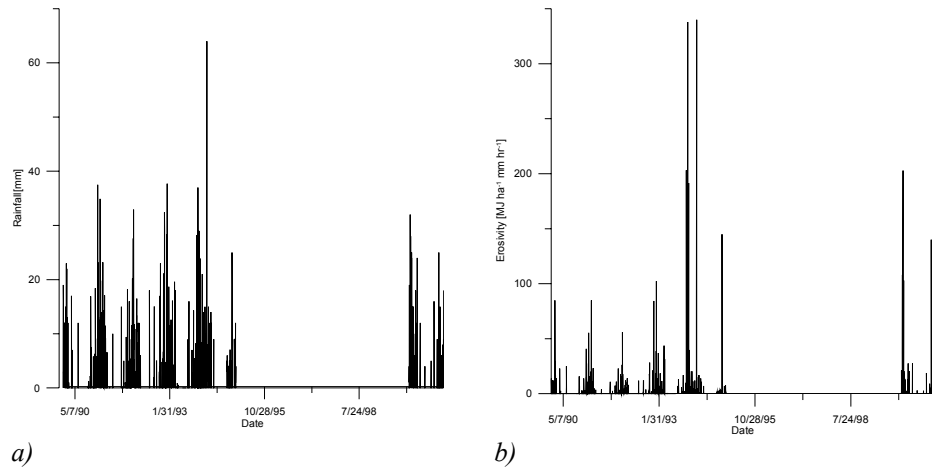
Figure 5.2 Scatterplot: *a)* daily rainfall, *b)* daily erosivity (EI_{30}) for 1990 to 1994 and 2000 (Pampa Chirigua station)

101
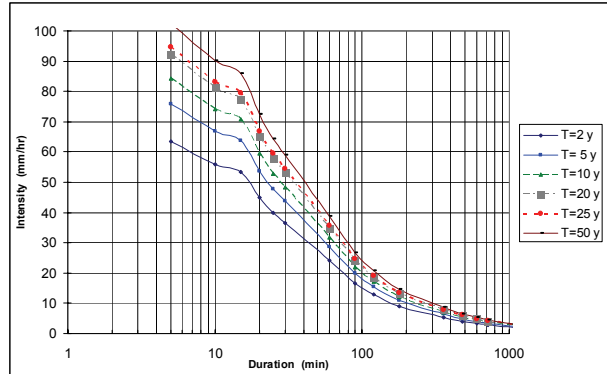
Figure 5.3 Intensity, duration and frequency (IDF) curve for Pampa Chirigua station
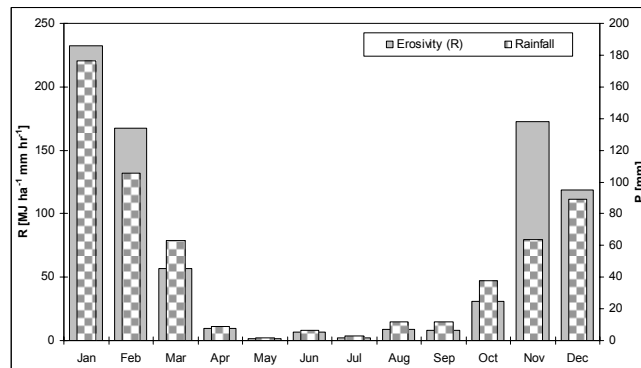
Figure 5.4 Monthly rainfall, P_i and the R factor distribution for the Laka-Laka catchment
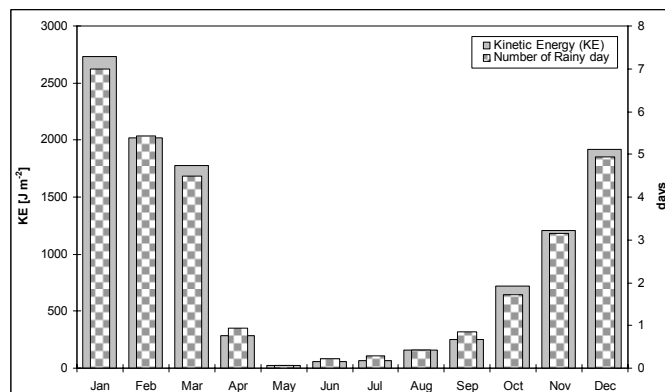
Figure 5.5 Monthly kinetic energy for 20 mm hr^{-1} rainfall intensity and mean rainfall per rainy day distribution for Laka-Laka catchment

The following equation was used to calculate the unit energy contained in the volume of rain:

$$E = 0.29 \left[1 - 0.72 \exp\left(-0.082 I \right) \right]$$ *(Eq 5.1)*

where E [MJ ha^{-1} mm^{-1}] is the kinetic energy and I [mm hr^{-1}] is the rainfall intensity.

On an annual basis, the R values were taken to be the summation of values of the erosive storms in an individual year. The average annual R factor is 815.5 MJ ha^{-1} mm hr^{-1} and the average number of erosive events is 30.

The monthly distribution of the R factor and rainfall is plotted in Figure 5.4. Because only hourly rainfall data were available, I_{30} values were estimated from I_{60} values using a ratio factor derived from the local intensity–duration–frequency curves available for Cochabamba airport meteorological station (Figure 5.3). More experimental short-duration rainfall data and research are needed to determine the effect of rainfall measurement interval on erosivity in these regions. Extreme variability in the relationship between annual rainfall erosivity and rainfall is observed in the region. Similar results have been reported by Renschler and Mannaerts (1999), Mannaerts and Gabriels (2000) and Diodato (2004).

An important factor required for estimating erosion in the MMMF model is the rainfall kinetic energy for soil detachment KE, which is a function of annual rainfall and rainfall intensity. The average annual kinetic rainfall energy was estimated at 11.2 kJ m^{-2}, the average rainfall intensity was 20 mm hr^{-1} and the mean rainfall per rainy day R_o (*i.e.,* mean annual rainfall R divided by the number of rainy days per year) was 16.6 mm. The monthly distribution of the KE and R_o is plotted in Figure 5.5.

5.2.2 Vegetation parameters

Vegetation plays a dominant role in controlling all the processes of erosion. It is an important factor when attempting to evaluate the spatial extent and intensity of erosion. The researched catchment presents typical landscape features that are vulnerable to water erosion processes. In such an environment, because vegetation cover is generally low, the signal of satellites is controlled by the spectral properties of bare soil.

Vegetation variables and parameters required for erosion model application, such as land cover and land use, fraction of vegetation cover and the cover management factor (C), were extracted by using different satellite-derived indices (*e.g.,* principal components (PC), NDVI, enhanced vegetation index (EVI)) and were monitored during the dry season of 2003 on the major land cover units.

The panchromatic/multispectral bands of SPOT-5 were orthorectified with 90 ground control points and the 30 m DEM using ERDAS 8.7 Ortho-Base with root mean square error (RMSE) of less than 0.89 cells. Next, a scatter diagram was made of the spectral responses from the sensor in the spectral bands, and a divergence matrix constructed for each dataset. Several interactions were required to keep overlap among the various land cover categories to a minimum. Furthermore, a stratified supervised classification employing the maximum likelihood method was used in combination with 65 ground truth georeferenced points to improve the classification of the land cover map (Figure 3.7c).

Table 5.1 Vegetation erosion parameters according to land use and land cover. SCC is the surface condition constant, C is the cover management factor, E_t/E_o is the ratio of actual to potential evapotranspiration, P_i is the rainfall canopy interception, n is the Manning roughness coefficient, R_d [m] is the hydrological root depth.

Land use and land cover	SCC	*C* factor	R_d	E_t/E_o	P_i	n
Bare exposed rock	0.15	0.005	0.01	1	2	0.1
Bare soils	0.16	0.25	0.05	1	5	0.07
Bushland	0.18	0.16	0.09	0.6	15	0.15
Fallow	0.22	0.26	0.1	0.7	5	0.13
Forestry	0.22	0.05	0.1	0.9	35	0.4
Irrigated cultivation	0.2	0.11	0.12	0.68	20	0.2
Lake	0	0	0	1	1	1
Open shrubland	0.19	0.12	0.08	0.75	18	0.16
Rainfed cultivation	0.15	0.09	0.11	0.73	19	0.22
Steppe shrubland	0.2	0.13	0.08	0.8	22	0.25

Table 5.3 Soil erosion parameters. K_m [m J^{-1}] is the erodibility factor according to Morgan, K_a is the soil erodibility [US units], K_i is the soil erodibility [SI units], *SM* [%] is the soil moisture, B_d [gr cm^{-3}] is the soil bulk density

Site	Horizon	K_m	K_a [US]	K_i [SI]	SM	B_d
1	HA1	0.8	0.55	0.072	0.12	1.34
2	HB1	0.75	0.36	0.047	0.12	1.46
3	HC1	0.8	0.54	0.071	0.15	1.7
4	HD1	0.75	0.35	0.046	0.12	1.2
5	HE1	0.73	0.32	0.042	0.11	1.41
6	HF1	0.8	0.33	0.043	0.17	1.52
7	HG1	0.7	0.32	0.042	0.11	1.46
8	HH1	0.85	0.45	0.059	0.27	1.25
9	HI1	0.7	0.37	0.048	0.08	1.38
10	HJ1	0.75	0.32	0.042	0.14	1.45
11	HK1	0.4	0.18	0.023	0.13	1.39
12	HL1	0.85	0.36	0.047	0.1	1.44
13	HM1	0.67	0.3	0.039	0.06	1.42
14	HN1	0.76	0.36	0.047	0.1	1.34
15	HT1	0.83	0.41	0.054	0.19	1.31
16	HR1	0.7	0.3	0.039	0.23	1.65
17	HQ1	0.82	0.25	0.032	0.16	1.36
18	HS1	0.75	0.3	0.039	0.12	1.4
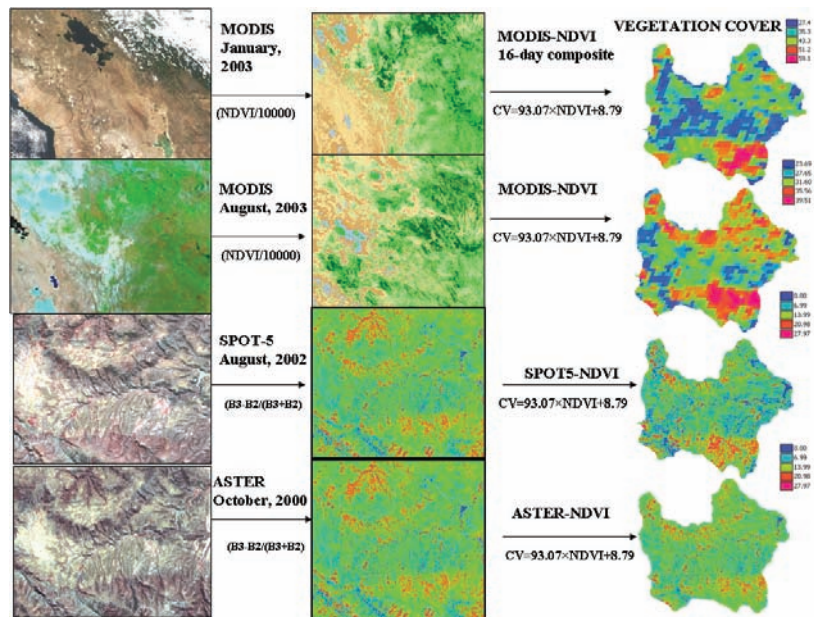
Figure 5.6 Use of MODIS satellite data (10-day composite NDVI) for land cover percentage determination
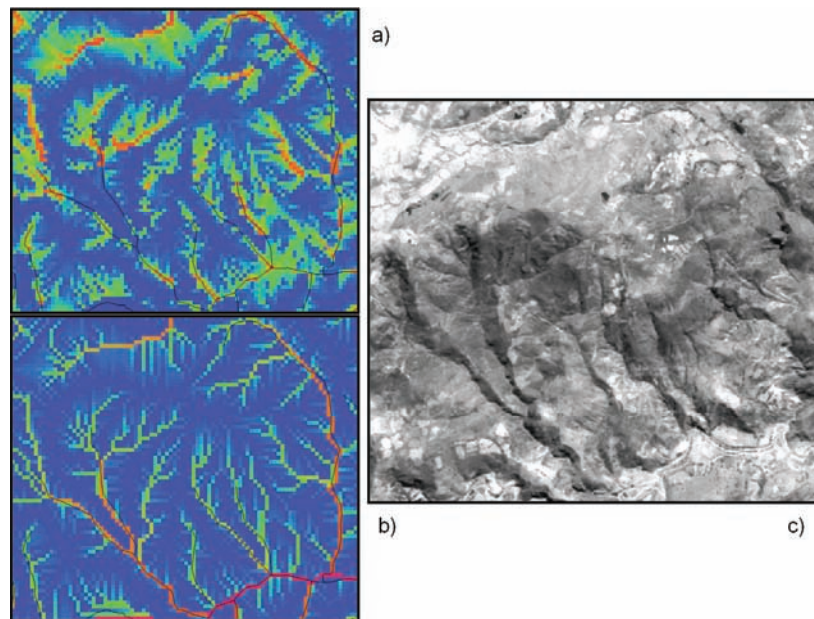
Figure 5.7 Flow accumulation pattern according to: *a*) multiple flow direction for prevalent convergent flow, *b*) single flow direction, *c*) mountain front in the northeastern region of the catchment in the panchromatic SPOT-5

The NDVI, a spectral ratio between near infrared and red reflectance, extracted from SPOT-5 was used to calculate the C values, bearing in mind that the NDVI is highly correlated with vegetative cover and biomass (Zhang, 2002). The C values were calibrated using RUSLE 1.6 software and field data from the individual field sample plots. A linear regression was computed between the NDVI values and the corresponding C values from the field. This regression equation was ultimately inverted and was used to compute distributed C values for the entire catchment. The C factor ranges from 0.45 for bare undisturbed soils to 1.0 for bare cultivated land. Literature values were employed for non-agricultural land uses (Table 5.1).

The effective hydrological depth R_d was considered a land use dependent input and set according to the model guidelines (Morgan, 2001). The ratio of actual to potential evapotranspiration Et_a/Et_o was estimated as the crop coefficient K_c of the FAO procedure for calculating crop water requirements (Allen et al., 1998).

The temporal variation of vegetation cover v_c [%] across the catchment was estimated using the MODIS-NDVI 16-day-interval time series data extracted for the period 2003. The MODIS gridded outputs are in integerized sinusoidal projection (ISIN). Because most of the conventional "off-the-shelf" software packages used for image processing and spatial data analysis do not accommodate the ISIN projection, the MODIS reprojection tool (USGS-EROS, 2003) was used to perform the geographical transformation to the coordinate system and cartographic projection required. The NDVI time series imagery was normalized using the equation suggested by Huete et al. (1999): $NDVI = \dfrac{DN}{10000}$, where *NDVI* is the Real NDVI with values ranging from -1 to 1 and *DN* is the per pixel digital number.

This new set was correlated and converted to monthly distributed maps of the vegetation cover fraction using the regression relationship developed by Zhang et al. (1999a), who assume that a high correlation between NDVI values and the fraction of vegetation cover image exists (Eq. 4.1). According to Symeonakis and Drake (2004), the fitted equation present a statistics of R^2=0.73; F=241.63 and p=4.26×10^{-27}. Figure 5.6 shows the scaled NDVI image and percentage of cover image for the driest and the wettest month of 2003.

5.2.3 Topographical parameters

Topography is one of the driving forces behind geomorphic processes. Slope steepness, slope length, tangential curvature, profile curvature and upstream contributing area represent the geometric properties of the terrain surface and are important parameters in modelling erosion, particularly in mountainous relief. The differences between processes on hillslopes and in channels make it important to properly map the physical extent of channels in catchments, and require the implementation of an effective flow-tracing algorithm (Tarboton, 1997).

If a high-resolution DEM is used, the application of a standard algorithm for flow tracing such as the D8, which uses only a limited number of flow directions from each grid cell (Jenson and Domingue, 1988), can lead to unrealistic situations, as it assumes the runoff flow only in the steepest downslope direction from any given point. Several

new algorithms for flow tracing proposed by Schauble (2003) and Schoorl (2002) help to overcome the aforementioned deficiencies. Most of these algorithms assume that the runoff flows occur in all downslope directions from any given point, so they are better suited for analysing complex flow divergence and convergence patterns that occur inevitably in mountainous terrain.

To select the suitable upslope contributing area $A_{(r)}$, results have been compared as obtained with the steepest descent (D8) algorithm, the multiple flow algorithm (Desmet and Govers, 1996a) and the flux composition algorithm (Tarboton, 1997) − a hybrid estimator that switches from multiple flow to single flow algorithm and is available in both TAUDEM (Tarboton, 2004) and Hydrotools (Schauble, 2003) software. Careful visual assessment of each output map, using an overlay of catchment stream tributaries, resulted in the selection of the multiple flow algorithm because of better approximation to the existing stream network and its accountability for the complicated flow divergence and convergence patterns common in mountainous areas (Figure 5.7). The RUSLE-3D model uses $A_{(r)}$ for estimating the $LS_{(r)}$ factor, whereas the USPED, SPL and MMMF models use $A_{(r)}$ as a proxy for runoff and sediment transport, respectively.

5.2.4 Hydrological parameters

Surface runoff plays a vital role in determining the rate of erosion, since sediment transport is accomplished mainly by runoff, especially in steep slopes. Large runoff events with high stream power may remobilize the coarser sediments deposited during past events. There is a well-established tendency for runoff to increase with land degradation. The rate of runoff is indeed a useful indicator of the land degradation process. Considering the fact that the data available for its estimation correspond to a single meteorological station and multitemporal coarse remote sensing data, the method of assessing its spatial and temporal variability in the catchment should rely on information obtained from remote sensing data (*i.e.,* soil and vegetation image indices). Hence, a modification of the Soil Conservation Service Curve Number (SCS-CN) method (SCS, 1972) developed by Zhang et al. (2002) was used.

The method assumes that the daily rainfall approximates an exponential frequency distribution within each month. As can be seen from Table 5.2, the value of the CN depends on factors such as land use, land cover, slope and soils, which the SCS method has divided into four groups according to their infiltration, retention and evaporation capacity.

These factors control not only the amount of water that becomes runoff but also the initial abstraction I_a [mm]. In order to estimate runoff, the hydrological soil group (HSG) map was derived based on the soil textural data. Next, the HSG map was integrated with the land cover theme to generate the CN map according to the antecedent moisture condition (AMC). The CN's values were assigned based on average AMC II condition. The resulting CN map was then used along with Eq 2.27 and rainfall data to estimate the monthly runoff OF_i [mm].

Another approach, proposed by Finlayson and Montgomery (2003), is the use of the runoff as a proxy for discharge, a parameter required for modelling fluvial erosion according to the SPL indices (Section 2.6.5). The annual discharge to the reservoir was

107

modelled by routing the annual rainfall across the DEM using the multiple flow algorithm with a weighted grid. The discharge was calibrated until the volumes stored corresponded to the volume measured in the reservoir. Overall, this modified rainfall weighted flow accumulation procedure accounts for spatial gradients in evapotranspiration and differences in runoff generation processes.

Table 5.2 Soil Conservation Service Curve Numbers (SCS-CN) for the Laka-Laka catchment

Land use/land cover	Hydrological condition	Curve number for hydrological soil group			
		A	B	C	D
Bare soils	Good	49	68	79	84
	Fair	55	72	81	86
	Poor	62	78	85	88
Forestry	Good	45	52	60	65
	Fair	49	50	63	69
	Poor	55	65	70	73
Irrigated cultivation	Good	45	50	55	60
	Fair	49	53	61	65
	Poor	51	55	60	70
Open shrubland	Good	48	51	55	61
	Fair	51	56	61	65
	Poor	55	62	65	69
Bushland	Good	47	49	52	57
	Fair	51	57	60	62
	Poor	54	60	66	67
Fallow	Good	54	56	58	61
	Fair	57	59	63	64
	Poor	62	66	67	68
Bare exposed rock	Good	50	53	58	64
	Fair	52	56	62	68
	Poor	56	61	66	70
Steppe shrubland	Good	47	51	56	61
	Fair	48	56	59	63
	Poor	50	55	60	65
Rainfed cultivation	Good	49	55	59	65
	Fair	52	58	64	68
	Poor	55	60	70	71

5.2.5 Soil parameters and erodibility

A soil unit map was generated based on the interpretation of pedoforms and landforms using the 1961 orthophoto mosaic. Basic data to estimate the erodibility values *K*, as well as the soil hydrological parameters (*e.g.,* texture, hydraulic conductivity, soil moisture, soil depth), were obtained from the soil reconnaissance survey conducted in

July 2003. Soil samples were derived from 18 representative soil profiles described and characterized according to the USDA Soil Survey Manual (1993) and representative of the major soils found in the catchment and region. Soil erosion parameters are summarized in Table 5.3.

Bulk densities B_d were in the range of 1.2 to 1.45 gr cm^{-3}. The low organic content and cohesion values of the topsoil indicate low resistance to soil particle detachment. The K factor values required for the RUSLE-3D and USPED models were estimated using the soil erodibility nomograph method of Wischmeier et al. (1971). This method uses percentage of silt plus very fine sand, percentage of sand, percentage of organic matter, and soil structure and permeability class. After assigning the appropriate values to each parameter, the K factors were assigned to each soil mapping unit. Soil moisture at field capacity MS and topsoil bulk density B_d were measured in the laboratory with standard methods. Cohesion was measured on saturated topsoil with a torvane in the fields. All the parameters were then averaged per soil type.

The soil detachability index K_m for the MMMF model was obtained from values published by Morgan (2001). The K_t values for the Thornes model are a quantitative description of the inherent erodibility of a particular soil. Mitchell and Bubenzer (1980) provide values for K_t according to the different soil textural classes and percentages of organic matter content. Conversely, the K_l values for the SPL model cannot be evaluated from the soil characteristics alone. Stock and Montgomery (1999), Barnes and Pelletier (2001) and Montgomery et al. (2001) used measured local incision rate data estimated in a range of geologic, climatic and tectonic settings to estimate values of K_l. A value of 5.4×10^{-5} m$^{0.2}$ yr^{-1} for weak and/or highly jointed rock units and a value of $2.03 \times 10^{-0.6}$ m$^{0.2}$ yr^{-1} for more resistant units were adopted because they best represent the geological characteristics of the study catchment.

5.2.6   Soil erosion assessment

Assessment of the actual erosion was conducted by classifying separately both orthorectified SPOT-5 and orthophoto-mosaic data in combination with field ground truth data. The method consisted of surveying erosion features together with major causes of erosion, such as land management, surface characteristics and runoff patterns (Hill and Schütt, 2000). The supervised classification was performed using the Gaussian maximum likelihood method in combination with ground verification data. Four main erosion feature classes were derived, namely, *No erosion*, *rill erosion*, *gullies*, and *channel erosion*, according to the degree of erosion intensity they present.

The map was checked in the field, where it was verified that it reproduced the actual situation. Accordingly, the 1:50,000 aerial photographs (1961) were orthorectified based on the SPOT-5 corrected images. Areas with similar intensity of water erosion were delineated using the visual classification (on-screen classification) method, distinguishing between areas with no visible signs of erosion, areas with rill erosion, and areas affected by gully and channel erosion.

a)

b)
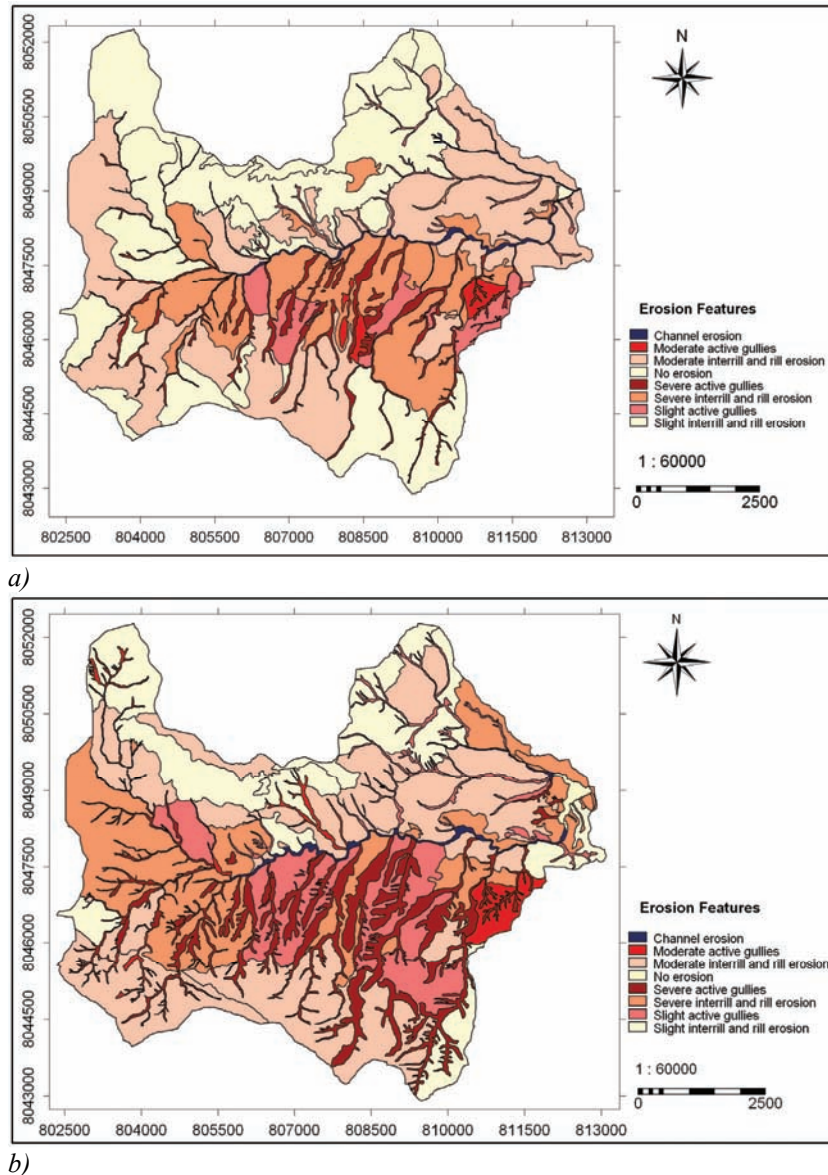
Figure 5.8 Erosion features delineated from: a) orthophoto mosaic (1961), *b)* orthorectified SPOT-5 (2002) imagery

It was determined that 9.3 km^2 of areas affected by rill erosion and ephemeral gullies 55 years ago have since become incised by deep gullies (Figure 5.8). This increase in gully density is related to land abandonment, to the natural degradation of the soil, and to a minor extent to the change in vegetation cover and/or soil erodibility caused by agricultural practices.

5.3   Results and discussion

5.3.1   Erosion model predictions

5.3.1.1   RUSLE-3D

The predicted spatial patterns of soil loss distribution are shown in Figure 5.9. Model soil loss estimates were grouped in five erosion intensity classes according to an exponential frequency distribution analysis. It was estimated that 11% of the catchment experiences low erosion rates, whereas 16% and 25%, respectively, encompass areas affected by medium and high rates of soil loss. In total, 49% is considered to be affected by very high and extreme soil loss rates. A comparison of the slopes and the spatial distribution of water erosion rates across the catchment indicate that the areas with the steepest slopes have the highest erosion rates. Predicted erosion rates in mountain areas with slope gradients higher than 50º (≈120%) are between 128 and 150 ton ha^{-1} yr^{-1}.
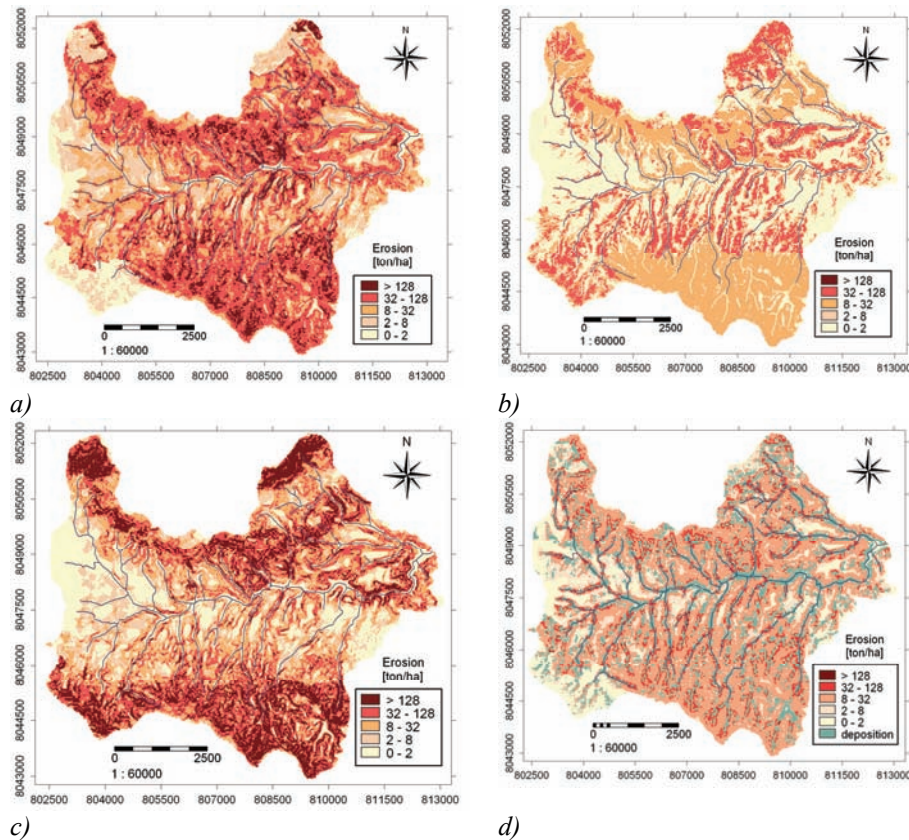
Figure 5.9 Predicted erosion rate using: *a)* RUSLE-3D, *b)* MMMF, *c)* THORNES, *d)* USPED

Notwithstanding, one should be cautious in interpreting these values as they are extremely influenced by the high $LS_{(r)}$ values. The effect of spatial resolution in predicting $LS_{(r)}$ was investigated by comparing the $LS_{(r)}$ maps obtained from the topographical map (30 m) and SRTM data (90 m). The results show marked differences in the spatial distribution and in the spatial variability of $LS_{(r)}$. The uncertainty in

111

predicting $LS_{(r)}$ came mainly from slopes in gentle areas and from the upslope contributing areas in steep areas where values of erosion increase exponentially. That is simply because the slope gradient is the major control on the $LS_{(r)}$ values.
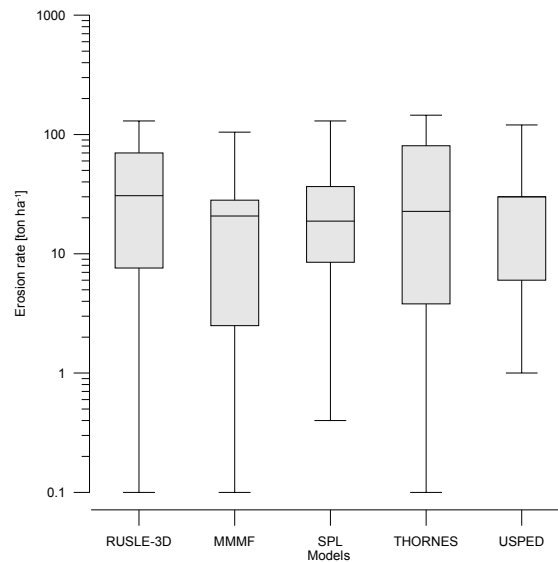
Figure 5.10 Box whisker plot with erosion rates from the model predictions

Table 5.4 Area of erosion intensity classes using field-surveyed data

N	Rate of erosion	Erosion risk class	RUSLE-3D		MMMF		SPL		THORNES		USPED	
	[ton ha^{-1}]		Area [km^2]	Area [%]	Area [km^2]	Area [%]	Area [km^2]	Area [%]	Area [km^2]	Area [%]	Area [km^2]	Area [%]
1	0 - 2	Low	6.5	10.9	22.4	37.3	13.1	21.8	12.0	20.0	6.0	10.0
2	2 - 8	Medium	9.4	15.7	6.9	11.5	26.1	43.7	8.7	14.6	7.5	12.5
3	8 - 32	High	14.9	24.9	20.3	34.0	18.3	30.6	13.6	22.7	26.3	44.0
4	32 - 128	Very high	23.9	40.0	10.2	17.2	2.2	3.7	15.6	26.0	6.6	11.0
5	> 128	Extreme	5.1	8.5	0.0	0.0	0.1	0.2	9.9	16.6	0.1	0.1
6	> 100	Deposition									13.5	22.5
Total			59.8	100.0	59.8	100.0	59.8	100.0	59.8	100.0	59.8	100.0

5.3.1.2   *Modified Morgan, Morgan and Finney (MMMF)*

Soil loss prediction using the MMMF model ranges from 5 to 87 ton ha^{-1} yr^{-1} (Figure 5.10). The detachment rate by raindrops F ranged from 10 ton ha^{-1} in agricultural low sloping lands to 80 ton ha^{-1} in mountain footslopes and erosive hillslopes, with a mean annual soil loss of 40 ton ha^{-1} for the whole catchment, while the transport capacity rates range from 1.5 to 150 ton ha^{-1}, with an average of 48 ton ha^{-1}. The model indicates that 49% of the area situated on low gradient slopes is undergoing low and medium erosion.

From the cumulative areal distribution of erosion, it can be seen that the detached material is originating mainly from an area of 10.2 km^2 (17%), whereby this area can be defined as the most active source of sediment.

A detailed analysis shows that the contributors of sediment to the river system are located in the southwest and southeast sections of the Calicanto river, where highly dissected footslopes are currently undergoing strong soil denudation. The contribution of soil detachment by surface runoff increased along the slope because of the runoff accumulation. Therefore, in 70% of the area, transport capacity was the erosion-limiting factor and erosion was detachment-limited only in a few areas on the medium and low terraces. On the other hand, the routing procedure introduced in the model allows for downslope accumulation of runoff, giving increased erosion rates for areas with scarce or medium vegetation cover. Table 5.4 divides the model predictions according to the area and intensity of erosion.
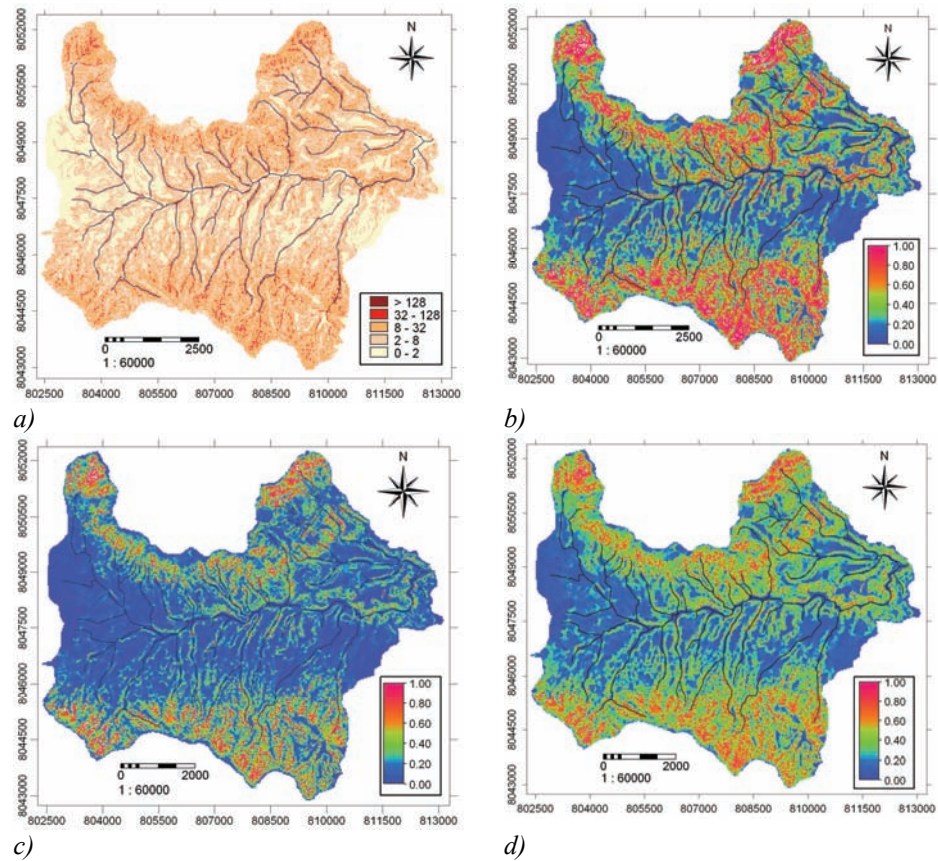
Figure 5.11 *a)* Predicted erosion rate using the Stream Power Law, *b)* erosion index (ε) per total stream power, *c)* erosion index (ε) for stream power per unit of length, *d)* erosion index (ε) per shear stress

Overall, the largest model estimates match accurately the areas where active erosion processes occur (*e.g.,* moderate and severe active gully erosion) as shown in Figure 5.8.

Steep gradients in the area cause overland flow to be erosive, especially where the ground has been disturbed or is otherwise denuded of vegetation.

5.3.1.3   Stream Power Law model (SPL)

The SPL model estimates the long-term rate of soil erosion, as well as the considerable influence of discharge and gradient on erosion rates (Figure 5.11a). The pattern of erosion reveals that 96% of the catchment is experiencing erosion in the range of 0 to 32 ton ha^{-1}; in turn, very high and extreme erosion rates are predicted only along the major tributary channels and the steep escarpment, encompassing 4% of the total area.

The SPL model is highly sensitive to local slope conditions (where the profile is steep, the erosion gets a spike) but because of the medium resolution of the DEM (30 m) a single spike in the output map may not accurately reflect the natural river conditions (Mitasova, 2000).

The spatial pattern of the catchment river network is closely tied to the gradient of the channel and reveals a more intense erosion process along the south section of the river and tributaries. Thus, rates of fluvial erosion in the catchment are high, but not exceptional considering the channel gradient and relatively low precipitation in the region.

The estimation of the three erosion indices (ε), namely, *total stream power*, *unit stream power per unit of length* and *shear stress*, reaffirms the theory that the SPL model overemphasizes the effect of the channel gradient and the flow accumulation. The indices displayed in Figures 5.11 b, c and d show that the specific formulation of the fluvial erosion law, with distinct *m* and *n* values representing different process rules, affects the magnitude and variance of ε, but has only limited effect on its spatial pattern. The spike nature of ε reflects large local changes in slope, which are amplified by large discharges linked with intense storms. The erosion index maps highlight distinct zones of high erosion associated with the steepest sections of the rivers. In applying both the SPL model and erosion-related indices, it is apparent that the control on erosion rates in the catchment involves the counter-intuitive phenomenon that in steep landscapes the rate of river incision governs the sediment flux, whereas rates of hillslope processes control sediment fluxes in low-gradient landscapes. Observations of the river channel beds and banks indicate that erosion has occurred primarily because of terrace failure and channel bank erosion. This implies that the rate-limiting process is some combination of joint-block loosening by physical weathering (frost shattering in these dry environments), fracture and loosening of joint blocks by bedload impacts, and hydrodynamic extraction and transport of blocks given extraordinary storms.

5.3.1.4   Thornes

The Thornes model predictions enable the high seasonal variation in erosion rates and dynamics to be verified. Spatial pattern predictions are shown in Figure 5.9c. In qualitative terms, in most areas the distribution of erosion seems reasonable. It is observed that around two quarters of the catchment (*i.e.,* 20.7 km^2) encompass areas affected by low and medium rates of erosion.

Accordingly, 26% and 17% (*i.e.,* 25.5 km^2) of the area are undergoing very high and extreme rates of erosion respectively, located on both sides of the water divides of the mountain ranges (*e.g.,* mountain escarpment and mountain footslopes). Although the highest erosion rates are associated with the steep mountain escarpment and cliffs, the actual soil erosion of these units, according to a visual field inspection can be categorized in the range from low to medium owing to protection by natural vegetation, so that the overemphasis of slope in the model conception is evident.

However, the predictions for the southwest and northwest sections of the catchment seem reasonable. Field inspection identified the increased amount of denudated soil provided by gully systems. The surface runoff generated within the cells (Eq 2.27) is low when compared with the runoff generated by the MMMF model (Eq 2.19); however, it is closely related to the pattern of precipitation and vegetation dynamics, reaching its maximum in January and February. By using average daily rainfall without considering the rainfall intensity distribution, short periods of rainfall that generate brief Hortonian overland flow may be masked. Moreover, its estimation at a monthly time step involves the derivation of the curve number, which depends on the land cover estimation and the hydrological soil group, which are both subject to uncertainty because of the land cover simplification.

Likewise, vegetation cover is a sensitive parameter, especially at low values. Although there is some uncertainty in using NDVI to estimate v_c, the most important aspect is that NDVI is a better predictor of green vegetation cover than of the total fraction of vegetation cover, and thus tends to underestimate v_c, which may produce higher erosion rates rather than low ones.

The ability of the Thornes model to provide monthly erosion estimates permitted to identify that most of the erosion occurs between December and February, when low vegetation coincides with high rainfall intensity. Although this model is based on modest data requirements, it can be readily implemented on an operational, near real-time basis to provide catchments with up-to-date realistic and quantitative information on erosion that could be used to identify target areas for mitigation measures.

5.3.1.5 *Unit Stream Power Erosion Deposition model (USPED)*

The USPED model was applied to the complex topography of the catchment in order to obtain quantitative information on the processes of soil detachment and sediment deposition. Model spatial pattern estimates are similar to those of the RUSLE-3D model, showing consistently that erosion prediction is controlled by relief and land cover. The ability of the model to identify depositional areas indicates that 22.5% of the catchment falls in areas of potential deposition.

Accordingly, Table 5.4 shows that areas experiencing low erosion rates encompass 6% of the catchment, whereas 12.5% and 44% of the area are affected by medium and high erosion rates respectively, corresponding to old planation levels, flat and medium alluvial terraces and moderately dissected hills (Figure 5.9d). The sources of sediment to the outlet cover 11% (6.7 km^2) of the area, which is consequently endangered by very high and extreme rates of soil loss. Although the high relief has a determinant effect on

the spatial pattern of erosion, in this model the local lithological, soil and climatological conditions modify the potential erosion in positive or adverse direction.

The model seems to predict satisfactorily the occurrence of erosion in areas where currently acute processes of erosion are taking place. However, the model fails (*e.g.,* in areas of steeper relief on both sides of the mountain chain along the water divide) to predict high erosion rates for areas where all arable land has already been long eroded. As expected, the highest values of deposition were found along the main tributaries, which is due to the temporary cumulative sedimentation on lower slopes. The use of the multiple flow direction favours the detection of bigger depositional areas. This is clearly an effect of increasing flow divergence and therefore the lowering of the dominant downslope flow gradient and the increasing of the length of the flow paths.

Borders between different land covers (*e.g.,* bare soil, bedrock and forest) cause abrupt changes in flow velocities, as well as in the transport and detachment capacities, with significant redistribution in the soil loss. The spatial pattern shows deposition at the sides and centres of the main tributaries, while erosion is observed in areas with convergent water flow as well as on steep and bare hillslopes.

5.3.2 Model intercomparison

From comparing the model predictions, it is observed that the area affected for each intensity class is slightly similar, as shown in Table 5.6. It is found that the highest annual denudation is provided by the Thornes model [2.8×10^5 tonnes], while the lowest is given by the MMMF model [1.5×10^5 tonnes]. Accordingly, the highest average predicted erosion rate is provided by the Thornes model [47.5 ton ha^{-1} yr^{-1}], whereas the MMMF model [17 ton ha^{-1} yr^{-1}] gives the lowest estimates. Overall, it is predicted that on average about 2.5×10^5 tonnes of soil are moved annually and the average erosion rate predicted is 30 ton ha^{-1} yr^{-1}. It has been evaluated that in general terms 20% of the catchment experiences low erosion, while about one quarter of the area [12.3 km^2] faces medium erosion. The figures for high, very high and extreme intensity of erosion are 31%, 20% and 6% of the area, respectively. In turn, 26% of the area [15.6 km^2] is suffering from high erosion rates, which contribute significantly to sediment yield in the catchment.

Zimmerer (1993) argues that 25 ton ha^{-1} is an appropriate measure of soil loss above which peasant farmers should be concerned; so this value was defined as the soil loss tolerance value for the catchment. Using this value for soil formation means that the catchment soil losses occur at a rate greater than the soil formation, highlighting the need for implementing conservation practices as part of future agricultural support.

It is observed that the dissected hills and footslopes present areas with high erosion rates because they are subject to long dry periods followed by heavy bursts of erosive rainfall, falling on steep slopes with thin fragile soils. Conversely, agricultural terraces, old planation levels and undulating hills present low soil loss rates because of a thicker topsoil. The short rainfall regime during the year influences the estimates and clearly highlights that under any land cover the reduction of protective ground cover increases the risk of soil losses. In terms of spatial patterns, reclassified erosion intensity classes appear rather well delineated, and cells containing high values for soil loss correspond

to severely degraded areas on the ground (*i.e.,* steep footslopes, steep hills and active gullies). By using the MODIS-NDVI multitemporal imagery, it was possible to identify areas where the density of vegetation is very low or absent, as the time series cover the phenological vegetation.

As mentioned above, the highest values are predicted by the RUSLE-3D model owing to the cumulative nature of the model in steep areas, generating large values of $LS_{(r)}$. In addition to the clear effects of erosion factors such as soil, vegetation and climate on the erosion estimates, the RUSLE-3D, USPED and MMMF estimates demonstrate the influence of relief on the distribution of erosion and deposition in areas with complex topography. Likewise, the RUSLE-3D and USPED models are able to represent the impact of a wider range of flow types. In turn, they include the combined, averaged impact of sheet and rill flow on hillslopes, as well as concentrated flow erosion and potential for gully formation, so it may not be necessary to add the impact of gullies as observed in the field, because gullies are already incorporated.

Although in general terms the spatial pattern of erosion across the catchment can be considered at least satisfactory, the predictions in steep mountain areas are still only fair in terms of absolute values. Consistently, errors and uncertainty associated with the model results are more dependent on the resolution, density and quality of the input data than on the model structure itself. Uncertainty in the prediction at the catchment scale is related mainly to the parameters extracted from the soil unit map, where spatial resolution and detail are very low (*i.e.,* texture, erodibility), and to the extrapolation of the meteorological data over the whole catchment from a single station located outside the area of interest.

Predictions suggest that natural factors and anthropogenic disturbance on medium-gradient slope sites may have led to accelerated runoff and erosion, and these conditions may have prevailed since 1953. The results suggest that anthropogenic disturbance alters the effects of scale on runoff and erosion. Results in degraded areas are fundamentally different from those in non-degraded areas because more runoff escapes off site and consequently erosion rates are much higher. In addition, they show the existence of a slope threshold, below which semi-arid landscapes may eventually recover from the anthropogenic disturbance and above which there could be no recovery without mitigation or remediation.

5.3.3   Model validation

The accuracy of the predicted soil loss rates depends on how exactly the erosion parameters are quantified, but will never be absolute (Brazier et al., 2000). Even if the quantitative estimates are contestable, qualitative results concerning the spatial distribution of soil loss are of value. From comparing the models, it was evident that model estimates in terms of spatial distribution and absolute values depend on the weights each individual model assigns to the erosion triggering factors (*i.e.,* lithology, rainfall, gradients, land cover). Yet though the field survey in the catchment allowed the collection of at least the minimum data to run the models with a certain level of confidence, it is still clear that there is uncertainty in their estimations.

Hence, it is important to validate the accuracy of the predicted erosion rates to ensure the predictive accuracy of the model and to demonstrate to potential users that sound decisions can be made based on the estimates (Jetten et al., 2003; Van Rompaey et al., 2003a). However, van Rompaey et al. (2003c; 2005) state that it is difficult to validate the soil erosion rates at catchment scale for a number of reasons: (i) there is a lack of direct soil erosion field measurements, (ii) the time frame of field measurements is often short and does not correspond to that of the model, and (iii) measuring soil erosion rates are fraught with methodological and practical problems, and different techniques of measurement of the same erosion processes give quite different results.

The lack of soil erosion measurement in the Laka-Laka catchment hampered the application of a quantitative validation. Instead, the method adopted by the Pan European Soil Erosion Risk Assessment (PESERA) research group (Gobin and Govers, 2003b) was used. This method relies on the degree of agreement [%] derived from the comparison between the distributed predicted erosion pattern and the actual soil erosion map extracted from SPOT-5 (Figure 5.13).

The analysis reveals that the MMMF and RUSLE-3D predictions are in agreement with the locations where severe erosional features (*e.g.,* ephemeral gullies, active gullies and bank erosion) have been observed. For example, when the Thornes erosion estimates are validated, it is shown that 64% of the area is mapped in the same class or differs by one class from the validation set. Areas overestimated by the Thornes model by two classes or more represent 9% of the catchment area, while 24% of the area is underestimated by two or more classes (Figure 5.12).

The validation indicates that areas classified as slight, moderate and severe rill/inter-rill erosion in the feature map are correctly predicted with an average of 44%, 35% and 37% respectively by all models,. The overall degree of agreement is slightly improved to an average of 49%, 39%, 39% and 35% in the case of prediction for areas affected by slight active gully, moderate active gully, severe active gully and channel erosion, respectively (Table 5.7).

Performances of the models is lower than those reported in Tanzania (Vigiak, 2005), Italy (Amore et al., 2004), Belgium (Verstraeten et al., 2003b) and Mexico (Millward and Mersey, 1999). That may be because small homogenous catchments were used, whereas the Laka-Laka catchment includes a wider range of landscapes, ranging from highly dissected mountains, dissected hills and footslopes to terraces and plateaus. Moreover, the results obtained are in accordance with Nearing (2000), who states that most soil erosion models overpredict small soil losses and underpredict large soil losses.
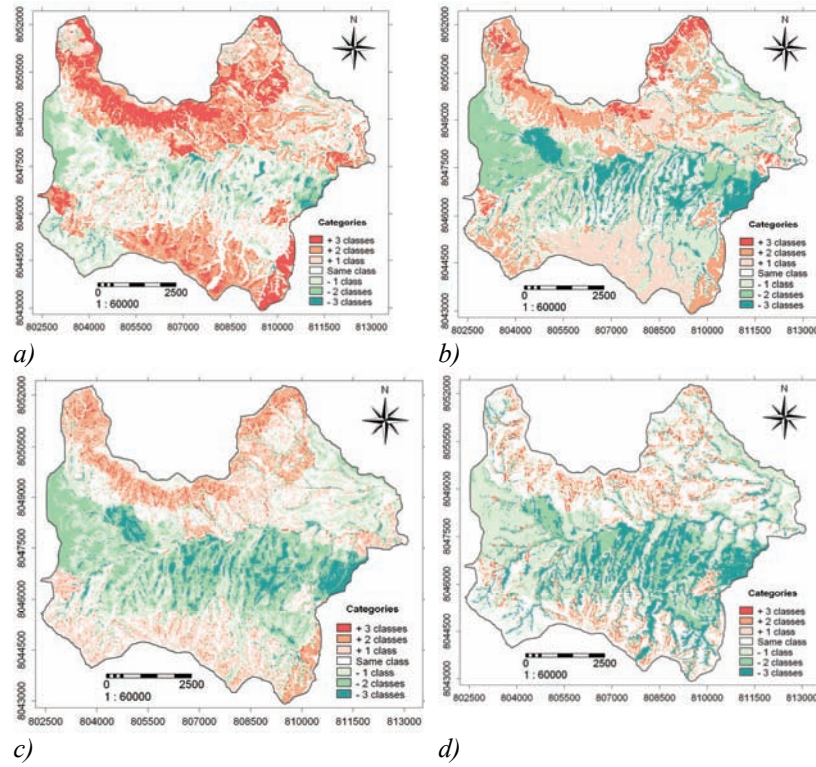
Figure 5.12 Semi-quantitative validation outputs: *a)* RUSLE-3D, *b)* MMMF, *c)* SPL, *d)* USPED model
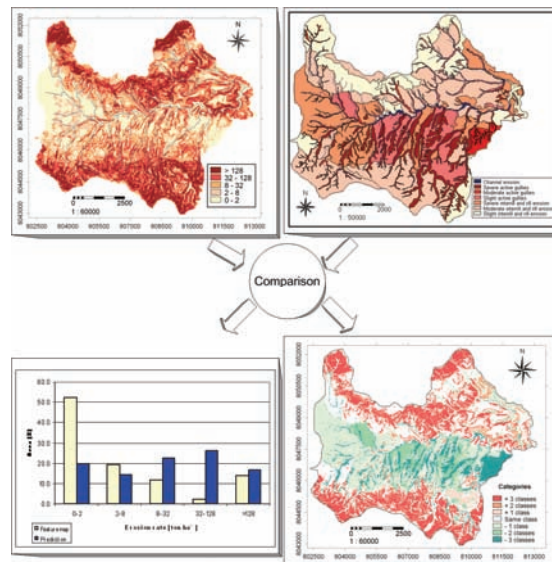
Figure 5.13 Scheme of the model validation

119

Table 5.5 Area of erosion intensity classes using continental geodata set

N	Rate of erosion [ton ha^{-1}]	Erosion risk class	RUSLE-3D Area [km^2]	Area [%]	MMMF Area [km^2]	Area [%]	SPL Area [km^2]	Area [%]	THORNES Area [km^2]	Area [%]	USPED Area [km^2]	Area [%]
1	0 – 2	Low	24.4	40.7	27.3	45.6	23.3	39.0	36.7	61.4	14.1	23.5
2	2 – 8	Medium	7.0	11.7	10.1	16.8	6.0	10.0	10.1	16.8	13.8	23.0
3	8 - 32	High	16.4	27.4	17.0	28.5	20.4	34.2	4.5	7.5	16.0	26.7
4	32 – 128	Very high	10.1	16.9	5.4	9.1	9.1	15.2	4.6	7.7	1.1	1.8
5	> 128	Extreme	2.0	3.3	0.0	0.0	1.0	1.6	4.0	6.67	0.0	0.0
6		Deposition									14.9	25.0
	Total		59.8	100.0	59.8	100.0	59.8	100.0	59.8	100.0	59.8	100

Table 5.6 Total annual denudation and annual soil loss average for the catchment using both the regional and catchment input datasets

Input datasets	Prediction	Units	RUSLE-3D	MMMF	SPL	THORNES	USPED
Catchment field-surveyed data	Annual denudation	[tonnes]	2.8×10^5	1.5×10^5	1.8×10^5	2.8×10^5	1.6×10^5
	Annual average soil loss	[tn ha^{-1}]	42.4	17	29.4	47.5	25.1
Continental data	Annual denudation	[tonnes]	1.3×10^5	0.7×10^5	1.0×10^5	1.2×10^5	0.5×10^5
	Annual average soil loss	[tn ha^{-1}]	26.9	11.3	25	17.7	13.3

From the validation analysis, it can be seen that the RUSLE-3D, Thornes and SPL models overpredict the amount of eroded soil on steeper slopes. The SPL model is driven by the shear stress effect so that it overemphasizes the effect of fluvial bedrock incision occurring in the main rivers and steep areas; the RUSLE-3D and Thornes models overemphasize the effect of slope. Notwithstanding, the degree of overestimation decreases as the capacity of the soil to produce runoff increases. Conversely, the MMMF and Thornes models underestimate the soil loss for areas with less than 40% of slope. This can be explained by the effect of vegetation cover and overland flow. The processes of soil detachment by overland and soil soil crusting are not considered in the MMMF model and any of these processes may play an important role in semi-arid catchments.

Overall, these fair prediction rates can be related to five factors: (i) the response of vegetation to rainfall is low; (ii) rainfall intensity gradually intensifies as the wet season progresses; (iii) intense rainfall events in steep mountains produce a high runoff that induces a major potential for the transport capacity of the eroded soil; (iv) overland flow affects the energy triggering soil erosion, especially after the end of the dry season; and (v) the nonlinear relationship between vegetation cover and erosion means that erosion is very high in bare areas, but low when the fraction of vegetation cover exceeds 40%. In synthesis, the model performance when using field-surveyed data in combination with medium and fine spatial resolution imagery can be categorized in the following order: SPL<USPED<THORNES<MMMF<RUSLE-3D.

Table 5.7 Mapping validation using an erosion feature map on the catchment outputs

Erosion features	Erosion rates	RUSLE-3D		MMMF		SPL		THORNES		USPED	
	[ton ha-1]	AAP [km2]	DA [%]	AAP [km2]	DA [%]	Area [km2]	DA [%]	Area [km2]	DA [%]	Area [km2]	DA [%]
Slight inter-rill and rill erosion	0-2	5.0	45.2	6.1	55.2	5.4	48.9	3.4	30.8	4.2	38.0
Moderate inter-rill and rill erosion	2-8	6.2	30.5	7.9	38.8	9.4	46.1	6.5	32.0	5.5	27.0
Severe inter-rill and rill erosion	8-32	3.7	31.7	4.5	38.6	3.5	30.0	5.1	43.7	4.8	41.2
Slight active gullies	32-128	3.5	49.9	3.1	44.2	2.5	35.6	4.8	68.4	3.1	44.2
Moderate active gullies	32-128	0.5	50.0	0.6	60.0	0.3	30.0	0.2	16.5	0.4	40.0
Severe active gullies	>128	4.0	50.5	3.0	37.9	3.2	40.4	2.5	31.6	2.9	36.6
Channel erosion	>128	0.2	34.0	0.2	34.0	0.2	36.3	0.2	40.8	0.1	22.7
Total		23.0		25.4		24.4		22.6		21.0	
Weighted accuracy			40.8		43.7		42.3		42.1		36.5

AAP: Accurate Area Prediction, DA: Degree of agreement

Table 5.8 Mapping validation using an erosion feature map on the regional outputs

Erosion features	Erosion rates	RUSLE-3D		MMMF		SPL		THORNES		USPED	
	[ton ha-1]	AAP [km^2]	DA [%]	AAP [km^2]	DA [%]	Area [km^2]	DA [%]	Area [km^2]	DA [%]	Area [km^2]	DA [%]
Slight inter-rill and rill erosion	0-2	6.5	58.9	7.0	63.6	6.1	55.3	6.3	56.8	3.7	33.7
Moderate inter-rill and rill erosion	2-8	1.7	8.5	3.1	15.2	1.7	8.4	3.7	18.3	4.2	20.7
Severe inter-rill and rill erosion	8-32	3.3	28.5	4.3	37.2	2.4	21.0	0.6	5.5	4.2	35.9
Slight active gullies	32-128	1.3	18.8	0.6	8.2	1.5	21.4	0.3	3.8	0.1	1.1
Moderate active gullies	32-128	0.1	9.5	0.1	7.2	0.1	7.9	0.0	1.8	0.0	0.0
Severe active gullies	>128	0.2	2.4	0.6	7.1	0.1	1.0	0.8	10.0	0.0	0.0
Channel erosion	>128	0.1	22.7	0.0	0.0	0.2	55.7	0.0	10.4	0.0	0.0
Total		13.3		15.7		12.2		11.8		12.2	20.4
Weighted accuracy			39.2		42.3		36.9		37.2		29.8

Given the degree of agreement obtained through the cross comparison, the quality and resolution of the input data, and the scale of the predictions, it is considered that the results obtained are at least promising.

5.3.4 Comparison of regional and catchment erosion predictions

The applicability of a purely continental dataset for catchment erosion assessment in terms of absolute values as well as spatial pattern is not encouraging. Soil loss estimates for the Laka-Laka catchment, clipped from the regional estimation of the Cochabamba province, are significantly lower than those obtained from field-surveyed catchment data (Table 5.5). Compared with the estimates at catchment scale, an underprediction by a factor of two in the total amount of eroded soil is found. It is predicted that an average of about 1×10^5 tonnes of soil are moved annually across the catchment, with an average erosion rate of 15 ton ha^{-1} yr^{-1} (Table 5.7).

There are a number of reasons for this underprediction. First, the runoff decreases when larger grid cell sizes are considered because a larger portion of the water is infiltrated. Secondly, smaller average slopes and the progressive vanishing of the larger slopes in the larger grids increase the opportunity for water to infiltrate. Thirdly, in larger grid cells the concavities and convexities of the terrain tend to disappear and thus the rates of local erosion decrease respectively. Fourthly, the slope lengths become shorter, which causes lower soil loss estimates. Lastly, overestimation of the fraction of vegetation cover is observed when using the SPOT-VGT time series.

5.3.4.1 Model intercomparison

The patterns of soil loss redistribution are similar in part to the catchment prediction outputs as a whole. However, it is evident that the large variation attributable to the pixel resolution (1 km) has taken place by reducing the soil erosion intensity in large parts of the catchment, on the one hand, and increasing areas of concentrated high soil loss, on the other. The total denuded soil, as well as the average erosion rate across the catchment, is shown in Table 5.6. A comparison of the slopes and spatial distribution of the soil loss rates pinpoints those areas with predicted highest erosion rates on the steepest slopes in all the models. Even at larger scales (regional scale) and considering the average effect on the SRTM-DEM data when resampled to 1 km cell size, the slope gradient and runoff are still the major triggering factor in erosion.

In general, it is evident that the models have a similar pattern of prediction, thus on average 43% of the catchment is considered to experience low values of erosion, 15% is exposed to medium soil loss, and an area of 13% is considered as being affected by very high and extreme soil loss rates. When these results are compared with the predictions at the catchment scale, it is observed that 33% of the area has shifted from the medium intensity class to the low erosion group, whereas the proportion of area affected by very high to extreme erosion is approximately similar in both cases.

5.3.4.2 Validation using mapped erosion features

Accordingly, the predicted regional outputs and the catchment feature erosion map were overlaid and the degree of agreement was estimated (Table 5.8). The model validation shows a significant reduction in the degree of agreement as compared with the catchment-scale validation. The overall mapping accuracy for areas classified as slight

inter-rill and rill erosion is 10% higher than on the catchment assessment. The overall accuracy for areas with moderate, high and severe intensity of erosion reduces to 20%, 10% and 5%, respectively. The possible causes for this underprediction are described in Section 5.4.1. However, three additional assumptions are made: (i) NDVI values from SPOT-VGT image time series overestimate the extent of the vegetation cover; (ii) intense rainfall events in steep mountain fronts produce a high runoff, whose effect is attenuated when using TRMM rainfall data, reducing the transport capacity of the eroded soil; and (iii) although the general pattern of erosion can be differentiated, individual patterns of gully and channel erosion are less sensitive when coarse DEM data is used.

5.4   Conclusions

In this chapter, the ability to predict catchment erosion based on satellite imagery in combination with models such as the RUSLE-3D, MMMF, Thornes, USPED, and SPL has been illustrated. These models try to capture the complexity of the landscape, using topographical parameters and basic thematic data to represent the variety of soil loss redistribution processes.

These kinds of approaches are considered more appropriate than sophisticated, physically based erosion models for data-scarce areas and when the aim is to simulate erosion and seasonal time step. Physically based erosion models include state-of-the-art knowledge of the system and provide good tools for understanding the erosion process. However, they require a large amount of data most of the time unavailable for many regions in the world, in particular for developing countries.

The integration of the topographic, meteorological, field-surveyed and remotely sensed data within a GIS provides an environment for an effective evaluation of various modelling approaches for soil erosion and deposition assessment at catchment scale. The use of the high temporal resolution MODIS-NDVI time series, and the high spatial resolution imagery SPOT-5 proved to be valuable for the continuous monitoring of vegetation dynamics and the derivation of vegetation parameters, including the analysis of the actual erosion in the catchment required for the different soil erosion models, as well as for their validation.

Likewise, when paucity of erosion measurements exists, model calibration and validation are hampered. The use of remote sensing imagery provided a spatially explicit background for an indirect model validation. The results of the validation demonstrated that none of the five models enables an accurate estimation of soil erosion across the catchment. It is therefore concluded that, although the spatial erosion patterns predicted by the different models are reliable, quantitative erosion rates should be interpreted with caution.

In terms of spatial distribution, the RUSLE-3D and USPED models proved more adequate in pinpointing ephemeral gullies. The MMMF model is more appropriate for identifying the detachment or transport limitation of potential sediment sources in the catchment. In turn, the RUSLE-3D and Thornes models show sufficiently reliable results and, since the input data required for them are lower and easier to obtain, they

are probably more suitable for predicting soil erosion in situations where detailed catchment data are not readily available.

Moreover, the ability of Thornes to estimate erosion at different time steps (*e.g.,* monthly, daily) enables the time periods where intense denudation is occurring to be identified. In the region of the Laka-Laka catchment, the period from December to March (rainy season) corresponds to the stage when significant erosion rates are predicted, following the Andean and regional climatic trend.

All the implemented models are based on modest data requirements, a common limitation in Bolivia. Their practical utility is based on providing a means of evaluating the spatial patterns of erosion and deposition and the impacts of erosion factors, besides predicting soil loss or deposition rates for a particular location.

Chapter 6

Reservoir sedimentation assessment using acoustic georeferenced sonar sounding and GIS

Chapter 6

Reservoir sedimentation assessment using acoustic georeferenced sonar sounding and GIS

6.1 Introduction

Sediments originate in the catchment mainly through land and channel erosion processes and are transported in river systems in the direction of the coast with the ocean being the final sink. Sediment transport depends on the water discharge of the river system. However, for a given river catchment size there is often a large temporal difference in the amount of sediment transported. Often sediment transport occurs in pulses. This effect is most pronounced for smaller catchments (up to 500 km^2), where 50% to 90% of the annual sediment fluxes are transported during periods lasting from days to weeks. In the largest basins (exceeding 100,000 km^2), this effect still occurs but is far less pronounced. Hence, independent of the catchment size, sediment inflow to and outflow from most natural rivers tend to reach equilibrium. Dam construction dramatically alters this balance, creating an impounded river reach characterized by extremely low flow velocities and efficient sediment trapping.

The impounded reach will accumulate sediment and lose storage capacity until the balance is again achieved. This would normally occur after the impoundment has become filled up with sediment and can no longer provide water storage and other related benefits. It diminishes the storage capacity, reducing and eventually eliminating the ability for flow regulation, and with it all water supply and flood control plus the benefits for hydropower, navigation, recreation and the environment that depend on the release from storage (Morris and Fan, 1997). Upstream of the dam, it causes aggradation of tributaries, deposition at diversions and increase in flood frequency; it leads to scouring of the riverbed, degradation of tributaries, and undercutting at diversions downstream (Tarela and Menendez, 1999). These combined impacts can substantially erode the net socio-economic benefits of dam or reservoir projects over time.

It is estimated that the annual loss in storage capacity of the world's reservoirs owing to sediment deposition is around 0.05% to 1% (Salas and Shin, 1999). However, for many reservoirs, annual siltation rates are much higher and can reach 5%, and they lose their storage capacity within 25 to 30 years (Verstraeten et al., 2003a).

On the other hand, catchment sediment mobilization, transport and yield are extremely variable in both space and time (Kothyari, 1996). Verstraeten and Poesen (2002) state that there is variation within and between catchments, such that it is suggested that drainage catchments are "fuzzy systems", with internal catchments constantly changing, thus causing major difficulties in estimating catchment sediment yields. To date, simple

statistical models such as the sediment rating curves and advanced physically based models such as WEPP (Flanagan and Nearing, 1995) or SHETRAN (Bathurst et al., 1995) still fail to produce reliable estimates of sediment yield, particularly at catchment and basin scales (Tarela and Menendez, 1999).

The absence of streamflow and sediment concentration records at these scales have led researchers such as Saavedra (2000) and Zarris et al. (2002) to prefer the use of reservoir sedimentation studies for establishing catchment sediment yields. Others have used the sediment deposited behind dams to understand transport and erosion rates at the watershed or regional scale (Verstraeten and Poesen, 2002; Dadson, 2003). Furthermore, de Vente et al. (2005) consider that the sediment stored in lakes and reservoirs offers considerable potential for reconstructing the history of sediment mobilization and transport in the catchment over the past 100 years.

These recent investigations demonstrate the importance of collecting high-quality datasets documenting the rates, physical properties, and morphology of sediment accumulation behind dams. Consequently, measurements of sedimentation in reservoirs can then be used (i) for analysis and prevention of many sediment-related problems, both upstream and downstream of the dam; (ii) for analysis of the reservoir life expectancy; and (iii) for monitoring the periodic build-up of sediments in the reservoir.

Classical surveys are conducted with standard single-beam echo sounders or high-resolution multibeam echo sounders. Survey standards follow those outlined in the engineering and design hydrographic surveying manual (HQUSACE, 2002). They involve repeated field measurements and they are probably the most costly and time-consuming methods. Notwithstanding, a number of errors arise when using these data. Sources of errors and uncertainties are associated with the surveying techniques used, density of depth sampling points, and interpolation and averaging during map preparation. Conventional estimation of the spatial distribution of sediments deposited in reservoirs requires a very dense network of control points (Hicks and Hume, 1997). Several methods have been proposed for the interpolation of bathymetric data to obtain a continuous surface (Mills, 1998).

The simplest approach consists of assigning the record of the closest point to the unsampled location. The U.S. National Weather Service developed another method whereby the unknown depth is estimated as a weighted average of the surrounding values, the weights being reciprocal to the square distance from the unsampled location (Yfantis et al., 1987). The isoline approach was designed to overcome limitations of the aforementioned method. The objective is to use the location of a registered depth, as well as the knowledge of the factors affecting the registered values, to draw lines of equal depth (*i.e.*, isolines). The correct depth at the unsampled location is then estimated by interpolation within the isolines. A limitation of this technique is that it requires an extensive sample network to draw the isolines accurately (Poon et al., 2000).

Most practitioners are aware that many sedimentation estimates are consequently uncertain and that such uncertainty must be accounted for in the decision-making process (Goovaerts, 1999). Geostatistics, which is based on the theory of regionalized variables, is increasingly preferred because it allows the spatial correlation between

neighbouring observations to be integrated in the prediction of attribute values at unsampled locations (Goovaerts, 2001). Although individual points define the accuracy of a bathymetric survey, all points within the focus area determine the overall accuracy of bathymetric analysis describing the geomorphic changes in the lake or reservoir (Woodcock and Gopal, 2000).
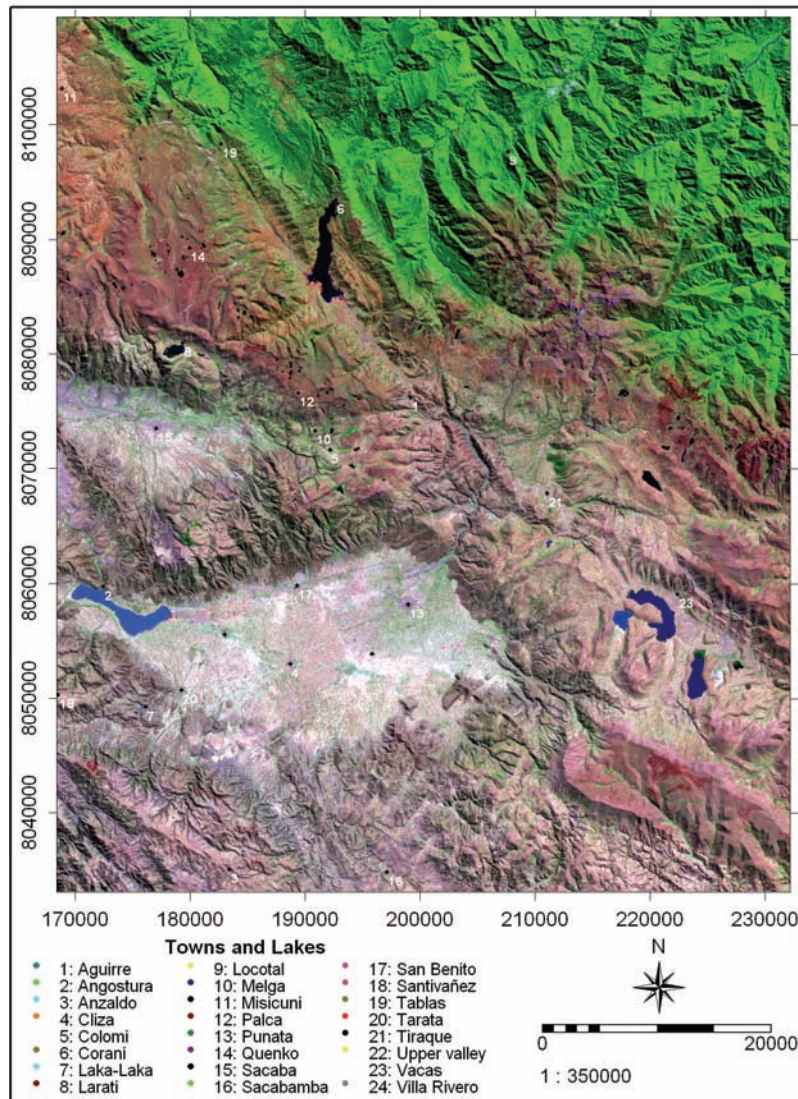
Figure 6.1 Location of towns, upstream catchments, reservoirs and lakes on a Landsat-7 ETM false-colour composite (July 2000)

Hence, a rapid, accurate and versatile method that combines low-cost technology and geostatistics is proposed, on the one hand, to provide quantitative estimates and spatial distribution of sediments deposited in reservoirs and, on the other, to indirectly provide

sediment yield from the drainage catchment by efficiently combining the reservoir sedimentation rates with the sediment bulk density and reservoir sediment trap.

The aim of this chapter is therefore to assess the use of a low-cost GPS coupled to an acoustic sonar sounder, in combination with ancillary satellite data, to map reservoir and lake bathymetry.

In order to fulfil this aim five specific objectives were considered: (i) to analyse the effect of the sample size or point density of sonar soundings on the accuracy of the bathymetric surface generation, (ii) to evaluate the interpolation methods for generating bathymetric surfaces, (iii) to estimate historical changes in storage volume and sediment deposition in three important reservoirs of the study area, (iv) to determine actual storage capacity and life expectancy of the three reservoirs, and (v) to derive the sediment yield of the Laka-Laka reservoir catchment from multitemporal reservoir sedimentation data.

6.2 Methods and data

Bathymetric surveys are generally conducted with a transducer (usually attached to the boat), which both transmits a sound pulse from the water surface and records that same signal when it bounces from the bottom of the water body. An echosounder attached to the transducer filters and records the travel time of the pulse. At the same time as the pulse occurs, a differential GPS unit can record the location of the reading. After many of these readings have been taken, corrections are made based on fluctuations in the water surface elevation that may have occurred during the survey.

The volumetric accumulation of sediments in the reservoirs is estimated by differencing bathymetric surveys taken at different time spans. This method is an effective means of quantifying deposition rates, particularly in reservoirs where the topography of the river prior to the dam construction is available. The proposed bathymetric survey method was implemented in three reservoirs and two lakes (Figure 6.1) located in the research area. Interpolated surfaces were derived from the acoustic depth-sounding data, and detailed maps of the pre-dam river and valley topography were obtained from previous studies. The dam and reservoir site characteristics are described in Chapter 3. The various datasets relevant to this study are outlined briefly below.

6.2.1 Historical reservoir bathymetry data

6.2.1.1 Corani reservoir

Topographical data of the reservoir site before construction (1967) was made available by the CORANI enterprise headquarters. In 1987, the National Hydrographic Navy Service conducted a bathymetry survey in which approximately 5,000 depth points along the ship track-lines were used to construct the surface of the reservoir bed. These data were prepared based on an irregular point network distribution throughout the reservoir. The minimum distance among nearby points was about 300 to 400 m. The points were converted into a contour map to allow the estimation of the area-volume relationship. In 1997, a second bathymetric and topographical survey was carried out by the Geodesic and Topographic Service (SGT, 1998). These data were collected along transects across the reservoir. The transects were generally 300 m apart, with a

minimum distance of 100 m between sampling points. The survey data were available in CAD format.

6.2.1.2 Angostura reservoir

Topographical survey data prepared in 1939 by the Mexican Corps of Engineers at the reservoir site prior to the dam construction were made available by the Angostura Irrigation System Farmer Association (ARSN-1). The 23 1:1,000 topographical sheets encompassing the reservoir site were digitized (Figure 6.2) in order to obtain the DEM at the dam site. In September 1990, the ARSN-1 contracted an engineering firm to conduct a topographical/bathymetric survey. The survey provided four 1:5,000 topographical maps with 2 m contour lines and the depth-area-capacity curve that is currently used for dam operation. Note that neither of the two datasets presented geographical coordinates.

6.2.1.3 Laka-Laka reservoir

In April 1990, a pre-dam topographical survey was carried out at the location of the future reservoir. The survey registered the lowest elevation at 2,775 masl. These topographical data yielded the area-capacity curve of the reservoir. Owing to the high rates of sediment deposition observed in the reservoir (rainy season 1993 to 1994) after a short period of operation (2.4 years), the Canadian Agency for International Cooperation (CAIC) entrusted an update of the bathymetric survey to the Hydraulic Laboratory of the Major University of San Simon (LH-UMSS) in July 1994. The survey reported that the reservoir had lost almost 21% of its original capacity. One year later, a new survey was carried out as the sedimentation was progressively reducing the capacity of the reservoir.

In order to reduce the sedimentation of the reservoir, the CAIC decided to construct a bottom-withdrawal spillway for sediment flushing in 1995 (Lai and Shen, 1996; White, 2001). The first sediment flushing was carried out in November 1996, releasing a volume of 60,000 m^3 of sediments. Since then, either one or two operations have been carried out at the beginning of each rainy season (Torrico, 1999). To evaluate the effectiveness of the sediment flushing, the last topographical/bathymetric survey was carried out in May 2001 as part of the research project entitled "Sedimentation in small irrigation reservoirs and implications for the design" that was funded by the National Programme of Irrigation (PRONAR, 2001). All bathymetric data were available in CAD format.

6.2.2 GPS-guided acoustic sonar survey

A GPS-guided bathymetric survey was designed, tested and conducted in the research reservoirs and lakes, and executed during April and May 2003. A low-cost Fishfinder-100 Garmin sonar sounding device and a handheld GPS-72 Garmin system recorded location at user-defined intervals of five seconds. The GPS-72 provides precise positioning coordinates when using the correction data obtained from the Wide Area Augmentation System (WAAS). An accuracy of less than 3 m was obtained when receiving WAAS corrections. The GPS-72 is also able to record the data provided by the sonar using the GARTRIP software (Pfeifer, 2005).
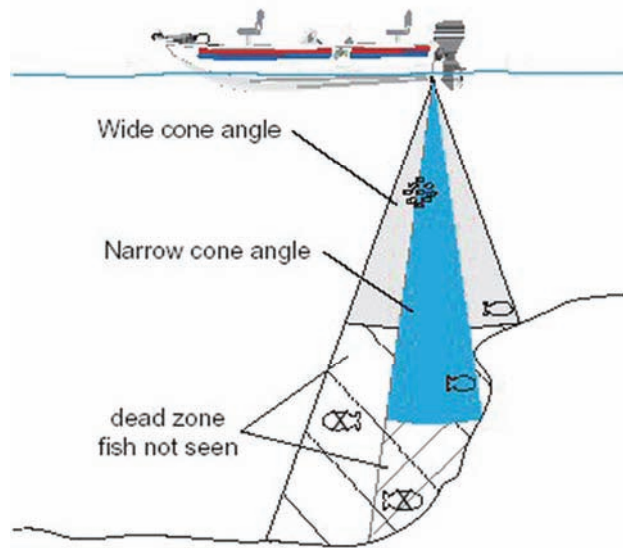
Figure 6.2 Schematic representation of the handheld GPS-guided sonar survey
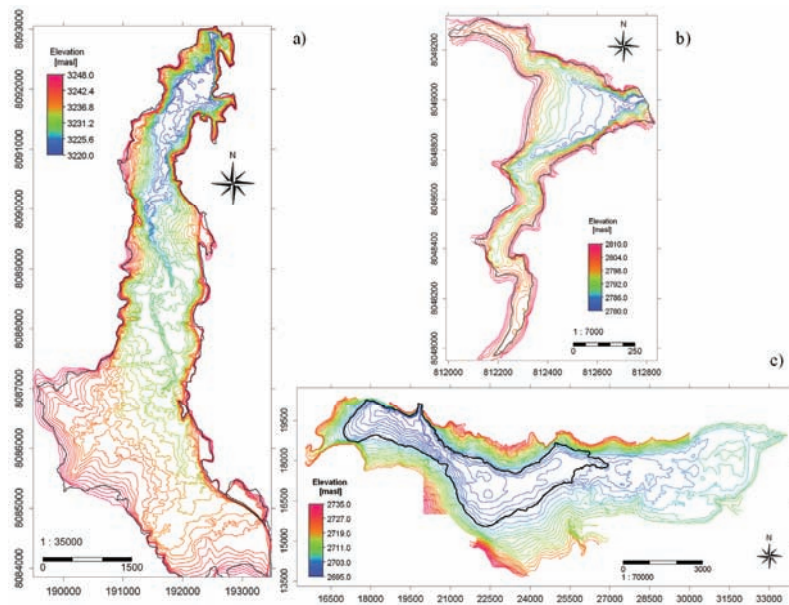
Figure 6.3 Maps of the pre-dam river topography: *a)* Corani (1967), *b)* Laka-Laka (1990), *c)* Angostura (1947)

The Fishfinder-100 acoustic sonar sounder operates at a frequency of 200 kHz and outputs digital depths with a precision of 15 cm. A schematic setup of the GPS bathymetric survey is shown in Figure 6.2. In principle, the transducer transmits sound waves towards the bottom in a cone shape. The larger the cone angle, the larger the coverage area at a given depth. A wide cone angle transducer works best in shallow water. The wide cone angle provides a large coverage area, but a decreased bottom resolution. A narrow cone angle transducer is better suited to deep-water installations (Banks and LaMotter, 1999). The surveyed data (*sampling points*) have a horizontal location accuracy of ±3 m and a vertical accuracy of ±15 cm. These accuracies comply with the standards of the International Hydrographic Organization Order (HQUSACE, 2002).

The bathymetric survey was carried out along previously designed transects. The GPS recorded the geographical location of the boat on the lake and the acoustic sonar determined the depth to the top of the bottom sediment (Baker and Morlock, 2001). The survey was conducted so that the distance between parallel track-lines was less than 25 m (Leonard and Coughlan, 2002). To minimize the effect of line transect surveying, complementary data were collected in a random distribution and with a very high temporal resolution, yielding a scattershot pattern. The points were digitally recorded and stored in a laptop, where additional processing was done to adjust to the pool elevation and to compare both original and previous reservoir data with available bathymetric surveys (Listh et al., 1997). For comparison purposes, the different bathymetric datasets were georeferenced to a unique coordinate system (Van der Wal and Pye, 2003). All datasets were reprojected to the UTM coordinate system and the WGS84 geodetic datum.

Besides the GPS-tracked sonar sounding, an innovative key element of the methodology was the derivation of the extra lake contour height information from remote sensing data. With this information, the digital surface of the reservoir bed was constructed from data corresponding to three different datasets: (i) topographical survey prior to the dam construction, (ii) existing bathymetric/topographical surveys, and (iii) GPS-guided bathymetric survey in combination with the lake land/water line contours from satellite imagery. Figure 6.3 shows the topographical maps prepared prior to the dam construction. They were constructed by digitizing the original topographical maps referred to a Cartesian coordinate system, and used to assess the initial reservoir storage capacity. The original topographical data for the Corani, Angostura and Laka-Laka reservoirs were reprojected and geocoded using 36, 32, 22 control points respectively. A linear contour interpolation algorithm method was used to obtain the bathymetric surface from the original topographical surveys (Koolhoven et al., 2005).

6.2.3 Spatial interpolation

The geostatistical analysis may provide valuable insight into the spatial deposition pattern of sediments in a reservoir, even with a limited number of data (Pebesma and Wesseling, 1998). Once an assessment is made of the sediment pattern as a function of distance, contours can be produced and additional detailed sampling and/or dredging activities can be performed with more confidence (Saito and Goovaerts, 2002). When using kriging methods, weights are assigned to measurement points on the basis of the

distance in which spatial autocorrelation is quantified, in order to weight the spatial arrangement of measured sampling locations (Isaaks and Srivastava, 1989).

The kriging procedure requires the covariance structure of the "depths" in the form of a variogram that is a measure of the average dissimilarity between data separated by a distance *h*. The practice of ordinary kriging involves calculating and modelling variograms. By accounting for statistical distance with a variogram model, as opposed to Euclidean distance utilized in deterministic interpolation, customization of the estimation method to a specific analysis is possible. As expected, this variogram quantifies the commonly observed relationship between the values of the samples and the proximity of samples. Given the statistical properties of this method, measures of the uncertainty and accuracy of the predictions can be produced using a cross-validation process.

6.2.3.1 *Sample size*

Spatial heterogeneity is a fundamental environmental characteristic that is also present in aquatic systems such as lakes and reservoirs (Krivoruchko and Gribov, 2002). The spatial analysis of different sample-size datasets requires an appreciation of the stationary and data variography factors, as well as consideration of optimal sampling design (*i.e.*, location and size), to optimize the quality of the geostatistical model. The analysis starts from the hypothesis that the sample locations and the size of sample points affect the reliability of the bathymetric surface. Since any geostatistical method is influenced by spatial relationships, it is presumed that the relationship between both locations and size sample will have an effect on the overall assessment.

This is in agreement with Kitsiou et al. (2001), who state that the reliable interpolated surface depends greatly on the sample design and variogram modelling. For the geostatistical analysis, individual reservoir depth samples were randomly split into six subsets. For each lake, sets containing 1.56%, 3.12%, 6.25%, 12.5%, 25%, 50% and 100% of the total sampling were thus individually analysed and interpolated. Accordingly, 98.4%, 96.8%, 93.7%, 87.5%, 75% and 50% of these sets randomly removed served as verification data points. The verification points provided ground truth comparison for the various interpolation methods and for identifying associated errors. In other words, the accuracy of each interpolated surface was estimated by comparing the estimates of the surface model (*prediction points*) with actual measurements (*observed points*). In turn, an assessment of the optimal sampling size required for an accurate bathymetric surface was made. The descriptive statistical analysis of each sampling subset is presented in Table 6.1.

6.2.3.2 *Ordinary kriging*

Kriging methods utilize statistical models that incorporate autocorrelation among a group of measured points to create prediction surfaces (Desbarats, 1996). For a detailed presentation of the different kriging algorithms, readers are referred to Deutsch and Journel (1998) and Pebesma and Wesseling (1998). The univariate kriging methods consider the estimation of values of a continuous attribute *z* (depth) at any unsampled location *u*, using the depth data available over the study area *A*.

Table 6.1 Descriptive statistics of the prediction subsets. **ID** is the subset sample identification, **P** is the percentage of sample size, **PS** is the number of samples used for the prediction, **VS** is the number of samples used for validation, **ȳ** is the mean, **PD1** is the sampling density per 100 m cell, **PD2** is the sampling density per 1 km cell, **SE** is the standard error, **Me** is the median, **Mo** is the mode, **SD** is the standard deviation, **SV** is the sample variance, **K** is kurtosis, **S** is the skewness, **R** is the range, **Min** is the minimum values, **Max** is the maximum values and **C** is the confidence coefficient at 95%.

ID	P [%]	P.S	V.S	PD1	PD2	ȳ [m]	S E	Me [m]	Mo [m]	S.D.	S.V.	K	S	R [m]	Min [m]	Max [m]	C
Angostura [100%]	100	11752		10	983	2701.5	0.01	2701.83	2703.10	1.56	2.42	-0.9	-0.6	6.01	2698	2704	0.03
Angostura [50%]	50	5860	5892	5	490	2701.5	0.02	2701.83	2702.90	1.56	2.44	-0.9	-0.6	6.01	2698	2704	0.04
Angostura [25%]	25	2933	8819	2	245	2701.5	0.03	2701.75	2702.90	12.54	2.37	-0.9	-0.6	5.91	2698	2704	0.06
Angostura [12%]	12.5	1467	10285	1	123	2701.5	0.04	2701.85	2703.00	1.54	2.36	-0.9	-0.6	5.81	2698	2704	0.08
Angostura [6%]	6.25	734	11018	1	61	2701.6	0.06	2701.95	2703.00	1.54	2.37	-0.8	-0.7	5.47	2698	2704	0.11
Angostura [3%]	3.125	367	11385	0	31	2701.5	0.08	2701.84	2703.00	1.6	2.56	-1	-0.6	5.2	2698	2704	0.16
Angostura [1%]	1.56	184	11568	0	15	2701.4	0.12	2701.75	2703.00	1.61	2.61	-1.1	-0.5	5.2	2698	2704	0.24
Corani [100%]	100	17051		12	1202	3236.4	0.05	3238.64	3243.19	7.12	50.7	-0.6	-0.7	32.1	3213	3246	0.11
Corani [50%]	50	8526	8525	6	601	3236.4	0.08	3238.69	3243.19	7.08	50.1	-0.6	-0.8	30.7	3215	3246	0.15
Corani [25%]	25	4264	12787	3	301	3236.3	0.11	3238.69	3243.09	7.24	52.5	-0.6	-0.7	30.8	3215	3246	0.22
Corani [12%]	12.5	2133	14918	2	150	3236.4	0.15	3238.54	3242.99	7.14	51	-0.6	-0.7	28.9	3217	3245	0.30
Corani [6%]	6.25	1066	15985	1	75	3236.5	0.22	3238.59	3242.89	7.07	50	-0.6	-0.7	27.4	3218	3245	0.43
Corani [3%]	3.125	534	16517	0	38	3236.3	0.31	3238.54	3242.69	7.10	50.4	-0.8	-0.7	27.1	3218	3245	0.61
Corani [1%]	1.56	268	16783	0	19	3236.4	0.46	3238.79	3242.89	7.33	53.70	-0.7	-0.7	27.1	3218	3245	0.90
Laka-Laka [100%]	100	6790		283	28291	2796.4	0.06	2796.1	2789.48	4.55	20.8	-1.3	0.1	18.7	2786	2805	0.11
Laka-Laka [50%]	50	3375	3415	141	14065	2796.5	0.08	2796.1	2792.7	4.5	19.8	-1.2	0.1	16.8	2788	2805	0.15
Laka-Laka [25%]	25	1705	5085	71	7104	2796.4	0.11	2796	2792.8	4.6	20.9	-1.3	0.1	17.8	2787	2805	0.22
Laka-Laka [12%]	12.5	873	5917	36	3637	2796.5	0.16	2796.4	2792.7	4.6	20.8	-1.3	0.1	16.3	2788	2805	0.31
Laka-Laka [6%]	6.25	444	6346	19	1850	2796.4	0.22	2796	2792.8	4.6	21	-1.2	0.1	17.8	2787	2805	0.44
Laka-Laka [1%]	1.56	119	6671	5	496	2796.2	0.4	2796.1	2792.7	4.1	16.6	-1	0.3	16.3	2788	2805	0.79

The basic idea behind kriging is that observations that are close to each other on the lake tend to be more alike than those further apart. Instead of the Euclidian distance, kriging uses the semivariogram as a measure of dissimilarity between observations. According to Burrough and McDonell (1998), the semivariogram γ_h for a separation distance h between sample points is the first step towards a quantitative description of the spatial variance in the data and is defined as half the average squared difference between the paired data values:

$$\gamma_h = \frac{1}{2N(h)} \sum_{\alpha=1}^{N(h)} \left[z(u_\alpha) - z(u_\alpha + h) \right]^2 \qquad\qquad \textit{(Eq 6.1)}$$

where $\{z(u_\alpha), \alpha=1,...,n\}$ is the set of depth data measured at n points and locations u, h is the lag distance, N is the number of observation pairs, $N(h)$ is the number of point pairs of data locations a vector h apart, z is the attribute value of interest, in this case elevation, and u is an index notation denoting the location of z. Here h is the distance between two points used to calculate the variance (Borga and Vizzaccaro, 1997). In order to extract valuable information for the interpolation, first a theoretical variogram model must be fitted to the experimental variogram. The experimental variogram is the plot of the variances calculated at each lag distance. Once it is calculated, the modelled variogram can be represented using several equations, such as linear, spherical, exponential and circular, among others.

The modelled variogram equation parameters are used to interpolate the depth at the unknown points. The change in the three features of a variogram (*i.e., sill, range* and *nugget*) for each lake sample set and with different sample size were consequently evaluated. The sill describes the variance within the data at distances far enough apart that there is no spatial correlation. The range is the distance at which spatial correlation is no longer evident and the sill has been reached. The nugget is the variance at lag distances smaller than the sampling interval or noise in the data (Deutsch and Journel, 1998). The models cannot be any randomly chosen function. Only certain mathematical functions are a permissible model for covariance functions and so only certain functions are valid for variograms. The three different types of permissible models for fitting the experimental semivariogram of depths can be observed in Figure 6.4 and its mathematical representation reads as:

Spherical model with a range a

$$\gamma_{(h)} = Sph\left(\frac{h}{a}\right) = \left\{ 1.5\frac{h}{a} - 0.5\left(\frac{h}{a}\right)^3 \qquad if \quad h \leq a \right.$$

$$\textit{(Eq 6.2)}$$

Exponential model with practical range a:

$$\gamma_{(h)} = 1 - \exp\left(\frac{-3h}{a}\right) \qquad\qquad \textit{(Eq 6.3)}$$

otherwise,
Gaussian model with practical range a:

$$\gamma_{(h)} = 1 - \exp\left(\frac{-3h^2}{a^2}\right) \qquad\qquad \textit{(Eq 6.4)}$$

The first two models have been fitted using regression and are such that the weighted sum of squares (WSS) of differences between experimental $\hat{\gamma}_{(h)}$ and model $\gamma_{(h)}$ semivariogram values is minimum.

$$WSS = \sum_{k=1}^{K} \omega(h) \left[\hat{\gamma}(h) - (\gamma(h) \right]^2 \qquad \text{(Eq 6.5)}$$

The weight $\omega(h)$ given to each lag h is often taken proportional to the number of data pairs $N(h)$ that contribute to the estimate $\hat{\gamma}_{(h)}$. The implicit assumption is that the reliability of an experimental semivariogram value increases with statistical mass. The value of the *WSS* criterion is frequently used to rank alternative models, say to compare the goodness of fit of a spherical model versus an exponential one.
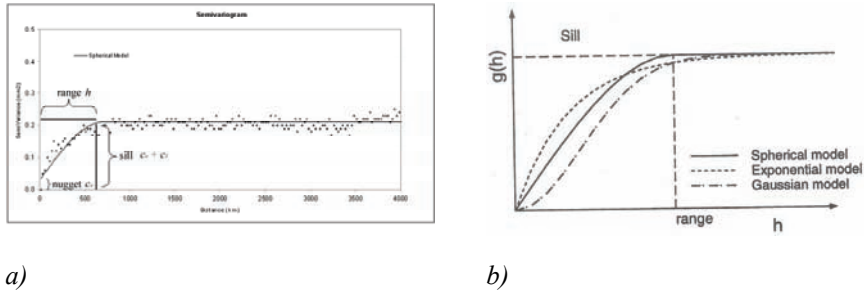
Figure 6.4 *a)* Features of an experimental semivariogram, *b)* semivariogram models with the same practical range (source: (Goovaerts, 1997)

To conclude, as a general rule, when a variogram is best fitted by a Gaussian model, this suggests that the variation in the spatial process is smooth. When the variogram is modelled by a spherical model, then it has a clear transition point, which means the one pattern is dominant. If an exponential model is chosen, this may suggest that the pattern of variation shows a gradual transition over a spread of ranges or that a number of patterns are present. The semivariogram modelling is not the prime objective (Saito and Goovaerts, 2003); the goal is to estimate the elevation (*depth*) at unsampled locations.

Heuvelink (2002) states that in contrast to simple kriging (*sk*), ordinary kriging (*ok*) allows one to account for the local variation of the mean by limiting the domain of stationarity of the mean to the local neighbourhood $W_{(i)}$ centred on the location i being estimated. The ordinary kriging estimator $z*_{ok(i)}$ reads as:

$$z_{ok}^*(u) = \sum_{\alpha=1}^{n(u)} \lambda_{\alpha}^{ok}(u) z(u\alpha) \quad with \quad \sum_{\alpha=1}^{n(u)} \lambda_{\alpha}^{ok}(u) = 1 \qquad Eq\ 6.6$$

The number $[n(u)]$ of weights $[\lambda_{\alpha}^{ok}(u)]$ are determined such as to minimize the estimated variance $[Var\{z_{ok}^*(u) - z(u)\}]$ while ensuring the unbiasedness of the estimator $[E\{z_{ok}^*(u) - z(u)\} = 0]$. These weights are obtained by solving a system of *[n(u)+1]* linear equations with *[n(u)+1]* unknowns, which is known as the "ordinary kriging system":

$$\begin{cases} \sum_{\beta=1}^{n(u)} \lambda_\beta^{ok}(u) \, C_R\left(u_\alpha - u_\beta\right) - \mu_{(ok)}(u) = C_R(u_\alpha - u) \\ \qquad \alpha = 1,..,n(u) \\ \qquad \sum_{\beta=1}^{n(u)} \lambda_\beta^{ok}(u) = 1 \end{cases}$$

(Eq 6.7)

where $\mu_{(ok)}(u)$ is the Lagrange parameter accounting for the constraints of weights. The only information required by the kriging system (Eq 6.7) is semivariogram values for different lags, and these are derived from the modelled semivariogram.

6.2.3.3 Cross validation

The ordinary kriging was implemented using the R freeware software (Pebesma and Wesseling, 1998; Paradis, 2002) to derive the bathymetric surfaces as well as the error residuals for each reservoir data subset. As one of the aims of this section was to assess the accuracy of the estimation at unsampled locations with progressive reduction in the sample size, only the omnidirectional semivariogram for each subset was estimated, assuming that the spatial variability was isotropic. The kriging strategy effectively assumes that semivariances are estimated without error. However, studies have shown that in practice different choices of variogram models or use of different range and sill parameters within a family of models can have quite significant effects on model predictions (Goovaerts, 1999).

The performances of the seven bathymetric surfaces were assessed and compared using cross validation (Isaaks and Srivastava, 1989). The technique consists of removing a percentage of the original sample and re-estimating these values from the remaining data using different semivariogram models. Interpolated and actual values are compared, and the subsample that produces the more accurate predictions is retained. The objective is to compare observed values of the prediction subset with the estimated value of the interpolated grid. On the basis of the cross-validation results, accuracy can be determined regarding the chosen model and method of interpolation for each prediction.

Comparison of prediction among different subsets was based on seven measures of accuracy: bias (B), goodness of fit (r^2), coefficient of correlation (r), root mean square error ($RMSE$), mean square error (MSE), mean absolute error (MAE) and the Nash-Sutcliffe coefficient (R_{NS}^2). The bias measures the average deviation of the statistics and is expressed as:

$$B = \frac{\sum_{i=1}^{N} \hat{z}_i - z_i}{N}$$

(Eq 6.8)

where $\hat{z}_i$ refers to the estimator of the parameter z_i and N is the number of samples. The goodness of fit or coefficient of determination (r^2) verifies the percentage of the data that can be explained by the algorithm.

$$r^2 = \frac{\sum\limits_{i=1}^{N}\left[\hat{z}_i - \bar{z}_i\right]^2}{\sum\limits_{i=1}^{N}\left[z_i - \bar{z}_i\right]^2}$$

(Eq 6.9)

where $\bar{z}_i$ refers to the average of the parameter z_i and N is the number of samples. The coefficient of correlation reads as:

$$r = \sqrt{r^2}$$

(Eq 6.10)

The *RMSE* is a commonly employed measure of estimator performance. The *RMSE* is used by the USGS to indicate the vertical accuracy of an entire grid. Here, the *RMSE* represents the expected accuracy of the grid considering each point under the simulated uncertainty conditions. The *RMSE* is expressed as:

$$RMSE = \sqrt{\frac{\sum\limits_{i=1}^{N}\left\{\hat{z}_i - z_i\right\}^2}{N}}$$

(Eq 6.11)

The *MSE* of prediction measures the average square differences between the true elevation z_i and its estimate $\hat{z}_i$. The value of this criterion should be close to zero if the algorithm is accurate.

$$MSE = \frac{1}{N}\sum\limits_{i=1}^{N}\left[\hat{z}_i - z_i\right]^2$$

(Eq 6.12)

The *MAE* is computed as the average absolute difference between actual and estimated value at the N sampled locations:

$$MAE = \frac{1}{n}\sum\limits_{i=1}^{N}\left|z_i - \hat{z}_i\right|$$

(Eq 6.13)

The Nash-Sutcliffe coefficient R_{NS}^2 compares estimated values with the observed average values ($\bar{z}_i$).

$$R_{NS}^2 = 1 - \frac{\sum\limits_{i=1}^{N}\left[z_i - \hat{z}_i\right]^2}{\sum\limits_{i=1}^{N}\left[z_i - \bar{z}_i\right]^2}$$

(Eq 6.14)

Finally, the interpolated sample subset that yields the more accurate predictions is retained.

6.2.4   Reservoir sedimentation volumes

To determine the net change in sediment deposition as a function of time, the ultimate (2003) bathymetric surface was subtracted from the earlier and original topographical pre-dam surfaces. The total volume and rate of sediment deposition in the reservoirs were determined by comparing recent reservoir bottom elevations and those prior to the impoundment (Radoane and Radoane, In Press). The difference in elevation between the periods is primarily the result of sediment deposition. To convert volumetric

changes to sediment yield in mass units, the material properties of the deposited sediment were also investigated by collecting core samples from the reservoir.

Direct measurements of sediment densities were not carried out because of the impossibility of collecting submerged undisturbed core samples. However, density was estimated from the proportion of sand, silt and clay in the samples by using the Lane and Koelzer (1943) formula and the sediment compaction equation (Julien, 1995). Further, sediment volumes were converted into weight (Morris and Fan, 1997). As not all sediment entering the reservoir is trapped, the trap efficiency of the reservoirs was estimated using the Brune (1953) capacity inflow ratio curve, based on the ratio of reservoir capacity to total annual inflow. The catchment sediment yield was estimated from the sediment weight, adjusted for trap efficiency and specific catchment area.

6.3   Results and discussion

6.3.1   Lake shoreline extraction from ancillary satellite data

The boundary of the reservoirs or lakes was extracted from enhanced colour composite images derived from SPOT-5, ASTER and Landsat-7 ETM (Figure 6.2). Accurate shoreline and additional elevation contours for the lake or reservoir can be obtained if the lake level at the time of satellite overpass is known. As the surveyed dates did not coincide with satellite overpasses, an alternative approach was to use the GPS track along the shoreline derived at the date of the survey and to overlap this information with the most up-to-date available satellite image (Landsat ETM-7, SPOT-5) for comparison purposes. The shorelines obtained using this approach show acceptable levels of accuracy, also when compared with other sources (*e.g.,* LH-UMSS (1994), LH-UMSS (1995), SGT (1998))

6.3.2   Variogram analysis

The variograms of each reservoir subset were evaluated using Eq 6.1. Both the estimated experimental semivariogram and the model fitted for the Angostura and Corani reservoirs are shown in Figure 6.5 and Figure 6.6. The modelled variograms for the Angostura reservoir present a remarkable similarity in pattern and shape. In all subsets, semivariogram values increase with the lag distance, reflecting correlation among nearby points.

However, consecutively the semivariogram computed with the whole sample size shows variations between lags because of the existence of areas with high depth variability. Unlike Angostura, variograms for the Corani subsets were calculated up to a distance of 1 km. The fitted semivariogram depicted a large nugget variance, which reaffirms the existence of little spatial dependence at distances greater than 1 km (Table 6.2).

Angostura [1%][(a,b)]

Angostura [6%]

Angostura [12%]

Angostura [25%]

Angostura [50%]
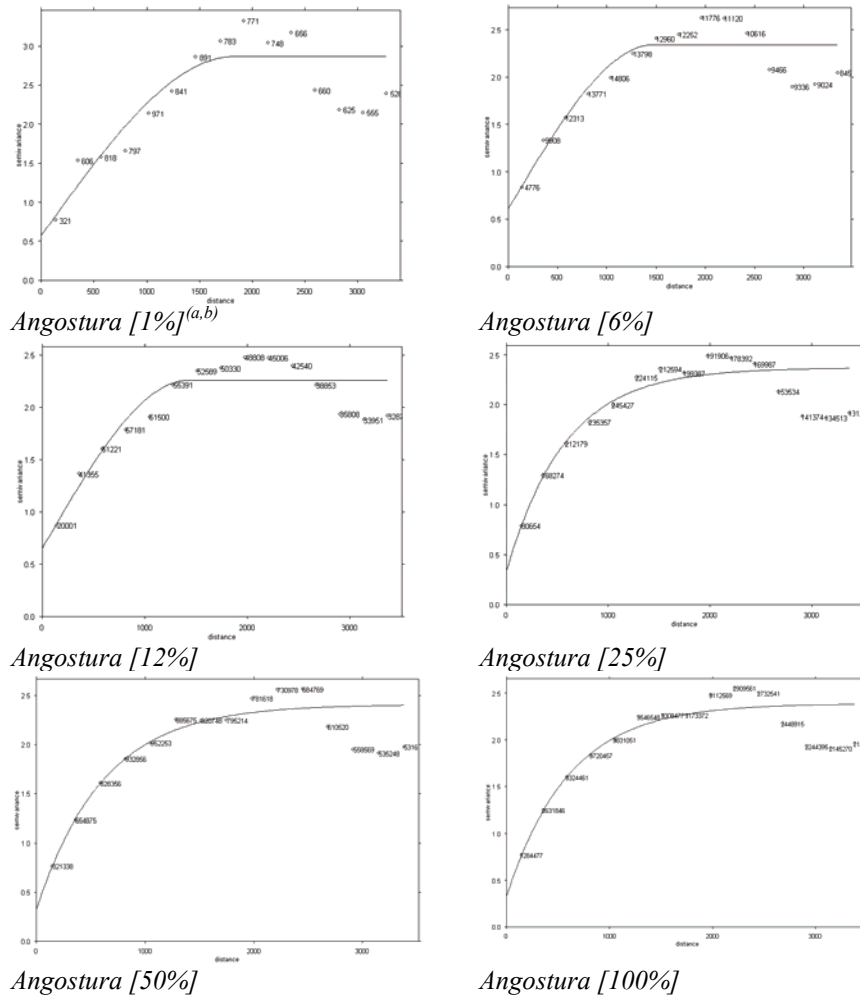
Angostura [100%]

Figure 6.5 Experimental and fitted semivariograms for Angostura subsets: *a)* subset 1 with 1.65 % of the total sampling, *b)* distance expressed in metres

Considering both the high sedimentation reported at the reservoir and its small size, the semivariograms for the Laka-Laka reservoir were calculated up to a distance of 150 m, showing the high spatial variability among nearby points.

The spherical model was used to fit most of the experimental semivariograms. However, in cases where the spherical model did not perform correctly, the exponential model was selected. For sample sizes greater than 10,000 points, as in the case of the Angostura and Corani reservoirs, it was necessary to estimate heterogeneous (*local*) semivariograms (Whelan et al., 2001). In other words, a moving window or kernel was centred on the location to be predicted and a semivariogram created for each local area. The prediction of each point in the reservoir was mapped sequentially as the window moved through the reservoir. Within each neighbourhood, the data are assumed to be locally stationary, and hence the assumptions of the ordinary kriging algorithm were not violated.

Corani [0.75%]$^{(a,b)}$

Corani [1%]

Corani [3%]

Corani [6%]

Corani [12%]

Corani [25%]

Corani [50%]

Corani [100%]
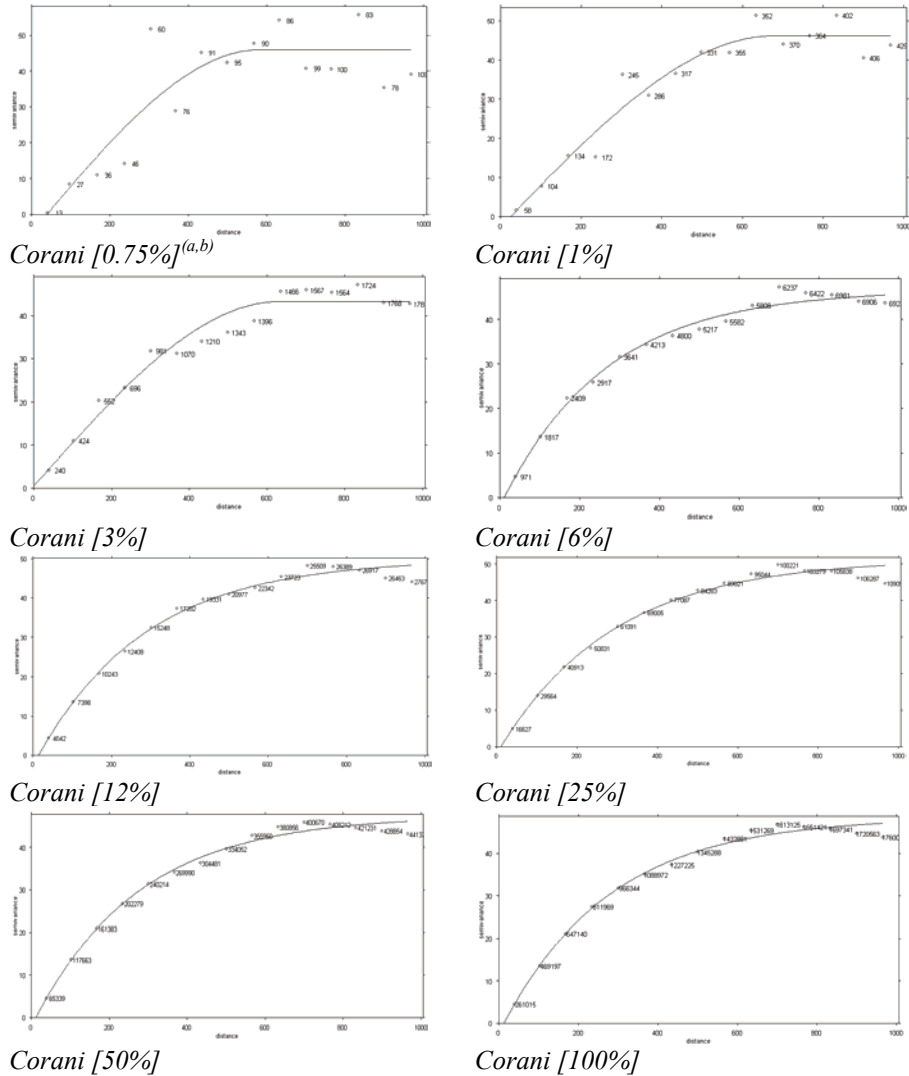
Figure 6.6 Experimental omnidirectional semivariograms with the fitted model (Corani reservoir): *a)* subset 1 with 0.75 % of the total sampling, *b)* distance expressed in metres

6.3.3 Cross validation

The performance of the bathymetric surface with the optimal sample size was assessed using cross validation. The cross-validation statistics were calculated as goodness of fit (r^2), *RMSE*, *MSE* and the Nash-Sutcliffe coefficient. The cross-validation results are displayed in Table 6.3. These summary statistics were utilized to determine, on average and for the entire lake, uncertainty under the six different error scenarios. The statistics of each estimator incorporate the spatial distribution of simulated uncertainty for every cell location in the reservoir.

Table 6.2 Fitted semivariogram parameters per sample subset

Subset			Fitted variogram parameters				
Sample size ID	Percentage	Nº samples	Model	Nugget	Sill	Range [m]	SEE [c]
Angostura [100%]	100	11752	Exp[a]	0.33	2.06	607.41	0.240
Angostura [50%]	50	5860	Exp	0.33	2.08	616.48	0.059
Angostura [25%]	25	2933	Exp	0.34	2.03	579.92	0.019
Angostura [12%]	12.5	1467	Sph[b]	0.65	1.60	1420.08	0.011
Angostura [6%]	6.25	734	Sph	0.61	1.73	1480.10	0.003
Angostura [3%]	3.125	367	Sph	0.64	2.00	1634.35	0.001
Angostura [1%]	1.56	184	Sph [e]	0.57	2.29	1831.31	0.001
Corani [100%]	100	17051	Exp	-2.16	50.67	268.76	73.740
Corani [50%]	50	8526	Exp	-2.04	49.48	266.18	20.218
Corani [25%]	25	4264	Exp	-1.85	53.06	279.17	7.402
Corani [12%]	12.5	2133	Exp	-0.23	52.00	281.78	0.920
Corani [6%]	6.25	1066	Exp	-2.40	45.24	216.00	0.368
Corani [3%]	3.125	534	Sph	-1.65	48.92	282.99	0.428
Corani [1%]	1.56	268	Sph	-0.78	44.05	572.09	0.107
Corani [0.7%]	0.757	135	Sph	-14.57	60.26	449.00	0.039
Laka-Laka	100	6790	Exp	-0.15	15.65	51.78	83.840
Larati	100	3538	Sph	0.25	0.36	179.61	0.031
Acero Qocha	100	4622	Sph	0.55	40.36	4971.87	1.175
Parco Qocha	100	3819	Sph	0.60	0.32	1289.9	0.013
Jutuntuyo	100	1701	Sph	0.03	0.15	976.18	0.003
Pilahuito	100	834	Sph	0.015	0.91	520.93	0.042

a) Exponential model b) Spherical model c) Sum of Square Errors.

Figure 6.7 displays the *MSE* prediction scatterplot according to the reduction in the sample size. A reduction in the *MSE* values can be observed as the sample size grows, especially when using a subset of 25% of the total sampling (>3 sampling points per 100 m cells) and onwards in both prediction and validation sets. A similar behaviour was observed for the rest of the statistical estimators, such as the *RMSE* and R^2_{NS}. The fairly large goodness of fit, especially in small sample sizes, was primarily due to the fact that most of the estimation standard errors tended to increase in value with increase in error. Negative values of R^2_{NS} should be considered as failure of the variogram model used, in general because of the too-small sample sizes. Bathymetric elevations are therefore considered unbiased as the *bias* values are not significantly different from zero. Because the systematic error is insignificant, uncertainty can be explained by random error as described by the *MSE* and *RMSE* values.

Figure 6.8 shows two bathymetric maps obtained with a global and a local semivariogram. The spatial patterns, as well as the absolute values, seem similar; therefore it can be argued that it was unnecessary to produce maps based on locally estimated semivariograms. However, when the global semivariogram is used, the

predicted standard errors are large in areas with higher values of altitude. Local variograms restore some of the local variability because the changes in spatial dependence between the local neighbourhoods are included. The results indicate that overall interpolation performance of ordinary kriging deteriorates consistently and significantly as the sampling size and pattern are reduced, and therefore the uncertainty in the bathymetric surface is manifested in higher depth variations.

Figure 6.9 displays results obtained for the eight different sample sizes in the Corani reservoir. In general, the results appear to agree with previous surveys. In regions where many points conveyed, the estimated error is significantly lower than in areas where only few points have been interpolated. It is also observed that along the track-lines the error is lower and in larger depressions the error is proportionally higher.

6.3.4 Deposition patterns in the reservoirs

Input of sediments into reservoirs is a function of several factors (*i.e.,* catchment area and geology, catchment and drainage network topography, drainage system density, soil erodibility, climate and land use, including human influences). From the accumulated sediment deposition maps of the three reservoirs, it can be observed that sediments are largely deposited in a non-uniform pattern.

As reaches and rivers drain into the reservoirs, their water velocities and turbulence begin to decrease, resulting in reduced sediment transport capacity of the flow. As shown in Figures 6.10 and 6.11, the accumulation of sediments near the mouths of the reaches and rivers has resulted in the formation of deltas. The large particles transported as bedload are the first to be deposited. As water velocities and turbulence further decrease, smaller particles are deposited, which results in a longitudinal sorting of particles near the mouth of the reaches or river.

On the left in Figure 6.10, the estimated thickness or height of sediment accumulation from 1967 to 2003 at the Corani reservoir is presented. In spatial terms, the analysis reveals that the rate of sedimentation can be categorized in the range from none to slight. Few areas with more than 3 m of sediment deposition were identified. Areas with more than 5 m of sedimentation are either susceptible to being affected by uncertainty in the measurement of the previous bathymetric surveys or a result of lack of sample points in these regions, which increases the inaccuracy of the interpolation. Sediment mobilization is observed where scouring of the bed floor has occurred and negative depth values are registered.

The estimated rates of sedimentation in the Angostura reservoir are low. Prior belief that high rates of sedimentation encountered in the lake were based on the *a priori* observation at the Angostura reservoir that the sediment-laden flow plunges in the water body and moves along the bed surface to form a turbidity current carrying silt and clay, making the reservoir permanently muddy, proved to be wrong.

Angostura [a]

Angostura [b]

Corani [a]

Corani [b]

Laka Laka [a]

Laka Laka [b]

Pilahuito [a]

Pilahuito [b]
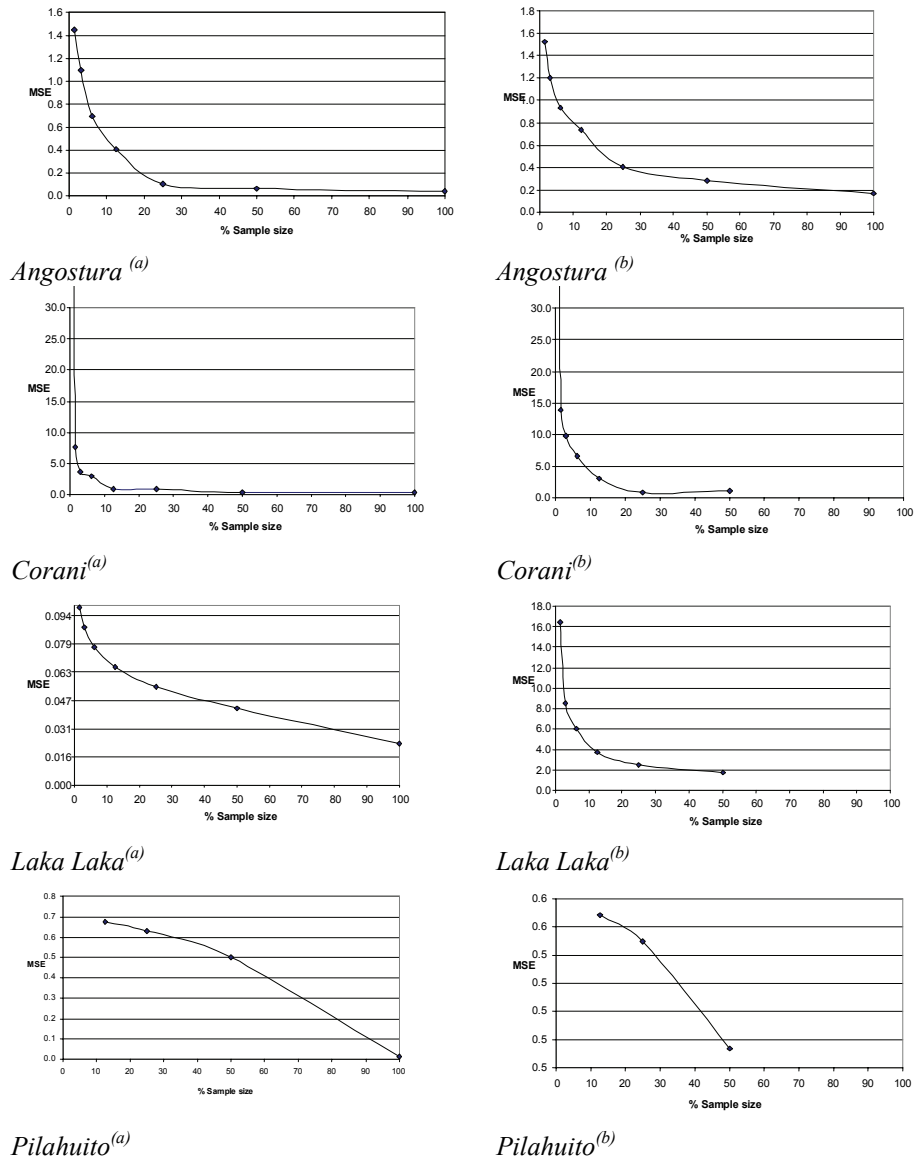
Figure 6.7 Mean square error estimated by different sample-size sampling: *a)* prediction subset, *b)* validation subset
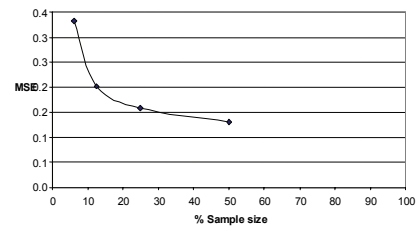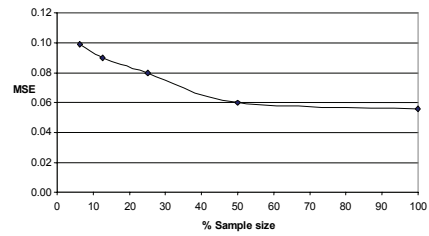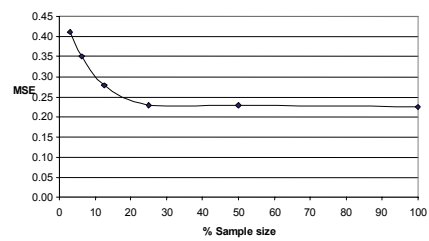
Jutuntuyo[a]   *Jutuntuyo[b]*
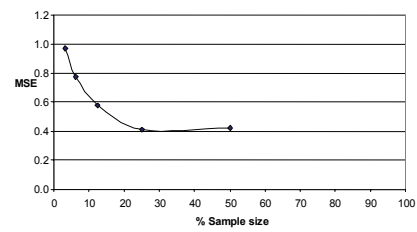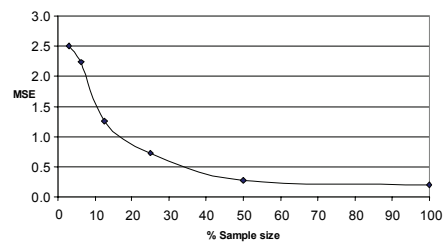
Larati [a]   *Larati [b]*
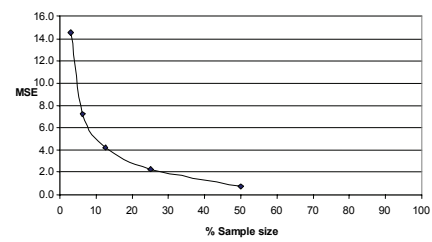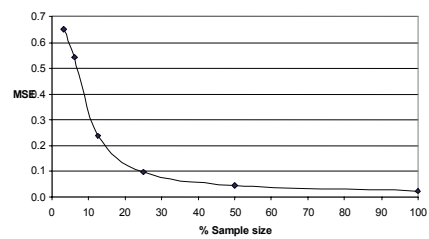
Acero Qocha[a]   *Acero Qocha[b]*
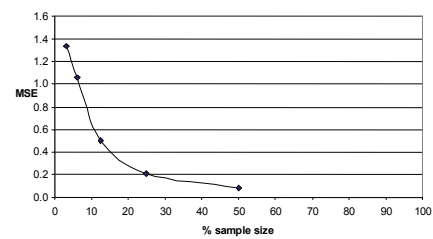
Parco Qocha[a]   *Parco Qocha[b]*

Figure 6.7 Continuation. Mean square error estimated by different sample-size sampling: *a)* prediction subset, *b)* validation subset

Table 6.3 Statistical accuracy of the estimators for prediction and verification of the sample sets

Subset	Statistics	Corani [1%]	Corani [3%]	Corani [6%]	Corani [12%]	Corani [25%]	Corani [50%]	Corani [100%]
Prediction	$r2$	1.13	1.01	1.00	1.01	1.00	1.00	1.00
	r	1.06	1.00	1.00	1.01	1.00	1.00	1.00
	$RMSE$	2.76	1.88	1.69	0.92	0.90	0.54	0.58
	MSE	7.62	3.55	2.85	0.84	0.81	0.29	0.33
	R^2_{NS}	0.86	0.93	0.94	0.98	0.99	0.99	0.99
Verification	$r2$	1.09	1.03	1.01	1.02	1.00	1.01	
	r	1.04	1.01	1.01	1.01	1.00	1.00	
	$RMSE$	3.72	3.13	2.57	1.73	0.93	1.03	
	MSE	13.88	9.81	6.60	3.01	0.87	1.07	
	R^2_{NS}	0.73	0.81	0.87	0.94	0.96	0.98	
		Angostura [15]	Angostura [3%]	Angostura [6%]	Angostura [12%]	Angostura [25%]	Angostura [50%]	Angostura [100%]
Prediction	$r2$	0.991	0.952	0.904	0.901	0.939	0.948	0.960
	r	0.995	0.975	0.951	0.949	0.969	0.974	0.980
	$RMSE$	1.202	1.048	0.835	0.637	0.325	0.253	0.199
	MSE	1.444	1.098	0.697	0.406	0.106	0.064	0.039
	R^2_{NS}	0.443	0.571	0.706	0.828	0.955	0.974	0.984
Verification	$r2$	1.228	1.062	0.953	0.928	0.936	0.948	1.000
	r	1.108	1.031	0.976	0.963	0.968	0.974	1.000
	$RMSE$	1.528	1.205	0.932	0.738	0.405	0.280	0.170
	MSE	2.334	1.451	0.868	0.544	0.164	0.078	0.029
	R^2_{NS}	0.035	0.400	0.642	0.776	0.933	0.967	0.988
		Laka-Laka [1%]	Laka-Laka [3%]	Laka-Laka [6%]	Laka-Laka [12%]	Laka-Laka [25%]	Laka-Laka [50%]	Laka-Laka [100%]
Prediction	$r2$	0.999	1.001	1.000	1.000	1.000	0.999	0.999
	r	1.000	1.000	1.000	1.000	1.000	0.999	0.999
	$RMSE$	0.315	0.297	0.277	0.257	0.235	0.207	0.152
	MSE	0.099	0.088	0.077	0.066	0.055	0.043	0.023
	R^2_{NS}	1.000	1.000	1.000	1.000	0.999	0.999	0.996
Verification	$r2$	1.421	1.412	1.325	1.212	1.100	1.035	
	r	1.192	1.188	1.151	1.101	1.049	1.017	
	$RMSE$	4.050	2.910	2.451	1.919	1.581	1.326	
	MSE	16.404	8.471	6.009	3.682	2.500	1.757	
	R^2_{NS}	0.193	0.581	0.703	0.817	0.875	0.915	
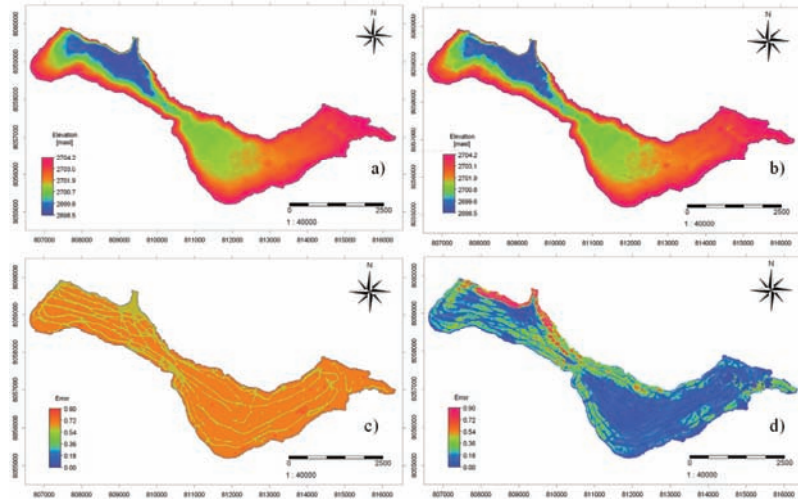
Figure 6.8 Angostura bathymetric surface [masl] and error map constructed using two interpolation procedures: *a)* ordinary kriging with global semivariogram, *b)* error map with global semivariogram, *c)* ordinary kriging with local semivariogram, *d)* error map with local semivariogram
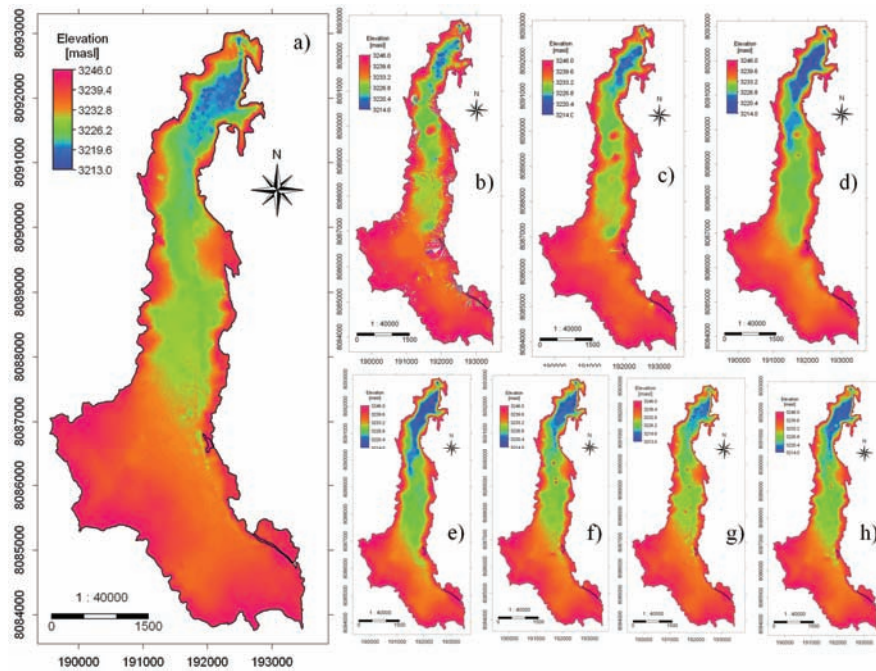
Figure 6.9 Corani bathymetric surface [masl] for different sample sizes: *a)* full sampling set, *b)* 0.75% sample size, *c)* 1.56% sample size, *d)* 3.12% sample size, *e)* 6.25% sample size, *f)* 12.5% sample size, *g)* 25% sample size, *h)* 50% sample size

Geographically, depth of sediment accumulation is higher in the southeastern section of the reservoir, where sediment concentrations are highest and thickness of the sediments reaches 1.5 m, decreasing gradually down to the dam. The average sediment accumulation is about 0.6 m. In the eastern part of the reservoir, the largest particles are deposited at the head of the delta areas. As flow velocities and turbulence continue to diminish, the longitudinal axis of the reservoir experiences a reduction in the depth of sedimentation.

Fine clays and colloidal material are settling very slowly in the area surrounding the dam, with depths ranging from 0.3 to 0.8 m. The pattern of sedimentation results in a smooth surface. Negative values (scouring) are also observed, although they can be explained by local mapping inaccuracies in the topographical survey of 1990.

Conversely, the Laka-Laka reservoir has suffered from high rates of sedimentation despite its small catchment area. In Figure 6.11, the height of sediment accumulation in the different surveys of the Laka-Laka reservoir is presented (1994, 1995, 2001 and 2003).

From the height of sediment accumulated during the whole period of the dam operation, it can be observed that most of the sediments were deposited in and around the dam and the former river channels. Geographically, the sediments took up the most volume in the northeastern section of the reservoir, with an average greater than 5 m of sediment, whereas in the northwestern section the sediment depth is less than 1.5 m. Furthermore, the area close to the shoreline shows a much lower thickness of sedimentation. However, some large variability at certain points in the shoreline (*e.g.,* negative values) is due to datum shifting.

In general, the pattern of deposition results in a rough bottom surface compared with the deposition in the Angostura and Corani reservoirs. This basic clinoform structure favours sediment discharge, with coarse bedload material deposited as lag in the topset section, sand building the prograding foreset deposits, and suspended load silt, clay and fine sand in the bottomset beds. The steep topography, scarce vegetation, frequent fires, weak lithology, erodible soils and heavy precipitation after a long period of drought contributed to increasing the transport of sediments to the Laka-Laka reservoir.

6.3.5 Estimation of sediment deposition in the reservoirs

6.3.5.1 Corani reservoir

The amount of sediment volume accumulated during the 36 years of operation of the Corani reservoir was estimated at 1.4 Mm^3, resulting in an annual average sedimentation of 39,800 m^3 yr^{-1}. This value is low compared with the other two reservoirs. This can be explained by the favourable location and geomorphological setting of the reservoir, as well as the geological, climate, soil and vegetation conditions in the upstream catchments.
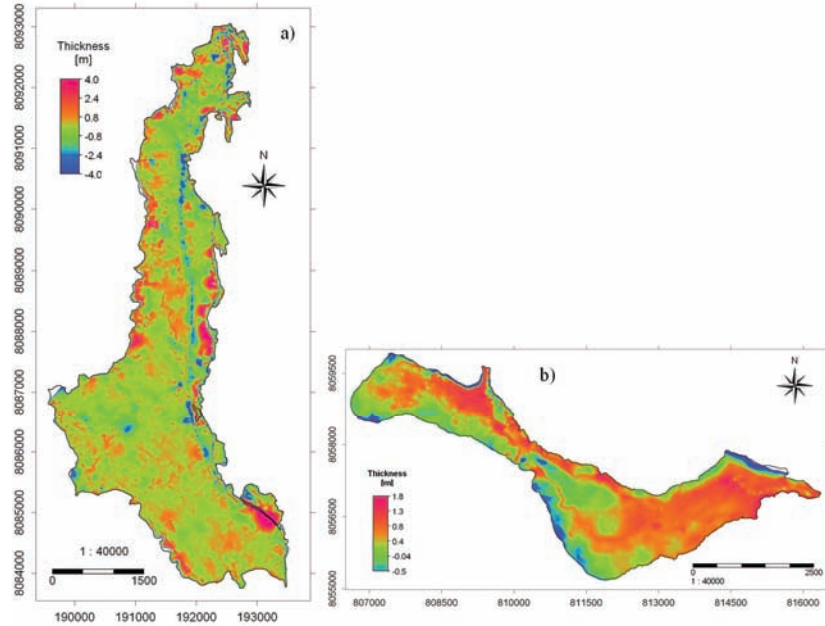
Figure 6.10 Accumulated sediment deposits [m] in *a*) the Corani reservoir (1967 to 2003), *b*) the Angostura reservoir (1947 to 2003)
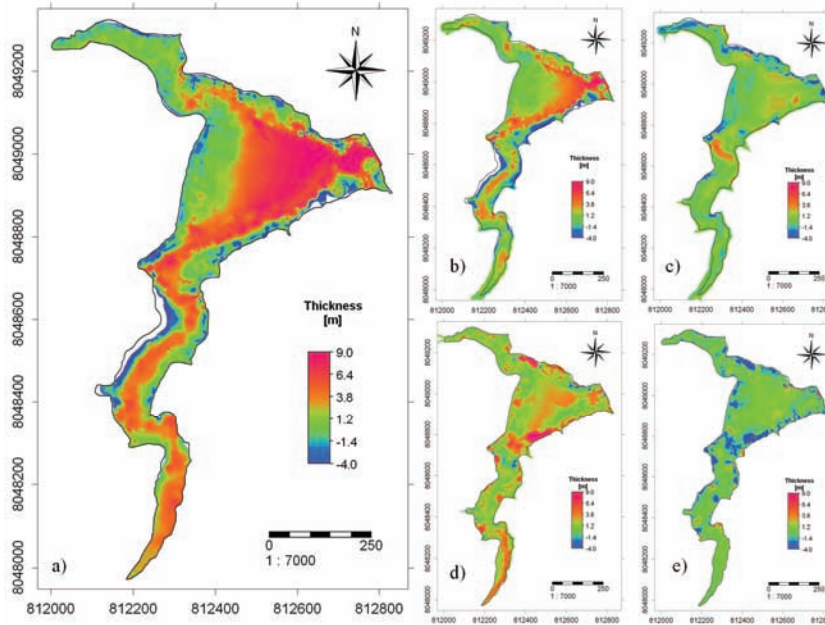
Figure 6.11 Accumulated sediment deposits [m] in the Laka-Laka reservoir: *a*) 1990 to 2003, *b*) 1990 to 1994, *c*) 1994 to 1995, *d*) 1995 to 2001, *e*) 2001 to 2003

From the reservoir operating rules and trap efficiency analysis, it was estimated that 5% of sediment entering the Corani reservoir is flushed through by the streamflow releases. This resulted in a specific sediment yield of 141 m^3 km^{-2} yr^{-1} or 152 ton km^{-2} yr^{-1} for the Corani basin. The total sedimentation within the reservoir was estimated at 1.6×10^6 tonnes, with a mean annual sediment inflow of 45,300 ton yr^{-1}.

Table 6.4 Summary of the reservoir sedimentation rates and long-term catchment sediment yield

Reservoir	Original capacity [Mm³]	Dam operation [Years]	Total volume of sedimentation [Mm³]	Total mass of sedimentation [10⁶ tonnes]	Mean annual sedimentation rate [m³ yr⁻¹]	Sediment accumulation per catchment area [m³ km⁻² yr⁻¹]	Sediment yield per catchment area [ton km⁻² yr⁻¹]
Laka-Laka	2.6	11.2	0.92	1.1	82,400	1,376	1,650
Angostura	100	56	10.2	12.5	182,000	91.4	111.6
Corani	145.5	36	1.41	1.5	39,800	133.9	145.0

6.3.5.2 Angostura reservoir

Estimation of the sedimentation in the reservoir shows that about 10.2 Mm^3 of sediment were deposited in the reservoir. The water capacity in the reservoir decreased from 100 Mm^3 to 89.8 Mm^3 during the period 1947 to 2003. This represents a mere 10.2% reduction in the overall water storage capacity over the past 56 years (Table 6.4). Sediment has accumulated at an average annual rate of about 182,000 m^3 yr^{-1}, far lower than the rate predicted during the design phase of the reservoir. The sediment trap efficiency was estimated at 90%, and the total sediment yield in the period of operation was estimated at 13.7×10^6 tonnes, with a mean annual specific sediment yield of 244,600 ton yr^{-1} or 123 ton km^{-2} yr^{-1}. The Angostura reservoir drains the upper valley river basin.

6.3.5.3 Laka-Laka reservoir

Due to its severe siltation problems, sediment accumulation in the reservoir was monitored several times (*i.e.,* four bathymetric surveys in 11.2 years), allowing the decline in reservoir capacity to be determined for different span periods. The total deposition of sediments in the reservoir for the 11.2 years of operation was estimated at 0.92 Mm^3. Likewise, the total sediment mass accumulated in the reservoir was estimated at 1.1×10^6 tonnes, with a mean annual sedimentation rate of 82,400 m^3 yr^{-1}.

Table 6.5 Reservoir life expectancy, volume and specific sediment yield of the reservoirs considering the reservoir trap efficiency

Reservoir	Trap efficiency [%]	Drainage catchment area [km²]	Reservoir area [km²]	Accumulated volume [Mm³]	Percent of loss capacity [%]	Accumulated mass [10⁶ tonnes]	Mean sediment yield [ton km⁻² yr⁻¹]	Reservoir life expectancy [years]
Laka-Laka	89	59.8	0.24	1.9	36	1.22	1,831	12.9
Angostura	90	1,992	12	80	10.2	13.7	122.8	>100
Corani	95	297.7	14.18	144.4	1	1.6	152.2	>1000

The total sedimentation, considering an 89% sediment trap efficiency in the reservoir, is considerable, given the relatively small size of the catchment (59.8 km^2), and was estimated to be 1.2×10^6 tonnes, with a mean annual specific sediment yield of 109,500 ton yr^{-1} or 1,831 ton km^{-2} yr^{-1}. The final results in terms of accumulated volume and accumulated mass after sediment trap efficiency estimation are presented in Table 6.5.

An important source of the sediment delivered to the Laka-Laka reservoir is the gully and streambank erosion, owing to their close connectivity with the drainage system,

whereby runoff and sediments are rapidly conveyed downstream. Steep topographical relief, weak lithology, important areas of siltstones and marls and scarce vegetation contribute to the important volumes of sediment.

6.3.6   Intercomparison of sedimentation rates of the reservoirs

Large differences in total volume of sedimentation are observed among the three reservoirs. Total sediment deposition estimates were lowest for the Laka-Laka reservoir [0.92 Mm^3] and higher for the Angostura reservoir [10.2 Mm^3]. Notwithstanding, when differences in the reservoir contributing drainage area and age of the reservoir were accounted for, mean annual sediment deposition, in m^3 per km^2 of contributing area drainage, was larger in the Laka-Laka reservoir [1,376 $m^3 km^{-2} yr^{-1}$], followed by the Corani reservoir [134 $m^3 km^{-2} yr^{-1}$], and finally the Angostura reservoir [91 $m^3 km^{-2} yr^{-1}$].

Likewise, when the mean annual sediment yields were determined using the reservoir sediment volume, sediment-specific weight and reservoir trap efficiency, there were also large differences, the smallest being for the Angostura reservoir with 123 ton km^{-2} yr^{-1} [244,600 ton yr^{-1}] and the largest for the Laka-Laka catchment with 1,831 ton km^{-2} yr^{-1} [109,500 ton yr^{-1}]. Considering the time of the operation of the reservoirs, it was estimated that the water storage capacities in the three reservoirs declined on an annual basis by 0.03% at the Corani reservoir, by 0.2% at the Angostura reservoir and by 3.2% at the Laka-Laka reservoir.

The evaluation of sediment deposition for the Angostura and Corani reservoirs showed that deposition was lower than expected on the basis of the 100-year reservoir design life, historically used by engineers. Alarming sedimentation, however, was observed in the Laka-Laka reservoir.

Several reasons exist for explaining the differences in total volumes and rates of sedimentation among the three reservoirs: the location of the dam, and the lithology, underlying geology, and relief in the vicinity of the reservoir (up to 10 km) being the most important. Notwithstanding, the basin area, the occurrence of depositional areas (sediment sinks) and localized high-intensity rainstorms common during summer are factors that should also be considered.

For example, although the Laka-Laka catchment area is relatively small [59.8 km^2], it presents a varied lithology, including sedimentaries, metamorphics and granites. In this tertiary stratum, siltstones, limestones, phyllites and schists are observed, being the most easily erodible and deeply weathered material. This, in combination with the prevailing steep slopes, low presence of croplands, intense short storms, renders them highly susceptible to erosion. Thus, the geological material underlying the Laka-Laka catchment strongly affects the mechanisms and rates of erosion, providing most of the sediments supplied to the reservoir and contributing to the development of badlands topography.

Conversely, sedimentation in the Angostura reservoir is low considering the basin area, time of operation, and the extensive production of alluvial sediments. The presence of extended coarse-grained alluvial fans, which act as depositional sinks (Punata and Tarata fan), prevents higher deposition in the reservoir and favours sediment

redistribution. Under the latter circumstances, although soil erosion might be severe on the upstream mountainous areas (*e.g.,* Anzaldo and Tiraque zones), the source of fluvial suspended sediment may be reworked material deposited in the alluvial stores (Figure 6.1).

Yet although the characteristics of the Corani basin are somewhat in contrast (*i.e.,* steeper topography, semi-humid climate) to the contributing Angostura basin and Laka-Laka reservoir, lower rates of sedimentation were found. This transport-limited basin may present low sediment yields for a number of reasons: (i) adequate location of the dam site, (ii) the semi-humid climate, (iii) exuberant vegetation that favours the production of deep organic soils, (iv) low rates of channel incision, and (v) agricultural valley floors, fans and rivers that trap much of the sediment supplied from the hillslopes.

Lastly, it is evident that variables such as runoff, discharge and basin area cannot be correlated directly and associated with modern denudation rates alone. For example, Aalto et al. (In press) investigated 47 Bolivian drainage basins and found a huge variation when runoff [17 to 2,660 mm yr^{-1}] was directly scaled to the stream power (per unit of contributing area) throughout a channel network and sediment yield [34 to 18,300 ton km^{-2} yr^{-1}].

6.4   Conclusions

Few studies have evaluated the influence of sample size or point density on bathymetric surface generation using acoustic sonar surveys. Results obtained in this research clearly illustrate the effect of point density or sample size on the mapping accuracy. The accuracy of the bathymetric surface was statistically estimated based on the uncertainty of the individual data points. In datasets lower than 25% (<3 points per 100 m cell) of the total sampling set, the instrument error of the survey at individual points was determined to be greater than the interpolation error. Increasing the dataset reduces the uncertainty. Based on the r^2, r, *RMSE, MSE* criteria, it can be concluded that the variogram model and sample size have a significant effect on uncertainty, especially for sets with sample sizes lower than 50% (<6 points per 100 m cell) of the total sampling. The optimization process resulted in a reduction of the sample size by 50% without diminishing the quality of the surface map.

The ordinary kriging method for creating bathymetric surveys is recommended because it performed better than the triangulated irregular network (TIN) and the inverse distance weighting method. The ordinary kriging that uses a local semivariogram appears well suited as a spatial prediction method for bathymetric data. To increase the efficiency of a computer analysis, it may be convenient to thin large datasets. In the study cases, thinning the data did not increase the interpolation uncertainty until the sample size was less than 50%. This corresponds to point densities of five and six soundings per 100 m cell size (1 ha) of reservoir bed for the Angostura and Corani reservoirs respectively, whereas it corresponds to a density of 141 soundings per 100 m cell of reservoir bed at Laka-Laka reservoir owing to its large bed variability. The use of spatial correlation can save unnecessary effort in collecting enormous datasets to obtain a certain level of reliability when estimating reservoir sedimentation rates.

The uncertainty in the bathymetric surfaces was more pronounced if higher depth variations were present. Comparing all the outputs of bathymetric surfaces obtained for all sample sizes, it was concluded that sample sets with a minimum of six sample points per 100 m cell size are adequate for an accurate interpolation when a uniform bed exists and a minimum of 71 sample points per 100 m cell size (25% of the total sampling) are required if a large bed variability exists.

For large sample sizes, the uncertainty associated with interpolation is smaller than the instrument error of the low-cost sonar sounder. Although the elevation error (depth) at any location may be as much as 15 cm, the cumulative effect on the entire survey is small because the instrument measuring error is random.

The use of ancillary remote sensing imagery as a complementary dataset for delimitation of the lake/reservoir shoreline and for yielding additional contour information is very useful. When shoreline tracks, imagery and lake or reservoir water-level information of different dates are available, it enables additional reservoir contours (*e.g.,* above the present water level) to be generated.

The satisfactory results obtained for the three different reservoirs demonstrate the applicability of this rapid GPS-guided bathymetric acoustic sonar sounding technique, combined with satellite data, for determining sedimentation or deposition volumes of lakes and reservoirs. The rapid geomatic method is capable of producing bathymetry maps comparable in accuracy and quality to traditional surveying, but using only a fraction of the labour and finances.

The advantages of this labour-saving are two-fold. First, the low cost makes it practical to map lakes and reservoirs that otherwise would never have been mapped because of the expenses involved in traditional bathymetric surveying. Second, visiting and surveying lakes or reservoirs on a more regular basis to evaluate sedimentation rates is affordable. Results can be used for establishing a time series of sediment accumulation, which can then be used for updating reservoir rule curves and analysing catchment sediment yields. Of course, ideally the method should be expanded with sediment core sampling, to determine more accurate values of the sediment bulk density.

Considering that the original volumes of the Corani, Angostura and Laka-Laka reservoirs were 145.5, 100 and 2.6 Mm^3, the loss in reservoir capacity through sedimentation for periods of respectively 36, 56 and 11 years was determined to be 1.4, 10.2 and 0.9 Mm^3, yielding average annual sedimentation rates of 39,900, 182,000 and 82,400 m^3 yr^{-1}, respectively.

The trap efficiencies of the reservoirs were estimated at 95%, 90% and 89%; consequently the total sediment yields from the three drainage basins were estimated at 1.6×10^6, 13.7×10^6 and 1.2×10^6 tonnes, respectively. The specific sediment yield was highest in the Laka-Laka reservoir catchment: 1,831 ton km^{-2} yr^{-1}. For the Corani basin a value of 152 ton km^{-2} yr^{-1} was derived. The lowest specific sediment yield value of 123 ton km^{-2} yr^{-1} was obtained for the upper valley basin, discharging in the Angostura reservoir.

An analysis of spatial distribution of the sediment deposits in the reservoirs showed that the concept of designing the "dead volumes" near the dam is doubtful. The researched reservoirs tend to occupy a significant (in absolute terms) part of the reservoir's useful volume while the nominal dead volume is somehow free of sediments. Only in the Laka-Laka reservoir is the dead storage completely occupied by accumulated sediments, while just part of the nominally useful water storage remains free of deposited sediments. This obviously means that the total loss of water stored is significantly larger than originally assumed. This reduces the useful life expectancy of this small reservoir to a mere 13 years.

The use of reservoir sedimentation records for direct evaluation of catchment sediment yields provided a cheap alternative to more common standard procedures such as sediment rating curves or suspended sediment sampling, which require long-term measurement of both accurate runoff discharges and suspended sediment concentrations. No expensive monitoring equipment has to be installed, nor are frequent field visits and maintenance operations required.

Furthermore, this methodology allowed the total sediment yield from a catchment to be measured, including suspended as well as bedload sediment transport. A weakness of the method is that it gives only an average of the sediment yield for the monitoring intervals and not a detailed temporal evolution. However, as the method is inexpensive when compared with conventional surveys, more frequent bathymetric surveying can be carried out, and then the sediment yield can be estimated at shorter time scales. Alternatively this method can be combined with distributed hydrological models, as well as sediment discharge measurements in upstream locations, to reconstruct the detailed temporal evolution of catchment sediment production and reservoir sedimentation.

Chapter 7

Analysing linkages between catchment gross erosion and reservoir sedimentation

Chapter 7

Analysing linkages between catchment gross erosion and reservoir sedimentation

7.1   Introduction

In general, mountainous catchments in the Andean region and upper Amazon basin in Bolivia, where the study area is located, exhibit relatively high geological and man-made soil erosion and sedimentation rates (Guyot et al., 1999; Aalto et al., 2003; Aalto et al., In press). Among the various processes of soil erosion, sediment delivery to river channels is probably one of the more natural and important off-site consequences of soil erosion. It occurs on hillslopes and sloping land surfaces where active soil detachment and sediment production processes take place. For example, South America alone contributes 13% of the global sediment load to the ocean. The Amazon, Orinoco and Paraná rivers are responsible for most of the water discharge and sediment load from the South American continent (Restrepo et al., In Press).

Sediment delivery from hillslopes to streams becomes particularly important when the sediments can affect and seriously reduce the capacity of rivers and reservoirs, enhance the risk of flooding and muddy floods, and shorten the design life of reservoirs (Yu et al., 2000b). Storage capacity of existing reservoirs is a valuable non-renewable resource that must be protected, especially in semi-arid and arid regions.

Hence, an understanding of the linkages between sediment sources and mobilization, sediment delivery and transport, and ultimately deposition in floodplains or sedimentation in reservoirs, is essential for the appropriate design and implementation of efficient catchment sediment management.

However, sediment production by erosion, transportation and deposition is extremely variable in both time and space at the catchment scale, and in general only a small portion of the eroded soil from hillslopes leaves a catchment at an event or annual time step (Wainwright et al., 2003). This suggests considerable time lags, temporary storages and associated residence times of sediment in a catchment, which is of particular importance in the context of sediment delivery to rivers and ultimately to reservoirs (Lu et al., 2004). The erosional response to rainfall of semi-arid mountain streams is generally very intense, leading to steep storm hydrograph rises and recessions. This makes the transport of sediment in natural drainage systems extremely variable in both time and space and, moreover, dependent on particle size (Renschler et al., 1999).

Although most erosion, sediment transport and sediment deposition processes have been studied in detail, the linkages between (i) soil erosion and sediment production from upland areas, (ii) sediment yield as a measure of the total sediment transported to the

catchment outlet, and (iii) deposition of sediment into the reservoir or impoundments have until today been less studied and analysed.

During the last decades, many different models and relations have been proposed for describing and predicting the linkages mentioned above, varying considerably in their objectives and the time and spatial scales involved, as well as in their conceptual basis. In some cases, estimates of sediment yields are based on the use of either empirical lumped models such as the USLE, or on the inverse relation between specific sediment yield and basin area (Guyot et al., 1996). Physical models (Wicks and Bathurst, 1996) produce a fairly good understanding of how most erosion and sediment yield processes work, and what factors are important at the scales of plot and small catchments.

Typical of most of these models is that they focus on a limited number of soil erosion and sediment transport processes. Most models focus on rill and inter-rill erosion and some models specifically on gully and bank erosion. Altogether, the limitations in the ability to model soil erosion and sediment yield at the catchment scale (>50 km^2) are due to the high data requirements of each individual model and the lack of a good description of connectivity and sediment transport through the basin.

An approach that may be capable of providing accurate and reliable estimates of the sediment yield at the scale of medium-sized basins with relatively low data requirements is the sediment delivery ratio (SDR). Although some argue that the SDR is essentially a "performance" factor that simply relates observed or modelled amounts at the plot scale to observed amounts at a larger scale (Kinnell, 2004), there are others who argue that the SDR concept can be used to explain the spatio-temporal heterogeneity of sediment transport processes and their interactions with rainfall and catchment characteristics in a more physical way (Lu et al., 2004; Lenhart et al., 2005). In turn, over the last decade the use of SDR has become increasingly accepted by the scientific community. Walling (1983) defines the SDR as the fraction of gross erosion that is transported in a given time interval from the sediment source to the catchment outlet. It is a dimensionless scalar and can be expressed as:

$$SDR = \frac{Y}{E}$$ *(Eq 7.1)*

where Y is the average sediment yield per unit of area and E is the average gross erosion over a specific time step in the same area. It often has a value between zero and one owing to sediment deposition caused by change in flow regime and reservoir storage. Methods of estimating *SDR* are roughly grouped in three categories. The first category deals with specific sites where sufficient sediment yield and streamflow data are available. In this category, methods such as sediment rating curve-flow duration and reservoir sediment deposition are often used (Collins and Walling, 2004; Fan et al., 2004). In general, such approaches are not suitable for estimating the spatial distribution of sediment yields for a large catchment because the measurements required are mostly unavailable at the subcatchment level.

The second category uses empirical relationships that relate *SDR* to the morphological characteristics of a catchment, such as the catchment area, average local relief or lithology. A widely used method is the *SDR* area power function:

$$SDR = \varphi \times A^\lambda$$ *(Eq 7.2)*

where A is the catchment area [km^2], and φ and λ are empirical parameters. Statistical regression based on sediment measurements shows that the exponent λ is in the range of -0.01 to 0.25, suggesting that SDR decreases with drainage area (Holliday et al., 2003). Despite its practical simplicity Eq 7.2 provides little understanding of the physical processes that underlie sediment transport in a large catchment. It carries no description of the mechanisms that cause sediment transport, fails to identify the separate effect of climate (*e.g.,* erosive rainfall) and catchment conditions, and provides limited assistance beyond the description of likely load magnitudes.

For a given catchment area, differences in the values of φ and λ cause variation in the orders of magnitude in SDR, suggesting the strong dependence of SDR on additional properties that represent catchment heterogeneity. It is known that factors influencing SDR include hydrological regime (*e.g.,* rainfall runoff), catchment properties (*e.g.,* vegetation, topography, and soil properties) and their complex interactions. Mathematical derivation of the dynamical spatial properties of SDR in terms of those causal factors is far from trivial.

The third category attempts to build models based on fundamental hydrological and hydraulic processes. In most of these models, sediment delivery and deposition are predicted through the coupling of runoff and erosion/deposition conditioning on sediment transport capacity (van Oost et al., 2004). Despite the merit of a physical description, these complex models are often not suited to ungauged catchments.

In order to overcome some of the difficulties mentioned above, several attempts to predict the export of sediment from catchments, by coupling catchment erosion to an SDR in a spatial modelling approach, have been investigated. The approach has been applied with relative success in non-mountainous catchments in Italy (Ferro et al., 2003), Belgium (Van Rompaey et al., 2001), the USA (Veith, 2002) and Australia (Lu et al., 2003). However, few studies have applied this concept to mountainous catchments or compared the results of the varied distributed SDR approaches in the same catchment. A summary of the relevant literature is given by Lenhart et al. (2005). Comparative studies are needed to assess the applicability and limitations of catchment models, but most studies to date have tended to focus on either model performance (Hessel, 2002) or differences in model structure (Bhuyan et al., 2002).

Svorin (2003) states that comparative studies tend to interpret significant differences, which can usually be used later as evidence of model quality. It is equally important to determine which model is more reliable in its estimation of sediment yield, given the conditions of model structure. Determination of this reliability is difficult in ungauged catchments owing to the lack of records of sediment concentrations of streamflow and soil erosion measurements in upland areas (Ferro et al., 1998). In order to overcome this limitation, researchers such as Saavedra (2000) and Verstraeten et al.(2003b) have promoted the use of reservoir sedimentation studies to define erosion, transport and sedimentation processes in drainage basins. Haregeweyn et al. (2005) suggest that, given the absence of long-term high-resolution data at basin or catchment scale, reservoir data provide information over relatively large time spans, and thus they not only represent the effect of frequent and rare events but also include the contribution of bedload in the measurement. The sediment trapped in a reservoir reflects, after

correction for trapping efficiency, the net sediment export or yield of the catchment or basin since the construction of the reservoir or impoundment.

Therefore, the aim of this chapter is to compare the performance of four distributed SDR approaches, namely, (i) the soil erosion assessment tool (SEAGIS) (DHI, 2003), (ii) the sediment delivery distributed model (SEDD) (Ferro and Porto, 2000), (iii) the Veith algorithm (Veith, 2002), and (iv) the hillslope sediment delivery ratio (HSDR) model (Lu et al., 2003), in their ability to predict net sediment delivery and yield from a 59.8 km^2 semi-arid mountainous catchment. All four SDR models used as input the distributed catchment gross erosion estimates obtained and described in Chapter 5. The specific objectives of this chapter are (i) to test spatial SDR methods and their suitability for semi-arid mountain catchments, and (ii) to estimate the spatial distribution of sediment yield (*i.e.,* per cell across the catchment) and to identify the sediment source areas. A multitemporal sedimentation dataset measured at the Laka-Laka reservoir was used as a validation dataset for the SDR model performances. First, all the input data for the erosion model were prepared. Next, the dataset with the observed sediment yield values was used to calibrate the SDR model parameters. Finally, the agreement between the predicted and observed sediment yield was examined.

7.2   Spatial sediment delivery ratio models

7.2.1   Soil erosion assessment tool (SEAGIS)

MIKE BASIN for Land and Water (MILW) is a river basin model developed at the Danish Hydraulic Institute (DHI, 2003), which operates on the basis of a digitized river network directly established in ArcView® GIS. It contains a series of tools (*i.e.,* land classification, catchment delineation, soil erosion assessment) that enable the managing of spatial and temporal data for comprehensive analysis of land and water systems. The component for soil erosion assessment is referred to as SEAGIS and contains a set of equations to calculate the amount of eroded sediment that is transported to a stream or a catchment outlet. SEAGIS outputs include the spatially distributed delivery index and ratio, as well as the sediment yield. In SEAGIS, the grid showing the *SDR* requires the estimation of a *delivery index* or DI_p. The DI_p for a cell is estimated as:

$$DI_p = \min\left[P_a^{0.7} \times \left\{ H^{0.5} \times S^{1.67} \right\} \right] \qquad \text{(Eq 7.3)}$$

where *H* is a flow parameter determined by the aspect-driven routing algorithm (Lea, 1992), P_a [mm] is the annual rainfall and *S* [m m^{-1}] is the channel slope. The SDR map is obtained by setting an upper threshold value for the delivery index above which all source erosion is transported and none is redeposited, and a lower threshold value below which all source erosion is redeposited. The transported erosion map [tonnes] is found by multiplying the source erosion map by the *SDR* map. The sediment yield (*SY*) per cell is calculated as:

$$SY = SE \times SDR \times k \qquad \text{(Eq 7.4)}$$

where *SE* [tonnes] is the source erosion map and *k* is a scaling constant depending on the size of the catchment. The predicted erosion rate maps obtained in Chapter 5 are used as a source erosion map. Total sediment yield in the catchment is found by summarizing the values of the transported erosion grid within the catchment theme.

7.2.2   Sediment delivery distributed model (SEDD)

For a given temporal scale, Pilotti and Bacchi (1997) proposed to model the within-basin variability of the hillslope sediment delivery process using a sequential approach. Basically, this approach follows the sediment mass Lagrangian scheme and applies appropriate delivery factors to each sequential modelling of morphological units *i* into which the catchment is divided. Ferro et al. (2003) improved on the previous approach and proposed to model the variability of the sediment delivery process within a catchment by calculating the *SDR* per cell (*SDR$_i$*) using the sediment delivery distributed model (SEDD). According to Stefano et al. (2005), the *SDR$_i$* indicates the probability that eroded particles mobilized from an individual cell will be transported to the nearest stream pixel and can be derived according to:

$$SDR_i = \exp\left(-\beta \times t_i\right)$$

(Eq 7.5)

where t_i [hr] is the travel time per cell *i* and β is a catchment-specific parameter. The time for runoff water to travel from one point to another in a catchment is determined by the flow distance and the velocity along the flow path (SCS-TR-55, 1972). The equation for particle travel time per cell t_i reads as:

$$t_i = \sum_{i=1}^{m} \frac{l_i}{v_i}$$

(Eq 7.6)

where l_i [m] is the length of segment *i* in the flow path and is equal to the length of the side or diagonal of a cell depending on the flow direction in the cell. v_i [m s^{-1}] is the flow velocity for the cell. Flow velocity of both overland flow and shallow channel is estimated from the relationship:

$$v_i = \delta_i \times \sqrt{s_i}$$

(Eq 7.7)

where s_i [m m^{-1}] is the slope of cell *i* and δ_i [m s^{-1}] is a coefficient for cell *i* dependent on the surface roughness characteristics. After combining equation Eq 7.5, Eq 7.6 and Eq 7.7, the *SDR$_i$* per cell reads as:

$$SDR_i = \exp\left[-\beta \sum_{i=1}^{m} \frac{l_i}{\delta \times s_i^{0.5}}\right]$$

(Eq 7.8)

If S_{Ei} is the amount of soil erosion produced in cell *i*, then the sediment yield for the catchment S_y during the time step considered is obtained as:

$$S_y = \sum_{i=1}^{N} SDR_i \times S_{E_i}$$

(Eq 7.9)

where *N* is the total number of cells over the catchment and the term *SDR$_i$* is the fraction of S_{Ei} that ultimately reaches the nearest channel. Since *SDR$_i$* is a function of travel time to the nearest channel, it implies that the gross erosion in that cell multiplied by the *SDR$_i$* value of the cell becomes the sediment yield contribution of that cell to the catchment outlet.

7.2.3   The Veith algorithm

To estimate the sediment yield in the catchment, Veith (2002) routed the eroded sediment from each cell to the catchment outlet, using a sediment delivery function. According to Veith (2003), the sediment routing component accounts for the downstream effects of sediment delivery such as variation in land use, flow length and slope steepness. Sediment delivery through overland cells *d* is modelled as a function of land cover, slope steepness and flow length:

$$d = \chi \times \sqrt{\frac{s}{l}}$$ *(Eq 7.10)*

where s [m m^{-1}] is the slope, χ is a land cover and land use coefficient related to the flow velocity of the overland cells, and l [m] is the flow length path across the cells.

The sediment yield contribution of each cell is determined by routing sediment from the cell through downstream cells to the outlet. For each cell, the gross erosion is multiplied by the *SDR* of cells in the flow path from the cell to the outlet:

$$Y_i = A_i \times a_i \times \prod SDR_j$$ *Eq 7.11)*

where Y_i [tonnes] is the sediment loss of cell i reaching the outlet, A_i [ton ha^{-1}] is the gross erosion from cell i, a_i [ha] is the area of cell i, SDR_j is the *SDR* of cell j, and j is the indices of all flow path cells between cells i and the outlet. None of the GIS programs provides a function for multiplying cell values along a flow path. However, a flow length function can be used to closely approximate *Eq 7.11* by rewriting the product of the delivery ratios as an additive exponential function:

$$\prod SDR_j = \exp^{\sum \ln(d)} \approx \exp^{-FlowLength\left[t_j \times \frac{-\ln(d)}{f_j}\right]}$$ *(Eq 7.12)*

where d is the sediment delivery ratio of the cell, f_j is the flow length assigned to cell j, and t_j is the travel distance of flow between cell j and the next cell in the flow path.

7.2.4 Hillslope sediment delivery ratio (HSDR)

In order to measure the catchment response to the upland erosion rate, Lu et al. (2003) developed the hillslope sediment delivery ratio (HSDR) method. The HSDR model routes the sediment as two lumped linear storages arranged in series: hillslope transport to the nearest stream and flow routing in the channel network (Figure 7.1).
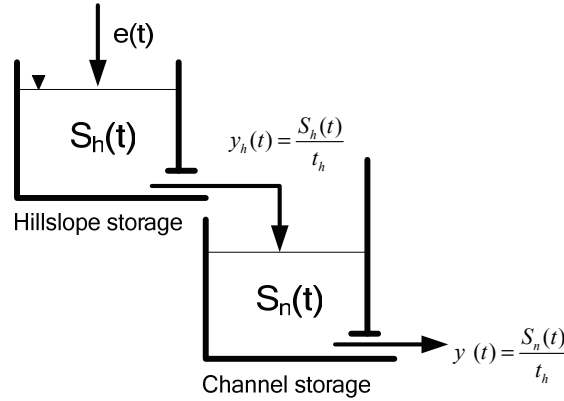
Figure 7.1 Diagram of a two-storage lumped linear model of HSDR at catchment scale (adapted from Sivapalan et al. 2001)

The hillslope storage is supplied with sediment by soil erosion at a rate e [mass area^{-1} time^{-1}] over an *effective storm duration* t_{er}. The hillslope stores part of the eroded sediment and delivers the rest to the channel network storage located downstream of it

at a rate y_h [mass area^{-1} time^{-1}]. y_h is assumed to be a linear function of the mass of sediment stored in the hillslope per unit of area, denoted by S_h [mass area^{-1}]. The area-specific sediment yield from the network store Y [mass area^{-1} time^{-1}], which is the same as the area-specific sediment yield from the catchment outlet, is assumed to be a linear function of the sediment store in the channel network, denoted by S_n [mass area^{-1}]. The continuity equation of sediment for the two storages can be expressed as:

$$\frac{dS_h(t)}{dt} = e(t) - y_h(t)$$

$$y_h(t) = \frac{S_h(t)}{t_h}$$

$$\frac{dS_n(t)}{dt} = y_h(t) - y(t)$$

$$Y(t) = \frac{S_n(t)}{t_n}$$

(Eq 7.13)

where t_h is the mean *hillslope residence time* and t_n is the mean *channel residence time*. The final expression for the ratio between the sediment yield denoted by y_p [mass area^{-1} time^{-1}] and the upland erosion rate e is written as follows:

$$\frac{y_p}{e} = \left[\frac{t_n}{t_n - t_h}\right] \times \left\{1 - \exp\left(-\frac{t_{er}}{t_n}\right)\right\} - \frac{t_h}{t_n - t_h}\left\{1 - \exp\left(-\frac{t_{er}}{t_h}\right)\right\} \quad t_h \geq 0 \quad t_n \neq t_h$$

(Eq 7.14)

$$\frac{y_p}{e} = \frac{1}{2}\left(\frac{t_{er}^2}{t_n^2}\right) - \frac{1}{3}\left(\frac{t_{er}^3}{t_n^3}\right) + \ldots \ldots \qquad t_n = t_h$$

The residence time for both hillslope and channel is estimated as a function of the sediment particle size. The *travel time* of the water particles is estimated as:

$$t_h(\theta) = t_h \times F_h(\theta)$$

$$t_n(\theta) = t_n \times F_n(\theta)$$

(Eq 7.15)

where $t_h(\theta)$ and $t_n(\theta)$ are the hillslope and channel residence times for particles with diameter θ, and t_h and t_n are the hillslope and channel travel times of water particles, respectively.

$F_h(\theta)$ and $F_n(\theta)$ are the enlargement functions describing the influence of particle size θ. The mathematical forms of $F_h(\theta)$ and $F_n(\theta)$ are modelled as:

$$F_h = \exp[\gamma_h \times w_t(\theta)]$$

$$F_n = \exp[\gamma_n \times w_t(\theta)]$$

(Eq 7.16)

where $w_t(\theta)$ is the settling velocity for particles with a diameter equal to θ. γ_h and γ_n are the parameters inversely related to water depth. The settling velocity was estimated according to:

$$w_t(\theta) = \left[\frac{4 \times \rho_p \times g \times \theta}{3 \times \rho \times C_D \times \text{Re}_p}\right]^{\frac{1}{2}}$$

(Eq 7.17)

where ρ_p is the particle density, ρ is the water density, g is the acceleration due to gravity, and Re_p is the particle Reynolds number at the settling velocity. It is calculated using:

$$Re_p = \frac{w_t \times \theta}{\nu}$$

(Eq 7.18)

C_D is the drag coefficient and is modelled as a function of the particle Reynolds number *Re_p*:

$$C_D = \frac{24}{Re_p}\left[1 + 0.15\,Re_p^{0.687}\right]$$

(Eq 7.19)

The *travel time* of water particles is calculated separately for overland flow and streamflow. The travel time is inversely related to the flow velocity. During a storm event when overland flow occurs, the flow carries sediment surface runoff until it reaches a stream. In the stream component, the runoff water is influenced by a set of factors affecting travel time that are different from those in the overland flow component. For hillslope cells, the overland flow velocity V_o [m s^{-1}] is estimated by combining a kinematic wave approximation with the Manning equation:

$$V_o = \frac{[i_e \times L]^{0.4} \times s^{0.3}}{n^{0.6}}$$

(Eq 7.20)

where L [m] is the travel distance along the flow path, n is the Manning roughness coefficient, i_e [mm s^{-1}] is the rainfall excess rate and s [m m^{-1}] is the slope. The travel time through each hillslope cell t_o [s] can be estimated as:

$$t_o = \frac{D}{V_o}$$

(Eq 7.21)

where D [m] is the distance travelled through that cell. For an orthogonal flow, the flow distance is the cell width, while for diagonal flow, it is equal to $\sqrt{2} \times D$. The excess rainfall i_e is generated using the SCS method (SCS, 1972).

$$i_e = \frac{Q}{t_r}$$

(Eq 7.22)

where t_r [s] is the rainfall event duration and Q [mm] is the total excess rainfall for the event.

The travel time in channels t_c [s] is calculated based on the SCS flow velocity equation:

$$V_{ch} = \psi \times \sqrt{s}$$

(Eq 7.23)

where V_{ch} [m s^{-1}] is the flow velocity, s [m m^{-1}] is the slope, and ψ is a coefficient relating to stream roughness condition. Similar to overland flow, the travel time through each channel cell t_c [s] can be estimated as:

$$t_c = \frac{D}{V_{ch}}$$

(Eq 7.24)

where D is the distance travelled through that cell (equal to horizontal, vertical or diagonal distance across a cell flow direction).

Finally, *SDR_i* is calculated for each particle-size group and then weighted by the particle-size distribution to get an overall *SDR* as follows:

$$SDR = \sum_{i=1}^{N} w_i \times SDR_i \qquad \sum_{i=1}^{N} w_i = 1$$

(Eq 7.25)

where N is the total number of particle groups, and w_i and SDR_i are the mass percentage and SDR for particle group i, respectively. Five particle sizes are considered.

7.3 Data processing

The research was undertaken in the 59.8 km^2 Laka-Laka reservoir catchment. The general settings and biophysical characteristics of the catchment are given in Chapter 3.

General data requirements for creating the inputs for the distributed erosion and SDR models included a DEM, land cover and soil characteristics, and precipitation. The DTM was obtained from contour interpolation of a 1:50,000 scale topographical map with 20 m contour line intervals derived from the Military Geographic Institute (IGM).

The vegetation parameters such as the C factor in the RUSLE-3D, USPED and MMMF models; the rainfall interception factor P_i, and the ratio of actual to potential evapotranspiration E_t/E_o in the MMMF model; and the monthly fraction of vegetation cover v_c in the Thornes model were extracted by combining high temporal resolution remotely sensed data (MODIS-NDVI), high spatial resolution imagery (SPOT-5), and field verification data.

The soil-related parameters such as the K factor in the RUSLE-3D and USPED models; the soil moisture at field capacity MS, bulk density B_d, rooting depth R_d and the detachability index K_m, in the MMMF model; and the K_t in the Thornes model were derived from the attributes of the geomorphic map delineated from the 1:50,000 aerial photographs and the soil physical characteristics were derived from the soil reconnaissance survey.

The spatial and temporal variations of runoff were estimated using the method developed by Zhang (1999), which is based on information obtained from the remote sensing data (*i.e.,* rainfall, soil and vegetation parameters). The spatial gross catchment erosion estimates obtained from the five erosion models were used as inputs and coupled to the spatial SDR predictions. The structure of the erosion models is described in Chapter 2 and the model implementation and results are detailed in Chapter 5.

The porosity in the Laka-Laka reservoir was estimated using field data on the specific dry weight of sediment as a function of the known specific dry weight and the specific solid weight of sediments, which is assumed to be equal to 2.65 ton m^{-3}.

In the SEAGIS model, the delivery index DI_p was calculated using the long-term rainfall average value of the catchment, the slope map, and the catchment boundary map. By using Eq 7.3, each grid cell is checked for grid cells with lower values downstream and, if found, the lower value is assigned to the grid cell. A downstream grid cell with lower value is considered a limiting factor in sediment transport. In this way, grid cells closest to the recipient got the highest values of the delivery index. To convert the DI_p into an SDR_i map, two threshold values were applied: a lower value (100) under which all source erosion is redeposited (*SDR of zero*), and an upper value (220) over which all sediment reaches the outlet (*SDR of unity*). Between the two threshold values, the DI_p is converted to values between zero and one.

In the SEDD model, the time for runoff water to travel from one cell to another in a catchment t_i [s] is determined by the flow distance and velocity along the flow path. If the flow path from cell i to the nearest channel cell traverses m cells, then the t_i from that cell is calculated by adding the travel time for each of the m cells located along the flow path.

The values of δ_i depend on the surface roughness characteristics and they were related to the land cover by Haan et al. (1994). The δ_i values used in this research according to the different land covers are presented in Table 7.1.

To ensure the proper use of Eq 7.7, a lower limit of velocity for the catchment is generally established by setting the minimum of a slope cell to a small value (*e.g.,* 0.03%). The catchment-specific parameter β depends primarily on the catchment morphological characteristics and was modelled until acceptable sediment yield predictions were obtained, using an inverse modelling approach.

When using the Veith algorithm, a much higher sediment delivery is expected for channel cells than for overland cells. To model this distinction, Eq 7.9 is used to model SDR_i for overland flow cells, whereas the SDR_i for channel cells (*i.e.,* shallow concentrated flow and streamflow through ephemeral and perennial streams) is defined by adopting a minimum accumulation threshold value. In the catchment, shallow concentrated flows are identified as cells with flow accumulation from at least 100 cells but less than 150 cells, using the 30 m DEM. A cell is considered as streamflow if it receives flow accumulation from more than 150 cells, so that d values of 0.90 and 0.95 were assigned for shallow concentrated flow and streamflow cells, respectively. Values for the empirical coefficient χ were derived from the work carried out by Veith (2003), who used the RUSLE2 model to estimate a delivery ratio for a slope/soil combination. Values adopted in this research are presented in Table 7.1.

In the HSDR model, the *cumulative travel time* for a given cell i was estimated by summing the travel time along its flow path – more specifically, if a sediment particle in cell i travelled through m_o overland cells and m_c channel cells to reach the catchment outlet. Eq 7.19 and Eq 7.20 were used in each of the m_o upland cells to calculate the concentrated shallow flow travel time and Eq 7.22 and Eq 7.23 were used in each of the m_c stream cells and aggregated to estimate the total streamflow time T_{ic}. Figure 7.2 shows the overall procedure for calculating travel time t_h and t_n. Five particle sizes were considered in this research.

Estimated values for the Reynolds number (Re) and the settling velocity according to the particle size are given in Table 7.2 and Table 7.3. Likewise, particle diameters larger than 2,000 μm are considered too large to be transported far away from their source areas. For simplicity, the Manning roughness coefficient was estimated using available land cover and vegetation cover data (Table 7.4). The channel roughness parameter ψ is parameterized as in Table 7.5.

Table 7.1 Values of χ and δ according to the different land cover units

Land cover/land use	χ	δ_i
Bare exposed rock	1	*6.5*
Bare soil	10	*5.8*
Bushland	5	*5.5*
Fallow	7	*5.5*
Forestry	1.2	*1.5*
Irrigated cultivation	4.9	*4.6*
Open shrubland	6	*4.2*
Rainfed cultivation	7	*4.9*
Steppe shrubland	*5*	*4.5*

Table 7.2 Particle diameter (θ), Reynolds number (Re) and settling velocity (v_i) according to five particle sizes

Particle class	Θ [μm]	Re	*vi [m s-1]*
Clay	2	9×10^{-7} -1.1×10^{-4}	9×10^{-7} - 5.7×10^{-5}
Silt	10-50	8.9×10^{-4} - 0.11	8.9×10^{-5} - 2.2×10^{-2}
Small aggregates	50 –200	0.15 - 3.5	2.8×10^{-2} - 2.01×10^{-2}
Large aggregates	200-500	6.5 - 38.3	2.8×10^{-2} - 7.6×10^{-2}
Sand	*500-1000*	*38.4 - 819.4*	*$7.8 \times 10_{-2}$ - 0.3*

Table 7.3 Settling velocity, v_i and mass percentage, w_i per particle group according to five particle sizes (sand, silt, clay, large aggregates, small aggregates)

P	Texture	v [sand]	v [clay]	v [silt]	v [S aggr]	v [L aggr]	w [clay]	w [silt]	w [sand]	w [S Aggr]	w [L Aggr]
P1	Silt loam	0.28	0.00001	0.00009	0.0014	0.0186	0.13	0.51	0.06	0.2	0.1
P2	Loam	0.268	0.00001	0.00013	0.0016	0.0213	0.17	0.41	0.05	0.22	0.15
P3	Silt loam	0.27	0.000012	0.00023	0.0023	0.0257	0.16	0.51	0.05	0.16	0.12
P4	Loam	0.25	0.000012	0.00018	0.0014	0.0213	0.16	0.47	0.07	0.2	0.1
P5	Sandy loam	0.248	0.000013	0.00013	0.0012	0.0187	0.12	0.35	0.06	0.35	0.12
P6	Loam	0.258	0.000008	0.00007	0.0011	0.01087	0.16	0.47	0.07	0.18	0.12
P7	Loam	0.26	0.00001	0.00013	0.0013	0.0186	0.12	0.41	0.06	0.31	0.1
P8	Silt loam	0.28	0.000011	0.00018	0.0014	0.0213	0.19	0.56	0.05	0.15	0.05
P9	Sandy loam	0.246	0.000012	0.00023	0.0016	0.0186	0.1	0.36	0.07	0.32	0.15
P10	Loam	0.255	0.000013	0.00009	0.0017	0.0213	0.14	0.47	0.05	0.24	0.1
P11	Sandy loam	0.266	0.000014	0.00013	0.0014	0.0257	0.13	0.34	0.06	0.33	0.14
P12	Loam	0.27	0.000012	0.00018	0.0013	0.0186	0.15	0.37	0.07	0.31	0.1
P13	Sandy loam	0.28	0.000013	0.00013	0.0012	0.0213	0.11	0.35	0.08	0.32	0.14
P14	Sandy loam	0.25	0.000014	0.00023	0.0013	0.0257	0.11	0.33	0.06	0.35	0.15
P18	Loam	0.248	0.000012	0.00018	0.0017	0.0312	0.19	0.41	0.05	0.25	0.1
P16	Clay loam	0.258	0.000013	0.00013	0.0023	0.0321	0.33	0.34	0.1	0.15	0.08
P15	Loam	0.2789	0.000012	0.00014	0.0014	0.0346	0.17	0.45	0.09	0.19	0.1
P17	Sandy loam	0.2689	0.000011	0.00014	0.0014	0.0369	0.17	0.35	0.08	0.25	0.15

Table 7.4 Values of Manning's *n* according to the land cover and vegetation cover groups

Land cover/land use	cv≤30 %	30%< cv ≤70%	cv ≥70%
Bare exposed rock	0.2	0.3	0.5
Bare soil	0.1	0.25	0.45
Bushland	0.15	0.29	0.5
Fallow	0.12	0.25	0.6
Forestry	0.2	0.5	0.8
Irrigated cultivation	0.15	0.2	0.4
Open shrubland	0.2	0.25	0.5
Rainfed cultivation	0.2	0.3	0.45
Steppe shrubland	*0.25*	*0.33*	*0.55*

Table 7.5 Channel roughness parameter ψ values

Channel section	ψ
Concentrated shallow flow	4
Intermittent stream	4.5
Permanent stream	5
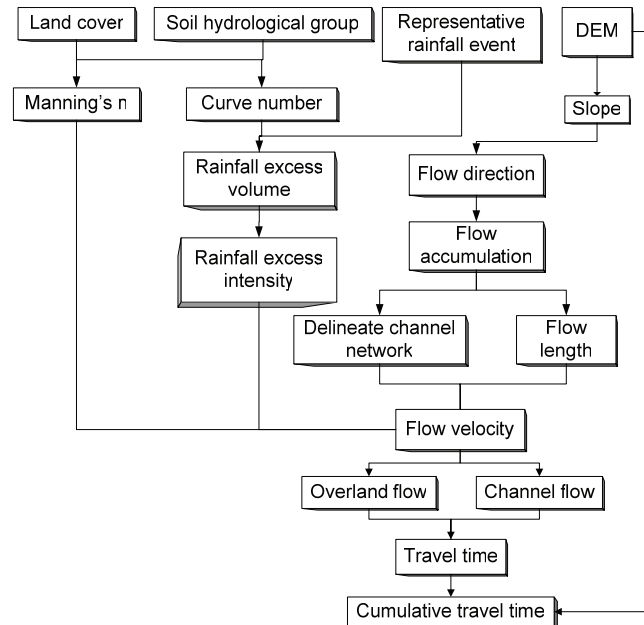
Figure 7.2 Flowchart for the calculation of travel time of water particles (source: Lu et al., 2003)

7.4 Results and discussion

7.4.1 Comparison of the sediment delivery ratio models

The four model approaches for sediment delivery from uplands to the drainage system and eventually catchment outlet, and reflecting the connectivity between the land surfaces and the drainage system of a catchment, were evaluated by comparing the results obtained with the SEAGIS, SEDD, Veith algorithm and HSDR models. The spatial patterns of the SDR_i derived for the central section of the catchment from the four models are shown in Figure 7.3. The spatial analysis immediately highlights the

fact that SDR_i redistribution strongly depends on the choice of model and parameter estimation method.

The SEDD and HSDR models present a similar pattern, whereas the Veith and the SEAGIS model predictions exhibit more contrasting patterns. This may be explained because both models emphasize the topographical forcing in sediment delivery by using the cumulative slope length and the aspect-driven routing algorithm, respectively.

Regardless of the model, it is observed that SDR_i values follow the well-established trend of decreasing values with increasing catchment surface. As would be expected, the further away an area is from a drainage line, the longer the travel time and the lower the SDR_i, whereas the greater the flow velocity along the flow path, the shorter the travel time and the higher the SDR_i. Note that any two locations at equidistance from the outlet may not have the same travel time because the travel time distribution does not follow concentric zones (Figure 7.4a).

a)   *b)*

c)   *d)*
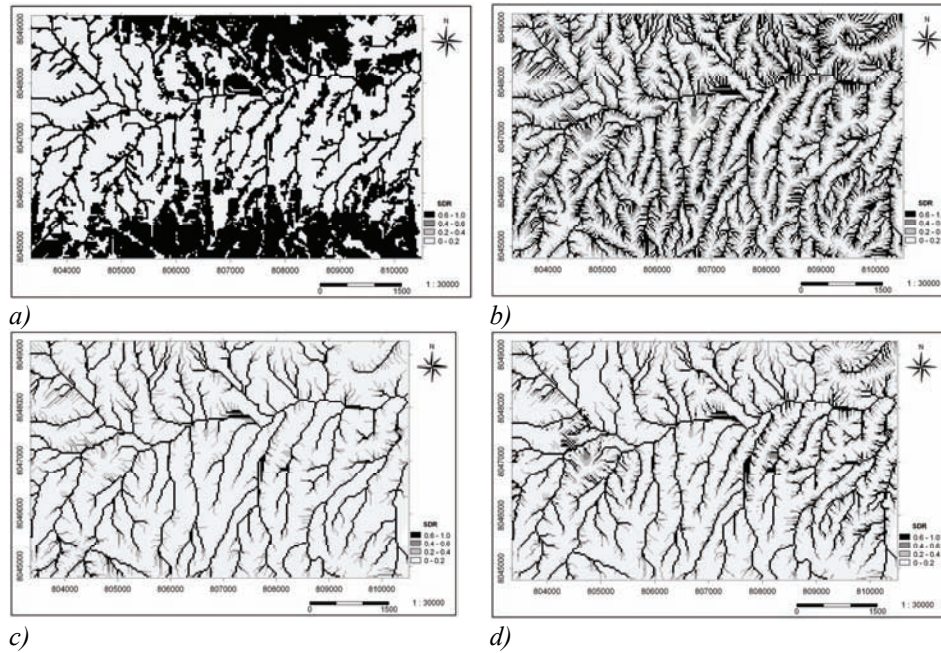
Figure 7.3 Distributed SDR maps: *a)* SEAGIS, *b)* SEDD approach, *c)* the Veith algorithm, *d)* HSDR

Therefore, the same distance does not imply that they will have the same SDR because they may have different travel times owing to surface roughness and overland slope. Overall, the mean estimated travel times of water particles for the catchment after adding the hillslope and channel travel times show that parts of the western, southwestern and northwestern regions have a large hillslope travel time owing to flat topography in the area and poor stream connectivity, respectively. The effects of land use are secondary and localized, and are translated into the overland flow velocities of runoff.

171
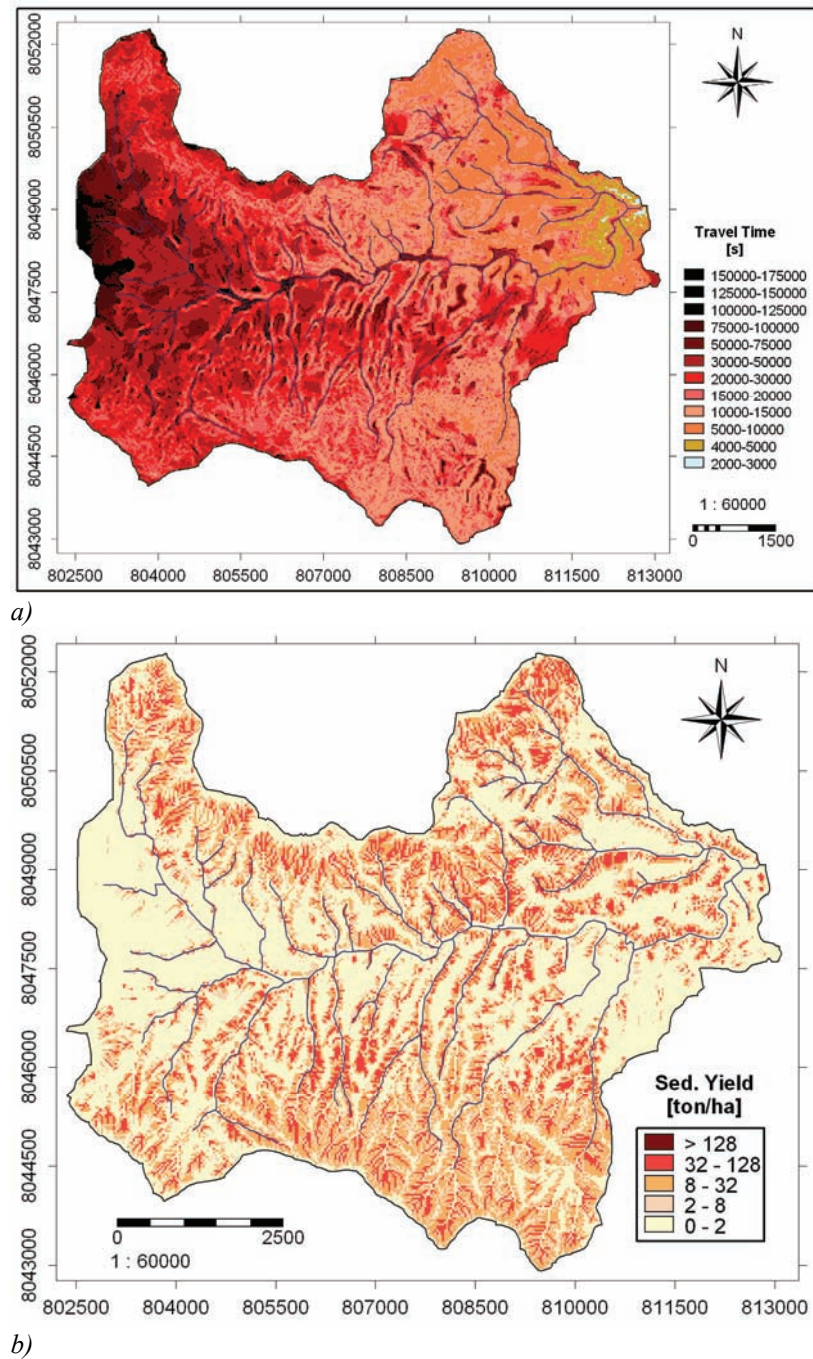
Figure 7.4 Spatial distribution of: *a*) hillslope travel time using the SEDD model, *b*) sediment yield using the SEDD and MMMF erosion model outputs

172

Notwithstanding, not all eroded particles of a sediment source area are expected to make their way to the catchment outlet. Such particles are stored or deposited somewhere in the system until a heavy rainfall is the means of routing these deposited sediments further downstream. Consequently, rainfall events both bigger in size and shorter in duration that occur in semi-arid catchments are more erosive than events that occur with the same intensity in more temperate or humid catchments.

From the SEDD predictions, it can be seen that only certain cells have the potential to contribute sediment to streams, with a significant portion deposited on gentle slopes as sediment travels from the source cells to the streams. A similar pattern is observed in the HSDR model estimates. Likewise, from the HSDR prediction for each of the five particle sizes, it can be noted that SDR_i decreases rapidly from the clay particle size to the sand-size class. SDR_i values for the sand-sized particles are close to zero everywhere. Thus, SDR changes with particle-size diameter (θ) in a nonlinear fashion. However, it remains almost constant for small particles (Lu and Higgitt, 2001). Large variations in SDR_i values are due mainly to heterogeneity in catchment properties, represented by the t_h, t_n and t_r.

The result suggests that large amounts of sediment are being deposited in the stream network. This is due to the difference in the time dimensions for upland erosion and sediment transport in the channels used in the HSDR approach. Upland runoff and associated erosion processes such as diffusive sheet-wash and rill erosion often occur at shorter time scales and in a strong ephemeral and intermittent fashion, whereas the sediment transport in the channels occurs over longer time periods. Overall, some of the key factors that control the estimation of the distributed SDR are potential runoff, slope steepness, slope shape, drainage pattern and density, land cover, soil surface and sediment characteristics, each of which were adjusted in the integrated spatial analysis and included in the SDR estimation.

In turn, the SEDD, HSDR and Veith spatial sediment delivery ratio algorithms provided more physically supported evidence for generating spatial sediment delivery maps. These maps can give useful indications and permit the analysis of the impact of sediment controls. In contrast, the theoretical basis of some algorithms of the SEAGIS is somewhat approximate, and the estimation of model parameters such as the thresholds and the scaling factor needs a stronger theoretical basis.

7.4.2 Sediment yield estimates

A holistic long-term approach to minimizing the amount of sediments entering a reservoir is to reduce soil erosion in the catchment upstream through soil conservation measures. Optimal application of these measures relies on an accurate estimation of erosion rates, proper location of erosion sources, and sediment yield estimation at the catchment scale (Van Rompaey et al., 2003a). Input erosion estimates required for the estimation of the spatial distribution of the sediment yield were derived from the application of five erosion models, namely, the RUSLE-3D, MMMF, SPL, Thornes and USPED models in Chapter 5.

After coupling the spatial soil erosion prediction with the four spatial SDR outputs, it is estimated that the two main rivers export relatively large amounts of sediment each year

in relation to their catchment size, with an average annual sediment yield per pixel of 14 ton ha^{-1} (Figure 7.5). For example if the *SDR$_i$* estimates provided by the SEDD model are modelled in terms of sediment yield, it is observed that the highest sediment yield was predicted by the Thornes model [112,000 tonnes], while the lowest values were estimated by the MMMF model [73,000 tonnes].

Likewise, when the SEAGIS sediment delivery output is used, the proportion of sediment yield in the catchment increases significantly, with the highest estimates being provided by the RUSLE-3D model [127,000 tonnes] and the lowest estimates by the MMMF model [87,000 tonnes]. A more complete evaluation of the quantitative results is given in Table 7.6. Overall, the sediment yield predictions obtained using the SEDD or HSDR sediment delivery approaches and the Thornes, RUSLE-3D and MMMF models for soil erosion estimation are similar to those registered in the reservoir, considering that the 10-year average deposition rate is 109,500 tonnes.

The fraction of eroded upland sediment delivered from hillslope to the channels is reduced by the presence of vegetation cover or increase in slope length (Ferro, 1997). Although SEDD neglects the channel sediment delivery component, results obtained are as satisfactory as with the application of HSDR. The spatial distribution of sediment yield obtained using the SEDD model can be observed in Figure 7.6.
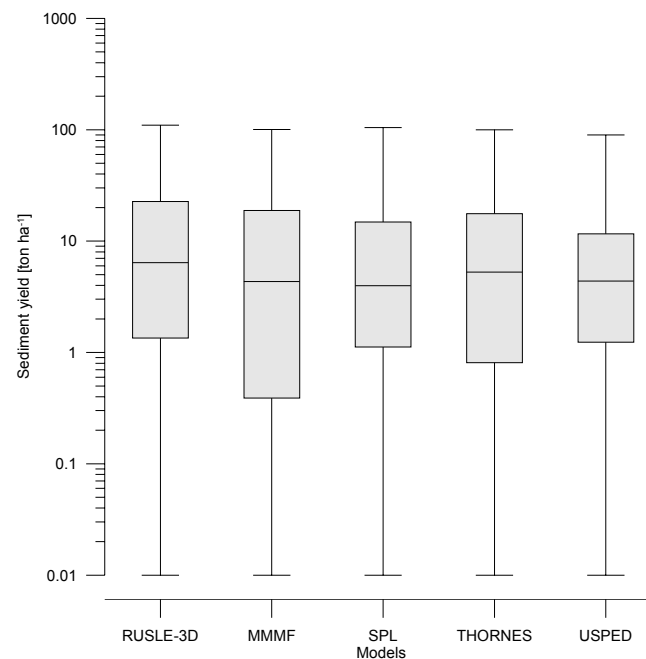
Figure 7.5 Box-plot of sediment yield using the SEDD sediment delivery ratio estimates
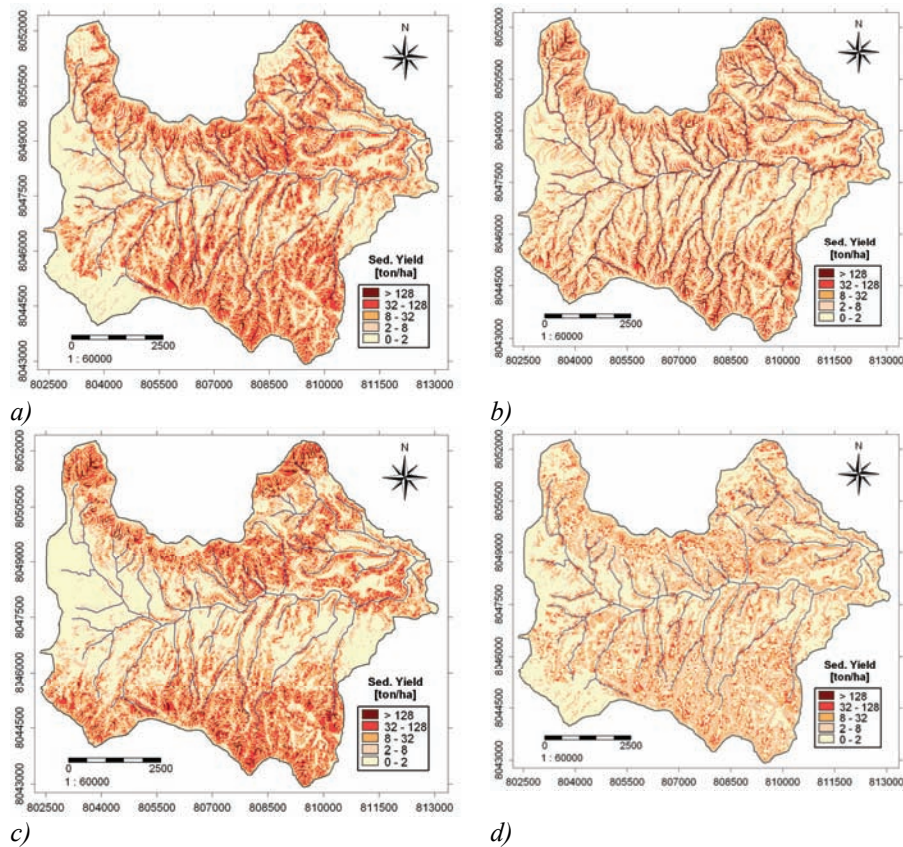
Figure 7.6 Sediment yield per cell [ton ha^{-1}] predicted using SEDD estimates: *a)* RUSLE-3D, *b)* SPL, *c)* THORNES, *d)* USPED

In terms of land cover distribution, most of the sources of sediment come from the steep shrubland. About 45% of the sediment reaching the channels was produced in the steep shrublands. This means that irrigated and rainfed cultivated areas have a reduced impact on the sediment yield generation. The average sediment yield to the outlet at steppe shrubland was 20 ton ha^{-1}, whereas values of 6 ton ha^{-1} and 7 ton ha^{-1} were found for irrigated areas and rainfed cultivation, respectively. The fallow areas and bare soils are the next most important source of sediment yield to the channel. They contribute about 15% and 10%, with an average of 15 ton ha^{-1} and 17 ton ha^{-1}, respectively.

In order to validate the performance of the SDR models, a methodology adopted in Verstraeten et al. (2003a) and van Rompaey et al. (2005) was used. The method consists of comparing the annual sediment yield predicted using the SDR approaches with the measurements of deposited sediment in the reservoir, bearing in mind that there is a direct connectivity between sedimentation in the reservoir and erosion in the upstream catchment.

After correcting the measured values of sedimentation in the Laka-Laka reservoir for trapping efficiency, the 15-year average sediment yield was derived and compared with

175

the model predictions. In order to perform a valid comparison with measured volumes, estimated volume at the Laka-Laka reservoir was calculated by multiplying estimated sediment yield by the relevant catchment area and by the proper number of years and dividing the result both specific solid weight of sediments and by the term (1-porosity). Table 7.6 summarizes the correlation between predicted annual sediment yields in the catchment with those estimated from reservoir sedimentation data.

Table 7.6 Predicted annual sediment yield using the distributed *SDR* approaches

Models	Gross erosion [tonnes]	SEAGIS [tonnes]	E. P.	SEDD [tonnes]	E.P.	Veith algorithm [tonnes]	E.P.	HSDR [tonnes]	E.P.
RUSLE-3D	280000	127000	16.0	107000	-2.3	117000	6.8	106000	-3.2
MMMF	148000	82000	-25.1	73000	-33.3	76000	-30.6	75000	-31.5
SPL	177000	113000	3.2	91000	-16.9	103000	-5.9	95000	-13.2
THORNES	284000	139000	26.9	112000	2.3	118000	7.8	115000	5
USPED	151000	87000	-20.5	83000	-24.2	85000	-22.4	84000	-23.3

E.P.: Percentage of error prediction. (-) underprediction, (+) overprediction

The validation shows that total sediment yield estimates given by SEAGIS are less accurate. For example, sediment yield is overestimated by 27%, 16% and 3%, respectively, when erosion predictions from the Thornes, RUSLE-3D and SPL models are used, whereas it is underestimated by 25% and 20% when the MMMF and USPED model predictions are used. A much better approximation with the observed sediment yield values is obtained when the SEDD, HSDR and Veith spatial distribution of SDR are used. For example, predictions provided by the SEDD model overestimate sediment yield by 2% when the erosion estimates derived from the Thornes model are used. However, total estimates are underpredicted by 2%, 17%, 24% and 34%, respectively, when the RUSLE-3D, SPL, MMMF and the USPED models are used. Notwithstanding, when compared with the other predictions, the spatial patterns of sediment yield per pixel seem more accurate when the MMMF model is used as catchment gross erosion estimator.

This is partly explained by the use of the minimum evaluation criteria by the MMMF model (*i.e.,* transport capacity limitation of *G*, the transport capacity rate of overland flow versus the detachment limitation of *F*, the rate of soil detachment by raindrop impact). It can be noted that *F* is not topographically dependent. The MMMF model is, however, sensitive to certain rather poorly defined soil moisture variables such as the typical rooting depth of vegetation types, and the calculated values of *G* vary considerably.

Another factor that of course can explain inaccuracies in the prediction of the sediment yield is related to uncertainty in the catchment gross erosion maps. As stated earlier, the difficulties in accommodating gully erosion and channel erosion, both particularly active processes in this semi-arid region, render these relatively simple model predictions less accurate. As Nearing (2004) states, hardly any of these factors can be fully or partly included in the distributed erosion models that are used nowadays. Sediment that is produced on upland areas far from any river channel has a much lower probability of being delivered to that river and hence to the reservoir. However, gully

erosion is a process that provides an almost direct link between sediment source (*e.g.,* the gully headcut) and the river channel. Models overpredict sediment yield for steep slopes located in the most upstream areas of the catchment; visual inspection demonstrates that low rates of sediment yield exist in these areas.

Thus, the spatial distribution of sediment yield is relatively inaccurate. This can be explained by the very pronounced topography and the presence of sizeable gullies (as large as 8 to 10 m deep, 20 m wide and 2.2 km long) that have developed in the weak siltstones, particularly in the south flank of the catchment. They extend easily into the reservoir but cannot be included in any of the models.

Considering the results obtained, which consider the total deposition over the entire erosion versus sediment transport periods, it is believed that the channel network is capable of transporting a major part of the sediments delivered to it when high torrential rainfall runoff events occur in the summer rainfall season.

As can be seen, the four spatial SDR methods described, when coupled to a gross catchment erosion estimate, produced reasonably reliable annual estimates of sediment yield. Note that the coefficient values used in the various equations were determined using standard procedures and without any field calibration. Hence, the reliability of the SEDD, HSDR and Veith models can be rated as satisfactory, particularly considering the fact that predictions from more sophisticated process-based models also show large differences between observed and computed sediment yields.

The sensitivity of dimensionless coefficients, namely, δ, ψ, χ, β, shows a high variability. The use of measured sediment yield data in combination with inverse methods seems to provide a sound method for their estimation. Due to the lack of sediment yield records in similar catchments in the region, the parameters were optimized by trial and error. For example, the β coefficient of the SEDD model was analysed and the value optimized empirically. The value of β varied from 0.0089 to 1, with increments of 0.001. The variation in the computed values of sediment yield S_y shows the high sensibility of the parameter β. A β value of 0.015 gave the best SDR estimate for these catchment conditions.

7.5   Conclusions

Distributed gross catchment erosion predictions were coupled to different spatial SDR models in order to evaluate the amount of sediment transferred annually from eroding sources through hillslopes and the channel network to the catchment outlet. Multiple reservoir sedimentation records were used to validate the computed sediment yields at the outlet. The aim was to evaluate four spatial sediment delivery ratio models in their capacity as sediment yield estimators of mountainous medium-sized catchments in the Andes.

The SEAGIS model predictions of sediment delivery depend largely on a subjective selection of the upper and lower threshold values to transport or deposition. Together with a scaling factor hard to define, the parameters of this model make it difficult to estimate sediment yield values. More extensive field data and research are needed on the SEAGIS model in order to establish proper parameter values and estimation criteria.

The sediment delivery estimations of the Veith and SEDD models depend upon a (semi-physically based) sediment travel time concept, defined as the time for eroded soil particles to travel from an erosion source area and be transported through the hillslope conveyance system to the channel network and eventually to the catchment outlet.

The HSDR model is a conceptual model based on linear reservoir storage and is driven by an effective rainfall duration (*i.e., t_r*), which is considered as the primary driving force of the sediment transport. The incorporation of rainfall characteristics permits this model to simulate the ephemeral nature of runoff and sediment transport, especially in semi-arid catchments and regions. This allows the HSDR model to evaluate the nonlinear effects on sediment delivery of rainfall and climate (*e.g.,* changes in climate and land use). In addition, the HSDR gives a spatial distribution of sediment delivery, using five sediment particle-size classes.

Overall, it was found that the local sediment delivery ratios and sediment yields are quite low in more than 50% of the catchment. High values (SDR>0.8) were obtained in 10% of the catchment area (*i.e.,* in the upland areas located in the southeastern and south-central part of the catchment).

From analysing the theoretical model backgrounds and assumptions, preference should be given to the HSDR model because it includes the sediment delivery process in the channel network. However, considering that the SEDD model provided rather reliable results, and since the input data required for the SDR estimation are relatively easy to obtain in a catchment, the SEDD approach is probably more suitable for predicting distributed SDR in situations where detailed catchment data are scarce or not readily available.

When using the SEDD model for spatial sediment delivery and sediment yield evaluation, it was estimated that an average of approximately 45% of the total gross catchment erosion was transported on an annual basis from the upland areas into the reservoir. This high proportion of sediment delivered to the reservoir can be explained by the erodible soils and prevalent sedimentary lithology (*e.g.,* siltstone, shale, mudstone), in combination with a steep catchment and drainage network topography and sparse vegetation cover.

For steep sloping areas, the production of sediment might be higher, particularly if insufficient vegetation cover exists and the area is exposed to a relatively more intense rainfall. However, a lower or higher sediment delivery in this area will not only depend on the slope, but on the rainfall duration and the interannual variability of the rainfall. For example, rainfall events both bigger in size and shorter in duration that occur in arid or semi-arid catchments are more erosive than when they occur with the same intensity in humid or temperate catchments.

The use of reservoir sedimentation records as shown in this chapter offers an alternative method for both erosion and sediment yield model validation. The collection of datasets with sedimentation records of lakes and reservoirs should therefore be encouraged both by the scientific community and by regional governments.

Overall, the introduction of spatially distributed SDR models might contribute to the development of cost-effective strategies for erosion control by identifying areas that have higher potential to deliver sediment to the reservoir.

In this chapter, the ability to predict erosion and sediment yield based on satellite imagery in combination with spatial erosion and SDR models has been demonstrated. Methods used in this analysis have illustrated how promising results can be obtained with a minimal amount of data collection.

Chapter 8

Evaluation

Chapter 8

Evaluation

Problem statement and objectives

The study of the behaviour of soil erosion, deposition and sediment redistribution processes in catchments and river basins is of major importance to natural resources managers, as well as hydrologists and water resources engineers. Soil erosion intensity determines to a large extent the long-term sustainability and productivity of agriculture, rangelands and forest systems. Sediment deposition can be seen as a beneficial process under certain circumstances, as in the case of alluvial floodplain aggradations. However, in most cases, excessive sedimentation adversely affects watercourses, drainage networks, and water resource structures such as dams and reservoirs, and with it limits the source of drinking water supply.

Soil erosion and sediment transport processes in shallow flows theoretically concern the dislocation and movement of soil particles, ranging from clay size to sand, and represent physical processes acting on a very small space and time continuum. However, predictive capabilities far beyond these theoretical microscales are required by resource managers and society in general.

Soil erosion assessments for fields and farmland usually rely on plot- to hillslope-scale erosion and deposition data analysis, using typical spatial length scales from 1 to 100 m. Catchment and larger regional-scale evaluations of process intensities and rates will in practice depend on larger-scale generalizations and coarser-resolution data and information. Scales of spatially distributed assessments ranging from 0.01 km^2 to 1 km^2 or even 10 km^2 are common and needed in practice when analysing large river basins or ecoregions. In global environmental and climate research, assessment and modelling tools using 10 to 100 km^2 grids, or approximately 1 arc-second degree geographical resolutions, are customarily used. Hence, understanding and appropriate handling of the scale factor is important when using modelling approaches for the assessment of erosion and deposition processes.

In many tropical and subtropical regions of the world, lack of *in situ* ground data and experiments presents the main hindrance to effective soil and water resources management and consequent protection of natural resources. Current progress in remote sensing and geo-information techniques has led to large amounts of data being made available nowadays to the scientific community and public. Therefore, spatial assessment methods are needed that combine remote observations from satellite and airborne sensors with the scarce *in situ* data.

This thesis has attempted to develop and compare geospatial methods of estimating spatial and temporal distributions of soil erosion and deposition rates in ground-data-poor environments. Spatial patterns and process rates of erosion and deposition were

obtained by combining satellite imagery and available *in situ* data with different relatively low data demanding erosion model approaches. The analysis was done at regional (54,100 km^2) and catchment (59.8 km^2) scales, using different data and different model resolutions. Regional spatial patterns of erosion and deposition were validated by comparing model estimates with semi-detailed erosion intensity or risk assessment studies available for a number of watersheds in the study area. For the catchment scale analysis, besides a validation using multitemporal remote sensing data, a quantitative validation of the gross catchment erosion–sediment yield relation was obtained by linking erosion and sediment yield estimates with reservoir sedimentation data, using spatial SDR concepts. Reservoir sedimentation data were collected for three important water and hydropower-generating reservoirs in the area. A novel rapid GPS-guided acoustic sonar surveying method was developed and evaluated for this purpose.

Erosion model selection

A review of erosion models was made in order to analyse and describe existing approaches in their capacity to represent erosion, deposition and sediment transport dynamics at various spatial and temporal scales and in relatively data-poor environments. Input data requirements and accommodation of the remote sensing of reviewed model data were also evaluated. The application of existing and powerful complex physically based models such as SHETRAN and WEPP was judged unfeasible at regional and catchment scales in this environment, owing to their extensive data and parameterization requirements, the difficulties in accommodating remotely sensed data, and the lack of necessary hydrological field data for calibration.

Five conceptual and spatially distributed erosion models were selected that had relatively low input data requirements, were able to accommodate satellite data, and were executable within a georeferenced environment. All models had proven ability of use in a broader range of climatic and topographical environments.

The RUSLE-3D model, variant of the famous Universal Soil Loss Equation (USLE) developed originally by Wischmeier and Smith (1978), enables an analysis of the impact of flow convergence in complex topography, such as found in the study area, to be carried out by replacing the hillslope length and steepness factor by an algorithm incorporating the upslope contributing area.

The modified version of the well-known Morgan, Morgan and Finney model (MMMF) was also used. This model analyses the erosion processes from two competing subprocesses (*i.e.,* soil detachment by rainfall impact and the transport of detached particles by runoff). The strength of this model lies in its ability to determine whether the erosion process is detachment- or transport-limited. The simplified Stream Power Law (SPL) model predicts long-term fluvial erosion incision based on the upstream contributing area and lithology. Thornes (1985) presents a geomorphic model that combines runoff rate, soil erodibility, the effects of topography, and vegetation protection in a simple physical equation. The Unit Stream Power Erosion Deposition model (USPED) of Mitasova et al. (1998) computes net erosion and deposition as the divergence in the sediment transport capacity.

Likewise, all five implemented models allowed the integrated use of (i) coarse-resolution multitemporal imagery (*i.e.,* NOAA-AVHRR, SPOT-VGT and MODIS) to account for vegetation properties and to monitor seasonal changes of vegetation cover, (ii) high spatial resolution imagery (*i.e.,* SPOT-5, Landsat-7 ETM) to map land cover, erosion features and types, and soil surface features at the catchment scale, (iii) DTMs (*i.e.,* HYDRO-1k, SRTM and 1:50,000 topographical map data) for terrain and topographical analysis, and (iv) climate data (*i.e.,* the global CRU CL-2 and TRMM satellite rainfall data and local meteorological station data) for hydrological parameterization.

Study area

The investigations were conducted in Cochabamba province, central Bolivia (Figure 3.1). A large part of the regional research and catchment areas located in the middle valleys in the proximity of Cochabamba city are representative of the Andes, and pertain geographically to the upper part of the Amazon river basin (Rio Grande basin). The gross area of 54,100 km^2 used in the regional assessment has elevations ranging from a mere 100 masl to over 5,200 masl. A high diversity of climates, topographies and vegetation types, ranging from high alpine to semi-arid mountain to tropical lowland environments, can be observed in the area. The region of the middle and upper valleys of Cochabamba (Figures 4.11 and 6.1), a focal part of the study area used for the catchment analysis and reservoir sedimentation surveys, is located at elevations ranging from 2,500 to 5,200 masl.

The middle valleys of Cochabamba have a dry subhumid to semi-arid climate with a potential evaporation [1,200 mm yr^{-1}] exceeding the annual rainfall in the range of 450 to 700 mm yr^{-1}. Rainfall shows a strong seasonal concentration with annual erosivity in the range of 800 to 1,400 MJ mm ha^{-1} hr^{-1}. Annual 24-hour rainfall depths are in the range of 25 to 45 mm, with storm erosivity of 150 to 300 MJ mm ha^{-1} hr^{-1}, and present medium-sized storms when compared with other tropical locations. This is due in part to the effect of the higher altitude and less exposure of the valleys to the rainfall-bearing weather systems during the summer.

Furthermore, the area of the upper valley, and more specifically the catchment study area, is characterized by a generally low vegetation cover and a relatively large abundance of old sedimentary lithologies (*i.e.,* the Anzaldo and Capinota formations), consisting of siltstones, sandstones and shales and weathering to medium-textured erodible soils. Tertiary and Quaternary alluvial and fluvio-lacustrine deposits, alluvial fans and terraces also present erosion-sensitive areas in many places. All this makes the region prone to general erosion and sensitive to rainfall erosion. The signatures of erosion and sedimentation processes are clearly visible in the landscape and have an important impact on the well-being of the rural and local populations in general. Both land (*i.e.,* soil productivity) and water resources are impacted by the processes (*e.g.,* siltation of reservoirs and irrigation canal structures).

Regional-scale analysis

The main objective of the regional erosion assessment was to evaluate the use of global coarse-resolution satellite data and geodata in combination with the selected models for erosion assessment and monitoring at the regional scale. Two evaluation scenarios using

different datasets were implemented. First, a baseline evaluation was done using the IPCC baseline climate data (1961 1990, 30-year long-term average) for the region, in combination with the 1 km global DEM HYDRO-1k, the NOAA-AVHRR 10-day composite NDVI time series for vegetation cover, and the global soil data and map. The second "present-day" evaluation used more recently available global or continental data and/or increased data resolution, such as the 1998 to 2003 satellite rainfall data from the Tropical Rainfall Monitoring Mission (TRMM), the 90 m Shuttle Radar Topographic Mission (SRTM-DEM), the SPOT-VGT sensor NDVI time series data for vegetation cover, and the 1:250,000 regional soil mapping information.

More consistent spatial patterns and erosion estimates were obtained using the current evaluation data. It was estimated that 56% of the region was slightly affected by rainfall erosion or erosion rates below 200 ton km^{-2} yr^{-1}, and 10% of the province faced medium erosion levels [200 to 800 ton km^{-2} yr^{-1}]. The relative proportions with high [800 to 3,200 ton km^{-2} yr^{-1}] and very high erosion [3,200 to 12,800 ton km^{-2} yr^{-1}] were 15% and 13%, respectively. Extreme erosion rates [>12,800 ton km^{-2} yr^{-1}] were found in 6% of the area. In general, 19% of the overall area faces very high to extreme soil degradation.

Regional erosion/deposition patterns and rates were validated by categorical comparison of estimated erosion patterns and rates, and classified according to existing catchment erosion intensity maps obtained from geomorphological field surveying combined with aerial photo interpretation. Although overall regional-scale model performance was generally poor (<50% area accuracy), the models could be ranked as follows regarding performance: MMMF, Thornes, RUSLE-3D, USPED and finally the SPL model. It was shown that especially the scale sensitivity of the DEM data and the generalizations observed in the soil information in the datasets are the cause of most inaccuracies in the predictions at this scale.

Catchment-scale analysis

The use of satellite data combined with limited *in situ* data as input for erosion models was further analysed. An attempt was made to integrate medium- to fine-resolution satellite images with *in situ* soil and land cover observations and meteorological station data at the catchment scale.

The data used were (i) recent (2002) high-resolution SPOT-5 data and 1:50,000 aerial photographs (1961) for mapping land cover, erosion features, soil types and geomorphology; (ii) the 250 m MODIS-NDVI time series for monitoring the temporal variation of cover vegetation; (iii) a reconnaissance soil and erosion survey for determining physical soil parameters; (iv) the 90 m SRTM-DEM and 1:50,000 topographical sheets with 20 m contour intervals for landscape representation; and (v) meteorological data for rainfall characterization in the catchment area. When compared with the regional assessment, more satisfactory predictions were obtained, owing to increased spatial model (30 m) and data resolutions ranging from 5 to 250 m.

For the 59.8 km^2 Laka-Laka catchment, average annual gross erosion for the five-year evaluation period (1998 to 2003) was estimated at 2.5×10^5 tonnes, or an area-specific erosion rate of 30 ton ha^{-1} yr^{-1} or 3,000 ton km^{-2} yr^{-1}. This relatively high denudation rate is explained in first instance by the sedimentary lithology of siltstones interbedded with

quartzite and green marls (Anzaldo formation) dominating large areas in the catchment and smaller occurrences of shales (Capinota formation) in combination with steep topographical gradients. This value is not equal to the sediment delivery or area-specific sediment yield.

From the spatial distribution analysis, it was observed that a total area of 32.3 km^2 or 54% of the catchment is affected by medium [200 to 800 ton km^{-2} yr^{-1}] to high [800-3,200 ton km^{-2} yr^{-1}] erosion intensities, whereas 15.6 km^2 or 26% of the area is undergoing very high [3,200 to 12,800 ton km^{-2} yr^{-1}] to extreme [>12,800 ton km^{-2} yr^{-1}] erosion rates, which are the major contributors of sediment to the reservoir.

The catchment erosion model performances were evaluated by comparing the spatial patterns obtained using the models with an erosion feature and intensity map derived from a combination of field surveying, the 1961 orthophoto mosaic, and the 5 m orthorectified SPOT-5 panchromatic image (acquisition date August 2002). Although diffusive wash and small rill erosion phenomena are not easily identifiable, larger erosion features such as gully initiation and growth, drainage system widening, bank erosion and small landslides can be easily extracted from the images. Comparison of the two image dates, the airborne photo mosaic, and the SPOT-5 enabled visual identification of active erosion areas in the catchment.

The semi-quantitative model validation indicates reasonable model agreement if minus (-) or plus (+) one class difference in estimation between observed and modelled erosion is considered to be acceptable. In terms of spatial patterns, the RUSLE-3D and USPED models were judged to be more adequate in pinpointing gully and stream network erosion.

Likewise, the MMMF model was found to be more appropriate for identifying sediment sources, owing to its evaluation of detachment or transport limitation and the decoupling of local erosion to *a priori* topographical forcing by most models. Although the effect of topography is most dominant in the Thornes model, its ability to evaluate erosion at a monthly time step is considered useful for analysing the seasonal distribution of erosion intensity and evaluating causal factors such as vegetation cover and rainfall erosivity.

Concerning the utility of the flow algorithms derived from the DEMs, the multiple flow algorithm was preferred to the steepest decent or D8 algorithm because it more closely approximated the existing stream network and accounted to a greater extent for flow divergence and convergence patterns observed on the images of the mountainous study area.

Reservoir sedimentation

In the absence of streamflow and sediment concentration records of watersheds, as in the case of the Laka-Laka catchment, reservoir sedimentation data offer considerable potential for reconstructing sediment yields from the contributing catchment. A rapid bathymetric survey method was therefore developed for the purpose, and was evaluated in a number of important reservoirs and natural lakes in the study area.

The novel geomatic method consisted of a low-cost GPS coupled to a portable acoustic sonar sounder, in combination with satellite data. Four specific research objectives were pursued in the reservoir studies: (i) to analyse the effect of sample size (or point density) of sonar soundings on the accuracy of the bathymetric surface generation; (ii) to evaluate interpolation methods for generating bathymetric surfaces; (iii) to estimate historical changes in storage volume, sediment deposition and to determine the actual capacity and life expectancy of the three reservoirs; and (iv) to derive the area-specific sediment yields of the reservoir catchments from the multitemporal reservoir sedimentation records.

The methodology for reconstructing sedimentation records for the reservoirs relied on the determination of the reservoir bed topography from data corresponding to three different time stages: (i) topographical survey prior to the dam construction, (ii) previous bathymetric surveys, and (iii) the 2003 GPS-guided sonar surveys. Historical bathymetric map data were scanned, digitized and interpolated using contour interpolation. Ordinary kriging was used for interpolation of measured sonar point data.

A split sampling technique, applying a progressive reduction in observed data points, was used to evaluate the effect of sample size (or point density) on the accuracy of the bathymetric surface generation. Based on a cross validation of results, the accuracy was determined taking into account the variogram model and interpolation method for each prediction. Comparison of predictions among different subsets was evaluated using several statistics of accuracy (*i.e.*, bias (B), goodness of fit (r^2), coefficient of correlation (r), root mean square error ($RMSE$), mean square error (MSE), mean absolute error (MAE) and the Nash-Sutcliffe coefficient (R^2_{NS}).

The validation analysis and accuracy test statistics clearly indicated that the accuracy of the interpolated bathymetric surfaces deteriorated consistently and significantly as the sampling size was reduced below 50% of the initial number of sample points. This corresponded to a point density of five or six soundings per 100 m cell size of the reservoir bed for the Angostura and Corani reservoirs, respectively, whereas it corresponded to a density of 141 soundings per 100 m cell size for the bottom of the Laka-Laka reservoir owing to its large bottom variability.

The uncertainty in the bathymetric surfaces was more pronounced if larger depth variations were present. Comparing all the bathymetric surface outputs obtained for all sample sizes, it was concluded that sample sets with a minimum of six sample points per 100 m cell size are adequate for an accurate interpolation when a uniform bed exists, whereas a minimum of 71 sample points per 100 m cell size are required if a large bed variability is detected (25% of the total sampling).

This statement is based on the fact that the elevation difference between the surface grid obtained with the total sampling sets (100%) and the surface grid of both 25% and 50% of the sample size were less than 0.5 and 0.2 m, respectively. With higher point sampling densities, differences between observed and interpolated bed depths were below the measurement error of ±0.1 m of the acoustic sonar instrument (Fishfinder-100 Garmin) and therefore redundant.

Owing to the different sizes, lifetimes and upstream basin characteristics of the reservoirs, considerable variation was found among the total sediment deposition in the three reservoirs. Values ranged from 0.92 Mm^3 for the Laka-Laka reservoir to 1.4 Mm^3 for the Corani reservoir, and 10.2 Mm^3 for the Angostura reservoir. Sediment trapping efficiencies were estimated at 95%, 90% and 89% for the Corani, Angostura and Laka-Laka reservoirs.

Considering these efficiencies, the total sediment yields accumulated during 36, 56 and 11 years of dam operation were estimated at 1.6×10^6, 13.7×10^6 and 1.2×10^6 tonnes respectively for the Corani, Angostura and Laka-Laka reservoirs. In terms of specific sediment yield or SSY prediction, the highest SSY estimate [1,831 ton km^{-2} yr^{-1}] was obtained for the Laka-Laka reservoir with an upstream catchment area of about 59.8 km^2, while a much lower value [123 ton km^{-2} yr^{-1}] was predicted for Angostura reservoir with an upstream area of 1,992 km^2. The SY of the 297 km^2 Corani basin derived from the reservoir sedimentation records was evaluated at 152 ton km^{-2} yr^{-1}.

Several possible reasons exist for the significant differences in sedimentation rates among the three reservoirs, the more important being basin area, general basin relief, lithology and land cover. The results are in agreement with recent findings that consider that the topographical gradients and presence of depositional environments such as alluvial fans or floodplains within of 5 km of the reservoir influence the sediment yield.

However, it is clearly shown that the commonly used variable "basin area" alone is a very poor predictor of specific sediment yield, although still in use and proliferating in scientific literature. Additional evidence for the high sediment yields of the smaller Laka-Laka catchment can be found when considering the lithological and geomorphic settings of the catchment and the geographical location of the dam site.

As stated earlier, the sedimentary geology underlying large parts of the Laka-Laka catchment, and the steep relief of the land areas and drainage network strongly affect the mechanism and rates of erosion and sediment supply. Conversely, sedimentation at the Angostura reservoir is low considering the total basin area (1,992 km^2) of the upper valley, the present lifetime of the reservoir of 56 years, and the relatively high erosion rates observed in the upper catchment areas (*e.g.,* Santivañez, Anzaldo and Sacabamba villages). However, the presence of the extended infilled alluvial upper valley and the large coarse-grained alluvial fans at the outlets of the main rivers entering the valley depression (*e.g.,* Punata, Villa Rivero and Cliza fans on Figure 6.1), which act as a huge depositional sink, prevent much sediment from travelling towards the reservoir, with the exception of very fine wash load transported during active flood events. Thus, although soil erosion may be severe in the upstream mountainous catchment areas, sediments generated upstream by the rainfall erosion process are deposited in alluvial fan storages and depositional floodplains.

Although the high internal relief and hydrological drainage pattern of the Corani river basin would *a priori* suggest important basin sediment yields, low rates of reservoir sedimentation were also found. Field observations and satellite image analysis indicate that in this subhumid basin the vegetation cover is quasi permanent, with small

perennial grasses, shrubs, forest patches and local agricultural fields (beans, potatoes) typical of the high sub-Andean environment.

Also soil development (*i.e.,* organic matter decomposition) shows typical features observed at these higher elevations (>3,000 masl) and near-tropical latitudes, resulting in relatively low soil erodibilities in combination with good vegetative cover. The Corani basin is fed from several subcatchments through two main rivers draining large U-shaped, old glacial alluvial valleys (*i.e.,* Colomi, Palca, Tablas, Melga, Quenko, Aguirre), which act as depositional environments and areas. Gradients of the main river courses in the proximity of the reservoir are low (<0.1%), impeding strong high-density sediment fluxes towards the reservoir. In turn, it can be stated that the dam site selections for the Angostura (1939) and Corani (1968) reservoirs were properly done, in contrast to the inadequate site selection carried out for the Laka-Laka dam and reservoir (1991), at least in terms of sedimentation and useful life expectancy.

The satisfactorily results obtained in the three studied reservoirs demonstrate the applicability of the handheld GPS-guided acoustic sonar survey technique for updating bathymetric records of lakes and reservoirs. It should be stated that, in order to be fully accurate, the method should be complemented with *in situ* reservoir sediment coring for direct determination of bulk densities. The use of additional satellite images provides the necessary additional reservoir contours (water versus land boundaries and above the present waterline) that allow reservoirs with lower water levels also to be monitored. Because of the low equipment cost (<€ 2,500) and the speed at which the method can be executed, the method can be used on a regular and frequent basis for establishing baseline data on reservoir sedimentation and catchment sediment yields.

Linking gross catchment erosion to reservoir sedimentation

Finally, an alternative method of establishing linkages between gross catchment erosion and sediment delivery to reservoirs, based on a spatial sediment delivery ratio (SDR) concept, was implemented for the 59.8 km^2 Laka-Laka catchment. Modelling the SDR on a spatial cell basis and coupling it to a gross erosion estimate enables estimation of the net amounts of eroded soil that are delivered from upland cells to the nearest river cell and further to the catchment outlet and reservoir. Four recently developed spatial SDR models (*i.e.,* the soil erosion assessment tool (SEAGIS), the sediment delivery distributed model (SEDD), the Veith algorithm, and the hillslope sediment delivery ratio (HSDR) model) were applied and evaluated.

Conceptually, the HSDR model considers a catchment as a system of two lumped linear storages coupled in series: hillslope transport to the nearest stream and sediment flow routing in the channel network. When using this method, the most important control factor in the sediment delivery processes is given by the ratio of catchment sediment residence time to average effective rainfall duration.

The Veith algorithm and the SEDD model present a similar theoretical background and consider the SDR to be a function of the sediment travel time of each cell. They define the SDR as a function of flow path length, slope and surface roughness. The SEAGIS approach considers the SDR as a function of the amount of runoff expected to travel

through a cell, weighted by the slope and the likelihood of sediment deposition further downstream.

Applying the four SDR models and using catchment gross erosion estimates obtained from the erosion models as input showed that the predictions were similar for all approaches, although differences in spatial SDR patterns were visible, leading to identification of different source areas. In general, the SDR and sediment yields on a cell basis were distinctly lower (*e.g.,* SDR<0.2) than the erosion rates in more than 50% of the catchment. Higher delivery values (*e.g.,* SDR>0.6) were found in 25% of the area, especially in the upland areas located in the southeastern and south-central part of the catchment. On average for the evaluation period, 45% of the total gross rainfall erosion was mobilized and transported from the upland areas through the stream network to the reservoir and catchment outlet, resulting in a gross catchment SDR of 0.45.

The HSDR approach, because of its strong theoretical basis and the inclusion of rainfall parameters, was considered more suitable for predicting distributed sediment deliveries at the catchment or basin scale. However, considering that the SEDD approach also showed sufficiently reliable results and since the input data requirement for this approach is easier to obtain, it is probably more suitable for estimating spatial SDR of catchments in data-poor environments.

A quantitative validation of the modelled sediment deliveries for the Laka-Laka catchment was carried out by comparing the annual sediment delivery prediction with the sediment yields derived from the measured reservoir sedimentation data. When using the SEDD model predictions (*e.g.,* SDR estimates coupled to the respective erosion models), higher catchment sediment yield estimates were derived for the Thornes [110,000 tonnes] and the RUSLE-3D [107,000 tonnes] models, whereas lower values were estimated by the SPL [91,000 tonnes], USPED [82,000 tonnes] and MMMF [73,000 tonnes] models. The annual predictions were in line with measured reservoir sedimentation, considering that the annual average deposition (11 years of reservoir life) in the reservoir was 109,500 tonnes.

Final remarks

The magnitude of the environmental and social consequences of soil erosion and sediment delivery issues in the Andean region of Bolivia has long been recognized and has attracted scientific attention. This research has shown that geo-information techniques such as geospatial erosion and sediment delivery modelling approaches, in combination with satellite data and supported by limited *in situ* measurements, enable the screening of larger regions and catchments for erosion and sedimentation hazards.

The methodology can be used to produce national, regional and catchment erosion and deposition estimates at appropriate spatial and temporal resolutions, using either freely available or affordable remotely sensed data. The implemented methodology, based on modest model data requirements, produced realistic estimates at monthly and annual time scale resolutions and at 1 km and 30 m spatial resolutions.

Using the rapid assessment and monitoring method developed in this study for lakes and reservoir sedimentation, the combined geospatial modelling framework for gross catchment erosion and sediment delivery estimation can be extended to other ungauged river basins with scarce *in situ* observation data.

The method may also find practical use in land use planning and land management, where it can supplement extrapolations from small-scale field experiments. The results of this research have also indicated other potential environmental fields and ecological issues where erosion and sediment production estimates could be of substantial use (*e.g.,* land desertification and climate change research).

References

Aalto, R. et al., 2003. Episodic sediment accumulation on Amazonian flood plains influenced by El Niño/Southern Oscillation. Nature, 425(2): 493-497.

Aalto, R., Dunne, T. and Guyot, J.L., In press. Geomorphic controls on Andean denudation rates. Journal of Geology.

Agash, M., 2003. Regional scale assessment of water balance and soil erosion using global climate and internet geodataset. Unpublished MSc Thesis, International Institute for Geo-Information Science and Earth Observation, Enschede, The Netherlands, 150 pp.

Allen, R., Pereira, L.S., Raes, D. and Smith, M., 1998. Crop evapotranspiration: guidelines for computing crop water requirements. FAO, Rome, Italy.

Alonso, C.V., Bingner, R.L. and Kuhnle, R.A., 1995. Sediment yield from watersheds with eroding channels. In: W.H. Espey and P.G. Combs (Editors), Water Resources Engineering: Proceedings of the First International Conference. American Society of Civil Engineers, pp. 1183-1187.

Amarsaikhan, D. and Douglas, T., 2004. Data fusion and multisource image classification. International Journal of Remote Sensing, 25: 3529-3539.

Amore, E., Modica, C., Nearing, M.A. and Santoro, V.C., 2004. Scale effect in USLE and WEPP applications for soil erosion computation from three Sicilian basins. Journal of Hydrology, 293: 100-114.

Angima, S.D., Stott, D.E., O'Neill, M.K., Ong, C.K. and Weesies, G.A., 2003. Soil erosion prediction using RUSLE for central Kenyan highland conditions. Agriculture, Ecosystems and Environment, 97: 295-308.

Arnold, J.G., 1996. SWAT: Soil and Water Assessment Tool / User's Manual, USDA-ARS.

Arnold, J.G. and Fohrer, N., 2005. SWAT2000: current capabilities and research opportunities in applied watershed modelling. Hydrological Processes, 19(3): 563-572.

aus Yarina-Kocha, K.S., 2002. Soil erosion in Andean cropping systems. PhD Dissertation. Der Facultät III - Agrarwissenchaften I. Pflanzenproduktion und Landschaftsökologie der Universität Hohenheim., Hohenheim, Germany, 178 pp.

Baban, S.M. and Yusuf, K.W., 2001. Modelling soil erosion in tropical environments using remote sensing and geographical information systems. Hydrological Sciences, 46(2): 191-198.

Baker, N.T. and Morlock, S.E., 2001. Use of a Global Positioning System and an Acoustic Doppler Current Profiler to map river and lake bathymetry, U.S. Geological Survey, Indiana, USA.

Banis, Y.N., Bathurst, J.C. and Walling, D.E., 2004. Use of caesium-137 data to evaluate SHETRAN simulated long-term erosion patterns in arable lands. Hydrological Processes, 18(10): 1795-1809.

Banks, W.S.L. and LaMotter, A.E., 1999. Sediment Accumulation and water volume in Loch Raven Reservoir, Baltimore county, Mariland, U.S. Geological Survey, Maryland, USA.

Barnes, J. and Pelletier, J., 2001. Erosion Mapping of the Bolivian Central Andes Using the Stream Power Law and a Digital Elevation Model. Department of GeoSciences. University of Arizona, Tucson, USA.

Bartsch, K.P., Van Miegroet, H., Boettinger, J. and Bobrowolski, J.P., 2002. Using empirical erosion models and GIS to determine erosion risk at Camp Williams, Utah. Journal of Soil and Water Conservation, 57(1): 29-36.

Bathurst, J.C., Wicks, J.M. and O'Connell, J.A., 1995. The SHE/SHESED basin scale water flow and sediment transport modelling system. In: V.P. Singh (Editor), Computer Models of Watershed Hydrology. Water Resource Publication, Highlands Ranch, Colorado, USA, pp. 63-94.

Beasley, D.B., Huggins, L.F. and Monke, E.J., 1989. ANSWERS: a model for watershed planning. Transactions of ASAE, 23(4): 938-944.

Beck, S., 1988. Las regiones ecológicas y unidades fitogeograficas de Bolivia. In: C. Morales (Editor), Manual de Ecología. Universidad Mayor de San Andres, La Paz, Bolivia.

Beck, S.G., Killen, T. and Garcia, E., 1993. Vegetación de Bolivia. In: T. Killen, E. Garcia and S. Beck (Editors), Guia de Arboles de Bolivia. Herbario Nacional de Bolivia - Missouri Botanical Garden. Quipus, La Paz, Bolivia, pp. 6-24.

Belward, A.S., Estes, J.E. and Kline, K.D., 1999. IGBP-DIS 1-km land cover data set DISCover: a project overview. Photogrammetric Engineering and Remote Sensing, 65(9): 1013-1020.

Beven, K., 1995. Linking parameters across scales: subgrid parameterizations and scale dependent hydrological models. Hydrological Processes, 9(507-525).

Bhuyan, S.J., Kalita, P.K., Keith, A.J. and Barnes, P.L., 2002. Soil loss predictions with three erosion simulation models. Environmental Modelling & Software, 17: 137-146.

Bhuyan, S.J., Marzen, L.J., Koelliker, J.A., Harrington, J.A. and Barnes, P.L., 2001. Asssessment of runoff and sediment yield using remote sensing, GIS and AGNPS. Journal of Soil and Water Conservation, 57(6): 351-363.

Biscaia, R.C., 1987. Dealing with erosion problems in Parana State, Brazil. In: I. Pla (Editor), Soil Conservation and Productivity. UCV-SVCS, Caracas, Venezuela, pp. 349-358.

Bishopa, M.P., Shroder, J.F. and Colby, J.D., 2003. Remote sensing and geomorphometry for studying relief production in high mountains. Geomorphology, 55: 345-361.

Bissonnais, Y.L., Montier, C., Jamagne, M., Daroussin, J. and King, D., 2000. Mapping erosion risk for cultivated soil in France. Catena, 46(2-3): 207-220.

Bocco, G. and Valenzuela, C.R., 1993. Integrating satellite remote sensing and geographic information systems technologies in gully erosion research. Remote Sensing Review, 7: 233-240.

Bogena, H.R. and Diekkrüger, B., 2002. Modelling solute and sediment transport at different spatial and temporal scales. Earth Surface Processes and Landforms, 27(13): 1475-1489.

Bolivar, G. and Mendez, R., 2000. Integrated and participatory watersheds management in the Tunari mountain range in the Andean zone of Cochabamba, Bolivia. An impact evaluation concerning watershed management, risk and productive rural development, PROMIC, Cochabamba, Bolivia.

Borga, M. and Vizzaccaro, A., 1997. On the interpolation of hydrologic variables : formal equivalence of multiquadratic surface fitting and kriging. Journal of Hydrology, 195(1-4): 160-171.

Brazier, R.E., Beven, K.J., Freer, J. and Rowan, J.S., 2000. Equifinality and uncertainty in physically based soil erosion models: application of the GLUE methodology to WEPP (the Water Erosion Prediction Project) for sites in the UK and USA. Earth Surface Processes and Landforms, 25: 825-845.

Brazier, R.E., Rowan, J.S., Anthony, S.G. and Quinn, P.F., 2001. MIRSED: towards an MIR approach to modelling hillslope soil erosion at the national scale. Catena, 42(1): 59-79.

Brown, J.F., Loveland, T.R., Ohlen, D.O. and Zhu, Z., 1999. The Global Land-Cover Characteristics Database: the users' perspective. Photogrammetric Engineering and Remote Sensing, 65(9): 1069-1074.

Brown, T. and Schneider, H., 1999. From plot to basins: the scale problem in studies of soil erosion and sediment yield. In: D. Harper and T. Brown (Editors), The Sustainable Management of Tropical Catchments. Wiley, Chichester, London, UK, pp. 7-12.

Brune, G.M., 1953. Trap efficiency of reservoirs. American Geophysical Union Transactions, 22: 649-655.

Bull, L.J. and Kirkby, M., 1997. Gully processes and modelling. Progress in Physical Geography, 21(3): 354-374.

Burrough, P. and McDonnell, A., 1998. Principles of Geographic Information Systems. Oxford University Press, New York.

Cabelguenne, M., Jones, C.A., Marty, J.R., Dyke, P.T. and Williams, J.R., 1990. Calibration and validation of EPIC for crop rotations in southern France. Agricultural Systems, 33(2): 153-171.

Cerdan, O., Bissonnais, Y.L., Couturier, A., Bourennane, H. and Souchère, V., 2002. Rill erosion on cultivated hillslopes during two extreme rainfall events in Normandy, France. Soil and Tillage Research, 67(1): 99-108.

CLAS, 2000. Diagnostico de riesgos de erosión y degradación de tierras de la cuenca Corani, Centro de Levantamientos Aeroespaciales y Aplicaciones SIG (CLAS), Cochabamba, Bolivia.

CLAS, 2003. Plan del uso de la tierra (PLUS) del departamento de Cochabamba, Centro de Levantamientos Aeroespaciales y Aplicaciones SIG (CLAS), Cochabamba, Bolivia.

Claure, B., 1996. Riesgos naturales de las cuencas de la Cordillera del Tunari, Programa de Manejo Integrado de Cuencas. CORDECO-COTESU, Cochabamba, Bolivia.

Collins, A.L. and Walling, D.E., 2004. Documenting catchment suspended sediment sources: Problems, approaches and prospects. Progress in Physical Geography, 28(2): 159-196.

Coppus, R., 2002. Landscape Sensitivity in Three Semi-arid Central Andean Geo-ecosystems. PhD Dissertation. Universiteit van Amsterdam, Amsterdam, the Netherlands, 150 pp.

CORDECO, 1991. Programa: manejo y control de la cuenca del Rio Calicanto, Corporación Regional de Desarrollo de Cochabamba (CORDECO) y Centro de Investigación y Desarrollo Regional (CIDRE), Cochabamba, Bolivia.

Dabral, S. and Cohen, M., 2001. ANSWERS-2000: Areal Non-point Source Watershed Environment Response Simulation with Questions Graphical User Interface, Virginia Polytechnic Institute and State University, Blacksburg, VA, USA.

Dadson, S.J., 2003. Links between erosion, runoff variability and seismicity in the Taiwan orogen. Nature, 426: 648-651.

de Jong, S.M., 1994. Applications of Reflective Remote Sensing for Land Degradation Studies in a Mediterranean environment. PhD Dissertation Thesis, Nederlandse Geografische Studies 177, Utrecht, the Netherlands, 179 pp.

de Jong, S.M. et al., 1999. Regional assessment of soil erosion using the distributed model SEMMED and remotely sensed data. Catena, 37(3-4): 291-308.

De la Rosa, R., Mayol, F., Diaz-Pereira, E., Fernandez, M. and de la Rosa, D., 2004. A land evaluation decision support system (MicroLEIS DSS) for agricultural soil protection with special reference to the Mediterranean region. Environmental Modelling & Software, 19: 929–942.

de Roo, A.P.J., 1998. Modelling runoff and sediment transport in catchments using GIS. Hydrological Processes, 12(6): 905-922.

de Roo, A.P.J., Hazelhoff, L. and Burrough, P.A., 1989. Soil erosion modelling using "ANSWERS" and geographical information systems. Earth Surface Processes and Landforms, 14: 517-532.

de Roo, A.P.J. and Jetten, V.G., 1999. Calibrating and validating the LISEM model for two data sets from the Netherlands and South Africa. Catena, 37: 477-493.

de Roo, A.P.J., Wesseling, C.G. and Ritsema, C.J., 1996. LISEM: a single event physically-based hydrologic and soil erosion model for drainage basins. I: Theory, input and output. Hydrological Processes, 10: 1107-1117.

de Vente, J., Poesen, J. and Verstraeten, G., 2005. The application of semi-quantitative methods and reservoir sedimentation rates for the prediction of basin sediment yield in Spain. Journal of Hydrology, 305: 63-86.

Dehn, M., 1995. An evaluation of soil conservation techniques in the Ecuadorian Andes. Mountain Research and Development, 15(2): 175-182.

Denniston, D., 1995. High priorities: conserving mountain ecosystems and cultures, Washington, D.C. USA.

deRose, R.C., Prosser, I., Wilkinson, L.J., Hughes, A.O. and Young, W.J., 2003. Regional patterns of erosion and sediment nutrient transport in the Goulburn and Broken River Catchments, Victoria, CSIRO Land Water Technical Report 11/03, Canberra, Australia.

Desbarats, A.J., 1996. Modelling spatial variability using geostatistical simulation. In: S. Rouhani, R.M. Srivastava and A.J. Desbarats (Editors), Geostatistics for environmental and geogchemical applications. American Society for Testing and Materials, Philadelphia, pp. 32-48.

Desmet, P.J.J. and Govers, G., 1995. GIS based simulation of erosion and deposition patterns in and agricultural landscape. A comparison of model results with soil map information. Catena, 25: 389-401.

Desmet, P.J.J. and Govers, G., 1996a. Comparison of routing algorithms for DEM and their applications for predicting ephemeral gullies. International Journal of Geographical Information Sciences, 10: 311-331.

Desmet, P.J.J. and Govers, G., 1996b. A GIS procedure for automatically calculating the USLE LS factor on topographically complex landscape units. Journal of Soil and Water Conservation, 51: 427-433.

Deutsch, C. and Journel, A.G., 1998. GSLIB: Geostatistical Software Library and User's Guide. Oxford University Press, New York.

DHI, 2002. MIKE BASIN: Soil Erosion Assessment. Documentation and User Guide, DHI, Horsholm, Denmark.

DHI, 2003. MIKE BASIN 2003. A Versatile Decision Support Tool for Integrated Water Resources Management Planning, DHI, Horsholm, Denmark.

Diodato, N., 2004. Estimating RUSLE's rainfall factor in the part of Italy with Mediterranean rainfall regime. Hydrology and Earth System Sciences, 8(1): 103.-107.

Doe, W., Saghafian, B. and Julien, P., 1996. Land-use impact on watershed response: the integration of two dimensional hydrological modelling and geographical information systems. Hydrological Processes, 10: 1503-1511.

Doe, W.W., Jones, D.S. and Warren, S.D., 1999. The Soil Erosion Model Guide for the Military Land Managers: Analysis of Erosion Models for Natural and Cultural Resources Applications, Center for Ecological Management of Military Lands. Colorado State University, Colorado, USA.

Dwivedi, R.S., Kumar, A.B. and Tewari, K.N., 1997. The utility of multi-sensor data for mapping eroded lands. International Journal of Remote Sensing, 18(11): 2303-2318.

Escadafal, R., 1994. Soil spectral properties and their relationships with environmental parameters - examples from arid regions. In: J. Hill and J. Megier (Editors), Imaging Spectrometry - A Tool for Environment Observations. Kluwer Academic Publishers, Dordrecht, pp. 71-87.

Eva, H.D., Miranda, E.E., di Bella, C.M. and Gond, V., 2002. A vegetation map of South America, European Comission: Joint Research Centre, Luxembourg.

Fan, J.R., Zhang, J.H., Zhong, X.H. and Liu, S.Z., 2004. Monitoring of soil erosion and assessment for contribution of sediments to rivers in a typical watershed of the upper Yangtze river basin. Land Degradation & Development, 15: 411-421.

FAO, 1998. Soil and Terrain Database for Latin America and the Caribbean (CD Rom), FAO Land and Water Digital Media Series. FAO, Rome, Italy.

FAO, 2003. Digital Soil Map of the World and Derived Soil Properties. Rev. 1. (CD Rom), FAO Land and Water Digital Media Series. FAO, Rome, Italy.

Ferro, V., 1997. Further remarks on a distributed approach to sediment delivery. Hydrological Sciences Journal, 42(5): 633-647.

Ferro, V., di Stefano, C., Giordano, G. and Rizzo, S., 1998. Sediment delivery process and the spatial distribution of caesium-137 in a small Sicilian basin. Hydrological Processes, 12: 701-711.

Ferro, V., Di Stefano, C. and Minacapilli, M., 2003. Calibrating the SEDD model for Sicilian ungauged basins. In: D.H. de Boer, W. Froehlich, T. Mizuyama and A. Pietroniro (Editors), Erosion Prediction in Ungauged Basins (PUBs): Integrating Methods and Techniques. IAHS, Sapporo, Japan, pp. 151-161.

Ferro, V. and Porto, P., 2000. Sediment delivery distributed (SEDD) model. Journal of Hydrologic Engineering, 5(4): 411-422.

Finlayson, D. and Montgomery, D.R., 2003. Modeling large-scale fluvial erosion in geographic information systems. Geomorphology, 53: 147-164.

Finlayson, D., Montgomery, D.R. and Hallet, B., 2002a. Spatial coincidence of erosional and metamorphic hot spots in the Himalayas. Geology, 30: 219-222.

Finlayson, D., Montgomery, D.R. and Hallet, B., 2002b. Spatial coincidence of rapid inferred erosion with young metamorphic massifs in the Himalayas. Geology, 30(3): 219-222.

Fistikoglu, O. and Harmancioglu, N.B., 2002. Integration of GIS with USLE in assessment of soil erosion. Water Resource Management, 16: 447-467.

Flanagan, D.C. and Nearing, M.A., 1995. USDA-Water Erosion Prediction Project: Hillslope Profile and Watershed Model Documentation, NSERL.

Flugel, W.-A., Marker, M., Moretti, S., Rodolfi, G. and Sidrochuk, A., 2003. Integrating geographical information systems, remote sensing, ground truthing and modelling approaches for regional erosion classification of semi-arid catchments in South Africa. Hydrological Processes, 17: 929-942.

Foster, G.R., 1982. Modelling the erosion processes. In: C.T. Haan (Editor), Hydrologic Modelling of Small Watersheds. ASAE Monograph, pp. 297-380.

Foster, G.R., 1996. Process-based modelling of soil erosion by water on agricultural land. In: J. Boardman, I.D.L. Foster and H.D. Dearing (Editors), Soil Erosion on Agricultural Land. Wiley, Chichester, pp. 429-445.

Foster, G.R. and Meyer, L.D., 1977. Soil erosion and sedimentation by water: an overview. In: ASAE (Editor), Proceedings of the National Symposium on Soil Erosion and Sedimentation by Water, pp. 1-13.

Fournier, F., 1960. Climate and Erosion. University of Paris, Paris, France.

Fu, B.J. et al., 2005. Assessment of soil erosion at large watershed scale using RUSLE and GIS: a case study in the Loess Plateau of China. Land Degradation & Development, 16(1): 73-85.

Garcia, E., 1992. El Pastoreo y los recursos forrajeros de Bolivia. In: CDC-Bolivia (Editor), Conservacion de la Diversidad Biologica en Bolivia. USAID, La Paz, Bolivia.

Geerken, R. and Ilaiwi, M., 2004. Assessment of rangeland degradation and development of a strategy for rehabilitation. Remote Sensing of Environment, 90: 490-504.

GEOBOL, 1992. Mapa geologico de Bolivia. GEOBOL - YPFB, La Paz, Bolivia.

GEOBOL, 1998. Mapa geologico de los valles de Cochabamba. Esc: 1:100,000. GEOBOL - YPFB, La Paz, Bolivia.

Gobin, A. and Govers, G., 2003a. Pan-European Soil Risk Erosion Assessment, Laboratory for Experimental Geomorphology Katholieke Universiteit Leuven. School of geography University of Leeds. Estacion Experimental de Zonas Aridas, Almeria Consejo Superior de Investigaciones Cientificas. Unité de Science du Sol, Orléans Institut National de la Recherche Agronomique European Soil Bureau, Environment Institute DG

- Joint Research Centre, Ispra. Agricultural University of Athens. International Soil Reference and Information Centre Wageningen University and Research Centre, Rome, Italy.

Gobin, A. and Govers, G., 2003b. Pan-European Soil Risk Erosion Assessment, Contract no. QLK5-CT-1999-01323. Third Annual Report (1 Apr '02 - 1 Apr '03). Laboratory for Experimental Geomorphology. Katholieke Universiteit Leuven: School of Geography. University of Leeds. Estacion Experimental de Zonas Aridas, Almeria Consejo Superior de Investigaciones Cientificas. Unité de Science du Sol, Orléans Institut National de la Recherche Agronomique European Soil Bureau. Environment Institute DG - Joint Research Centre, Ispra. Agricultural University of Athens. International Soil Reference and Information Centre Wageningen University and Research Centre, Rome, Italy, pp. 145 pp.

Goitia, J., 1990. Determinacion del riesgo potencial de erosion en la subcuenca del Rio San Pedro a nivel del reconocimiento. Unpublished Thesis Thesis, Juan Misael Saracho, Tarija, 120 pp.

Goovaerts, P., 1997. Geostatistics for Natural Resource Evaluation. Applied Geostatistics Series. Oxford University Press, Oxford, 483 pp.

Goovaerts, P., 1999. Geostatistics in soil science: state of the art and perspectives. Geoderma, 89: 1-45.

Goovaerts, P., 2001. Geostatistical modelling of uncertainty in soil science. Geoderma, 103: 3-26.

Griguolo, S., 2003. CROP-VGT. Win32 v 0.6. A user-defined region image extraction program from a set of SPOT-VEGETATION files (HDF format, zipped). Institute of Architecture, Department of Planning University of Venice, Italy.

Grimm, M., Jones, R. and Montanarella, L., 2002. Soil Erosion Risk in Europe. European Soil Bureau. Institute for Environment and Sustainability JRC Ispra. European Comission. Joint Research Centre., Rome, Italy.

Grunwald, S. and Norton, L.D., 1999. An AGNPS-based runoff and sediment yield model for two small watersheds in Germany. Transactions of ASAE, 42(6): 1723-1731.

Guyot, J.L., Filizola, N., Quintanilla, J. and Cortez, J., 1996. Dissolved solids and suspended sediment yields in the Rio Madeira basin, from the Bolivian Andes to the Amazon. In: IAHS (Editor), Erosion and Sediment Yield: Global and Regional Perspectives. IAHS, pp. 55-63.

Guyot, J.L., Jouanneau, J.M. and Wasson, J.G., 1999. Characterization of river bed and suspended sediments in the Rio Madeira drainage basin (Bolivian Amazonia). South American Earth Sciences, 12: 401-410.

Guyot, J.L., Roche, M.A., Noriega, L., Calle, H. and Quintanilla, J., 1990. Salinity and sediment transport in the Bolivian Highlands. Journal of Hydrology, 113: 147-162.

Haan, C.T., Barfield, B.J. and Hayes, J.C., 1994. Design Hydrology and Sedimentology for Small Catchments. Academic Press, 588 pp.

Haboudane, D., Bonn, F., Royer, A., Sommer, S. and Mehl, W., 2002. Land degradation and erosion risk mapping by fusion of spectrally based information and digital geomorphometric attributes. International Journal of Remote Sensing, 18: 3795-3820.

Haregeweyn, N. et al., 2005. Specific sediment yield in Tigray-Northern Ethiopia: assessment and semi-quantitative modelling. Geomorphology, 69: 315-331.

Harmon, R.S. and Doe, W.W., 2001. Landscape Erosion and Evolution Modelling. Kluwer Academic / Plenum Publishers, New York, USA, 540 pp.

He, Q. and Walling, D.E., 2003. Testing distributed soil erosion and sediment delivery models using ^{137}Cs measurements. Hydrological Processes, 17: 901-916.

Hessel, R., 2002. Modelling Soil Erosion in a Small Catchment on the Chinesse Loess Plateau. PhD Dissertation. NGS 307. Nederlandse Geografische Studies, Utrecht, the Netherlands, 317 pp.

Heuvelink, G.B.M., 2002. Is the ordinary kriging variance a proper measure of interpolation error? In: G.B.M. Heuvelink and P.M. Lemmens (Editors), 4th International Symposium on Spatial Accuracy Assessments in Natural Resources and Environmental Sciences. Delft University Press, Amsterdam.

Hicks, M.D. and Hume, T.M., 1997. Determining sand volumes and bathymetric changes on an ebb-tidal delta. Journal of Coastal Research, 13(2): 407-416.

Hill, J. and Schütt, 2000. Mapping complex patterns of erosion and stability in dry Mediterranean ecosystems. Remote Sensing of Environment, 74: 557-569.

Holliday, V., Higgit, D.L., Warburton, J. and White, S., 2003. Reconstructing upland sediment budgets in ungauged catchments from reservoir sedimentation and rainfall records calibrated using short-term streamflow monitoring. In: D.H. de Boer, W. Froehlich, T. Mizuyama and A. Pietroniro (Editors), Erosion Prediction in Ungauged Basins: Integrating Methods and Techniques. IAHS, Sapporo, Japan, pp. 59-67.

Howard, A., Dietrich, W. and Seidl, A., 1994. Modelling fluvial erosion on regional to continental scales. Journal of Geophysical Research, 99(13): 971-986.

HQUSACE, 2002. Engineering and Design Hydrographic Surveying. EM 1110-2-1003, U.S. Army Corps of Engineers, Washington, D.C.

Huang, C., Wells, L.K. and Norton, L.D., 1999. Sediment transport capacity and erosion processes: Model concepts and reality. Earth Surface Processes and Landforms, 24: 503-516.

Huete, A., Justice, C. and van Leuwen, W., 1999. MODIS Vegetation Index (MOD 13). Algorithm theoretical basis document. Version 3, University of Virginia. Department of Environmental Sciences, Tucson, Arizona.

IGBP-DIS, 2000. Global-Soil-Data-Task. Global soil data products CD-Rom (IGBP-DIS). In: O.R. National Laboratory Distributed Active Archive Center (Editor). International Geosphere-Biosphere Programme, Data and Information System, Tennessee, USA.

IPCC, 1996. Climate Change 1995: The Science of Climate Change. Cambridge University Press, Cambridge, 572 pp.

Isaaks, E. and Srivastava, R.M., 1989. An Introduction to Applied Geostastitics. Oxford University Press, New York, 561 pp.

Jain, M.K. and Kothyari, U.C., 2000. Estimation of soil erosion and sediment yield using GIS. Hydrological Sciences Journal, 45(5): 771-786.

Jensen, J.R., 1996. Digital Image Processing: A Remote Sensing Perspective. Prentice Hall, New Jersey, USA.

Jenson, S.K. and Domingue, J.O., 1988. Extracting topographic structure from digital elevation model data for geographic information system analysis. Photogrametric Engineering and Remote Sensing, 54(11): 1593-1600.

Jette, C. and Rojas, R., 1998. Cochabamba. Pobreza, Genero y Medio Ambiente. Embajada Real de los Paises Bajos, La Paz, Bolivia, 243 pp.

Jetten, V., Govers, G. and Hessel, R., 2003. Erosion models: quality and spatial predictions. Hydrological Processes, 17: 887-900.

Johnson, A.M., 1976. The climate of Peru, Bolivia, and Ecuador. In: W. Schwerdtfeger (Editor), Climates of Central and South America, World Survey of Climatology. Elsevier, Amsterdam, the Netherlands, pp. 147-202.

Johnson, B.E., Julien, P.Y., Molnar, D.K. and Watson, C.C., 2000. The two-dimensional-upland erosion model CASC2D-SED. Journal of the American Water Resource Association (AWRA), 36(1): 31-42.

Julien, P.Y., 1995. Erosion and Sedimentation. Cambridge University Press, Cambrige, USA, 279 pp.

Julien, P.Y. and Saghafian, B.l., 1991. CASC2D Users Manual - A Two Dimensional Watershed Rainfall-Runoff Model, Colorado State University, Fort Collins, Colorado.

Julien, P.Y. and Saghafian, Y., 1995. Raster based hydrologic modelling of spatial varied surface runoff. Water Resource Bulletin, 31(3): 523-536.

Julien, P.Y. and Simmons, D.B., 1985. Sediment transport capacity of overland flow. Transactions of ASAE, 28: 755-762.

Kandel, D.D., Western, A.W., Grayson, R.B. and Turral, H.N., 2004. Process parameterization and temporal scaling in surface runoff and erosion modelling. Hydrological Processes, 18: 1423-1446.

Karssenberg, D., 2002. Building dynamic spatial environmental models. Phd Dissertation. NGS 305. Nederlandse Geografische Studies, Utrecht, the Netherlands, 222 pp.

Kessler, M., Parris, B.S. and Kessler, E., 2001. A comparison of the tropical montane pteridophyte floras of Mount Kinabalu, Borneo, and Parque Nacional Carrasco, Bolivia. Journal of Biogeography, 28: 611-622.

King, C., Baghdadi, N., Lecomte, O. and Cerdan, O., 2005. The application of remote sensing data to monitoring and modelling of soil erosion. Catena, 62: 79-93.

Kinnell, P.I.A., 2003. Event erosivity factor: the errors in erosion predictions by some empirical models. Australian Journal of Soil Research, 41(5): 991-1003.

Kinnell, P.I.A., 2004. Sediment delivery ratios: a misaligned approach to determining sediment delivery from hillslopes. Hydrological Processes, 18(16): 3191-3194.

Kinnell, P.I.A. and Risse, L.M., 1998. USLE-M: empirical modelling rainfall erosion through runoff and sediment concentration. Soil Science Society of America Journal, 62(6): 1667-1672.

Kirkby, M. et al., 2004. PAN-European Soil Erosion Risk Assessment: The PESERA Map, Version 1 October, 2003, European Soil Bureau Research, Luxembourg.

198

Kirkby, M.J., Abrahart, R.J., McMahon, M.D., Shao, J. and Thornes, J.B., 1998. MEDALUS soil erosion models for global change. Geomorphology, 24: 35-49.

Kirkby, M.J., Bissonais, Y.L., Coulthard, T.J., Daroussin, J. and McMahon, M.D., 2000. The development of land quality indicators for soil degradation by water erosion. Agriculture, Ecosystems and Environment, 81: 125-136.

Kitsiou, D., Tsirtis, G. and Karydis, M., 2001. Devoloping an optimal sampling design: a case study in a coastal marine ecosystem. Environmental Monitoring and Assessment, 71: 1-12.

Knisel, W.G., 1995. CREAMS: A Field-Scale Model for Chemicals, Runoff, and Erosion from Agricultural Management Systems., US Dept of Agriculture. Agricultural Research Service.

Koolhoven, W., Hendrikse, J., Nieuwenhuis, W., Retsios, B. and Schouwenburg, M., 2004. ILWIS (v 3.21). Integrated Land and Water Information System. ITC, Enschede, The Netherlands.

Koolhoven, W., Hendrikse, J., Nieuwenhuis, W., Retsios, B. and Schouwenburg, M., 2005. ILWIS (v 3.3). Integrated Land and Water Information System. ITC, Enschede, the Netherlands.

Kothyari, U.C., 1996. Erosion and sedimentation problems in India. In: D.E. Walling and B.W. Webb (Editors), Erosion and Sediment Yield: Global and Regional Perspectives. IAHS. Publ. N 236, Exeter, U.K.

Krivoruchko, K. and Gribov, A., 2002. Working on Nonstationarity problems in geostatistics using detrending and transformation techniques: An agricultural case study. In: ESRI (Editor), Joint Statistical Meetings. ESRI, New York.

Lai, J. and Shen, H.W., 1996. Flushing sediments through reservoirs. Journal of the Hydraulics Research, 4: 3237-3255.

Lal, R., 2001. Soil degradation by erosion. Land Degradation & Development, 12: 519-539.

Lane, E.W. and Koelzer, V.A., 1943. Density of sediment in reservoirs. In: USCE (Editor), A study of methods used in the measurements and analysis of sediment loads in streams. US Corp of Enginneers. Iowa University, Iowa, USA.

Lane, L.J., Nichols, M.H. and Paige, G.B., 1995. Modeling erosion on hillslopes: concepts, theory and data. In: P. Binning, H. Bridgman and B. Williams (Editors), Proceedings of the International Congress on Modelling and Simulation (MODSIM'95).

Lara, R., 1985. Mapa de vegetación de Bolivia. In: I.G.M. Bolivia (Editor), Atlas de Bolivia. Geomundo, Barcelona, España.

Lea, N.J., 1992. An aspect-driven kinematic routing algorithm. In: A.J. Parsons and A.D. Abrahams (Editors), Overland Flow. UCL Press, New York, pp. 393-408.

Lenhart, T. et al., 2005. Considering spatial distribution and deposition of sediment in lumped and semi-distributed models. Hydrological Processes, 19: 785-794.

Leon, L.F., Soulis, E.D., Kouwen, N. and Farquhar, G.J., 2001. Nonpoint source pollution: a distributed water quality modelling approach. Water Resources, 4: 997-1007.

Leonard, T.J. and Coughlan, D.J., 2002. Reservoir Bathymetry: Mapping the pitfalls, Duke Power Company, Huntersville.

Leprieur, C., Kerry, Y.H., Mastorchio, S. and Meunier, J.C., 2000. Monitoring vegetation cover across semi-arid regions: comparison of remote observations from various scales. International Journal of Remote Sensing, 21(2): 281-300.

LH-UMSS, 1994. Batimetria del Embalse Laka-Laka. Informe Final. 1994, Laboratorio de Hidraulica de la UMSS, Cochabamba, Bolivia.

LH-UMSS, 1995. Batimetria del Embalse Laka-Laka. Informe Final 1995, Laboratorio de Hidraulica de la UMSS, Cochabamba, Bolivia.

LH-UMSS-PROMIC, 1999. Estimacion de tasas de aporte de sediments a nivel de cuencas, LH-UMSS - PROMIC, Cochabamba, Bolivia.

Li, Z., O'Neill, A.L. and Lacey, S., 1996. Modelling approaches to the prediction of soil erosion in catchments. Environmental Software, 11(1-3): 123-133.

Libermann, M., 1991. Situación del medio ambiente en Bolivia. In: E. Hajek (Editor), Analisis de la situación del medio Ambiente en America Latina: Algunos estudios de caso. Fundacion Konrad Adenauer, Buenos Aires, Argentina.

Lin, C.Y., Lin, W.T. and Chou, W.C., 2002. Soil erosion prediction and sediment yield estimation: the Taiwan experience. Soil & Tillage Research, 68: 143-152.

Listh, J.H., Jaffe, B.E., Sallenger, A.H. and Hansen, M.E., 1997. Bathymetric comparison adjacent to the Lousiana Barrier Islands: Processes of large-scale change. Journal of Coastal Research, 13: 670-678.

López, P.L. and Soto, B., 2004. Modeling wash load transport of soil in a headwater catchment cultivated by non-tillage methods. Journal of Hydrology, 287(1-4): 19-33.

Lopez, P.R., 2003. Phytogeographical relations of the Andean dry valley of Bolivia. Journal of Biogeography, 30: 1659-1668.

Loveland, T.R. et al., 1999. An analysis of the IGBP global land cover characterization process. Photogrammetric Engineering and Remote Sensing, 9: 1021-1032.

Lu, H., Gallant, J., Prosser, I., Moran, C. and Graeme, P., 2001. Prediction of sheet and rill erosion over the Australian continent, incorporating monthly soil loss distribution., CSIRO Land and Water, Canberra, Australia.

Lu, H., Moran, C., Prosser, I. and Sivapalan, M., 2004. Modelling sediment delivery ratio based on physical principles. In: C. Pahl-Wostl, S. Schmidt and T. Jakeman (Editors), IEMSS 2004 International Congress: "Complexity and Integrated Resources Management". International Environmental Modelling and Software Society, Osnabrueck, Germany, pp. 600.

Lu, H. et al., 2003. Sheet and rill erosion and sediment delivery to streams: a basin wide estimation at hillslope to medium catchment scale, CSIRO Land and Water, Camberra.

Lu, X. and Higgitt, D.L., 2001. Sediment delivery to the Three Gorges. 2: local response. Geomorphology, 41: 157-169.

Ma, J.W., Xue, Y., Ma, C.F. and Wang, Z.G., 2003. A data fusion approach for soil erosion monitoring in the Upper Yangtze River Basin of China based on the Universal Soil Loss Equation (USLE) model. International Journal of Remote Sensing, 24(23): 4777-4789.

Mannaerts, C.C.M. and Gabriels, D., 2000. Rainfall erosivity in Cape Verde. Soil & Tillage Research, 55: 207-212.

Mannaerts, C.M., 1993. Assessment of the Transferability of Laboratory Rainfall - Runoff and Rainfall - Soil Loss Relationships to Field and Catchment Scales : A Study in the Cape Verde Islands. PhD Dissertation. University of Gent, Gent, Belgium, 150 pp.

Marker, M. and Sidorchuk, A., 2003. Assessment of gully erosion process dynamics for water resources management in a semiarid catchment of Swaziland (Southern Africa). In: D.H. de Boer, W. Froehlich, T. Mizuyama and A. Pietroniro (Editors), Erosion Prediction in Ungauged Basins (PUBs): Integrating Methods and Techniques. IAHS, Sapporo, Japan, pp. 188-198.

Martínez-Casasnovas, J.A., Ramos, M.C. and Poesen, J., 2004. Assessment of sidewall erosion in large gullies using multitemporal DEMs and logistic regression analysis. Geomorphology, 58: 305-321.

Martínez-Casasnovas, J.A., Ramos, M.C. and Ribes-Dasi, M., 2002. Soil erosion caused by extreme rainfall events: mapping and quantification in agricultural plots from very detailed digital elevation models. Geoderma, 105(1-2): 125-140.

Mathieu, R., King, C. and Bissonnais, Y., 1997. Contribution of multi-temporal SPOT data to the mapping of a soil erosion index: the case of the loamy plateaux of northern France. Soil Technology, 10(2): 99-110.

MDSMA, 1996. Mapa Preliminar de Erosion de Suelos: Región Arida, Semi-arida y Sub-húmeda de Bolivia, La Paz, Bolivia.

Mellerowicz, K.T., Rees, H.W., Chow, T.L. and Ghanem, I., 1994. Soil conservation planning at watershed level using the Universal Soil Loss Equation with GIS and microcomputer technologies: a case study. Journal of Soil and Water Conservation, 33(3): 839-849.

Merrit, W.S., Letcher, R.A. and Jakeman, A.J., 2003. A review of erosion and sediment transport models. Environmental Modelling & Software, 18: 761-799.

Metternicht, G.I. and Fermont, A., 1998. Estimating erosion surface features by linear mixture modelling. Remote Sensing of Environment, 64: 254-265.

Metternicht, G.I. and Gonzalez, S., 2005. FUERO: foundations of a fuzzy exploratory model for soil erosion hazard prediction. Environmental Modelling & Software, 20: 715-728.

Mills, G.B., 1998. International hydrographic survey standards. International Hydrographic Review, 72(2).

Millward, A.A. and Mersey, J.E., 1999. Adapting the RUSLE to model soil erosion potential in a mountainous tropical watershed. Catena, 38(2): 109-129.

Mitas, L. and Mitasova, H., 1998. Distributed soil erosion simulation for effective erosion prevention. Water Resource Research, 34: 505-516.

Mitasova, H., 1996. GIS Tools for Erosion/Deposition Modelling and Multidimensional Visualization. Part III: Process-based Erosion Simulation, Geographic Modelling and Systems Laboratory, University of Illinois, Illinois.

Mitasova, H., 1997. GIS Tools for Erosion/Deposition Modelling and Multidimensional Visualization. Part IV: Process-

based Erosion Simulation, Geographic Modelling and Systems Laboratory, University of Illinois, Illinois.

Mitasova, H., 1999. Terrain Modelling and Soil Erosion Simulation, Geographic Modelling and Systems Laboratory, University of Illinois, Illinois.

Mitasova, H., 2000. Terrain Modelling and Soil Erosion Simulation. Final Report, Geographic Modelling and Systems Laboratory, University of Illinois, Illinois.

Mitasova, H., Hofierka, J., Zlocha, M. and Iverson, L.R., 1996. Modeling topographic potential for erosion and deposition using GIS. International Journal of Geographical Information Science, 10(5): 629-641.

Mitchell, J.K. and Bubenzer, G.D., 1980. Soil loss estimation. In: M.J. Kirkby and P.C. Morgan (Editors), Soil Erosion. Wiley, Chichester, London, UK, pp. 17-62.

Montes de Oca, I., 2002. Geografía y Recursos Naturales de Bolivia, La Paz, Bolivia, 300 pp.

Montgomery, D.R., Balco, G. and Willet, S.D., 2001. Climate, tectonics and the morphology of the Andes. Geology, 29(7): 579-582.

Moore, I. and Wilson, P., 1992. Length slope factors for the Revised Universal Soil Loss Equation: Simplified method of estimation. Journal of Soil and Water Conservation, 47(5): 423-428.

Morgan, R.P.C., 1995. Soil Erosion and Conservation. Longman Scientific & Technical, London, UK.

Morgan, R.P.C., 2001. A simple approach to soil loss prediction: a revised Morgan-Morgan-Finney model. Catena, 44: 305-322.

Morgan, R.P.C., Morgan, D.D.V. and Finney, H.J., 1984. A predictive model for the assessment of erosion risk. Journal of Agricultural Engineering Research, 30: 245-253.

Morgan, R.P.C. et al., 1998. The European soil erosion model (EUROSEM): a dynamic approach for predicting sediment transport from fields and small catchments. Earth Surface Processes and Landforms, 23: 527-544.

Morris, G.L. and Fan, J., 1997. Reservoir Sedimentation Handbook: Design and Management of Dams, Reservoirs, and Watersheds for Sustainable Use. McGraw-Hill, New York.

Mücher, C.A., Steinnocher, K.T., Kressler, E.P. and Heunks, C., 2000. Land cover characterization and change detection for environmental monitoring of pan-Europe. International Journal of Remote Sensing, 21: 1159-1181.

Nagashiro, K., 1992. Recursos forestales y caracteristicas de uso. In: CDC-Bolivia (Editor), Conservación de la Diversidad Biologica en Bolivia. USAID, La Paz, Bolivia.

Navarro, G., 1997. Contribucion a la clasificacion ecologica y floristica de los bosques de Bolivia. Revista Boliviana de Ecologia y Conservacion Ambiental, 2: 3-38.

Nearing, M.A., 1998. Why soil erosion models over-predict small soil losses and under-predict large soil losses. Catena, 32: 15-22.

Nearing, M.A., 2000. Evaluating soil erosion models using measured plot data: accounting for variability in the data. Earth Surface Processes and Landforms, 25: 1035-1043.

Nearing, M.A., 2004. Capabilities and limitations of erosion models and data. In: S.R. Raine, A.J.W. Biggs, N.W. Menzies, D.M. Freebairn and P.E. Tolmie (Editors), Conserving Soil and Water for Society: Sharing Solutions. Proceedings 13th International Soil Conservation Organisation Conference. ASSSI/IECA, Brisbane, Australia.

Nearing, M.A., Foster, G.R., Lane, L.J. and Finkner, S.C., 1989. A process-based soil erosion model for USDA: water erosion prediction project technology. Transactions of ASAE, 32: 1587–1593.

Nearing, M.A., Lane, L.J. and Lopez, J.L., 1994. Modelling soil erosion. In: R. Lad (Editor), Soil Erosion: Research Methods. CRC Press, New York, USA, pp. 127-156.

New, M., Lister, D., Hulme, M. and Makin, D., 2002. A high resolution data set of surface climate over global land areas. Climate Research, 21: 1-25.

Nichols, M.H. and Renard, K.G., 1999. Sediment yield from semi-arid watersheds, Agricultural Research Service, Southwest Watershed Research Center, Tucson, USA.

Pallaris, K., 2000. Terrain modelling for erosion risk assesment in the Cabuyal river catchment: comparison of results with farmer perceptions. Advances in Environmental Monitoring and Modelling, 1(1): 149-177.

Paradis, E., 2002. R for Beginners, Institut des Sciences de l'Evolution, Montpellier.

Paringit, E. and Nadaoka, K., 2003. Sediment yield modelling for small agricultural catchments: Landcover parameterization based on remote sensing data analysis. Hydrological Processes, 17: 1845-1866.

Pebesma, E.J. and Wesseling, C.G., 1998. GSTAT: A program for geostatistical modelling, prediction and simulation. Computer & Geosciences, 24(1): 17-31.

Pecknold, S., Lovejoy, S., Schertzer, D. and Hooge, C., 1997. Multifractals and resolution dependence of the remotely sensed data: GSI to GIS. In: D.A. Quattrochi and M.F. Goodchild (Editors), Scale in Remote Sensing and GIS. CRC Lewis, Boca Raton, Florida, USA, pp. 361-394.

Perrin, C., Michel, C. and Andreassian, V., 2001. Does a large number of parameters enhance model performance? Comparative assessment of common catchment model structures on 429 catchments. Journal of Hydrology, 242: 275-301.

Peters, N.E., Freer, J. and Beven, K., 2003. Modelling hydrologic responses in a small forested catchment (Panola Mountain, Georgia, USA): a comparison of the original and a new dynamic TOPMODEL. Hydrological Processes, 17,(2): 345-362.

Pfeffer, K., 2003. Integrating Spatio-temporal Environmental Models for Planning Sky Runs. PhD Dissertation. NGS 311. Nederlandse Geografische Studies, Utrecht, the Netherlands, 238 pp.

Pfeifer, H., 2005. GARTRIP 2.06: the windows PC shareware program for Garmin and Magellan GPS receivers, Berlin, Germany.

Phillips, J.D. and Marion, D.A., 2001. Residence times of alluvium in an east Texas stream as indicated by sediment color. Catena, 45: 49-71.

Picouet, C., Hingray, B. and Olivry, J.C., 2001. Empirical and conceptual modelling of the suspended sediment dynamics in a large tropical African river: the Upper Niger river basin. Journal of Hydrology, 250(1-4): 19-39.

Pilesjo, P., 1992. GIS and Remote Sensing for Soil Erosion Studies in Semi-arid Environments, PhD thesis, Institutioner, Avhandlingar CXIV. Meddelanden fran Lunds Universitets Geografiska, Lunds, Sweeden, 203 pp.

Pilotti, M. and Bacchi, B., 1997. Distributed evaluation of the contribution of soil erosion to the sediment yield from a watershed. Earth Surface Processes and Landforms, 22: 1239-1251.

Pimentel, D. et al., 1995. Environmental and economic costs of soil erosion and conservation benefits. Science, 267: 1117-1123.

Pla, I., 1993. La erodabilidad de los andisoles en Latinoamerica. Suelos Ecuatoriales. Sociedad Colombiana de la Ciencia del Suelo, 22(1): 33-43.

Pla, I., 1996. Degradación de suelos en zonas de ladera de America Latina. In: F. Bertch and C. Monreal (Editors), El Uso Sostenible de Suelo en Zonas de Ladera: El Papel Esencial de los Sistemas de Labranza Conservacionista. FAO-MAG, San Jose, Costa Rica, pp. 27-49.

Pla, I., 2003. Erosion research in Latin America. In: D. Gabriels and W. Cornelis (Editors), In: 25 Years of Assessment of Erosion. Gent Universiteit, Belgium, pp. 19-27.

Poesen, J., Nachtergaele, J., Verstraeten, G. and Valentin, C., 2003. Gully erosion and environmental change: Importance and research needs. Catena, 50: 91-113.

Poesen, J. et al., 2002. Gully erosion in dryland environments. In: L.J. Bull and M.J. Kirbby (Editors), Dryland Environments. Wiley, Chichester, London, UK.

Poon, K.R., Wong, W., Lam, M.H. and Yeung, J., 2000. Geostatistical modelling of the spatial distribution of sewage pollution in costal sediments. Water Research, 34: 99-108.

Prado, E.O., 1995. Estudios de Erosión: Uso de la Ecuación Universal de Perdida de Suelo, en los Cultivos de la Cuenca Taquiña, LH-UMSS - PROMIC, Cochabamba, Bolivia.

PRODEVAT, 1999. Plan de manejo integral de la cuenca Tintaya, Programa de Desarallo de los Valles de Arque y Tapacari. Cooperacion de la Union Europea en Bolivia, Cochabamba, Bolivia.

PROMIC, 1995. Estudio de priorización de cuencas en la cordillera del Tunari, Programa de Manejo Integrado de Cuencas. CORDECO-COTESU, Cochabamba, Bolivia.

PRONAR, 2001. Sedimentos en microcuenca y diseño de obras de almacenamiento, Programa Nacional de Riegos (PRONAR) y Dirección Nacional de Suelos y Riego (DNSR), Cochabamba, Bolivia.

Prosser, I.P. and Rustomji, P., 2000. Sediment transport capacity relations for overland flow. Progress in Physical Geography, 24(2): 179-193.

Prosser, I.P. et al., 2001. Large scale patterns of erosion and sediment transport in river networks, with examples from Australia. Marine and Freswater Research, 52: 81-99.

Pullar, D. and Springer, D., 2000. Towards integrating GIS and catchment models. Environmental Modelling & Software, 15: 451-459.

Qinke, Y., Rui, L., Zhang, X. and Hu, L., 2002. Regional evaluation of soil erosion by water: a case study on the Loess Plateau of China. In: T.R. McVicar, L. Rui, R. Fitzpatrick and L. Changming (Editors), Regional Water and Soil Assessment for Mannaging Sustainable Agriculture in China and Australia. ACIAR, Melbourne, Australia, pp. 304-310.

Radoane, M. and Radoane, N., In Press. Dams, sediment sources and reservoir silting in Romania. Geomorphology.

Ranieri, S.B.L., van Lier, Q.J., Sparovek, G. and Flanagan, D.C., 2002. Erosion database interface (EDI): a computer program for georeferenced application of erosion prediction models. Computer & Geosciences, 28: 661-668.

Reich, P., Eswaran, H. and Beinroth, F., 2000. Global dimensions of vulnerability to wind and water erosion, USDA, Washington D.C.

Renard, K.G., A., F.G., Weesies, G.A., McCool, D.K. and Yoder, D.C., 1997. Prediction of soil erosion by water: a guide to conservation planning with the revised universal soil loss equation (RUSLE). Agric. Handbook 703. USDA, Washington D.C.

Renard, K.G. and Freimund, J.R., 1994. Using monthly precipitation data to estimate the R-factor in the Revised USLE. Journal of Hydrology, 157: 287-306.

Renschler, C.S., 2003. Designing geo-spatial interfaces to scale process models: the GeoWEPP approach. Hydrological Processes, 17: 1005-1017.

Renschler, C.S. and Flanagan, D.C., 2003. Implementing a process-based decision support tool for natural resource management: the GeoWEPP example, Transactions of ASAE, pp. 189-209.

Renschler, C.S. and Harbor, J., 2002. Soil erosion assessment tools from point to regional scales: the role of geomorphologists in land management research and implementation. Geomorphology, 47(2-4): 189-209.

Renschler, C.S., Mannaerts, C.C.M. and Diekkruger, B., 1999. Evaluating spatial and temporal variability in soil erosion risk rainfall erosivity and soil loss ratios in Andalucia, Spain. Catena, 34: 209-225.

Restrepo, J.D., Kjerfve, B., Hermelin, M. and Retrepo, J.C., In Press. Factors controling sediment yield in a major South American drainage basin: the Magdalena River, Colombia. Journal of Hydrology.

Reusing, M., Schneider, T. and Ammer, U., 2000. Modelling soil loss rates in the Ethiopian Highlands by integration of high resolution MOMS-02/D2-stereo-data in a GIS. International Journal of Remote Sensing, 21(9): 1885-1896.

Ribera, M., Libermann, M., Beck, S. and Moraes, M., 1996. Vegetación de Bolivia. In: K. Mihotek (Editor), Comunidades, Territorios, Indigenas, Territorios Indigenas y Biodiversidad en Bolivia. CIMAR, Santa Cruz, Bolivia.

Rojas, R.S., 2002. GIS-based Upland Erosion Modelling, Geovisualization and Grid Size Effects on Erosion Simulations with CASC2D-SED. Ph.D. Dissertation Thesis Thesis, Colorado State University, Colorado, 124 pp pp.

Romero, C.C., 2005. A multi-scale approach for erosion assessment in the Andes. Phd Dissertation. Tropical Resource Management Papers, No. 61, Wageningen, the Netherlands, 145 pp.

Romero, C.C. and Stroosnijder, L., 2002. A multiscale approach for erosion impact assessment for ecoregional research in the Andes., Proceedings SAAD-III, Lima, Peru.

Römkens, M.J.M., Prasad, S.N. and Poesen, J.W.A., 1986. Soil erodibility and properties, Proceedings of the 13th Congress of the International Soil Science Society, pp. 492-504.

Rubio, J.L. and Bochet, E., 1998. Desertification indicators as diagnosis criteria for desertification risk assessment in Europe. Journal of Arid Environments, 39: 113-120.

Rustomji, P. and Prosser, I., 2001. Spatial patterns of sediment delivery to valley floors: Sensitivity to sediment transport capacity and hillslope hydrology relations. Hydrological Processes, 15(1003-1018).

Saavedra, C.P., 2000. Estimation of water & sediment yields of watersheds using RS, GIS & hydrologic modelling system: a case study in the High Valleys, Cochabamba, Bolivia, Unpublished MSc thesis. International Institute for Aerospace Survey and Earth Sciences, Enschede, the Netherlands, 120 pp.

Saavedra, C.P. and Mannaerts, C.C.M., 2003a. Modelamiento y monitoreo de la erosión a escala regional usando datos disponibles en servidores publicos de Internet: Estudio de caso en Bolivia. In: FAO (Editor), 3er Congreso Latinoamericano de Manejo Integrado de Cuencas: Hacia el Desarrollo Sostenible de Cuencas. FAO, Arequipa, Peru.

Saavedra, C.P. and Mannaerts, C.C.M., 2003b. Regional scale erosion modelling and monitoring using remotely sensed data: some spatial data scale issues. In: D. Gabriels and W. Cornelis (Editors), 25 Years of Assessment of Erosion. Universiteit Gent, Belgium, pp. 433-440.

Saito, H. and Goovaerts, P., 2002. Accounting for measurement error in uncertainty modelling and decision-making using indicator kriging and p-field simulation: application to a dioxin contaminated site. Environmentrics, 13: 555-567.

Saito, H. and Goovaerts, P., 2003. Selective remediation of contaminated sites using a two level multiphase strategy and geostatistics. Environment Science and Technology, 37: 1912-1918.

Salas, J.D. and Shin, H., 1999. Uncertainty analysis of reservoir sedimentation. Journal of the Hydraulic Engineering, 4(339-350).

Salazar, S. and Montenegro, E., 1997. Caracterización de la Precipitación en la Vertiente Sur de la Cordillera del Tunari, LH-UMSS - PROMIC, Cochabamba, Bolivia.

Santos, C.A.G., Srinivasan, V.S., Suzuki, K. and Watanabe, M., 2003. Application of an optimization technique to a physically based erosion model. Hydrological Processes, 17(5): 989-1003.

Schauble, H., 2003. Hydro Tools 1.0. Arcview extension. Schauble, H., Darmstad, Germany.

Schmidt, J. and von Werner, M., 2000. Modelling the sediment and heavy metal yields of drinking water reservoirs in the Osterzgebirge region of Saxony (Germany). In: S. Schmidt (Editor), Soil Erosion: Application of Physically-based Models. Springer, Berlin, Germany, pp. 59-77.

Schmidt, S., 2000. Soil Erosion: Application of Physically-based Models. Springer, Berlin Heidelberg, Germany, 318 pp.

Schoorl, J.M., 2002. Addressing the Multiscale LAPSUS of Landscape. PhD Dissertation Thesis, Wageningen University, Wageningen.

SCS, 1972. Soil Conservation Service (SCS). National Engineering Handbook, Section 4: Hydrology, US Department of Agriculture, USA.

SCS-TR-55, 1972. Urban hydrology for small watersheds. Technical Release No. 55, USDA Soil Conservation Service, Washington, DC.

SGT, 1998. Levantamiento Topografico y Batimetrico del Embalse Corani, Servicio de Geodesia y Topografia, Cochabamba, Bolivia.

Sharpley, A.N. and Williams, J.R., 1990. EPIC: Erosion/Productivity Impact Calculator:Model Documentation., USDA-ARS.

Shi, Z.H., Cai, S.F., Ding, S.W., Wang, T.W. and Chow, T.L., 2004. Soil conservation planning at the small watershed level using RUSLE with GIS: a case study in the Three Gorge area of China. Catena, 55: 33-48.

Shirazi, M.A. and Boersma, L., 1984. A unifying quantitative analysis of soil texture. Soil Science Society of America Journal, 48: 142-147.

Shrestha, D., Zinck, J.A. and Van Ranst, E., 2004. Modelling land degradation in the Nepalese Himalaya. Catena, 57: 135-156.

Singh, D., Herlin, I., Berroir, J.P., Silva, E.F. and Simoes-Meirelles, P., 2004. An approach to correlate NDVI with soil colour for erosion process using NOAA/AVHRR data. Advances in Space Research, 33(3): 328-332.

Sivapalan, M., Jothityangkoon, C. and Menabde, M., 2002. Linearity and non linearity of basin response as a function of scale: discussion of alternative definitions. Water Resources Research, 38(2).

Slattery, M., Gares, P.A. and Phillips, D., 2002. Slope-channel linkage and sediment delivery on North Carolina coastal plain cropland. Earth Surface Processes and Landforms, 27: 1377-1387.

Slaymaker, O., 2003. The sediment budget as conceptual framework and management tool. Hydrobiologia, 494: 71-82.

Smith, R.E., Goodrich, D.C., Woolhiser, D.A. and Unkrich, C.L., 1995. KINEROS: a kinematic runoff and erosion model. In: V.P. Singh (Editor), Computer Models of Watershed Hydrology. Water Resources Publications, Colorado, pp. 697-732.

SPOT, 2000. Vegetation User Guide: SPOT-5, VITO, Brussels, Belgium.

Springer, G.S., Dowdy, H.S. and Eaton, L.S., 2001. Sediment budgets for two mountainous basins affected by a catastrophic storm: Blue Ridge Mountains, Virginia. Geomorphology, 37: 135-148.

Stefano, C.D., Ferro, V., Porto, P. and Rizzo, S., 2005. Testing spatially distributed sediment delivery model (SEDD) in a forested basin by cesium-137 technique. Journal of Soil and Water Conservation, 60(3): 148157.

Stock, J. and Montgomery, D.R., 1999. Geologic constraints on bedrock river incision using the stream power law. Journal of Geophysical Research, 104: 4983-4993.

Sujatha, G., Dwivedi, R.S., Sreenivas, K. and Venkataratnam, L., 2000. Mapping and monitoring of degraded lands in part of Jaunpur district of Uttar Pradesh using temporal spaceborne multispectral data. International Journal of Remote Sensing, 21: 519-531.

Summer, W., Klaghofer, E. and Zhang, W., 1998. Modelling Soil Erosion, Sediment Transport and Closely Related Hydrological Process, IAHS-AISH Publication. Nº 249. IAHS, 453 pp.

Svorin, J., 2003. A test of three soil erosion models incorporated into a geographical information system. Hydrological Processes, 17: 967-977.

Symeonakis, E., 2001. Soil Erosion Modelling over Sub-Saharan Africa Using Remote Sensing and Geographical Information Systems. PhD Dissertation Thesis, University of London, London, UK.

Symeonakis, E. and Drake, N., 2004. Monitoring desertification and land degradation over sub-Saharan Africa. International Journal of Remote Sensing, 25(3): 573-592.

Tarboton, D.G., 1997. A new method for the determination of flow direction and upslope areas in grid digital elevation models. Water Resources Research, 33: 309-319.

Tarboton, D.G., 2004. TAUDEM: Terrain Analysis Using Digital Elevation Models. Utah State University, Logan, Utah, USA.

Tarela, P.A. and Menendez, A.N., 1999. A model to predict reservoir sedimentation. Lakes & Reservoirs, 4: 121-133.

Tateishi, R., Shimazaki, Y. and Gunin, P.D., 2004. Spectral and temporal linear mixing model for vegetation classification. International Journal of Remote Sensing, 25(20): 4203-4218.

Thieken, A.H., Lücke, A., Diekkrüger, B. and Richter, O., 1999. Scaling input data by GIS for hydrological modelling. Hydrological Processes, 13(4): 611-630.

Thornes, J.B., 1985. The ecology of erosion. Geography, 70: 222-234.

Thornes, J.B., 1990. Vegetation and Erosion: Processes and Environments. Wiley, Chichester, London, UK.

Thornes, J.B. et al., 1996. Testing the MEDALUS hillslope model. Catena, 26: 137-160.

Torri, D., Poesen, J. and Borselli, L., 1997. Predictability and uncertainty of the soil erodibility factor using a global dataset. Catena, 31(1-2): 1-22.

Torrico, M., 1999. Monitoreo de los Sedimentos en el Embalse Laka-Laka, Universidad Mayor de San Simon, Cochabamba, Bolivia, 184 pp.

Toy, T.J., Foster, G.R. and Renard, K.G., 2002. Soil Erosion: Processes, Prediction, Measurement and Control. John Wiley and Sons, New York, USA, 338 pp pp.

TRMM, 1998. Tropical Rainfall Measuring Mission Science Data and Information System (TSDIS) Interface Control Specification between the TSDIS and the TSDIS Science User (TSU). Volume 3: File Specifications for TRMM Products - Level 1. Volume 4: File Specifications for TRMM Products - Level 2 and Level 3., Tropical Rainfall Measuring Mission, Maryland, USA.

Tucker, G.E. and Whipple, K.X., 2002. Topographic outcomes predicted by stream erosion models: sensitivity analysis and intermodel comparison. Journal of Geophysical Research, 107(9): 2179-2194.

USDA, 1993. Soil Survey Manual. USDA-SCS Agricultural Handbook, Soil Survey Staff. USDA Soil Conservation Service, Washington, D.C.

USGS-EROS, 2003. MODIS reprojection Tool v 3.2. User's Manual, Departament of Mathematics and Computer Science. South Dakota School of Mines and Technology.

Vaidyanathan, N.S., Sharma, G., Sinha, R. and Dikshit, O., 2002. Mapping of erosion intensity in the Garhwal Himalaya. International Journal of Remote Sensing, 23(20): 4125-4129.

van der Knijff, J.M., Jones, R.J.A. and Montanarella, L., 2000. Soil Erosion Risk Assessment in Italy, European Soil Bureau, Joint Research Center of the European Commission, Rome, Italy.

van der Perk, M. and Slávik, O., 2003. Simulation of event-based and long-term spatial redistribution of Chernobyl-derived radiocaesium within catchments using geographical information system embedded models. Hydrological Processes, 17(5): 943-957.

Van der Wal, D. and Pye, K., 2003. The use of hystorical bathymetric charts in a GIS to asses morphological change in estuaries. The Geographical Journal, 169(1): 21-31.

van Oost, K., Beuselinck, L., Hairsine, P.B. and Govers, G., 2004. Spatial evaluation of a multiclass sediment transport and deposition model. Earth Surface Processes and Landforms, 29: 1027-1044.

Van Oost, K. et al., 2005. Spatially distributed data for erosion model calibration and validation. Catena, 61: 105-121.

van Oost, K., Govers, G. and Desmet, P., 2000. Evaluating the effects of changes in landscape structure on soil erosion by water and tillage. Landscape Ecology, 15(6): 577-589.

Van Rompaey, A.J.J., Bazzoffi, P., Jones, R.J.A. and Montanarella, L., 2005. Modelling sediment yields in Italian catchments. Geomorphology, 65: 157-169.

Van Rompaey, A.J.J., Govers, G., Verstraeten, G., van Oost, K. and Poesen, J.W.A. (Editors), 2003a. Modelling the geomorphic response to landuse changes. In; Long Term Hillslope and Fluvial System Modelling. Concepts and Case Studies from the Rhine River Catchment. Springer-Verlag, Bonn, Germany.

Van Rompaey, A.J.J., Krasa, J., Dostal, T. and Govers, G., 2003b. Modelling sediment supply to rivers and reservoirs in Eastern Europe during and after collectivization period. Hydrobiologia, 494: 169-176.

Van Rompaey, A.J.J., Montanarella, L., Bazzofi, P. and Govers, G., 2003c. Validation of Soil Erosion Risk Assessments in Italy, EUR 20676 EN. Office for Official Publications of the European Communities, Luxembourg.

Van Rompaey, A.J.J., Verstraeten, G., van Oost, K., Govers, G. and Poesen, J., 2001. Modelling mean annual sediment yield using a distributed approach. Earth Surface Processes and Landforms, 26: 1221-1236.

Vandekerckhove, L. et al., 2000. Characteristics and controlling factors of bank gullies in two semi-arid Mediterranean environments. Geomorphology, 33(1-2): 37-58.

Vaneberg, P., 1988. Reforestación y manejo de plantaciones en los valles y altiplano de Bolivia. PAF-BOL, Cochabamba, Bolivia.

Veith, T.L., 2002. Agricultural BMP placement for cost-effective pollution control at the watershed level. PhD dissertation Thesis, Virginia Polytechnic Institute and State University, Virginia, 195 pp.

Veith, T.L., 2003. Optimization procedure for cost effective BMP placement at a watershed scale. Journal of American Water Resources Association(03024): 1331-1343.

Veldkamp, A. et al., 2001. Multi-scale system approaches in agronomic research at the landscape level. Soil and Tillage Research, 58(3-4): 129-140.

Verstraeten, G. and Poesen, J., 2001. Factors controlling sediment yield from small intensively cultivated catchments in a temperate humid climate. Geomorphology, 40: 123-144.

Verstraeten, G. and Poesen, J., 2002. Using sediment deposits in small ponds to quantify sediment yield from small catchments: possibilities and limitations. Earth Surface Processes and Landforms, 27: 1425-1439.

Verstraeten, G., Poesen, J., de Vente, J. and Koninckx, X., 2003a. Sediment yield variability in Spain: A quantitative and semiqualitative analysis using reservoir sedimentation rates. Geomorphology, 50(2003): 327-348.

Verstraeten, G., van Oost, K., van Rompaey, A.J.J., Poesen, J. and Govers, G., 2002. Evaluating an integrated approach to catchment management to reduce soil loss and sediment pollution through modelling. Soil Use and Management, 19: 386-394.

Verstraeten, G., van Rompaey, A., Poesen, J., van Oost, K. and Govers, G., 2003b. Evaluating the impact of watershed management scenarios on changes in sediment delivery to rivers? Hydrobiologia, 494: 153-158.

Vigiak, K., 2005. Modelling Spatial Patterns of Erosion in the West Usambara Mountains of Tanzania. Phd Dissertation. Tropical Resource Management Papers, No. 64, Wageningen, the Netherlands, 176 pp.

Vigiak, O., Okoba, B.O., Sterk, G. and Groenenberg, S., 2005. Modelling catchment-scale erosion patterns in the East African Highlands. Earth Surface Processes and Landforms, 30(2): 183-196.

Viney, N.R. and Sivapalan, M., 1999. A conceptual model of sediment transport: application to the Avon river basin in Western Australia. Hydrological Processes, 13: 727-743.

Viney, N.R. and Sivapalan, M., 2001. Modelling catchment processes in the Swan-Avon river basin. Hydrological Processes, 15(13): 2671-2685.

von Werner, M., 2000. EROSION-3D Technical User Manual, Department of Soil Science and Water Protection. TU Bergakademie Freiberg, Berlin, Germany.

Vrieling, A., Sterk, G. and Beaulieu, A., 2002. Erosion risk mapping: a methodological case study in the Colombian Eastern Plains. Journal of Soil and Water Conservation, 57(3): 158-162.

Wainwright, J., 1994. Anthropogenic factors in the degradation of semiarid regions: a prehistoric case study from southern France. In: A.C. Millington and K. Pye (Editors), Environmental changes in Drylands. John Wiley and Sons, Chichester., London, pp. 285-304.

Wainwright, J., Parsons, A.J., Michaelides, K., Powell, D.M. and Brazier, R. (Editors), 2003. Linking short and long term soil erosion modelling. In: Long Term Hillslope and Fluvial System Modelling. Concepts and Case Studies from the Rhine River Catchment. Springer-Verlag, Bonn, Germany.

Walling, D.E., 1983. The sediment delivery problem. Journal of Hydrology, 69: 209-237.

Walling, D.E. and Fang, D., 2003. Recent trends in the suspended sediment loads of the world's rivers. Global and Planetary Change, 39: 111-126.

Walling, D.E. and Probst, J.-L., 1997. Human Impact on Erosion and Sedimentation, IAHS Publication N° 245. IAHS, Wallingford, Oxfordshire, UK., 311 pp.

206

Whelan, B.M., Bratney, M. and Minasny, B., 2001. VESPER: spatial prediction software for precision agriculture. In: G. Grenier and S. Blackmore (Editors), 3rd European Conference on Precision Agriculture, Montpellier, France, pp. 139-144.

Whipple, K.X., Snyder, N.P. and Dollenmayer, K., 2000. Rates and processes of bedrock incision by the Upper Ukak River since the 1912 Novarupta ash flow in the Valley of Ten Thousand Smokes, Alaska. Geology, 28(9): 835-838.

Whipple, K.X. and Tucker, G.E., 1999. Dynamics of the stream-power river incision model: Implications for height limits of mountain ranges, landscape response timescales, and research needs. Journal of Geophysical Research, 104(8): 17661-17674.

White, R., 2001. Flushing of Sediments from Reservoirs, World Commission on Dams, Cape Town.

Wickenkamp, V., Duttmann, R. and Mosimann, T., 2000. A multiscale approach to predicting soil erosion on cropland using empirical and physically based soil erosion models in a geographic information system. In: J. Schmidt (Editor), Soil Erosion: Application of Physically-based Models. Springer,, Berlin, Germany, pp. 109-133.

Wicks, J.M. and Bathurst, J.C., 1996. SHESED: a physically based, distributed erosion and sediment yield component for the SHE hydrological modelling system. Journal of Hydrology, 175: 213-238.

Wilkinson, S., Henderson, A. and Chen, Y., 2004. SEDNET: User Guide, CSIRO Land and Water Client Report for the Cooperative Research Centre for Catchment Hydrology. Canberra, Australia.

Williams, J.R., 1975. Sediment Yield Prediction with Universal Equation Using Runoff Energy Factor, U.S. Department of Agriculture.

Wilson, J.P. and Gallant, J.C., 2000. Terrain Analysis: Principles and Applications. Wiley, New York, USA.

Wischmeier, W.H., Johnson, C.B. and Cross, B.W., 1971. A soil erodibility nomograph for farmland and construction sites. Journal of Soil and Water Conservation, 26(5): 189-193.

Wischmeier, W.H. and Smith, D.D., 1978. Predicting rainfall erosion losses: A guide to conservation planning. Agriculture Handbook 537. U.S. Department of Agriculture, Washington, DC, USA.

Woodcock, C.E. and Gopal, S., 2000. Fuzzy set theory and thematic maps: Accuracy assessment and area estimation. International Journal of Geographic Information Science, 14(2): 153-172.

Wrigth, A., 2002. FS Terrain-2002. Graphics, London, England.

Xia, A. and Clarke, K.C., 1997. Approaches to scaling of geo-spatial data. In: D.A. Quattrochi and M.F. Goodchild (Editors), Scale in Remote Sensing and GIS. CRC Lewis, Boca Raton, Florida, USA, pp. 309-360.

Xiong, L. and O'Connor, K.M., 2000. Analysis of the response surface of the objective function by the optimum parameter curve: how good can the optimum parameter values be? Journal of Hydrology, 234(3-4): 187-207.

Yang, D., Kanae, S., Oki, T., Koike, T. and Musiake, K., 2003. Global potential soil erosion with reference to land use and climate changes. Hydrological Processes, 17: 2913-2928.

Yfantis, E.A., Flatman, G.T. and Behar, J.V., 1987. Efficiency of kriging estimation for square, triangular and hexagonal grids. Mathematical Geology, 19: 183-205.

Young, R.A., Onstad, C.A., Bosch, D.D. and Anderson, J.P., 1989. AGNPS: a non point-source pollution model for evaluating agricultural watersheds. Journal of Soil and Water Conservation, 44(2): 4522-4561.

Yu, B., Hashim, G.M. and Eusof, Z., 2000a. Estimating the R-factor with limited rainfall data: A case study from Peninsular Malaysia. Journal of Soil and Water Conservation: 101-105.

Yu, W.S., Lee, H.Y. and Hsu, S.M., 2000b. Experiments on deposition behaviour of fine sediment in a reservoir. Journal of Hydraulic Engineering, 126(12): 912-920.

Zarate, O. and Montenegro, E., 1999. Modelación Hidrologica en la Cuenca Taquiña a Nivel Diario, LH-UMSS - PROMIC, Cochabamba, Bolivia.

Zarris, D., Lykoudi, L. and Koutsoyiannis, L., 2002. Sediment yield estimation from a hydrographic survey: a case study for the Kremasta reservoir basin, Greece. In: G. Tsakiris (Editor), Proceedings of the 5th International Conference of European Water Resources Association: "Water Resources Management in the Era of Transition". European Water Resources Association, Athens, Greece, pp. 234-241.

Zehl, T. and Montenegro, E., 1996. Estimación de las Tasas de Erosión en las Cuencas Pintu Mayu y La Pajcha, LH-UMSS - PROMIC, Cochabamba, Bolivia.

Zhang, K., Li, S., Peng, W. and Yu, B., 2004a. Erodibility of agricultural soils on the Loess Plateau of China. Soil and Tillage Research, 76(2): 157-165.

Zhang, X., 1999. Remote Sensing and GIS for Modelling Soil Erosion at the Global Scale. PhD Dissertation Thesis, Kings College London, London, UK.

Zhang, X., 2002. Scaling issues in environmental modelling, Environmental Modelling: Finding simplicity in complexity. John Wiley & Sons Ltd.

Zhang, X., Drake, N. and Wainwright, J., 2002. Scaling land surface parameters for global-scale soil erosion estimation. Water Resources Research, 38(9): 1170-1180.

Zhang, X., Drake, N. and Wainwright, J., 2004b. Scaling issues in environmental modelling. In: J. Wainwright and M. Mulligan (Editors), Environmental Modelling: Finding simplicity in complexity. John Wiley & Sons Ltd., London, UK, pp. 319-332.

Zhang, X., Drake, N.A., Mulligan, M. and Berkhout, E., 1999a. Modelling soil erosion at global and regional scales using remote sensing and GIS techniques. In: M. Atkinson and N.J. Tate (Editors), Advances in Remote Sensing and GIS Analysis. John Wiley & Sons Ltd, pp. 241-261.

Zhang, X., Drake, N.A., Wainwright, J. and Mulligan, M., 1999b. Comparison of slope estimates from low resolution DEM's: scaling issues and a fractal method for their solution. Earth Surface Processes and Landforms, 14: 763-779.

Zhou, Q. and Liu, X., 2002. Error assessment of grid-based flow routing algorithms used in hydrological models. International Journal of Geographic Information Science, 16(8): 819-842.

Zimmerer, K.S., 1993. Soil erosion and labour shortages in the Andes with special reference to Bolivia, 1953-91: implications for "Conservation with Development". World Development, 21(10): 1659-1675.

Zimmerer, K.S., 1994. Local soil knowledge: answering basic questions in highland Bolivia. Journal of Soil and Water Conservation, 6: 29-34.

Zobeck, T.M. et al., 2003. Measurement and data analysis methods for field-scale wind erosion studies and model validation. Earth Surface Processes and Landforms, 28(11): 1163-1188.

Samenvatting

Probleemstelling en doelen

De studie van het gedrag van bodemerosie, depositie en herverdeling van geërodeerde materialen op hellingen en in stroomgebieden is van groot belang in het bodem- en waterbeheer. De intensiteit van bodemverliezen bepaalt in grote mate de duurzaamheid en productiviteit van onze landbouw, veeteelt en bosbouw systemen. Sedimentatie kan aanzien worden als een nuttig proces wanneer geërodeerde bodemdeeltjes bijvoorbeeld worden afgezet op alluviale overstromingsvlakten. In vele gevallen heeft overmatige sedimentatie als gevolg van versnelde bodemerosie echter negatieve gevolgen voor rivieren, irrigatiesystemen en infrastructuren voor het waterbeheer zoals waterbekkens en stuwmeren.

Op perceelsniveau wordt de evaluatie van bodemverliezen door erosie gewoonlijk uitgevoerd door middel van analyse aan experimentele erosieplots. Deze hebben een typische ruimtelijke lengteschaal van 1 tot 100 m. Erosie studies op het niveau van stroomgebieden en op meer regionale schaal hangt meestal af van generalisaties gecombineerd met algemene (grove ruimtelijke resolutie) gegevens en informatie. Ruimtelijke schalen voor erosie evaluaties van 0.01 km^2 tot 1 of zelfs 10 km^2 zijn echter nodig in de praktijk, wanneer men grote stroombekkens en gebieden wil analyseren op erosie of bodemdegradatie risico's. In mondiaal onderzoek naar klimaatsverandering en milieu is het gebruik van rasters van 10 tot 100 km^2 algemeen van toepassing. Het begrijpen van de factor ruimtelijke schaal bij de bestudering van erosie en sedimentatie is daarom van groot belang.

In vele tropische en subtropische gebieden in de wereld, vormt het gebrek aan kwantitatieve -in situ- waarnemingen, de grote hinderpaal voor effectief bodem- en waterbeheer. Vooruitgang in satellieten, sensoren en geografische gegevensverwerking stellen ons echter in staat om aanzienlijke hoeveelheden informatie te verkrijgen via deze weg. Methoden en technieken die satelliet waarneming koppelen aan schaarse -in situ- metingen zijn daarom dringend nodig.

Deze studie behandelt de ontwikkeling en vergelijking van methoden om ruimtelijke patronen van bodemerosie en sedimentatie te bepalen in gebieden met schaarste aan experimentele grondwaarnemingen of metingen. De ruimtelijke patronen werden verkregen door satelliet waarnemingen te combineren met de beschikbare veldgegevens en conceptuele erosiemodellen. De geografische analyse werd uitgevoerd op regionale schaal ($54,100$ km^2) en op klein stroomgebiedschaal (59.8 km^2), daarbij gebruik makend van verschillende satellieten en modelresoluties. De verkregen erosie en depositie patronen werden geverifieerd door middel van een categorische vergelijking met erosiekaarten, beschikbaar voor een aantal stroomgebieden in de regio. Model resultaten werden onderling vergeleken om hun toepasbaarheid in het Andes gebied te toetsen.

Voor de validatie van erosie model resultaten in het stroomgebied werd tevens gebruik gemaakt van een vergelijkende digitale beeldanalyse van historische (1961) luchtfoto's en een recent (2002) hoge resolutie (5 tot 10 m) satellietbeeld. Het verband tussen bodemerosie en sediment transport uit het gebied via het drainage systeem werd tevens

geverifieerd door middel van de sedimentatie historie van een stuwmeerdat het Laka-Laka stroomgebied begrenst. Reservoir sedimentatiegegevens van drie belangrijke stuwmeren en waterreservoirs in het gebied werden tevens verzameld. Hiervoor werd een nieuwe en snelle methode gebruikmakend van akoestische sonar en het globale plaatsbepalingsysteem GPS en ontwikkeld en getest

Selectie van erosiemodellen

Een overzichtstudie van beschikbare erosiemodellen werd uitgevoerd en beschreven in hoofdstuk 2. Doel was hier om modellen te selecteren die bruikbaar waren onder verschillende ruimtelijke resoluties en in gebieden met schaarse veldwaarnemingen. De toepassing van bestaande en krachtige complexe fysische modellen, zoals SHETRAN en WEPP, werd als niet haalbaar beoordeelt in stroomgebied- en regionale studies, vanwege hun grote vereiste aan experimentele gegevens, de moeilijkheid om satellietgegevens te accomoderen en het gebrek aan beschikbare hydrologische gegevens voor calibratie. Vijf conceptuele erosie - depositie modellen werden uiteindelijk geselecteerd, met relatief geringe invoer gegevensbehoefte, met mogelijkheid tot gebruik van satellietbeeld gegevens, en toepasbaar in een ruimetelijke context.

Al deze modellen hadden bewezen toepasbaarheid in een breed scala aan klimatologische en topografische omstandigheden. De RUSLE-3D variant van de befaamde Universal Soil Loss Equation van Wischmeier & Smith (1978) stelde ons in staat de invloeden van complexe topografie op bodemverliezen te simuleren. Een aangepaste versie van het bekende MMF model van Morgan, Morgan en Finney (MMMF, Morgan et al, 1982) werd ook gebruikt. Daarnaast werd ook het vereenvoudigde "Stream Power Law" of SPL model (Barnes en Pelletier, 2001) toegepast. Het model voorgesteld door Thornes (1985), dat de vier grote erosie factoren klimaat, bodem, topografie en vegetatie in een eenvoudige fysische relatie koppelt, werd ook geselecteerd. Het vijfde model, het "Unit Streampower Erosion Deposition" (USPED) model (Mitas en Mitasova, 1998), stelde ons in staat om expliciet ruimtelijke erosie depositie patronen te vergelijken. Voor de selectie van het ruimtelijke "sediment delivery ratio" of SDR concepten verwijzen we naar hoofdstuk 7 of later in deze samenvatting.

Studiegebied

Het onderzoek werd uitgevoerd in Cochabamba, een provincie in de centrale Andes van Bolivie (Figure1.3). Het gebied maakt hydrografisch deel uit van het Amazone stroomgebied. Bij de regionale studie vormde de hele provincie Cochabamba, het studiegebied. In dit gebied, variërend in hoogteligging van 300 tot 5,400 m wordt een grote variatie van locale klimaten en fysiografische eenheden waargenomen. De valleien rond Cochabamba stad vormden het kerngebied van deze studie en ook van het onderzoek in stroomgebieden en de stuwmeren. Jaarlijkse neerslag en erosiviteit variëren hier van 450 tot 700 mm jr^{-1} en van 800 tot 1,400 MJ ha^{-1} mm hr^{-1}. Bodem- en geologische erosie fenomenen zijn duidelijk zichtbaar aanwezig in het landschap en hebben een aanzienlijke invloed op de lokale bevolking en economie. Naast de lokale bodemproductiviteit worden ook water- en energievoorraden, zoals in stuwmeren, direct

beïnvloed door deze erosie en sedimentatie processen. Het studiegebied wordt verder beschreven in hoofdstuk 3.

Regionale analyse

Het hoofddoel van de regionale analyse was de evaluatie van globale en kleinschalige satellietbeelden (>= 1 km^2 resolutie) en andere ruimtelijke gegevens voor het regionaal kaarteren van erosie en depositie patronen en de bepling van bodemverliezen. Hiervoor werden twee analyse scenario's beschouwd, die gebruik maakten van verschillende gegevenssets. Bij de eerste, algemene ("Baseline") evaluatie werd gebruik gemaakt van de IPCC (International Panel of Climate Change) lange termijn klimaat normalen (1960-1990), een 1-km rooster globaal digitaal hoogtemodel, bekent als GTOPO30, in combinatie met een 10-dagen tijdserie composiet van NOAA-AVHRR satellietbeelden voor de vegetatie dichtheid en een globale bodemkaart en databank. In het tweede scenario werd de huidige situatie geevalueerd, met recentere satelliet- en terrein gegevens:i satelliet neerslag waarnemingen voor de periode 1998-2003 van de zogenaamde "Tropical Rainfall Monitoring Mission" (TRMM) satelliet, een globaal 90-m rooster digitaal hoogtemodel van Shuttle Radar Topographic Mission (SRTM), satellietbeelden van de SPOT vegetatie sensor en een regionale bodemkaart op 1:250,000 schaal. De begroting van de ruimtelijke erosie patronen en bodemverliezen wordt getoond in Figure 4.5 en zijn vervat in Tabel 4.3. De toetsing van de erosiepatronen en waarden werd uitgevoerd door middel van een categorische vergelijking met bestaande erosiekaarten voor een aantal stroomgebieden. In het algemeen werd vastgesteld dat alle modellen slechts matig tot zeer matig presteerden (<= 50% ruimtelijke nauwkeurigheid). Niet tegenstaande relatief kleine verschillen tussen de modellen gevonden werden, is een model ordening op basis van nauwkeurigheid als volgt (van hoger naar lagere nauwkeurigheid): MMMF, THORNES, RUSLE-3D, USPED en SPL. Voornamelijk de gevoeligheid van de modellen voor de resolutie van het digitale hoogtemodel, evenals de zeer lage informatiedichtheid van de globale en regionale bodemkaarten, verklaren de zeer lage efficiëntie van deze regionale erosie evaluatie op een 1-km rooster schaal.

Analyse op stroomgebiedschaal

Bij de studie op stroomgebied niveau werden zowel satellietgegevens met een hogere ruimtelijke en temporele resolutie gebruikt, als ook een finere ruimtelijke resolutie (30 m) bij de modellering toegepast. Een recent SPOT-5 satellietbeeld (2002) en een 1:50,000 topografische achtergrond werden gebruikt om landgebruik, bodembedekking en erosie fenomenen in kaart te brengen. Gegevens van het MODIS sensor systeem werden gebruikt om de temporele variatie in het vegetatiedek te evalueren. De bodemgegevens werden verkregen uit een veldstudie uitgevoerd in 2003. Op 18 referentie punten in het stroomgebied werden veld experimenten uitgevoerd en bodemmonsters genomen voor analyse in het laboratorium (tabel 3.1). In vergelijking met de regionale analyse werd een duidelijke verbetering waargenomen in de erosie analyse. Dit kan toegeschreven worden aan de hogere ruimtelijke resolutie van invoer gegevens (5-250 m) en aan de gebruikte model resolutie (30 m). Het gemiddelde jaarlijkse bodemverlies in het Laka-Laka stroomgebied is vrij hoog (3,000 ton km^{-2} jr^{-1}) en kan verklaard worden door de dominantie van sedimentaire lithologieën (Anzaldo leisteen, Capinota formaties), welke verweren tot erosiegevoelige lemige bodems. Ook het steile reliëf en lage efemere vegetatiedek dragen aanzienlijk bij tot de

erosiegevoeligheid van dit gebied. De prestaties van de vijf erosie modellen werd geanalyseerd door een vergelijking van de ruimtelijke patronen met een multitemporele analyse van een 5-m resolutie luchtfoto mozaïc (1961) en een panchromatisch SPOT-5 beeld (5-m resolutie), na orthorectificatie en digitale beeldverwerking van deze opnames. Wat betreft ruimtelijke patronen, bleken de RUSLE-3D en USPED beter in staat de visuele waargenomen erosiefenomenen in kaart te brengen. Het MMMF of Morgan model laat beter toe om de brongebieden van geërodeerde materialen en sediment in kaart te brengen, vanwege zijn vergelijkende evaluatie van aan de ene kant het losmaken van bodemmaetriaal door regenval en aan de andere kant afvoer capaciteit van sediment door oppervlakte transport

Evaluatie van sedimentatie in stuwmeren

In afwezigheid van hydrologische afvoergegevens en informatie over sediment concentraties, zoals in het studiegebied, vormen sedimentatiegegevens van stuwmeren een goed alternatief om de sediment balans, oftewel het verschil tussen het totale bodemverlies (of sediment productie) van een stroomgebied en de uiteindelijke sediment export, te bepalen. Een methode werd daarom ontwikkeld, gebruik makend van een globaal plaatsbepalingsysteem via satelliet (GPS) en een eenvoudige akoestische sonar of echosounder. De volgende specifieke onderzoeksdoelen werden hierbij nagestreefd: *i*) het effect van de bemonstering dichtheid van de echolodingen op de nauwkeurigheid van de methode*, ii*) de keuze van de interpolatie methode voor het verkrijgen van een nieuw bathymetrisch bodemoppervlak van het stuwmeer*, iii)* evaluatie van de historische veranderingen in opslagcapaciteit van de drie stuwmeren en *iv*) afleiden van specifieke sediment opbrengsten van de drie stroomgebieden. Er werd ook gebruik gemaakt van historische bathymetrische informatie van de stuwmeren, om het sedimentatie verloop in de tijd te bestuderen.

Bij de analyse van de sonar puntmetingen werd de "split sampling" methode gehanteerd en een progressieve gegevensreductie toegepast om de invloed van de waarnemingsdichtheid op de nauwkeurigheid te bepalen. Tevens werden ruimtelijke variogrammen en interpolatie technieken getoetst. Ordinary kriging werd toegepast voor ruimtelijke interpolatie van sonar gegevens. De nauwkeurigheden van resultaten van de verschillende methoden werden getoetst dmv. een aantal test statistieken.

Voor de twee grotere stuwmeren *i.e.,* Corani en Angostura (Figure 6.1), werd gevonden dat een waarnemingsdichtheid van 5 tot 6 echopeilingen per 100 m rooster of 1 hectare stuwmeer bodemoppervlak voldoende is. Een hogere dichtheid draagt niet bij tot de nauwkeurigheid. Voor de kleinere Laka-laka stuwmeer echter waren 71 waarnemingen per hectare vereist om tot nauwkeurige resultaten te leiden. Dit is vanwege de zeer grote variaties in diepte en geulen waargenomen in dit stuwmeer, daar waar de grotere reservoirs, een vlakkere bodem topografie vertoonden.

De specifieke sediment productie van de bovenstroomse stroombekkens werd begroot op respectievelijk 1,831 ton km^{-2} jr^{-1} voor het kleine erosiegevoelige 59.8 km^2 Laka-Laka stroomgebied. Voor het Angostura stuwmeer werd een waarde van 123 ton km^{-2} jr^{-1} afgeleid uit de sedimentatiemetingen. Dit stuwmeer bevindt zich (Figure 6.1) benedenstrooms de "Valle Alto" en draineert een gebied van 1,992 km^2. De specifieke sedimentatie snelheid van het Corani stuwmeer, met een stroombekken van 297 km^2,

werd begroot op 152 ton km^{-2} jr^{-1}. De verschillen in sediment producties van de drie bekkens kon verklaard worden door de gebiedskarakteristieken in acht te nemen. Vooral de aanwezigheid van alluviale afzettingsgebieden ("depositional areas, alluvial plains") op korte afstand van de stuwdammen is naar onze mening verantwoordelijk voor de relatief lage sediment opbrengsten van vooral de Corani en Angostura stuwmeren.

Verbanden tussen sedimentatie en erosie in stroomgebieden

In hoofdstuk 7 werden de verbanden tussen sedimentatie in het Laka-Laka stuwmeer en bodemverliezen in het stroomgebied bestudeerd. Een vrij nieuw concept van zogenaamde "spatial sediment delivery ratio" (SDR) werd hierbij gebruikt. Vier recent ontwikkelde SDR methodes werden vergeleken, te weten: het SEAGIS (DHI, 2003) en SEDD model (Pillotti et al, 1997), de methode van Veith (2002) en het HSDR model (Lu et al, 2003). Doel was hun toepasbaarheid in het studiegebied en in de Andes te evalueren. De ramingen van de bodemverliezen verkregen met de erosiemodellen (hoofdstuk 5) werden gebruikt als invoer voor de SDR modellen. Er werden duidelijke verschillen vastgesteld tussen de vier SDR benaderingen en modellen voor wat betreft ruimtelijke patronen in sediment afvoer en aldus in brongebieden van sedimenten. Hoge export ratio's (SDR>0.6) van geërodeerde materialen werden gevonden in het zuidoostelijke en centrale deel van het stroomgebied en 25% van het totale gebied. In andere subgebieden was de export van geërodeerde bodemmaterialen in de orde van 20% (SDR= ± 0.2). Een gemiddelde SDR=0.45 werd vastgesteld. Deze is in overeenstemming met de verhouding tussen de specifieke sediment opbrengst (1,830 ton km^{-2} jr^{-1}), bepaald door middel van stuwmeer sedimentatie waarnemingen en de totale jaarlijkse bodemerosie (3,000 ton km^{-2} jr^{-1}), welke modelmatig begroot werd door middel van zowel satelliet- als lokale terrein-waarneming als brongegevens. De HSDR benadering leek ons beter geschikt in deze regio, mede dank zij een sterke theoretische onderbouw en gebruik van gegevens van neerslaginstensiteit en duur. Het SEDD model, dat minder brongegevens vereist, is een goed praktisch alternatief voor de "Hillslope Sediment Delivery Ratio" methode in deze gebieden waar meteorologische en hydrologische waarnemingen en gegevens schaars zijn.

Eindconclusies

De ernst van de consequenties van bodemerosie en sedimentatie voor het milieu en de maatschappij in de Boliviaanse Andes regio wordt sinds geruime tijd erkend en krijgt nu ook meer wetenschappelijke aandacht. Dit onderzoek heeft aangetoond dat geo-informatie technieken, zoals ruimtelijke erosie, depositie en sediment export modellen, gekoppeld aan satelliet waarnemingen en beperkte terreingegevens, ons in staat stellen om bodemerosie en land degradatie in grotere gebieden te evalueren en in kaart te brengen tegen relatief geringe kosten. Men moet echter terdege rekening houden met de ruimte - tijd resolutie en de informatiedichtheid van de gegevensbronnen, alsook hun invloed op de modellen en fysische processen. De methode kan aanbevolen worden om eerste schattingen van bodemdegradatie op nationaal, regionaal en stroomgebied niveau uit te voeren, zodat interventies van de overheid of lokale autoriteiten op het gebied van land en waterbeheer meer gebied- of locatiespecifiek kunnen worden uitgevoerd . Een snelle methode voor inventarisatie en evaluatie van sedimentatie in meren en stuwmeren in combinatie met een ruimtelijk sediment export concept is een goed alternatief om sediment balansen op te maken in stroomgebieden met weinig hydrologische en sediment gegevens, zoals veel voorkomt in Bolivia. De voorgestelde methodiek zou ook

kunnen worden toegepast in landgebruik planning en landinrichting studies. Ook aan mondiale studies zoals verwoestijning en de studie van effecten van klimaatsverandering op het milieu kunnen de methoden ontwikkeld in dit werk bijdragen.

Resumen

Planteamiento del problema y objetivos

El estudio del comportamiento de la erosión hídrica de suelos, la deposición y el proceso de redistribución de los sedimentos en cuencas de media y gran extensión (*p.e.* cuenca Chocaya cuenca del río Grande, cuenca del rio Bermejo, cuenca del Pilcomayo) es de suma importancia para los especialistas del manejo de Recursos Naturales asi como tambien para los hidrólogos e ingenieros de Recursos Hídricos.

La intensidad de la erosión hídrica determina en gran manera la sostenibilidad del recurso suelo a largo plazo. Por lo tanto su adecuado control garantizara una agricultura productiva en serranías, tierras en pendiente y en sistemas forestales. La deposición de sedimentos se convierte en un proceso benéfico en ciertas circunstancias tales como el rellenamiento de planicies aluviales (*p.e.* lameo de tierras). Sin embargo en muchas casos la excesiva sedimentación producto de las altas tasas de erosión aguas arriba afecta adversamente los cursos de agua, la red de drenaje y las estructuras hidráulicas como presas y reservorios, todo ello limita el abastecimiento de agua potable y riego.

El proceso de erosión y de transporte de sedimentos teóricamente involucra el disgregamiento y movilización de las partículas de suelo desde las arcillas a arenas. Por lo cual representa un proceso físico que se desarrolla en una escala espacial y temporal muy pequeña (*p.e.* escala de parcela en un evento de tormenta). Capacidades para la determinación de estos procesos a través de modelos físicos de erosión tales como WEPP, EUROSEM, LISEM esta en una etapa muy avanzada. Sin embargo, las capacidades de predicción may allá de estas micro escalas (*p.e.* escala de parcela o terrenos en pendiente) no están desarrolladas al mismo nivel que la interior (*p.e.* escala de cuenca, provincial, regional) y son precisamente datos a esas escalas, los que son mas urgentemente requeridos por especialistas en manejo y conservación de cuencas.

La evaluación de la erosión hídrica para campos y terrenos agrícolas usualmente se basa en el análisis de datos colectados en parcelas y/o terrenos experimentales en pendiente en los cuales la típica escala de la longitud de pendiente analizada varía de 1 a 100 m. La evaluación de estos procesos a escala regional y de cuenca hasta el presente depende en gran manera en generalizaciones de información y datos medioambientales de resolución espacial muy gruesa.

En la practica, evaluaciones espaciales distribuidas a escalas que varían desde 0.01 km^2 a incluso 10 km^2 son comúnmente utilizadas cuando se analiza cuencas de gran extensión (*p.e.* Cuenca del Amazonas, cuenca de La Plata) o eco regiones. En investigaciones de calentamiento global y de caracterización continental de la vegetación y de varios otros procesos medio ambiéntales, la evaluación y herramientas de modelación típicamente utilizadas varían desde 10 km^2 a 100 km^2 o un arco segundo de resolución geográfica (tamaño de celda). Por lo tanto, entendimiento y apropiado manejo de los factores que afectan la escala espacial en la modelación es igualmente importante cuando se usa enfoques de modelación para la evaluación de los procesos de erosión y deposición de sedimentos.

En muchas regiones tropicales y sub-tropicales del mundo, falta de datos de campo –in situ-y experimentos, se constituye en la mayor limitante para la implementación de medidas efectivas de control y manejo del suelo y de recursos hídricos. Los últimos avances en sensores remotos (teledetección) y técnicas de geo información han conducido a la producción de una enorme cantidad de imágenes satelitales de variada resolución espacial y espectral, las cuales están disponible a la comunidad científica y público en general. Por lo tanto métodos de evaluación espacial son requeridos para combinar los datos brindados por estos satelitales de observación de la tierra en combinación con los escasos datos -in situ- disponibles.

Esta investigación ha tratado de desarrollar y comparar diferentes métodos para la estimación espacial y temporal de la distribución de los patrones y tasas de erosión y deposición de suelos en áreas con escasa información de campo (información –in situ-). Patrones espaciales y tasas de los procesos de erosión y deposición fueron obtenidos a través de la combinación de imágenes satelitales, algoritmos de transformación, y los pocos datos de campo con modelos conceptuales de erosión los cuales requieren información comúnmente disponible. El análisis fue hecho a escala regional (54,100 km^2) y de cuenca (59.8 km^2) usando diferentes datos y enfoques de modelación de la erosión.

Los patrones espaciales de erosión obtenidos a nivel regional fueron validados por comparación de los mapas de predicción con estudios de evaluación de la erosión en cuencas correspondientes a diferentes áreas del área de estudio regional

Para el análisis a la escala de cuenca, además de una validación usando datos multitemporales de alta resolución espacial, una validación cuantitativa fue llevada a cabo a través del establecimiento de una conexión entre la erosión, la producción de sedimentos y las tasas de sedimentación en reservorios en el concepto conocido como tasa de entrega de sedimentos (SDR).

La colección de datos de sedimentación en reservorios fue llevada a cabo para tres importantes reservorios de agua potable y energía eléctrica. Un novedoso, y rápido levantamiento batimétrico basado en un sonar acústico conectado a un GPS portátil fue desarrollado y evaluado para este propósito.

Selección de los modelos de erosión

Una revisión de los modelos de erosión existente hasta el presente fue llevado a cabo de manera de analizar y describir los enfoques existentes y sus capacidades de representación de la erosión, deposición y la dinámica del transporte de sedimentos a varias escalas espaciales y temporales para sitios con escasa información. El requerimiento de datos de entrada y la inclusión de datos de percepción remota (imágenes satelitales) en los modelos revisados fue tambien parte del analisis.

La aplicación de complejos y sofisticados modelos físicos tales como SHETRAN, WEPP, EUROSEM fue juzgada como no factible a la escala de cuenca y regional, debido a la extensa cantidad de datos requeridos para la parametrización y calibración del modelo, las características topográficas del terreno, la extensión del área de estudio, y las dificultades en la introducción de los datos de sensores remotos y la falta de datos hidrológicos medidos para la calibración de estos modelos.

Cinco modelos conceptuales y espacialmente distribuidos, con requerimiento mínimo de datos, capaces de acomodar información satelital y ejecutables dentro de un ambiente de GIS fueron seleccionados. Todos los modelos seleccionados han sido utilizados con cierto grado de éxito en diferentes ambientes climáticos y topográficos.

El modelo tridimensional RUSLE-3D, una variante del muy conocido modelo de la Ecuación Universal de Perdida de Suelo (USLE) desarrollada por Wischmeier y Smith (1978), permite un análisis del impacto de la convergencia de los flujos en terrenos con topografía compleja similares al área de estudio, al reemplazar los factores de longitud e inclinación de la pendiente por un algoritmo que incorpora áreas contribuyentes pendiente arriba.

La versión modificada del modelo de Morgan, Morgan y Finney (MMMF) fue también usado. Este modelo analiza los dos procesos que limitan la erosión *p.e.* desprendimiento del suelo por el impacto de la lluvia y el transporte de las partículas removidas por escurrimiento. De hecho, la solidez de este modelo radica en su habilidad para determinar si el proceso de erosión es inducido por el desprendimiento o transporte.

El modelo simplificado de la ley del poder de flujo (SPL) predice la tasa de erosión por incisión fluvial y esta basada en el concepto de área contribuyente pendiente arriba y la litología. Thornes (1985) presento un modelo geomorfico que combina la tasa de escurrimiento, la erodabilidad del suelo, los efectos de la topografía y la protección vegetal en una ecuación física sencilla.

El modelo unitario de poder de flujo para la erosión o deposición (USPED) desarrollado por Mitasova et al. (1998) estima la erosión neta y deposición como producción de la divergencia en la capacidad de transporte de sedimento.

Asimismo, todos los modelos implementados permiten el uso integrado de: (*i*) imágenes satelitales multitemporales de baja resolución espacial (*p.e.* NOAA-AVHRR, SPOT-VGT y MODIS) para incluir las propiedades de la vegetación y para monitorear los cambios estaciónales en la cobertura vegetal, (*ii*) imágenes de alta resolución espacial (*p.e.* SPOT-5, Landsat-7 ETM, ASTER) para el mapeo de la cobertura del terreno, rasgos y tipos de erosión y las características de la superficie del suelo a la escala de cuenca, (*iii*) modelos digitales del terreno (*p.e.* HYDRO-1k, SRTM y cartas topográficas a escala 1:50,000) para la caracterización del terreno y análisis topográfico, y (*iv*) datos climáticos (*p.e.* información satelital de la lluvia de TRMM y mapas globales de precipitación de la CRU CL-2 y datos estaciones meteorológicas locales), para la parametrización hidrológica.

Área de estudio

La investigación fue conducida en el departamento de Cochabamba, central área en Bolivia (Figura 1.3). Una gran extensión del departamento y el sistema de cuencas que rodean el valle central en las proximidades de la ciudad Cochabamba son representativas de la región de los Andes y geográficamente pertenecen a la parte alta de la cuenca del río Amazonas (cuenca del río Grande). El departamento que cuenta con un área aproximada de 54,100 km^2 fue usado en la evaluación regional. La elevación en Cochabamba, varía desde 100 m.s.n.m hasta cerca de 5,200 m.s.n.m. Una gran

diversidad de climas, topografía y tipos de vegetación, desde semi-alpina, semi-árida, hasta ambientes tropicales pueden ser observadas en el área.

Las regiones del valle central y del valle alto de Cochabamba (Figura 4.11) localizadas entre elevaciones de 2,400 a 4,200 masl se constituyeron en un área importante de esta investigación y fueron usadas para el análisis de cuencas y de la sedimentación en reservorios El valle central presenta un clima de seco sub-húmedo a semi-árido con una evaporación potencial [1,200 mm a^{-1}] que excede la precipitación la cual tiene un rango de 450 to 700 mm a^{-1}. La precipitación muestra una fuerte concentración estacional con índices anuales de erosividad en el rango de 800 a 1,400 MJ mm ha^{-1} hr^{-1}. Las láminas de lluvia de 24 horas están en el rango de 25 a 45 mm con una erosividad de tormenta de 150 a 300 MJ mm ha^{-1} hr^{-1}, y se caracteriza por eventos de precipitación de tamaño medio, en comparación a eventos de tormenta en áreas tropicales. Esto es debido al efecto orográfico, mayor altitud y una menor exposición de los valles a las lluvias durante el verano.

En adición, el área del valle alto y mas específicamente el área de la cuenca en consideración (Laka-Laka) esta caracterizada por una generalizada escasa cobertura vegetal, una relativa abundancia de litologías antiguas sedimentarias *p.e.* las formaciones de Anzaldo y Capinota, las cuales consisten de limonitas, calizas y lutitas y suelos meteorizados erodables de textura media. Rocas terciarias, aluviales cuaternarios depósitos fluvio-lacustrine, abanicos aluviales y terrazas presentan tambien áreas sensitivas a la erosión en muchos sitios.

Todo lo anteriormente mencionado, convierte a esta región en un área muy susceptible a la erosión y en particular sensible a la erosión hídrica. La evidencia de los procesos de erosión y sedimentación muy visibles en el paisaje tiene un impacto negativo en el bienestar de la población de esta área. Por lo tanto el suelo como los recursos hídricos y/o hidráulicos (*p.e.* sedimentación en reservorios y canales de riego) son impactados negativamente por estos procesos.

Análisis a escala regional

El principal objetivo de la investigación a esta escala de modelación fue evaluar el uso de datos de sensores remotos y medio ambientales con baja resolución espacial y de cobertura global en combinación con los modelos de erosión seleccionada para evaluación y monitoreo de la erosión en toda el área del departamento de Cochabamba.

Dos escenarios de evaluación fueron simulados utilizando un diferente conjunto de datos. El primero denominado evaluación de referencia (baseline) fue implementado usando los datos climáticos de referencia de la IPCC (promedio de 30 años, 1961-1990) en combinación con el modelo de elevación digital HYDRO-1k con 1-km de tamaño de celda, composiciones de imágenes de NDVI en series multitemporales del sensor NOAA-AVHRR con una resolución temporal de 10-dias, y datos y mapas globales de suelo. La segunda evaluación denominada actual, uso los datos de información de factores ambientales y sensores remotos mas reciente con una mejor resolución espacial para la representación de parámetros tales como la lluvia (*p.e.* precipitación derivada de los sensores infrarrojos de la TRMM o la Misión de Monitoreo de Lluvia Tropical) y topografía (*p.e.* DEM con 90-m de resolución de SRTM o del Trasbordador de Radar

con Misión Topográfica), cobertura vegetal (*p.e.* series multitemporales de NDVI del sensor SPOT-VGT) además de información de suelos a escala regional.

Patrones espaciales de erosión más consistentes fueron obtenidos, utilizando los datos seleccionados para la evaluación del scenario actual. Se estimo que el 56% del departamento esta ligeramente afectado por erosión hídrica con tasas de erosión menores a 200 ton $km^{-2} a^{-1}$ Asimismo el 10% del área se encuentra afectado por niveles de erosión media [200 a 800 tones $km^{-2} a^{-1}$]. La proporción relativa con una alta [800-3,200 ton $km^{-2} a^{-1}$] y muy alta erosión [3,200 a 12,800 ton $km^{-2} a^{-1}$] esta en 15% y 13%, respectivamente. Tasas extremas de erosión [>12,800 ton $km^{-2} a^{-1}$] fueron encontrada en 6% del departamento. En general, 19% del área presenta una muy alta y extrema degradación del suelo.

La validación de los patrones y tasas de erosión a escala regional fue hecha a través de una comparación categórica de las tasas de erosión reclasificada estimada con mapas existentes de intensidad de erosión a escala de cuenca, obtenidos de levantamientos de campo geomorfológico en combinación con interpretación de fotos aéreas. Aunque, en su conjunto el desempeño de los modelos a escala regional fue regular (<50% de exactitud de mapeo), los modelos fueron categorizados en cuanto a su desempeño en la forma siguiente *p.e.* MMMF, THORNES, RUSLE-3D, USPED y finalmente el modelo SPL. A través del análisis de comparación se ha demostrado que la sensibilidad de la escala en los datos del DEM y las generalizaciones observadas en los datos de información de suelos son la mayor causa de inexactitud y errores en las predicciones a esta escala.

Análisis a escala de cuenca

El uso de datos de sensores remotos (percepción remota) combinada con la escasa información de campo (información -*in situ*-) como fuente de datos de entrada en los modelos fue analizada a mayor detalle. Un intento fue hecho para integrar imágenes satélites con media a fina resolución con los mínimos datos recolectados producto del levantamiento de suelos y cobertura del terreno y la información de estaciones meteorológicas adyacente en la cuenca.

Los datos usados fueron (*i*) imágenes satelitales recientes (2002) de alta resolución (pancromática y multiespectrales) SPOT-5 y fotografías aéreas a escala 1:50,000 (1961) para el mapeo de la cobertura del terreno, los rasgos de erosión, los tipos de suelo y geomorfología, (*ii*) la serie satelital multitemporal de MODIS-NDVI con 250-m de resolución para el monitoreo de la variación temporal de la cobertura vegetal, (*iii*) un levantamiento a nivel del reconocimiento del suelo y la erosión para la determinación de los parámetros físicos del suelo, (*iv*) datos del SRTM-DEM de 90-m y las cartas topográficas 1:50,000 con 20-m de intervalo de curva para la representación del paisaje y (*v*) datos meteorológicos para la caracterización de la lluvia y el área de la cuenca.

Cuando las predicciones obtenidas a esta escala fueron comparadas con las predicciones a escala regional, se evidencio que las predicciones fueron mucho mas satisfactorias, esto debido a la mejor resolución espacial en la escala de modelación (30-m) y con datos de entrada con una resolución espacial que vario de 5-m a 250-m.

Para los 59.8 km^2 de la cuenca Laka-Laka, el promedio de la erosión bruta para los 5 años de periodo de evaluación fue estimado en 2.5×10^5 toneladas o una tasa de erosión con área especifica de 30 ton ha^{-1} a^{-1} o 3,000 ton km^{-2} a^{-1}. Esta relativa alta denudación puede ser explicada en primera instancia por la litología sedimentaria de lutitas intercaladas con cuarcitas y margas verduscas (Formación Anzaldo) las cuales dominan extensas áreas de la cuenca. Tambien existen pequeñas área con ocurrencia de pizarra (Formación Capinota) en combinación con gradientes topográficas muy inclinadas. Sin embargo esta claro que la cantidad de erosión bruta no es igual a la entrega de sedimento o la producción de sedimentos por área especifica.

Del análisis de la distribución espacial se observa que un área total de 32.3 km^2 o 54% esta afectadas por intensidades de erosión de media [200-800 ton km^{-2} a^{-1}] a alta [800-3,200 ton km^{-2} a^{-1}] mientras que 15.6 km^2 o 26% del área esta afectada por muy alta [3,200-12,800 ton km^{-2} a^{-1}] a extremas [>12,800 ton km^{-2} a^{-1}] tasas de erosión que son los mayores contribuyentes de sedimentos al reservorio.

El desempeño de los modelos de erosión fue evaluado por comparación de los patrones espaciales con el mapa de rasgos e intensidad de la erosión de la cuenca obtenidos de la combinación del levantamiento a nivel de reconocimiento, la interpretación del orthofoto mosaico (1961) y de las imágenes satélites orthorectificadas de la banda pancromática de SPOT 5 la cual tiene 5-m de resolución espacial (fecha de adquisición Agosto, 2002). Aunque los fenómenos de lavado difuso de sedimentos y la presencia de erosión en surcos es muy difícil de identificar, rasgos de erosión profundos tales como iniciación y profundización de las cárcavas, ensanchamiento del sistema de drenaje, erosión de canal y deslizamientos pueden ser extraídos de las imágenes satelitales. De hecho, la comparación de las dos imágenes multitemporales, la fotografía aérea y la SPOT-5 permitió una mejor identificación visual de las áreas activas de erosión en la cuenca.

La validación semicuantitativa de los modelos produjo una razonable coincidencia, si se considera que una clase con una diferencia de mas (-) o menos (+) una clase como aceptable entre un clase estimada con la indicada en el mapa de rasgos de erosión. En términos de los patrones espaciales, los modelos RUSLE-3D y USPED son juzgados como los más adecuados para indicar área con presencia de cárcavas y erosión de canal en los cursos de ríos. Asimismo, el modelo MMMF es considerado como el mas apropiado para la identificación de fuentes de sedimentos, debido al análisis que realiza sobre si la erosión es por desprendimiento o transporte y al hecho que descompone la erosión puntual a una -*a priori*- dependencia topográfica como la mayoría de los modelos asume.

Aunque, el efecto de la topografía es uno de los factores mas predominantes en el modelo Thornes, su habilidad para evaluar la erosión con una base multitemporal (diaria, decadal, quincenal, mensual) es considerada útil para el análisis de la distribución estacional de la intensidad de la erosión y la evaluación de los factores causales, tales como la cobertura vegetal y la intensidad de la lluvia.

En lo que concierne a la utilidad de los algoritmos de avance del flujo derivados del DEM, el algoritmo de flujo múltiple fue seleccionado en vez del algoritmo D8 o de

flujo en dirección de la pendiente mas inclinada, debido a que la red drenaje existente fue mas exactamente representada y debido a su mejor consideración de los patrones de flujo convergente y divergente, que toman lugar en los paisajes montañosos.

Sedimentación en reservorios

En la ausencia de registros de medición de caudales y de concentración de sedimentos en los cursos del río en la cuenca Laka-Laka, los datos de sedimentación en reservorios ofrecen un considerable potencial para reconstruir la historia de la producción de sedimentos de la cuenca contribuyente. Un método de levantamiento batimétrico sencillo y rápido fue por lo tanto desarrollado para cumplir este propósito y fue ejecutado en los más importantes reservorios y lagos del área de estudio.

El novedoso método geomático consistió en la utilización de un Sistema de Posicionamiento Global (GPS) portátil unido a un sonar acústico portable ambos de bajo costo económico en combinación con imágenes satelitales. Cuatro objetivos específicos fueron trazados en los reservorios estudiados: (*i*) analizar el efecto de reducción del tamaño de la muestras (o densidad de puntos de sondeo) de sondeos del sonar en la exactitud de la generación de la superficie batimétrica (área interpolada), (*ii*) evaluar los métodos de interpolación para la generación de las superficies batimétricas, (*iii*) estimar los cambios históricos en el volumen de sedimentos depositados en el reservorio y determinar la capacidad de captación y esperanza de vida los tres reservorios y (*iv*) derivar la producción de sedimentos por área especifica de lo registros multitemporales de sedimentación en reservorios

La metodología para la reconstrucción de los registros de sedimentación en los reservorios se basa en la determinación topográfica del lecho del reservorio de los datos correspondiente a tres diferentes periodos de tiempo: (*i*) levantamiento topográfico antes de la construcción de la presa, (*ii*) levantamiento topográficos existentes (datos previos) y (*iii*) el levantamiento topográfico con la metodología desarrollada en esta investigación (2003). Los Mapas batimétricos derivados del registro histórico fueron escaneados, digitalizados e interpolados usando el método de interpolación entre curvas de nivel. El método de interpolación denominado método de kriging convencional (ordinary kriging) fue usado para los puntos derivados del sonar.

La técnica de separación de muestras aplicando en una reducción progresiva en número total de puntos sondeados fue usada para evaluar el efecto de la reducción en el tamaño de muestreo y para obtener una superficie batimétrica exacta con un mínimo de datos. Con base a los resultados de validación cruzada (cross validation) la exactitud de los resultados fue determinada tomando en cuenta el modelo del variograma y los métodos de interpolación para cada predicción.

La comparación de las predicción con los diferentes tamaños de muestra fue evaluada usando pruebas estadísticas tales como el sesgo (*B*), prueba de bondad de ajuste (r^2), coeficiente de correlación (*r*), la raíz del error medio cuadrático (*RMSE*), error medio cuadrático (*MSE*), Error medio absoluto (*MAE*) y el coeficiente de eficiencia del modelo o Nash-Sutcliffe (R^2_{NS}).

El análisis de la validación y las pruebas de exactitud estadística indicaron que la exactitud en la interpolación de las superficies batimétricas fue deteriorada

221

significativamente a medida que el tamaño de la muestra fue reducida en menos de 50% del numero inicial de puntos de muestreo. Esto corresponde a una densidad de puntos de 5 o 6 sondeos por 100-m de tamaño de celda para la interpolación del lecho de fondo de los reservorios de Angostura y Corani, respectivamente, mientras que corresponde a una densidad de 141 puntos de sondeo por 100-m de tamaño de celda para el lecho de fondo del reservorio Laka-Laka, esto debido a una mayor variabilidad en el lecho del reservorio.

Por lo tanto, la incertidumbre en la superficie batimétrica seria mas pronunciada si largas variaciones de profundidad existieran. Comparando los resultados de todas las superficies batimétricas obtenidos con los diferentes tamaños de muestra, se concluye que los grupos de muestra con un mínimo de 6 puntos de muestras por 100-m de tamaño de celda es una cantidad optima para una adecuada interpolación cuando los lechos del reservorios son uniformes mientras que un mínimo de 71 muestras de puntos de sondeo es requerido para el mismo tamaño de celda si la superficie del lecho es variable (25% del muestreo total).

Esta afirmación esta basada en el hecho que la diferencia de elevaciones entre la superficie interpolada obtenida con el numero total de puntos de sondeo (100%) y la superficie interpolada con 25% y 50% del total de puntos es menos que 0.5 y 0.2 m respectivamente. Con una densidad de puntos mayor (75%) las diferencias entre las altitudes observadas y las interpoladas es menor que el error de medición del sonar acústico el cual es aproximadamente ±0.1 m (Fishfinder-100 Garmin) y por ello redundantes.

Debido a la diferente dimensión de los reservorios, el tiempo de vida, y las características de las cuencas contribuyentes, una considerable variación en el volumen total de sedimentación en los reservorios fue encontrado. Los volúmenes variaron de 0.92 Mm^3 para el reservorio Laka-Laka a 1.4 Mm^3 para el reservorio Corani y 10.2 Mm^3 en el caso del reservorio Angostura. La eficiencia de captura de sedimentos de los reservorios fue estimada en 95%, 90% y 89% para los reservorios Corani, Angostura y Laka-Laka, respectivamente.

Considerando estas eficiencias, la producción de sedimentos acumulada durante los 36, 56 y 11 años de operación de la presa fue estimada a 1.6×10^6, 13.7×10^6 y 1.2×10^6 toneladas de sedimento para los reservorios Corani, Angostura y Laka-Laka, respectivamente. En términos de la producción especifica de sedimentos estimado, la predicción mas alta [1,831 ton km^{-2} a^{-1}] fue para el reservorio Laka-Laka con una área de cuenca contribuyente de cerca de 59.8 km^2 mientras que una menor estimación [123 ton km^{-2} a^{-1}] fue calculada para el reservorio Angostura con una área de cuenca de 1,992 km^2. La producción de sedimentos especifica para la cuenca contribuyente del reservorio Corani (297 km^2) fue evaluada en 152 ton km^{-2} a^{-1}.

Muchas posibles razones existen para explicar estas significativas diferencias en tasas de sedimentación entre los tres reservorios siendo las más importantes el área de la cuenca, el relieve general de la cuenca, litología, cobertura del terreno y las características geomorfológicas y topográficas en la proximidad del reservorio (<5 km^2). Los resultados de esta tesis están de acuerdo con la literatura más reciente las

cuales hacen mención especial de las gradientes topográficas y la presencia de áreas deposiciones tales como abanicos aluviales o planos inundación en la proximidad del reservorio como los factores más importantes para la contribución de sedimentos.

Sin embargo, es claramente demostrado que la variable comúnmente usada "área de la cuenca" por si misma es un pobre estimador de la producción especifica de sedimentos, aunque aun es hasta el presente muy extensamente utilizada y mencionada en los ámbitos científicos. Evidencia adicional para la alta producción de sedimentos en la pequeña cuenca Laka-Laka puede ser encontrada cuando se considera la litología, la características geomorficas en la proximidad del reservorio y la inadecuada localización geográfica del sitio de presa.

Como se menciono en un comienzo, la geología sedimentaria en el área subyacente de la cuenca de Laka-Laka y el relieve inclinado y el tipo de red de drenaje de la cuenca fuertemente afectan los mecanismos y tasas de erosión y entrega de sedimentos. Al contrario la sedimentación en el reservorio Angostura es baja considerando el área total de la cuenca del valle alto (1,992 km^2), los 56 años de tiempo de vida del reservorio y la relativa alta tasa de erosión observada en las áreas altas de la cuenca (*p.e.* localidades de Santivañez, Anzaldo y Sacabamba). Sin embargo la presencia de áreas extensas de valles aluviales rellenados, extensos abanicos aluviales con textura gruesa a la salida de los principales ríos entrando a la depresión de los valles (*p.e.* en los abanicos de Punata, Villa Rivero, Figure 6.1), actúan como grande pozos deposicionales evitando que una gran parte del sedimento sea conducido al reservorio, con excepción la lavado de carga de sedimento fino, transportado en los eventos extraordinarios de inundación Asi de este modo, aunque la erosión de suelos se considera severa en las áreas de la montaña alta de la cuenca, los sedimentos generados aguas arriba debido a los procesos de erosión hídrica son depositados en los abanicos aluviales de almacenamiento y en los planos de inundación deposicionales.

Aunque el profundo relieve interno y el patrón hidrológico de drenaje de la cuenca Corani parecerían -*a priori*- sugerir que la cuenca produce una alta cantidad de sedimentos, se encontraron bajas tasas de sedimentación en el reservorio. Los levantamientos de campo y el análisis de las imágenes satelitales, indican que en la cuenca categorizada como sub-húmeda, la cobertura vegetal es casi permanente, con pastos de porte bajo perennes, arbustos, manchas de bosque y campos agrícolas (papas, maíz, verduras) típicas de un ambiente sub-andino húmedo.

Al mismo tiempo el desarrollo de los suelos (*p.e.* descomposición de materia orgánica) muestra típicos rasgos de su evolución y las cuales son comúnmente observadas a estas altas elevaciones (>3,000 m) y bajas latitudes tropicales resultando en una relativa baja erodabilidad en combinación con una buena cobertura vegetal

La cuenca Corani se abastece de varias sub-cuencas a través de los dos principales ríos que drenan los antiguos valles aluviales glaciales (*p.e.* Colomi, Palca, Tablas, Melga, Quenko y Aguirre) los cuales actúan como áreas y ambientes deposicionales. Las gradientes de los principales cursos del río en la proximidad del reservorio son bajas (<0.1%) lo cual impide un fuerte densidad de flujo de sedimentos hacia el reservorio. De hecho, se puede afirmar que la selección del sitio de presa para los reservorios

Angostura (1939) y Corani (1968) fue apropiadamente determinadas, en contraste con la inadecuada selección del sitio de presa para el reservorio de Laka-Laka (1991), al menos en términos de sedimentación y el tiempo de esperanza de vida de la presa.

Los satisfactorios resultados obtenidos en los tres reservorios estudiados demuestra la aplicabilidad de la técnica de levantamiento de sonar acústico guiado por un GPS portátil para la actualización y registro batimétrico de lagos y reservorios. Se debe afirmar que para que la técnica sea completamente exacta, el método debe ser complementado con un muestreo de los sedimentos de fondo para la determinación de la densidad aparente. El uso de imágenes satelitales provee las curvas del reservorio adicionales necesarias para la definición del borde del reservorio en la fecha del levantamiento batimétrico (agua versus los bordes de la orilla y por arriba de la línea de agua actual) permitiendo el análisis y monitoreo de los reservorios incluso con bajos niveles de agua. Debido al bajo costo económico de los instrumentos (<€ 2,500) y la rapidez con la cual el levantamiento puede ser ejecutado, el método puede ser usado con un periodo de tiempo frecuente para el establecimiento de datos de referencia de sedimentación en reservorios y producción de sedimentos en cuencas.

Uniendo la erosión bruta de una cuenca a la sedimentación en reservorios

Para finalizar, un método alternativo que conecta el proceso de producción bruta de erosión en la cuenca y la entrega de sedimentos al reservorio, basado en el concepto distribuido de la tasa de entrega de sedimentos (SDR) fue implementada en la cuenca de Laka-Laka. La modelación del SDR en una estructura especial de celda unida a los estimados de producción bruta de la erosión permite la estimación de las cantidades netas de suelo erodado y la cuales son entregadas de las celdas en áreas altas a las celdas de río mas cercanas y las cuales son transportadas hasta la salida de la cuenca y consecuentemente al reservorio. Cuatro modelos espaciales de SDR desarrollados recientemente, a nombrar, la herramienta de evaluación de la erosión de suelos (SEAGIS), el modelo distribuido de entrega de sedimentos (SEDD), el algoritmo de Veith y el modelo de la tasa de entrega de sedimento en serranías en pendiente (HSDR) fueron aplicados y avaluados.

Conceptualmente, el modelo HSDR considera a la cuenca como un sistema de dos almacenes lineares unidos en serie: transporte de sedimentos desde las serranías hasta el río más próximo y transición del flujo de sedimento en la red de drenaje. Cuando se usa este método el factor de control mas importante en el proceso de entrega de sedimento esta dado por la proporción del tiempo de residencia de los sedimentos (t_o y t_n) en la cuenca entre la duración promedio efectiva de la lluvia (t_{er}).

El algoritmo de Veith y el modelo SEDD presentan una base teórica similar y consideran que la SDR es una función del tiempo de viaje de las partículas (t_i) de sedimento en cada celda. El modelo SEAGIS considera que la *SDR* es una función de la cantidad de escurrimiento esperada para ser transportada a través de la celda, ponderada por la pendiente y la probabilidad de deposición de los sedimentos aguas abajo.

La aplicación de los cuatro modelos de *SDR* usando la estimaciones de erosión en la cuenca como datos de entrada, muestran que las predicciones fueron similares en todos los enfoques, aunque las diferencias en los patrones espaciales de SDR son visible,

conduciendo a una identificación de las fuentes de sedimentos. En general, la *SDR* y la producción de sedimentos en celdas fueron marcadamente menores (*p.e.* SDR<0.2) que las tasas de erosión en mas del 50% de la cuenca. Valores de tasa de entrega de sedimentos mas altos (*p.e.* SDR>0.6) fueron encontrados en un 25% del área de la cuenca, especialmente en las serranías y planicies altas localizadas en la zona mas sureste y sur de la cuenca. En promedio, en el periodo en evaluación, 45% del total de la erosión producida es movilizada y transportada desde las serranías altas a las redes de drenaje y finalmente al reservorio, resultando en un valor promedio de la tasa de entrega de sedimentos de 0.45.

El enfoque de *HSDR* es considerado el más apropiado para la estimación de la producción distribuida de la entrega de sedimento a la escala de cuenca media a grande, debido a su solida base teórica física y la inclusión de los parámetros de lluvia y transporte en la red de drenaje. Sin embargo, considerando que el modelo SEDD tambien mostró resultados confiables y puesto que los requerimientos de datos de entrada para este enfoque son mas fáciles de obtener, este método es probablemente el mas apto para le estimación distribuida de *SDR* en cuencas con una pobre o escasa colección de datos.

Una validación cuantitativa de los modelos de entrega de sedimentos de la cuenca de Laka-Laka fue llevada a cabo por comparación de las estimaciones de la tasa anual de entrega de sedimentos basado en la SDR, con la estimación de la producción de sedimentos de la cuenca contribuyente a parir de los datos de medición de las tasas de sedimentación en el reservorio.

Cuando se usa los patrones espaciales de la tasa de entrega de sedimentos del modelo SEDD (*p.e.* estimaciones de la SDR unidas a los estimados de los modelos de erosión respectivos) estimaciones de la producción de sedimentos en la cuenca fueron mayores para el modelo Thornes [110,000 toneladas] y el modelo RUSLE-3D [107,000 toneladas], mientras que los valores mas bajos fueron estimados por los modelos SPL [91,000 toneladas], USPED [82,000 toneladas], y el modelo MMMF [73,000 toneladas]. Las predicciones anuales fueron en el rango con los datos medidos de sedimentación en el reservorio, considerando que la tasa anual de deposición (11 años de vida) en el reservorio fue de 109,500 toneladas.

Consideraciones finales

La magnitud y consecuencias ambientales y sociales de los aspectos de erosión y entrega de sedimento en la región de los Andes de Bolivia han sido reconocidas y han atraído la atención científica de varios especialistas. Esta investigación ha demostrado que las técnicas de geo-información tales como la modelación espacial distribuida de la erosión y la tasa de entrega de sedimentos, en combinación con diversas fuentes de imágenes satelitales y con los escasos datos de campo (información -*in situ*-) disponibles permiten un escrutinio de extensas regiones, cuencas de tamaño medio a grande, en términos de las amenazas y/o riesgos de erosión y sedimentación.

Esta metodología puede ser usada para producir mapas de cobertura nacional, regional y de cuenca con estimaciones de erosión y deposición con una apropiada resolución espacial y temporal usando datos libremente disponibles o información de percepción

remota de bajo costo pero mayor resolución espacial y espectral. La implementación de esta metodología, basada en una muy modesta base de datos de campo, y con modelos con un requerimiento de datos mínimo, produjo estimaciones reales a una escala temporal mensual y anual y con resoluciones espaciales desde 30-m a 1-km.

Usando un novedoso y rápido método de evaluación y monitoreo de la sedimentación en reservorios, desarrollado en esta investigación, el marco del modelamiento geo-espacial combinado de la estimación de la erosión y la de entrega de sedimentos puede ser extendidas a otras cuencas hídricas sin redes de monitoreo y con escasos datos de observación -*in situ*-.

El método puede tambien encontrar muchas aplicaciones en la planificación del uso de la tierra, y el manejo de la tierra, donde puede suplementar información extrapolada de experimentos llevados a cabo en escala local (parcela o en terrenos en pendiente). Los resultados de esta investigaron indican tambien otras aplicaciones potenciales en el campo del medio ambiente y aspectos ecológicos donde la erosión y la estimación de la producción de sedimentos puede ser de uso sustancial, *p.e.* en investigación de la desertificación y degradación de la tierra, cambio climático, y calentamiento global.

Resumo

A previsão de padrões espaciais e intensidade de erosão e redistribuição sedimentar de solos, em paisagens naturais, pode ser problemática em áreas onde há pouca disponibilidade de dados experimentais. Entretanto, é nessas regiões de dados escassos onde a habilidade de extrapolar evidências locais de campo poderia ser muito útil em aplicações práticas. Convencionalmente, conservacionistas e tomadores de decisão consideram a escala de campo para julgar os impactos da erosão de solos na região. Diferentemente, gestores de recursos hídricos usualmente baseiam-se nos dados de produção de sedimentos, medidos nas áreas de captação, quando esses dados existem na região de interêsse, para avaliar a intensidade de erosão e produção de sedimentos. De fato, uma diferença de escala é observada nas abordagens usadas, respectivamente, por gestores de recursos de terra e recursos de água.

A crescente disponibilidade de dados de imagens de satélites, com resolução espacial variando de 5 m a 1 km e resolução temporal de 1 a 26 dias, oferece uma fonte significante de informações para mapeamento, monitoramento e predição da presente degradação da terra, bem como permite monitorar sinais que descrevem variações espacio-temporais nas caracaterísticas da superfície dos solos. Adicionalmente, o uso integrado de dados experimentais de campo com imagens de sensoriamento remoto, possibilita extender evidências de campo a áreas maiores. Por outro lado, modelos de distribuição de erosão tem evoluído devido à crescente capacidade de plataformas existentes de SIG e são atualmente usados como o eixo principal geo-referenciado para análise de processos hidrológicos e de erosão. Contudo, a acurácia das previsões é seriamente comprometida pela complexidade natural e heterogeneidade espacial dos processos que atuam na própria paisagem, associada à limitada disponibilidade de séries de dados espacio-temporais em captações sem medidores.

Portanto, esta tese visou a desenvolver e usar métodos existentes com abordagens espacialmente distribuídas, em combinação com diferentes técnicas de geo-informação, para analisar processos de erosão e sedimentação e permitir a definição de vínculos entre as escalas de campo e de bacia, em ambientes com escassez de dados. Neste estudo, modelos conceituais foram selecionados, por representarem um meio termo entre modelos que demandam dados complexos (com base física) e modelos simplificados de regressão (com base empírica).

A província de Cochabamba, na região Central Andina da Bolívia, constituiu o foco desta pesquisa. A região dos vales médios e altos de Cochabamba representa um ambiente semi-árido, onde os impactos de erosão do solo são claramente visíveis e desempenham um papel importante na sustentabilidade da vida rural e bem-estar da sociedade como um todo.

Mapas regionais de erosão e deposição para a província de Cochabamba, com uma área aproximada de 54.100 km^2, foram compostos usando clima global, topografia, dados de solos e imagens de satélite de baixa resolução para cobertura da terra. Cinco propostas de modelos conceituais foram comparados, quanto à sua habilidade de representar fenômenos de erosão e sedimentação ao nível regional. Um método de comparação

categórica foi usado para validar a predição dos modelos, com base em mapas temáticos existentes de intensidade de erosão. A precisão dos modelos variou de razoável a pobre, refletindo diferenças fundamentais em modelagem baseada em "pixels" e nas unidades de mapeamento do terreno. A generalização nas séries de dados globais de topografia e de solos foi considerada como a principal fonte de incerteza nas estimativas dos modelos, especialmente para o ambiente altamente variável dos Andes.

Uma análise mais detalhada da erosão, em uma captação semi-árida de 59,8 km^2, foi conduzida, usando dados de satélite de alta a média resolução (5 a 90 m) para cobertura e topografia da terra. Dados de precipitação e solos foram obtidos pela extrapolação, a partir de estações locais, e medições "in situ". Da mesma maneira, as estimativas dos cinco modelos foram comparadas e validadas em relação a um mapa de intensidade de erosão, obtido a partir de análise multi-temporal de um mosaico de orto-fotos de 1961 e uma imgem pancromática SPOT-5, orto-retificada, de 2002, em combinação com um modêlo digital de terreno e dados de campo. A validação semi-quantitativa indicou uma concordância razoável do modêlo, em termos de padrões espaciais. Entretanto, nenhum dos modêlos mostrou-se preciso, em termos de valores absolutos, e portanto essas estimativas de perdas de solos devem ser interpretadas com cautela.

A próxima escala de análise, para o entendimento de processos de condução de sedimentos às redes de canais e finalmente para a saída da captação, foi a escala local. Com esse propósito, três reservatórios contrastantes foram estudados, em termos de tamanho e processo erosivo à jusante. Constatou-se que estudos sedimentológicos detalhados de reservatóros fornecem históricos deposicionais de alta resolução, que ajudam a quantificar a produtividade média anual de sedimentos das captações contribuintes. Um nôvo e rápido sonar acústico e uma técnica de levantamento direcionado por GPS foram desenvolvidas para êsse propósito. A avaliação do tamanho de amostra, ou densidade pontual, sobre a geração de superfície batimétrica, foi avaliada por validação cruzada, usando várias estatísticas de acurácia. Foi constatado que a variabilidade da taxa de sedimentação, dentro dos reservatórios, variaram de acordo com a fisiografia (distância do canal do rio, vizinhança do reservatório), topografia (relêvo suave, moderado ou íngreme), clima (descargas e regimes de rios) e condições hidráulicas dos reservatórios (descargas anuais e requerimentos de irrigação). A variação temporal foi devida às variações de vazões incidentes do rio, o regime de exploração e as mudanças na capacidade de armazenamento do reservatório.

Finalmente, as relações entre as taxas brutas de erosão da captação e a sedimentação do reservatório foram analisadas, usando os conceitos de razão de transporte de sedimento espacialmente distribuída (SDR). Este conceito é baseado no tempo de deslocamento requerido para os sedimentos deslocados chegarem à saída da captação. Altas razões de transporte (SDR>0,6) foram encontradas em 25% da área de captação, enquanto valores de SDR inferiores a 0,2 foram encontrados em 50% da área.

A modelagem de SDR no domínio espacial e o seu acoplamento às estimativas prévias de erosão bruta da captação possibilitaram a estimativa das quantidades líquidas de solo erodido. Essas predições de produção de sedimentos foram validadas usando os registros de sedimentos do reservatório e foram verificadas para as condições fisiográficas e climáticas prevalecentes nesta parte dos Andes.

228

A coleta de informações ambientais "in situ" requer um forte suporte financeiro, na maioria das vezes não disponível em países em desenvolvimento, como a Bolívia. Estes resultados abrem possibilidades de usar escassos dados "in situ", junto a crescentemente disponíveis dados remotamente coletados, para a indentificação de "áreas fontes", ou para o desenvolvimento preliminar de estratégias de manejo de bacias.

Abbreviations and Acronyms

Abbreviations

AMC	*Antecedent Moisture Condition*
ASTER	*Advanced Spaceborne Thermal Emission and Reflection Radiometer*
ATSR-2	*Along Track Scanning Radiometer*
AVHRR	*Advanced Very High Resolution Radiometer*
CAD	*Computer Aided Design*
DEM	*Digital Elevation Model*
DTM	*Digital Terrain Model*
FCC	*False Colour Composite*
GCP	*Ground Control Points*
GOES	*Geostationary Operational Environmental Satellite*
GPI	*GOES Precipitation Index*
GPS	*Geographic Positioning Systems*
GSD	*Ground Sample Distance*
GTOPO30	*Global Digital Elevation Model from the US Geological Survey*
HSG	*Hydrological Soil Group*
JERS-1	*Japanese Earth Resources Satellite*
LAI	*Leaf Area Index*
Landsat ETM	*Landsat Enhanced Thematic Mapper*
Landsat MSS	*Landsat Multispectral Imagery Scanner*
Landsat TM	*Landsat Thematic Mapper*
MAE	*Mean Absolute Error*
masl	*Metres above sea level*
MERIS	*Medium Resolution Imaging Spectrometer*
METEOSAT	*Meteorological Satellite*
MODIS	*Moderate Resolution Imaging Spectroradiometer*
MSE	*Mean Square Error*
NDVI	*Normalized Difference Vegetation Index*
OLS	*Operational Linescan System*
RMSE	*Root Mean Square Error*
SDR	*Sediment Delivery Ratio*
SRTM	*Shuttle Radar Terrain Mission*
SSM/I	*Special Sensor Microwave Imager*
SSY	*Specific Sediment Yield*
UTM	*Universal Transversal Mercator projection*
VHR	*Very High Resolution*
WGS-84	*World Geodetic System 1984*

Acronyms

AGNPS	*Agricultural Non Point Source Pollution model*
ANSWERS	*Aerial Non Point Source Watershed Environment Response Simulation*
ARSN-1	*Irrigations Farmers Association of Angostura reservoir*
CAIC	*Canadian Agency for International Cooperation*
CASC2D-SED	*The Two Dimensional Upland Erosion model*
CLAS	*Centre for Aerospace Survey and GIS Applications for Natural Resources Management*
CORANI	*Electric Enterprise CORANI*
CORDECO	*Development Agency of Cochabamba*
CREAMS	*Chemicals, Runoff and Erosion from Agricultural Management Systems*
CRU	*Climatic Research Unit*
EOS	*Earth Observing System*
EPIC	*Erosion Productivity Impact Calculator*
EROS	*National Centre for Earth Resources Observation & Science*
EROSION-3D	*The Three Dimensional Storm Process Based Erosion model*
EUROSEM	*European Soil Erosion model*
FISHFINDER-100	*Full featured 200 khz GARMIN sounder with temperature*
GARTRIP	*The windows PC Shareware Program for GARMIN and Magellan GPS*
GEOBOL	*Bolivian Geological Survey*
GIS	*Geographic Information System*
GRASS	*Geographic Resources Analysis Support System*
HQUSACE	*International Hydrographic Organization Order*
HSDR	*Hillslope Sediment Delivery Ratio model*
HYDRO-1k	*Global Corrected Topographic data derived from GTOPO-30*
HYDROTOOLS	*Hydrological tools for ArcView GIS*
IGBP	*International Geosphere Biosphere Programme*
ILWIS	*Integrated Land and Water Information System software*
IPCC	*International Panel of Climate Change*
JRC	*European Join Research Centre*
KINEROS2	*Kinematic Runoff and Erosion model*
LA	*Latin America*
LASCAM	*Large Scale Catchment Model*
LH-UMSSS	*Hydraulic Laboratory of the UMSS*
LISEM	*Limburg Soil Erosion Model*
LISFLOOD	*Physically based model for Peak Flow and Flooding simulation*
LP DAAC	*Land Process Distributed Active Archive Centre*
MDSMA	*Ministry of Sustainable Development and Environment*
MMMF	*Modified Morgan, Morgan and Finney model*
MUSLE	*Modified Universal Soil Loss Equation*
NASA	*National Aeronautics and Space Administration*
NOAA	*National Oceanic & Atmospheric Administration*
NWS	*US National Weather Service*
PCRaster	*PCRaster Environmental Modelling software*

PESERA	*Pan European Soil Erosion Risk model*
PRODEVAT	*Development Programme for the Arque and Tapacari Valleys*
PROMIC	*Integrated Catchment Management Programme*
PRONAR	*Bolivian National Irrigation Programme*
RS	*Remote Sensing*
RUSLE	*Revised Universal Soil Loss Equation*
RUSLE-3D	*The Three Dimensional Revised Universal Soil Loss Equation*
SA	*South America*
SCS	*US Soil Conservation Service*
SEAGIS	*Erosion Assessment Tool of MIKE BASIN & MILW*
SEDD	*Sediment Delivery Distributed model*
SEDNET	*Sediment Budgeting Model*
SGT	*Geodesic and Topographic Service*
SHETRAN	*European Distributed Basin Flow and Transport Modelling System*
SPL	*Stream Power Law Model*
SWAT	*Soil and Water Assessment Tool*
TAUDEM	*Terrain Analysis using Digital Elevation Models*
TRMM	*Tropical Rainfall Measuring Mission*
UMSS	*Major University of San Simon*
USDA	*United States Department of Agriculture*
USLE	*Universal Soil Loss Equation*
USPED	*Unit Stream Power Erosion Deposition model*
WAAS	*Wide Area Augmentation System*
WEPP	*Water Erosion Prediction Project*

Symbols

Greek

α	Aspect of the elevation
$\beta_{(r)}$	Steepest slope angle
κ	Fractal coefficient
ε	Erosion index
ς	Calibration coefficient for rainfall and runoff
$\gamma_{(h)}$	Semivariance
φ	Coefficient for SDR determination as a function of the catchment area
λ	Coefficient for SDR determination as a function of the catchment area
β	Catchment specific parameter for SDR determination as a function of the sediment travel time
δ	Coefficient for flow velocity estimation according to the surface roughness
χ	Land cover and land use coefficient for flow velocity estimation
θ	Particle size diameter
ψ	Coefficient related to the stream roughness

Roman

A	Annual soil loss rate
R	Erosivity factor
K	Erodibility factor
C	Cover management factor
LS	Slope length factor
P	Support practice factor
$A_{(r)}$	Upslope contributing area
$LS_{(r)}$	Modified slope length factor
C_s	Sediment concentration
D	Fractal dimension
EI_{30}	Erosivity index for 30 minutes rainfall intensity
F	Modified Fournier index
D_g	Geometric mean particle diameter
E_d	Net erosion deposition index
E	Kinetic energy for splash detachment
I	Rainfall intensity
R_a	Annual rainfall
R_c	Soil moisture storage capacity
R_o	Mean rainfall per rainy day
MS	Soil moisture at field capacity
B_d	Soil bulk density
R_d	Hydrological root depth
E_t/E_o	Ratio of actual to potential evapotranspiration
Q	Overland flow
Q_{cum}	Cumulative overland flow
P_i	Rainfall interception by vegetative cover
F	Soil detachment by rainfall
T_c	Soil detachment by runoff or transport capacity
K_s	Hydraulic conductivity
K_m	Soil detachability index
CN	Curve number

OF	*Overland flow*
v_c	*Fraction of vegetation cover*
J_i	*Rain day frequency density*
I_a	*Initial abstraction*
S_a	*Potential retention*
s	*Slope*
K_t	*Soil erodibility factor in the Thornes model*
K_l	*Erosion coefficient encompassing the effects of lithology, soil and climate*
B	*Bias*
r^2	*Goodness of fit or coefficient of determination*
r	*Coefficient of correlation*
$R^2{}_{NS}$	*Coefficient of model efficiency or Nash Sutcliffe coefficient*
P_a	*Annual rainfall*
DI_p	*Delivery index*
H	*Flow parameter according to the flow routing algorithm*
t_i	*Sediment travel time*
l_i	*Flow path or flow length*
d	*Sediment delivery function in the Veith algorithm*
t_{er}	*Effective rainfall duration*
$t_h(\theta)$	*Hillslope residence time*
$t_n(\theta)$	*Channel residence time*
$w_t(\theta)$	*Settling velocity*
Re_p	*Reynolds number*
C_D	*Drag coefficient*
i_e	*Excess rainfall*
n	*Manning roughness coefficient*

236

Curriculum Vitae

Carlos Saavedra was born in Sucre, Bolivia, on the 14th of February 1974. After finishing secondary school in his hometown of Cochabamba, he enrolled at the Faculty of Agronomy of the Major University of San Simon (UMSS) in January 1991. He was awarded a two-year research contract (1996-1997) within the Bolivian-Dutch Research and Educational Programme of Irrigation in the Andes and Valleys (PEIRAV/WUR). After this period he concluded his thesis in the field of irrigation design processes, and in September 1997 he obtained a BSc degree in agronomic engineering, specializing in irrigation and drainage. In December 1998, he obtained the degree of Professional Master (PM) in water resource survey at the Centre of Aerospatial Survey and GIS Applications for Sustainable Natural Resource Management (CLAS), a joint educational programme between the International Institute for Geo-Information and Earth Observation (ITC), the Netherlands, and the UMSS, Bolivia. He worked as a junior consultant on environmental impact assessment studies for the Dames & Moore Engineering Firm in the first semester of 1999. He obtained an MSc degree in environmental system analysis and monitoring at the Department of Water Resources at ITC in April 2000. From June 2000 until December 2001, he held an appointment as a full-time lecturer for the three PM programmes at CLAS. In addition to teaching at this educational centre, he has carried out several projects and teaching duties at the Bolivian Catholic University (UCB) and the Bolivian Private University (UPB). In January 2002, he embarked on the PhD programme within the framework of the CLAS-SAIL project at the Department of Water Resources at ITC, which has resulted in this thesis.

contact address:
Carlo.Saavedra@gmail.com

ITC dissertation list

Akinyede (1990), Highway cost modelling and route selection using a geotechnical information system

Pan He Ping (1990), 90-9003-757-8, Spatial structure theory in machine vision and applications to structural and textural analysis of remotely sensed images

Bocco Verdinelli, G. (1990), Gully erosion analysis using remote sensing and geographic information systems: a case study in Central Mexico

Sharif, M. (1991), Composite sampling optimization for DTM in the context of GIS

Drummond, J. (1991), Determining and processing quality parameters in geographic information systems

Groten, S. (1991), Satellite monitoring of agro-ecosystems in the Sahel

Sharifi, A. (1991), 90-6164-074-1, Development of an appropriate resource information system to support agricultural management at farm enterprise level

Zee, D. van der (1991), 90-6164-075-X, Recreation studied from above: air photo interpretation as input into land evaluation for recreation

Mannaerts, C. (1991), 90-6164-085-7, Assessment of the transferability of laboratory rainfall-runoff and rainfall-soil loss relationships to field and catchment scales: a study in the Cape Verde Islands

Ze Shen Wang (1991), 90-393-0333-9, An expert system for cartographic symbol design

Zhou Yunxian (1991), 90-6164-081-4, Application of Radon transforms to the processing of airborne geophysical data

Zuviria, M. de (1992), 90-6164-077-6, Mapping agro-topoclimates by integrating topographic, meteorological and land ecological data in a geographic information system: a case study of the Lom Sak area, north-central Thailand

Westen, C. van (1993), 90-6164-078-4, Application of geographic information systems to landslide hazard zonation

Shi Wenzhong (1994), 90-6164-099-7, Modelling positional and thematic uncertainties in integration of remote sensing and geographic information systems

Javelosa, R. (1994), 90-6164-086-5, Active Quaternary environments in the Philippine mobile belt

Lo King-Chang (1994), 90-9006526-1, High quality automatic DEM (digital elevation model) generation from multiple imagery

Wokabi, S. (1994), 90-6164-102-0, Quantified land evaluation for maize yield gap analysis at three sites on the eastern slope of Mt. Kenya

Rodriguez, O. (1995), Land use conflicts and planning strategies in urban fringes: a case study of western Caracas, Venezuela

Meer, F. van der (1995), 90-5485-385-9, Imaging spectrometry and the Ronda peridotites

Kufoniyi, O. (1995), 90-6164-105-5, Spatial coincidence: automated database updating and data consistency in vector GIS

Zambezi, P. (1995), Geochemistry of the Nkombwa Hill carbonatite complex of Isoka District, north-east Zambia, with special emphasis on economic minerals

Woldai, T. (1995), The application of remote sensing to the study of the geology and structure of the Carboniferous in the Calañas area, pyrite belt, southwest Spain

Verweij, P. (1995), 90-6164-109-8, Spatial and temporal modelling of vegetation patterns: burning and grazing in the Paramo of Los Nevados National Park, Colombia

Pohl, C. (1996), 90-6164-121-7, Geometric aspects of multisensor image fusion for topographic map updating in the humid tropics

Jiang Bin (1996), 90-6266-128-9, Fuzzy overlay analysis and visualization in GIS

Metternicht, G. (1996), 90-6164-118-7, Detecting and monitoring land degradation features and processes in the Cochabamba valleys, Bolivia: a synergistic approach

Hoanh Chu Thai (1996), 90-6164-120-9, Development of a computerized aid to integrated land use planning (CAILUP) at regional level in irrigated areas: a case study for the Quan Lo Phung Hiep region in the Mekong Delta, Vietnam

Roshannejad, A. (1996), 90-9009284-6, The management of spatio-temporal data in a national geographic information system

Terlien, M. (1996), 90-6164-115-2, Modelling spatial and temporal variations in rainfall-triggered landslides: the integration of hydrologic models, slope stability models and GIS for the hazard zonation of rainfall-triggered landslides with examples from Manizales, Colombia

Mahavir, J. (1996), 90-6164-117-9, Modelling settlement patterns for metropolitan regions: inputs from remote sensing

Al-Amir, S. (1996), 90-6164-116-0, Modern spatial planning practice as supported by the multi-applicable tools of remote sensing and GIS: the Syrian case

Pilouk, M. (1996), 90-6164-122-5, Integrated modelling for 3D GIS

Duan Zengshan (1996), 90-6164-123-3, Optimization modelling of a river-aquifer system with technical interventions: a case study for the Huangshui river and the coastal aquifer, Shandong, China

Man, W.H. de (1996), 90-9009-775-9, Surveys: informatie als norm: een verkenning van de institutionalisering van dorp - surveys in Thailand en op de Filippijnen

Vekerdy, Z. (1996), 90-6164-119-5, GIS-based hydrological modelling of alluvial regions: using the example of the Kisaföld, Hungary

Pereira, Luisa (1996), 90-407-1385-5, A robust and adaptive matching procedure for automatic modelling of terrain relief

Fandino Lozano, M. (1996), 90-6164-129-2, A framework of ecological evaluation oriented at the establishment and management of protected areas: a case study of the Santuario de Iguaque, Colombia

Toxopeus, B. (1996), 90-6164-126-8, ISM: an interactive spatial and temporal modelling system as a tool in ecosystem management; with two case studies: Cibodas biosphere reserve, West Java Indonesia: Amboseli biosphere reserve, Kajiado district, central-southern Kenya

Wang Yiman (1997), 90-6164-131-4, Satellite SAR imagery for topographic mapping of tidal flat areas in the Dutch Wadden Sea

Saldana-Lopez, Asunción (1997), 90-6164-133-0, Complexity of soils and soilscape patterns on the southern slopes of the Ayllon Range, central Spain: a GIS assisted modelling approach

Ceccarelli, T. (1997), 90-6164-135-7, Towards a planning support system for communal areas in the Zambezi valley, Zimbabwe: a multi-criteria evaluation linking farm household analysis, land evaluation and geographic information systems

Peng Wanning (1997), 90-6164-134-9, Automated generalization in GIS

Lawas, C. (1997), 90-6164-137-3, The resource users' knowledge, the neglected input in land resource management: the case of the Kankanaey farmers in Benguet, Philippines

Bijker, W. (1997), 90-6164-139-X, Radar for rain forest: a monitoring system for land cover change in the Colombian Amazon

Farshad, A. (1997), 90-6164-142-X, Analysis of integrated land and water management practices within different agricultural systems under semi-arid conditions of Iran and evaluation of their sustainability

Orlic, B. (1997), 90-6164-140-3, Predicting subsurface conditions for geotechnical modelling

Bishr, Y. (1997), 90-6164-141-1, Semantic aspects of interoperable GIS

Zhang Xiangmin (1998), 90-6164-144-6, Coal fires in northwest China: detection, monitoring and prediction using remote sensing data

Gens, R. (1998), 90-6164-155-1, Quality assessment of SAR interferometric data

Turkstra, J. (1998), 90-6164-147-0, Urban development and geographical information: spatial and temporal patterns of urban development and land values using integrated geo-data, Villaviciencia, Colombia

Cassells, C. (1998), 90-6164-234-5, Thermal modelling of underground coal fires in northern China

Naseri, M. (1998), 90-6164-195-0, Characterization of salt-affected soils for modelling sustainable land management in semi-arid environment: a case study in the Gorgan region, northeast, Iran

Gorte B.G.H. (1998), 90-6164-157-8, Probabilistic segmentation of remotely sensed images

Tegaye, Tenalem Ayenew (1998), 90-6164-158-6, The hydrological system of the lake district basin, central main Ethiopian rift

Wang Donggen (1998), 90-6864-551-7, Conjoint approaches to developing activity-based models

Bastidas de Calderon, M. (1998), 90-6164-193-4, Environmental fragility and vulnerability of Amazonian landscapes and ecosystems in the middle Orinoco river basin, Venezuela

Moameni, A. (1999), Soil quality changes under long-term wheat cultivation in the Marvdasht plain, south-central Iran

Groenigen, J.W. van (1999), 90-6164-156-X, Constrained optimisation of spatial sampling: a geostatistical approach

Cheng Tao (1999), 90-6164-164-0, A process-oriented data model for fuzzy spatial objects

Wolski, Piotr (1999), 90-6164-165-9, Application of reservoir modelling to hydrotopes identified by remote sensing

Acharya, B. (1999), 90-6164-168-3, Forest biodiversity assessment: a spatial analysis of tree species diversity in Nepal

Akbar Abkar, Ali (1999), 90-6164-169-1, Likelihood-based segmentation and classification of remotely sensed images

Yanuariadi, T. (1999), 90-5808-082-X, Sustainable land allocation: GIS-based decision support for industrial forest plantation development in Indonesia

Abu Bakr, **Mohamed** (1999), 90-6164-170-5, An integrated agro-economic and agro-ecological framework for land use planning and policy analysis

Eleveld, M. (1999), 90-6461-166-7, Exploring coastal morphodynamics of Ameland (the Netherlands) with remote sensing monitoring techniques and dynamic modelling in GIS

Yang Hong (1999), 90-6164-172-1, Imaging spectrometry for hydrocarbon microseepage

Mainam, Félix (1999), 90-6164-179-9, Modelling soil erodibility in the semiarid zone of Cameroon

Bakr, Mahmoud (2000), 90-6164-176-4, A stochastic inverse-management approach to groundwater quality

Zlatanova, Z. (2000), 90-6164-178-0, 3D GIS for urban development

Ottichilo, Wilber K. (2000), 90-5808-197-4, Wildlife dynamics: an analysis of change in the Masai Mara ecosystem

Kaymakci, Nuri (2000), 90-6164-181-0, Tectono-stratigraphical evolution of the Cankori Basin (Central Anatolia, Turkey)

Gonzalez, Rhodora (2000), 90-5808-246-6, Platforms and terraces: bridging participation and GIS in joint-learning for watershed management with the Ifugaos of the Philippines

Schetselaar, Ernst (2000), 90-6164-180-2, Integrated analyses of granite-gneiss terrain from field and multisource remotely sensed data: a case study from the Canadian Shield

Mesgari, Saadi (2000), 90-3651-511-4, Topological cell-tuple structure for three-dimensional spatial data

Bie, Cees A.J.M. de (2000), 90-5808-253-9, Comparative performance analysis of agro-ecosystems

Khaemba, Wilson M. (2000), 90-5808-280-6, Spatial statistics for natural resource management

Shrestha, Dhruba (2000), 90-6164-189-6, Aspects of erosion and sedimentation in the Nepalese Himalaya: highland-lowland relations

Asadi Haroni, Hooshang (2000), 90-6164-185-3, The Zarshuran gold deposit model applied in a mineral exploration GIS in Iran

Raza, Ale (2001), 90-3651-540-8, Object-oriented temporal GIS for urban applications

Farah, Hussein (2001), 90-5808-331-4, Estimation of regional evaporation under different weather conditions from satellite and meteorological data: a case study in the Naivasha Basin, Kenya

Zheng, **Ding** (2001), 90-6164-190-X, A neural-fuzzy approach to linguistic knowledge acquisition and assessment in spatial decision making

Sahu, B.K. (2001), Aeromagnetics of continental areas flanking the Indian Ocean; with implications for geological correlation and reassembly of Central Gondwana

Alfestawi, Y. (2001), 90-6164-198-5, The structural, paleogeographical and hydrocarbon systems analysis of the Ghadamis and Murzuq Basins, west Libya, with emphasis on their relation to the intervening Al Qarqaf Arch

Liu, Xuehua (2001), 90-5808-496-5, Mapping and modelling the habitat of Giant Pandas in Foping Nature Reserve, China

Oindo, Boniface Oluoch (2001), 90-5808-495-7, Spatial patterns of species diversity in Kenya

Carranza, Emmanuel John (2002), 90-6164-203-5, Geologically-constrained mineral potential mapping

Rugege, Denis (2002), 90-5808-584-8, Regional analysis of maize-based land use systems for early warning applications

Liu, Yaolin (2002), 90-5808-648-8, Categorical database generalization in GIS

Ogao, Patrick (2002), 90-6164-206-X, Exploratory visualization of temporal geospatial data using animation

Abadi, Abdulbaset M. (2002), 90-6164-205-1, Tectonics of the Sirt Basin: inferences from tectonic subsidence analysis, stress inversion and gravity modelling

Geneletti, Davide (2002), 90-5383-831-7, Ecological evaluation for environmental impact assessment

Sedogo, Laurent G. (2002), 90-5808-751-4, Integration of participatory local and regional planning for resources management using remote sensing and GIS

Montoya, Lorena (2002), 90-6164-208-6, Urban disaster management: a case study of earthquake risk assessment in Carthago, Costa Rica

Ahmad, Mobin-ud-Din (2002), 90-5808-761-1, Estimation of net groundwater use in irrigated river basins using geo-information techniques: a case study in Rechna Doab, Pakistan

Said, Mohammed Yahya (2003), 90-5808-794-8, Multiscale perspectives of species richness in East Africa

Schmidt, Karin (2003), 90-5808-830-8, Hyperspectral remote sensing of vegetation species distribution in a saltmarsh

Lopez Binnquist, Citlalli (2003), 90-3651-900-4, The endurance of Mexican amate paper: exploring additional dimensions to the sustainable development concept

Huang, Zhengdong (2003), 90-6164-211-6, Data integration for urban transport planning

Cheng, Jianquan (2003), 90-6164-212-4, Modelling spatial and temporal urban growth

Campos dos Santos, Jose Laurindo (2003), 90-6164-214-0, A biodiversity information system in an open data/metadatabase architecture

Hengl, Tomislav (2003), 90-5808-896-0, Pedometric mapping: bridging the gaps between conventional and pedometric approaches

Barrera Bassols, Narciso (2003), 90-6164-217-5, Symbolism, knowledge and management of soil and land resources in indigenous communities: ethnopedology at global, regional and local scales

Zhan, Qingming (2003), 90-5808-917-7, A hierarchical object-based approach for urban land-use classification from remote sensing data

Daag, Arturo S. (2003), 90-6164-218-3, Modelling the erosion of pyroclastic flow deposits and the occurrences of lahars at Mt. Pinatubo, Philippines

Bacic, Ivan (2003), 90-5808-902-9, Demand-driven land evaluation with case studies in Santa Catarina, Brazil

Murwira, Amon (2003), 90-5808-951-7, Scale matters! A new approach to quantify spatial heterogeneity for predicting the distribution of wildlife

Mazvimavi, Dominic (2003), 90-5808-950-9, Estimation of flow characteristics of ungauged catchments: a case study in Zimbabwe

Tang, Xinming (2004), 90-6164-220-5, Spatial object modelling in fuzzy topological spaces with applications to land cover change

Kariuki, Patrick (2004), 90-6164-221-3, Spectroscopy and swelling soils; an integrated approach

Morales, Javier (2004), 90-6164-222-1, Model driven methodology for the design of geo-information services

Mutanga, Onisimo (2004), 90-5808-981-9, Hyperspectral remote sensing of tropical grass quality and quantity

Šliužas, Ričardas V. (2004), 90-6164-223-X, Managing informal settlements: a study using geo-information in Dar es Salaam, Tanzania

Lucieer, Arko (2004), 90-6164-225-6, Uncertainties in segmentation and their visualisation

Corsi, Fabio (2004), 90-8504-090-6, Applications of existing biodiversity information: capacity to support decision-making

Tuladhar, Arbind (2004), 90-6164-224-8, Parcel-based geo-information system: concepts and guidelines

Elzakker, Corné van (2004), 90-6809-365-7, The use of maps in the exploration of geographic data

Nidumolu, Uday Bhaskar (2004), 90-8504-138-4, Integrating geo-information models with participatory approaches: applications in land use analysis

Koua, Etien L. (2005), 90-6164-229-9, Computational and visual support for exploratory geovisualization and knowledge construction

Blok, Connie A. (2005), Dynamic visualization variables in animation to support monitoring of spatial phenomena

Meratnia, Nirvana (2005), 90-365-2152-1, Towards database support for moving object data

Yemefack, Martin (2005), 90-6164-233-7, Modelling and monitoring soil and land use dynamics within shifting agricultural landscape mosaic systems

Kheirkhah, Masoud (2005), 90-8504-256-9, Decision support system for floodwater spreading site selection in Iran

Nangendo, Grace (2005), 90-8504-200-3, Changing forest-woodland-savanna mosaics in Uganda: with implications for conservation

Mohamed, Yasir Abbas (2005), 04-15-38483-4, The Nile hydroclimatology: impact of the Sudd wetland (distinction)

Duker, Alfred, A. (2005), 90-8504-243-7, Spatial analysis of factors implicated in *mycobacterium ulcerans* infection in Ghana

Ferwerda, Jelle, G., (2005), 90-8504-209-7, Charting the quality of forage: measuring and mapping the variation of chemical components in foliage with hyperspectral remote sensing

Martinez, Javier (2005), 90-6164-235-3, Monitoring intra-urban inequalities with GIS-based indicators: with a case study in Rosario, Argentina

Saavedra, Carlos (2005), 90-8504-289-5, Estimating spatial patterns of soil erosion and deposition in the Andean region using geo-information techniques: a study case in Cochabamba, Bolivia.

WAGENINGEN UNIVERSITY
University for Life Sciences

International Institute for Geo-information Science and Earth Observation